This is to certify that the

dissertation entitled

BOND AND SLIP OF STEEL BARS IN FROZEN SAND

presented by

RIYADH M. ALWAHHAB

has been accepted towards fulfillment
of the requirements for

Ph.D. degree in Civil & Sanitary Engineering

Orlando B. Andersland
Major professor

Date November 10, 1983

BOND AND SLIP OF STEEL BARS IN FROZEN SAND

by

Riyadh M. Alwahhab

A DISSERTATION

Submitted to
Michigan State University
in partial fulfillment of the requirements
for the degree of

DOCTOR OF PHILOSOPHY

Department of Civil and Sanitary Engineering

1983

ABSTRACT

BOND AND SLIP OF STEEL BARS
IN FROZEN SAND

By

Riyadh M. Alwahhab

Structural members (reinforcement, piles, ground anchors) embedded in frozen ground for the transfer and distribution of loads, tensile or compressive, involve load transfer at their common interface. Engineering design requires prediction of both the short- and long-term adfreeze bond strength for a range of freezing temperatures and sand-volume fractions. The design method must account for surface type (steel, wood, concrete), roughness, loading geometry, and the presence of any impurities in the sand-ice material. Adfreeze bond strength at the interface can be described as the shearing stress between the structural member and surrounding frozen soil at failure. For steel bars embedded in frozen sand the adfreeze bond includes three components: ice adhesion to the bar, friction between the bar surface and sand particles, and mechanical interaction between frozen sand and the bar surface roughness.

This experimental study involved measurement of the adfreeze bond components using model structural members (steel bars) embedded in frozen sand samples. Pullout loads, bar displacements, and temperatures were monitored for both constant displacement rate tests and constant load (creep) tests. The observed behavior showed that initially ice adhesion combined with friction prevents slip. Very small bar displacements (about 0.002 in.) characterize the start of tertiary creep for shearing stresses below those required for rupture of ice adhesion. After rupture and partial slip

a much smaller residual adfreeze bond controlled the pullout load. When a single lug was added to the bar, bearing action of frozen sand on the lug greatly increased the pullout load. Larger displacements with higher adfreeze bond strengths are associated with mobilization of mechanical interaction forces between the frozen sand and bar surface asperities. Lug spacing for maximum adfreeze bond was shown to be a function of pressure bulb overlap between lugs and formation of a void space behind lugs. Experimental relations presented showed the dependence of creep displacement rates and/or adfreeze bond on lug size and spacing, sample dimensions, water impurities, bar surface roughness, temperature, sand volume fraction, and permitted development of empirical relationships for prediction of adfreeze bond strength.

TO MY FATHER WHO GAVE LOVE AND FATHERHOOD

THEIR IDEAL MEANING

ACKNOWLEDGEMENT

The author wishes to express a special appreciation to his major advisor, Dr. O.B. Andersland, professor of Civil Engineering, for his encouragement, initiative, and aid throughout the author's doctoral studies and for his guidance during the preparation of this thesis. Thanks are also due the other members of the author's doctoral committee: Dr. R.K. Wen, Professor of Civil Engineering; Dr. G.L. Cloud, Professor of Metallurgy, Mechanics, and Materials Science; and Dr. C.O. Horgan, Professor of Metallurgy, Mechanics, and Materials Science. Sincere appreciation is also given to the author's father for his love and support throughout the author's studies.

Thanks are also due the National Science Foundation, Division of Engineering Research, and the Department of Civil and Sanitary Engineering for their financial assistance which made this study possible at Michigan State University. The author also wishes to extend thanks to the University of Technology in Baghdad for financial support.

Special appreciation is also given to Margaret L. Cridge for her love, patience, and encouragement. Appreciation is also extended to the author's close friend, Dr. Saad M. Alhir and his family, for their moral support.

TABLE OF CONTENTS

LIST OF TABLES

LIST OF FIGURES

LIST OF SYMBOLS

a	Rod, pile, or footing radius, (d or B)/2,
a'	Constant (Equation 5.5),
b	Constant (Equation 2.16), or beam width (Equation 2.20),
b'	Constant (Equation 5.5),
c	Constant (Equation 2.16), or soil cohesion,
c_{lt}	Long-term soil cohesion,
d	Rod (or pile) diameter,
d'	Reinforcement depth in a frozen soil beam,
f	Flow value, $(1 + \sin\phi)/(1 - \sin\phi)$,
h	Lug height, or frozen soil beam (cross-section) height,
k	Constant (Equation 2.3),
k'	Constant (Equation 2.6),
m	Exponent (Equation 5.1),
m'	Exponent (Equation 5.3),
n	Strain-hardening parameter, 1/m,
n'	1/m',
p	Confining stress, $(\sigma_1 + \sigma_3)/2$,
p_i	Cavity expansion pressure,
p_o	Overburden (confining) pressure,
q	Maximum shear stress, $(\sigma_1 - \sigma_3)/2$, or lug (or footing) pressure,
q_{co}	"Proof" lug pressure at $\theta = 0^oC$ and $\dot{\delta}_c = 0.0005$ in./min. (Equation 6.4),

$q_{c\theta}$ "Proof" lug pressure at temperature θ and $\dot{\delta}_c$ = 0.0005 in./min. (Equation 6.4),

q_l Lug pressure, P_l/A_l,

q_o Pressure under the first lug in a deformed bar,

q_u Ultimate lug pressure, P_u/A_l,

r Radial dimension in a cylindrical or spherical coordinate system,

r_c Radius of a cylindrical plastic "cavity"

r_e "Cavity" radius at the elastic-plastic boundary,

r_s Radius of a spherical "cavity"

s Footing settlement,

$\dot{\delta}^c$ Creep settlement rate,

t Time,

t_f Time to failure,

t_o Time parameter (Equation 2.1),

t^* Soil dependent parameter (Equation 2.1), $\exp(\sigma_o/\sigma_i)$

u Vertical soil displacement at distance r,

u_a Soil displacement at $r=a$,

u_i "Cavity" expansion displacement,

v Creep deflection at the center of a frozen soil beam,

$\dot{v}$ Deflection rate at the beam center,

v_s Sand volume fraction,

x Horizontal coordinate,

z Vertical coordinate, or lug position relative to the reaction plate,

z_1 Neutral axis position in a frozen soil beam,

A Constant (Equation 2.7),

A_l Lug area,

A_r Rod area,

B Footing Width, or equivalent footing width (= d + 2h),

D Sample diameter,

D' Footing embeddment depth,

E Soil modulus of elasticity,

F_b Bond resisting force in tension zone,

F_c Soil resistance in compression zone,

F_t Resultant force in tension zone, ($F_b + T_s$),

H Sample height,

L Bond development length (embedded portion of rod in frozen sample or beam),

L' Constant (Equation 2.9), U/R', ^oK,

L_c Length of a standard chord,

L_r Length of "roughness" line,

L_t Total length of standard chords,

P Pull-out load,

$\dot{P}$ Loading rate,

P_c "Proof" load for any lug height, at $\dot{\delta}_c$ = 0.0005 in./min. (Figure 5.4),

$\dot{P}_c$ Arbitrary loading rate, 1 lb./min. (Equation 5.1),

P_{co} "Proof" load at $\theta = 0^oC$ and $\dot{\delta}_c$ = 0.0005 in./min. (Figure 6.23),

$P_{c\theta}$ "Proof" load at temperature θ and $\dot{\delta}_c$ = 0.0005 in./min. (Figure 6.23),

P^c Load from constant load (creep) tests,

P_{iy} "Initial yield" load for deformed rods,

P_l Lug load,

P_{lt} Long-term lug load,

P_r Residual load for plain rods,

P_u Ultimate load,

$P_{\dot{\delta}}$ Load from constant $\dot{\delta}$,

R Radius of beam curvature,

R' Universal gas constant,

$SP(max)$, $SP(min)$ Maximum and minimum aspirity heights observed on the profilometer,

$SR(max)$, $SR(min)$ Maximum and minimum aspirity heights as observed on the recorder strip chart,

T Temperature (^{o}C or ^{o}K),

T_s Soil resistance in tension zone

U Apparent activation energy,

V_s Displaced volume of soil under the footing,

V_u Displaced volume of an expanding "cavity"

α Wedging angle under the footing,

ϕ Angle of internal friction,

ϕ_{lt} Long-term angle of internal friction,

ε Strain,

ε^c Creep strain,

ε_c Compression strain at the beam outer fiber,

ε_f Failure strain,

ε_i "Psuedo" instantaneous strain,

$\varepsilon_{k'}$ Instantaneous plastic strain,

ε_r Strain at the reinforcement level,

ε_o Instantaneous strain,

$\dot{\varepsilon}$ Strain rate,

$\dot{\varepsilon}^c$ Creep strain rate,

$\dot{\varepsilon}_c$ Arbitrary strain rate

ε_1 Major principal strain rate,

λ Constant (Equation 2.3), or ratio (D-d)/2h,

η Ratio 10 s/B (Equation 2.18), or ratio A_1/A_r,

κ Constant (Equation 2.17),

ω Constant (Equation 2.4),

μ Constant (Equation 2.2),

ρ Roughness factor,

γ Soil shear strain, du/dr,

$\dot{\gamma}$ Shear strain rate,

$\dot{\gamma}$ Arbitrary shear strain rate,

θ Absolute value of temperature below freezing,

θ Tangential coordinate,

θ_o Reference temperature, 1^oC,

σ Stress,

σ^c Soil compressive strength,

σ_{co} Uniaxial compressive strength of soil at 0^oC, and arbitrary strain rate $\dot{\varepsilon}_c$,

$\sigma_{cu\theta}$ Uniaxial compressive strength at temperature θ, and arbitrary strain rate $\dot{\varepsilon}_c$,

σ_f Long-term, or failure, soil strength,

$\sigma_{k'}$ Compression stress corresponding to $\varepsilon_{k'}$,

σ_i Instantaneous strength,

σ_o Soil dependent parameter (Equation 2.1),

σ^t Soil tensile strength,

σ_1, σ_3 Major and minor principle stresses,

τ Bond (or shear) stress,

τ_c Soil shear strength corresponding to $\dot{\gamma}_c$,

τ_i Ice adhesive strength,

τ_{lt} Long-term bond strength,

τ_r Residual bond strength,

τ_{rf} Frictional component of residual bond,

τ_u Ultimate bond strength,

τ_{uf} Frictional component of ultimate bond,

ξ Reciprocal of viscosity (Equation 2.2),

δ Rod (or pile) displacement relative to the frozen sample,

δ^c Creep displacement,

δ_i "Psuedo" instantaneous rod displacement,

δ_r Rod displacement at rupture (Figure 5.1),

$\dot{\delta}$ Rod displacement rate,

$\dot{\delta}^c$ Creep displacement rate,

$\dot{\delta}_c$ Arbitrary displacement rate,

$\dot{\delta}_n$ Nominal (machine) displacement rate,

1.1 Gr

The

eration

agent, t

their co

work car

tight fr

frozen g

soils di

much mor

generall

temperat

projects

Usu

competit

bearing

a high w

unexpecte

construc

and the

inside a

CHAPTER I

INTRODUCTION

1.1 Ground Freezing:

The principle behind controlled ground freezing is the use of refrigeration to convert in-situ pore water to ice. The ice becomes a bonding agent, fusing together adjacent particles of soil or rock to increase their combined strength and make them impervious. Excavation and other work can then proceed safely inside of, or next to, a strong watertight frozen earth barrier. This frozen soil is analogous to perennially frozen ground in permafrost areas. Artifically and naturally frozen soils differ from unfrozen soils in that their mechanical behavior is much more time and temperature dependent. The strength of frozen soils generally decrease with time (due to creep) and increase with colder temperatures. Thus, temporary ground freezing can be used on construction projects.

Usually, one of the following conditions makes ground freezing more competitive than other methods (Sanger and Sayles, 1978): a water-bearing stratum is so deep that grouting is impractical; the lowering of a high water table by pumping may damage adjacent structures; a sudden unexpected flow of water into a tunnel or shaft has occurred during construction and a watertight barrier is needed; permafrost is present and the ground must remain frozen; a clear space (no bracing) is required inside a cofferdam; or the site is for a below-ground cold storage tank

where the
for low-te
Gener
provide te
shafts (Je
in this sc
competitiv
of creatin
clear area
systems (B

1.2 Groun
Previ
that the t
compressiv
frozen soi
because of
related to
regions is
the pipelir
soil adjace
In som
soil, the f
beam under
necessary t
Steel reinf
frozen cant

where the frozen soil would serve as a watertight retaining structure for low-temperature liquids.

Generally, controlled ground freezing has been profitably used to provide temporary support for large open excavations, tunnels, and mine-shafts (Jessberger, 1980; Klein and Jessberger, 1978). Recent improvements in this science and its refrigeration techniques have made it a competitive construction alternative. Ground freezing has the advantage of creating no smoke, vibration, shock or undue noise. It also provides clear areas within the excavation free of bracing and earth support systems (Braun, et al., 1979).

1.2 Ground Reinforcement:

Previous work (Bragg and Andersland, 1980; Eckardt, 1982) has shown that the tensile strength of sand-ice material is about one-fifth of its compressive strength, particularly at high strain rates. Therefore, a frozen soil mass (beam) subjected to an external bending moment may fail because of a weakness in tensile strength. One special application, related to natural gas pipeline construction in discontinuous permafrost regions is shown in Figure 1.1 (a and b). Operating temperatures for the pipeline would be in the range of $-8^{\circ}C$ to $-12^{\circ}C$, thus granular bedding soil adjacent to the pipeline would remain continuously frozen.

In some areas where ice lenses may form in the underlying unfrozen soil, the frozen sand backfill behavior can be simulated by a simple beam under a uniform load (Figure 1.1 c). In this case, it would be necessary to use steel reinforcement in zones of tensile stresses. Steel reinforcement would also be needed in other cases such as the frozen cantilevered retaining wall shown in Figure 1.2 (a). Without

reinforce
compressi
vertical
and they
section.
reinforce
frost (Fi
be transf

Use
pipe piles
successful
Luscher, 1
embedded i
pull-out c

1.3 Scope

Time
the struct
longer fol
and strain
temperatur
analysis a
and analyse
ice materi
frozen soil
studies are
with load t

reinforcement the frozen soil structural system would be limited to compressive stresses associated with a curved or circular arch wall. Vertical H-beams, could be easily installed as shown in Figure 1.2 (a), and they would permit a frozen soil wall to be designed as a cantilevered section. The space between H-piles could be designed as short non-reinforced frozen soil beams. Steel piles are often installed in permafrost (Figure 1.2 b) so that large (compressive or pull-out) loads can be transferred to the soil at a proper depth.

Use of corrugations can significantly improve the load capacity of pipe piles in frozen granular soils (Figure 1.2 c). This technique was successfully used on the trans-Alaska pipeline project (Thomas and Luscher, 1980). In other cases, power-installed screw anchors deeply embedded in warm permafrost (Figure 1.2 d), were used to provide a large pull-out capacity (Johnston and Ladanyi, 1974) for power line anchors.

1.3 Scope of the Investigation:

Time and temperature dependence of frozen soil behavior means that the structural analysis for a frozen earth ground support system would no longer follow conventional analytic procedures. The geometry, stresses, and strains at any point within the structure all vary with time and temperature. In general, a non-linear viscoelastic-plastic finite element analysis appears to be the future analytic method most effective for design and analyses. These analytic methods require information on the sand-ice material properties, bond adfreeze strength and creep behavior at the frozen soil/reinforcement bar interface. Beam tests and analytical studies are part of another project. This thesis is concerned primarily with load transfer at the interface between frozen sand and the model

structura

Bond

force bet

includes

action be

bars deper

primarily

This

friction,

roughness

tests incl

size, lug

diameter),

Initi

placement

pull-out l

of frozen

larger pul

creased th

comparison

based on c

structural member.

Bond at the interface can be described as the shearing stress or force between the reinforcement member and surrounding soil. Bond includes three components: ice adhesion; friction; and mechanical interaction between frozen soil and the bar surface roughness. Bond of plain bars depends primarily on the first two components. Deformed bars depend primarily on mechanical interlocking for bond properties.

This experimental study involved measurement of ice adhesion, sand friction, and mechanical interaction between frozen sand and surface roughness of steel bars. Test variables affecting results of pull-out tests included: temperature, bar displacement rate, loading rate, bar size, lug size and shape, lug position, sample dimensions (height and diameter), water impurities, steel surface type, and sand concentration.

Initially, adhesion of ice to the steel bar prevents slip. As displacement increased friction and mechanical interaction contributed to the pull-out load. When a single lug was added to the bar, bearing action of frozen sand on the lug restrained bar movement giving rise to much larger pull-out loads. Colder temperatures and high loading rates increased the pull-out load. Considering lug bearing on frozen sand, comparisons were made between observed and predicted pull-out loads based on cavity expansion theory.

Ground surface
Gas pipeline

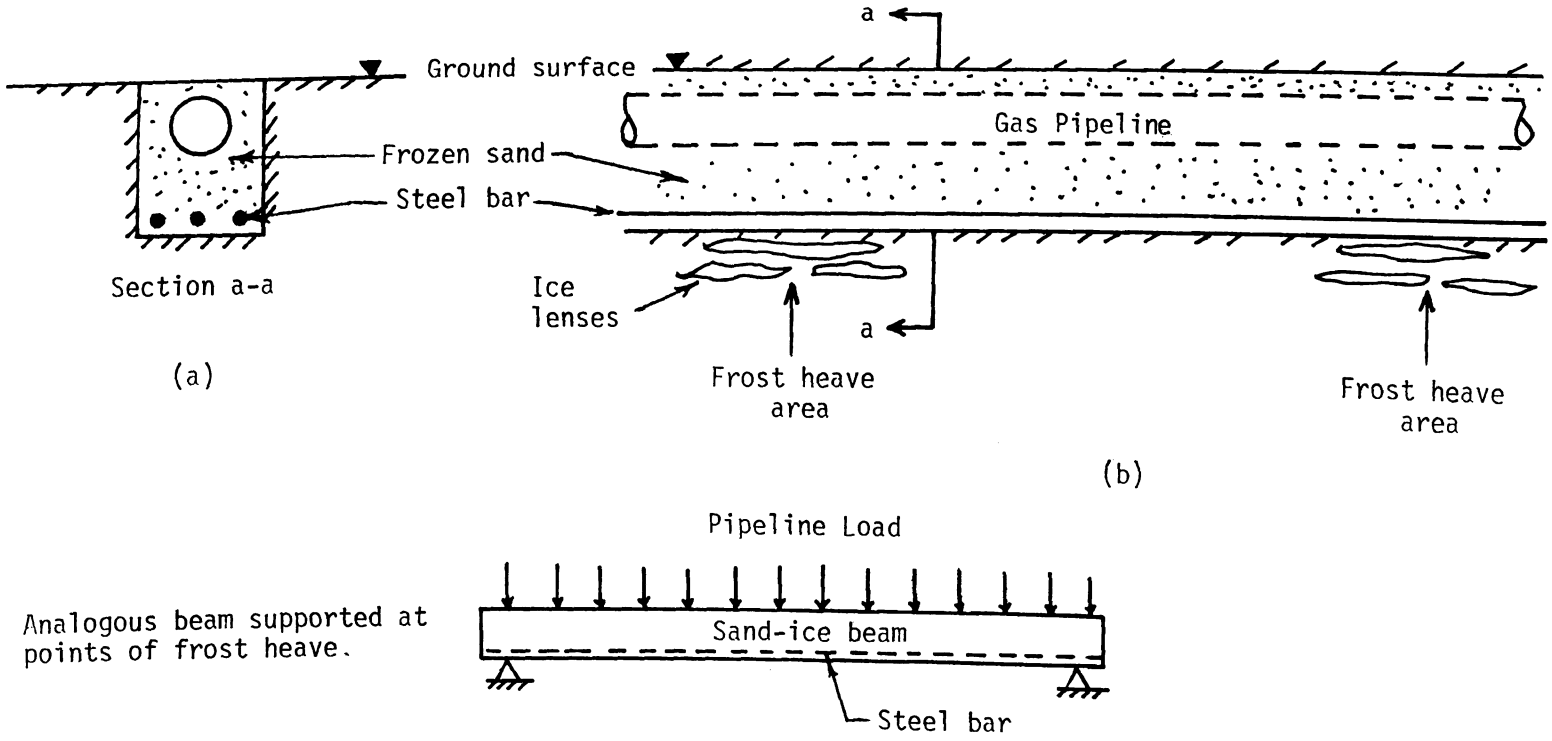

Figure 1.1: Frozen sand backfill with steel bars simulating a reinforced simple beam for partial support of a pipeline in areas of differential frost heave action.

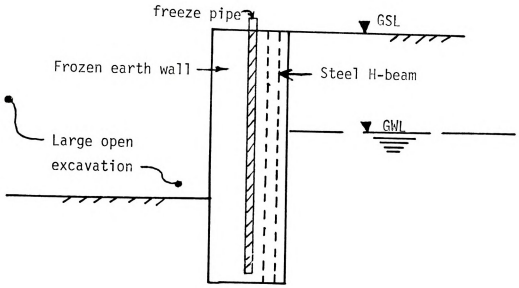

(a) Cantilevered frozen earth wall with H-beam reinforcement

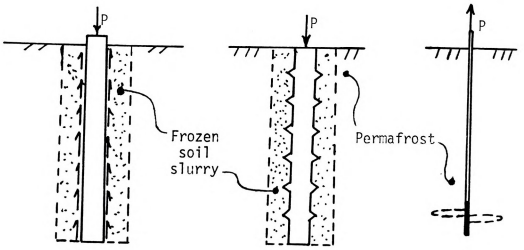

Figure 1.2: Ground Reinforcement

2.1

compl
the T
point
postu
consi
gators
Hosler
unfroz

I
to at
termin
(Jelli
1960 a;
experim
steel,
roughne
strengt
This fi
steel i

CHAPTER II

REVIEW OF LITERATURE

2.1 Ice Adhesion:

Studies on the adhesive properties of ice normally deal with complex physico-chemical phenomenon. There are numerous papers in the literature which report on ice studies based on a fundamental viewpoint. The existence of a liquid-like layer on the ice surface was postulated by Faraday (1859; 1860). This concept has since undergone considerable attention. Experiments carried out by several investigators (Nakaya and Matsumoto, 1953; Hori, 1956; Jensen, 1956; and Hosler et al., 1957) offer strong evidence for the existence of an unfrozen transition liquid film on the ice surface.

It is currently agreed that liquid-like water exists on ice down to at least $-25^{\circ}C$. However, it has been difficult to precisely determine the nature, and properties of this unfrozen water (Jellinek, 1967; Barnes et al., 1971). Jellinek (1957 a; 1957 b; 1960 a; 1960 b; 1960 c; 1970) carried out tensile and shear adhesion experiments on ice frozen to various surfaces including stainless steel, polystyrene, lucite, and fused quartz of varying surface roughness. These results, summarized in Figure 2.1, show the adhesive strength of ice to various materials as a function of temperature. This figure indicates that the adhesive strength of ice to stainless steel increases linearly with decreasing temperature until it becomes

larger than the cohesive strength of ice.

Cohesive type breaks (i.e. within the ice crystals) were observed only in the tensile experiments. Adhesive type breaks (i.e. at the interface between the ice and solid) were observed in the shear experiments. The transition from adhesion to cohesion appears to occur at about -14°C. These results are very similar to those reported by Hunsaker, et al. (1940) on the adhesion of ice to brass (Figure 2.1). The transition temperature in the latter case was close to -12°C.

The adhesive shear strength was also strongly dependent on surface finish, with strength decreasing significantly with decreasing roughness. This is also shown in Figure 2.1, where the surface of the polystyrene plate was much "smoother" than the stainless steel surface. The adhesive strength obtained from tensile experiments (Jellinek, 1957 b) was observed to be about fifteen times greater than that obtained from shear experiments (Figure 2.2).

To explain these results, Jellinek (1957 b) proposed that a continuous liquid-like transition layer exists between the ice and the material. For shear experiments, the adhesive strength was a function of the interfacial strength, and consisted of a viscous contribution from this thin film, as well as contribution due to surface roughness. For the tensile adhesion experiments, the measured strength was controlled by the ice cohesion as shown by the nature of the observed breaks (mostly cohesive). Jellinek proposed that the ice/solid interfacial strength was increased in the tensile mode due to the reinforcing effect of surface "tension" at the perimeter of the

inter

It

unfro

proper

induce

to dis

analys

been c

(1971)

sisten

Unfort

mechan

experi

uniform

of the

caused

(1957 t

consis

2.2 Me

Mec

Soviet

are a f

boundar

of unfr

Anders

interfacial transitional water.

If the two-dimensional liquid model for absorbed water in unfrozen soil were to be adopted (Martin, 1960), then these adhesive properties may be readily explained: while it was relatively easy to induce motions laterally parallel to the surface, it was very difficult to displace the absorbed water normal to the surface. Other tests and analyses related to the nature of the unfrozen water film in ice have been carried out. These are summarized by Jellinek (1967) and Barnes, et al. (1971). Generally, the results from these investigations are consistent with the concept of a liquid-like transitional film in ice. Unfortunately there are very few available data on this basic mechanical property of ice and there is a lot of scatter in the experimental results because of difficulty with control of the uniformity of the ice structure. Further, the extreme sensitivity of the interfaces to any small impurities, such as solutes or gases, caused poor reproducibility of the experimental results. Jellinek (1957 b) duplicated each data point 12 times to obtain the reasonably consistent variation shown in Figure 2.1.

2.2 Mechanical Properties of Frozen Soil:

Mechanical properties of frozen soils have been studied in the Soviet Union as early as 1920 (Tsytovich, 1975). Most frozen soils are a four-phase material; containing solid particles, ice, gas, and boundary water in equillibrium with ice (Vyalov, 1965). The amount of unfrozen water in frozen soil depends on the soil type (Dillon and Andersland, 1966), temperature (Nerseova and Tsytovich, 1963),

grain-to-grain contact pressure (Tsytovich, 1975), and hydrostatic pressure (Chamberlain, et al., 1972). In frozen sands nearly all water is frozen at 0°C under atmospheric pressure, as reported by Nerseova and Tsytovich (1963) and Dillon and Andersland (1966).

The mechanical properties of frozen soils are dependent on many factors including time, temperature, soil type, frozen and unfrozen water contents, ice content, etc. Owing to the varying nature of soils and experimental conditions, it is difficult to compare or correlate the data obtained by different authors. However, one can compare the results obtained for materials of the same type (such as quartz sands) tested under similar conditions.

The strength of frozen soils may take on different meanings depending on the engineering problem. It includes the concept of rupture and that of excessive deformation (Andersland, et al., 1978). Pressure melting of ice at points of contact with soil particles contributes to plastic deformation of the pore ice and readjustment in particle arrangement. This mechanism appears to be responsible for creep of frozen soil under constant stress and temperature (Vyalov, 1965; Andersland, et al., 1978). The increase in deformation with time, under constant stress and temperature, is represented by a typical creep curve in Figure 2.3 (a). After an initial strain ε_o (obtained immediately upon loading), the creep rate decreases over the primary stage, remains approximately constant during the secondary stage, and increases over the tertiary stage until terminated by rupture. Andersland (1963) and Vyalov (1963) attribute this creep behavior mainly

to the

remain

a heal

(i.e.

T

partic

cement

(Tysto

1965),

streng

theory

an ang

dependi

that fi

term s

Sayles

Vyalov

represe

σ_f

where f

t_f is f

$(\sigma_1-\sigma_3)$

t* equa

to the change in soil structure, otherwise, the creep rate would have remained constant. Refreezing of liquid water is also considered to be a healing mechanism which contributes to the time-hardening process (i.e. decreasing creep rate) over the primary stage, Figure 2.3 (b).

The strength of frozen soil develops from interparticle friction, particle interlocking, and cohesion. The latter is related to ice cementing of soil particles and from the shear strength of ice (Tystovich, 1958; Vyalov, 1965; Sayles, 1968). Tests by Vyalov (1959, 1965), Tsytovich (1966), and Sayles (1973) have shown that the shear strength of frozen soil can be described, using the Mohr-Coulomb failure theory, by a normal stress on the failure surface and two parameters; an angle of internal friction and cohesion. Time and temperature dependence is governed primarily by the cohesion. It is recognized that frozen soil has a high instantaneous strength and a smaller long-term strength. Test results (Figure 2.4) on Ottawa sand at -3.85°C by Sayles (1973) show a reasonable agreement with Vyalov's long-term strength. Vyalov (1959, 1963) suggested that the variation of strength can be represented by:

$$\sigma_f = \frac{\sigma_o}{\ln[(t_f + t^*)/t_o]} \simeq \frac{\sigma_o}{\ln(t_f/t_o)} \qquad (2.1)$$

where the parameters σ_o and t_o depend on soil type and temperature, t_f is the time to failure, σ_f is the long-term strength and equals $(\sigma_1-\sigma_3)$ as modified by Sayles (1973) to allow for triaxial conditions, t^* equals exp (σ_o/σ_i) and σ_i is the instantaneous strength.

may b

where

behav

stren

tinuo

idea

time,

that

term

of the

pointe

strain

would

it bec

follow

$$\frac{d}{d}$$

where

modifi

frozen

by Say

$$\varepsilon =$$

where

For long-term strengths Vyalov (1963) stated that the quantity t* may be neglected. This appears to be applicable to frozen soils where either primary or secondary creep dominates the deformation behavior. Equation 2.1 with t_f equal to infinity results in a long-term strength equal to zero, which is not consistent with the idea of continuous strength at some finite time. Vyalov (1963) stated that the idea is purely conventional, but in practice, after some long period of time, the additional strength reduction is so insignificant and so slow that the reduction can be neglected in engineering calculations. Long-term strengths reported by Vyalov (1965) ranged from 18 to 37 percent of the instantaneous cohesion for a frozen sandy silt. Vyalov (1963) pointed out that with a stress level below the long-term strength the strain rate would not change to the stationary (or secondary) stage, but would remain in the primary stage where it continues to decrease until it becomes zero. If $\sigma = \sigma_f$, then the rate goes to zero, according to the following equation:

$$\frac{d\varepsilon}{dt} = \dot{\varepsilon} = \xi\ (\sigma - \sigma_f)^{\mu} \qquad (2.2)$$

where $\mu > 1$ and ξ is the reciprocal of viscosity. Equation 2.2 is a modified version of the primary creep model Vyalov (1965) has proposed for frozen soils and which has been successfuly applied to various frozen soils by Sayles (1968, 1974) and others. In this model, the strain is expressed as:

$$\varepsilon = \varepsilon(t) = \left(\frac{\sigma t^{\lambda}}{\omega(\theta + \theta_0)^{k}} \right)^{1/m} \qquad (2.3)$$

where θ equals -T, θ_0 is a reference temperature, usually 1°C, and

u, t

ε ma

Note
thus
hard
from

(197
One

wher
proc
sele
the

where
Plast
(1972
inter
10 pe
time
Equat

ω, k, λ, m are soil parameters.

By differentiating Equation 2.3 with respect to time, the strain rate $\dot{\varepsilon}$ may be obtained:

$$\dot{\varepsilon} = \frac{\lambda}{m} \left(\frac{\sigma}{\omega(\theta + \theta_o)^k}\right)^{1/m} t^{(\lambda-m)/m} \qquad (2.4)$$

Note that the strain rate $\dot{\varepsilon}$ decreases continuously with time, for $\lambda < m$, thus confirming that Equation 2.3 represents the primary (strain and time hardening) creep model. The parameters in this equation may be obtained from a series of log-log curve fits based on experimental data.

Secondary creep models for frozen soils have been proposed by Ladanyi (1972) based on work in metals by Hult (1966), Odqvist (1966) and others. One model is based on a power law which may be written as:

$$\frac{d\varepsilon^c}{dt} = \dot{\varepsilon}^c = \dot{\varepsilon}_c \, (\sigma/\sigma_{cu\theta})^n \qquad (2.5)$$

where $\sigma_{cu\theta}$ and n are creep parameters, both dependent on temperature. The proof stress $\sigma_{cu\theta}$ (Hult, 1966) is the uniaxial stress for an arbitrarily selected creep rate $\dot{\varepsilon}_c$. Then, for a given material at a constant temperature, the total strain $\varepsilon(t)$ is:

$$\varepsilon(t) = \frac{\sigma}{E} + \varepsilon_{k'} \, (\sigma/\sigma_{k'})^{k'} + t \, \dot{\varepsilon}_c \, (\sigma/\sigma_c)^n \qquad (2.6)$$

where the first two terms represent the pseudo-instantaneous elastic and plastic strains respectively (ε_0 in Figure 2.3 a) as proposed by Ladanyi (1972). Vyalov (1959) provided experimental data showing that for time intervals greater than 24 hours these two terms together become less than 10 percent of the total creep strain. For engineering applications where time intervals are greater than one day, use of the third term only in Equation 2.6 gives good approximations of the total strains (Andersland,

et al.,

reaction

the temp

Akili, 1

1970; Ho

Eyring (

by Mitch

marized

(of mole

strained

riers se

flow uni

of suffi

energy")

perature

becomes

Using Equ

been done

where U i

stant, an

and U/R'

et al., 1978).

Several authors have attempted to apply the theory of absolute reaction rates, commonly known as the rate process theory, to explain the temperature-dependence of strength for frozen soils (Andersland and Akili, 1967; Goughnour and Andersland, 1968; Andersland and AlNouri, 1970; Hooke, et al., 1972). The theory was originally formulated by Eyring (1936) and later by Glasstone, et al. (1941). It was also applied by Mitchell, et al. (1968) and Mitchell (1976) to unfrozen soil, and summarized by Andersland and Douglas (1970).

The rate process theory is based on the assumption that flow units (of molecular size) participating in a deformation process are constrained from movement relative to each other by virtue of energy barriers separating adjacent equilibrium positions. The displacement of flow units to new positions requires their activation through acquisition of sufficient energy (thermal or mechanical called "the free activation energy") to overcome an energy barrier. In analytical terms, the temperature dependence of the creep rate $\dot{\varepsilon}$, when other factors are constant, becomes (Ladanyi, 1972):

$$\dot{\varepsilon} = A \exp(-U/R' T) \tag{2.7}$$

Using Equation 2.7 together with the power law (Equation 2.5), as has been done for ice (Glen, 1955; Gold, 1970), one can write:

$$\dot{\varepsilon} = \dot{\varepsilon} (\sigma/\sigma_c)^n = A \exp(-U/R' T) \tag{2.8}$$

where U is the apparent activation energy, R' is the universal gas constant, and the other parameters are as defined before. The constants A and U/R' can be found for different temperatures by plotting the

natur

of th

manip

σ_{ce}

where

stress

appli

to cre

to Hoe

the ac

corres

the th

but in

frozen

from o

be dis

Dougla

A

for a

In this

strain

absorbe

natural logarithm of the observed creep rates against the reciprocal of the absolute temperature. Finally, with some mathematical manipulations Ladanyi (1972) derived the following relationship:

$$\sigma_{c\theta} = \sigma_{co} \exp(L'\sigma / 273n(273-\theta)) \simeq \sigma_{co} \exp(L'\sigma / (273)^2 n) \qquad (2.9)$$

where $L' = U/R'$ with units of temperature, $\theta = (273-T)$ °k, σ_{co} = proof stress at -273°k.

While the rate process theory has fundamental significance when applied to reaction rates in pure chemical systems, its application to creep of frozen soils is primarily empirical in nature. According to Hoekstra (1969), Andersland and Douglas (1970), and Ladanyi (1972), the activation energy calculated from Equation 2.7 does not necessarily correspond to its physical definition, since in frozen soil not only the thermal energy of the moving molecules changes with temperature but in addition a gradual phase change also occurs. Moreover, in frozen soil a mechanically activated process (moving a soil particle from one equillibrium position to the next) is involved, which should be distinguished from a thermally activated process (Andersland and Douglas, 1970).

A more sophisticated "tertiary creep" model which does account for accelerating creep was proposed by Goughnour and Andersland (1968). In this model, the plastic strain rate is composed of the sum of a strain hardening term and a softening term which is dependent on the absorbed strain energy. Since integration of their (strain-based)

empi
empi
mode
(196
stre
stre
rate
sligh
sand,
obser
(due
Dilat
betwe
effec

in Fi
been
1968;
Alkir
Bragg
1980).
of inc
temper

Nouri,

empirical model was quite difficult, the two authors proposed a separate empirical relation in terms of time. Excellent correlations between their model and data on Ottawa sand was reported. Goughnour and Andersland (1968) studied the effect of sand concentration on the frozen soil strength. They obtained a bilinear relationship between the peak strength and sand concentration at different temperatures and strain rates (Figure 2.5). For low volume fractions of sand there was a slight linear increase in strength. When a critical volume fraction of sand, about 42 percent, was reached a rapid increase in strength was observed. At this point friction between sand particles and dilatancy (due to particle interlocking) began to contribute to the shear strength. Dilatancy must act against cohesion of the ice matrix and the adhesion between sand grains and ice, thus creating an effect analogous to higher effective stresses (Goughnour and Andersland, 1968).

The effect of strain rate and temperature on strength is also shown in Figure 2.5. These two factors, strain rate and temperature, have been studied by several investigators (Vyalov, 1959; Sayles, 1966, 1968; Sayles and Epanchin, 1966,; Goughnour and Andersland, 1968; Alkire and Andersland, 1973; Ladanyi and Arteau, 1978; Eckardt, 1979; Bragg and Andersland, 1980; Parameswaran, 1980; Parameswaran and Jones, 1980). Their experimental results showed that there was a general trend of increasing strength upon increasing strain rate and decreasing temperature below 0°C.

Other factors such as confining pressure (Andersland and Al-Nouri, 1970; Chamberlain, et al., 1972; Alkire and Andersland, 1973)

and sample size (Bragg and Andersland, 1980) on the strength of frozen soils have also been investigated. A summary of the results for strength testing by various investigators at low confining stresses is shown in Figure 2.6. Strength increases almost linearly with confining pressure. Note that the apparent friction angle for frozen sands is similar to that for unfrozen sand; however, a sigificant apparent cohesion exists in the frozen sand.

Chamberlain, et al. (1972) reported that at high confining stresses (greater than 10 kips/sq.in.) the shear strength begins to decrease (region II in Figure 2.7). The authors attributed the decrease in strength to the suppression of dilatancy due to a reduction in particle size caused by crushing under high pressures. Pressure melting of ice in frozen soil is also expected when hydrostatic or deviatoric stresses are applied. It develops from stress concentrations on the ice component between soil particles and from hyrostatic pressure on ice. Since global pressure melting occurs at a pressure of 15 kips/sq.in. and more (region III in Figure 2.7), the soil is analytically similar to unfrozen soil where friction becomes the major component. Since the strength measured in region III was relatively low, the observed quantity must be an undrained shear strength at effective stresses much less than the total stresses.

Strength tests on frozen soils are generally of two types: the constant strain rate and constant stress (creep) tests. Odqvist (1966) presents a theoretical discussion of the relationship between

these two test types. Since engineering strain (in the compression test) is nearly equal to the true strain for small strains, and if primary creep may be neglected, the peak stress (at failure) determined from constant strain rate tests may be related to the creep parameters determined from creep tests as shown below:

$$\dot{\varepsilon} = \dot{\varepsilon}_c (\sigma_f / \sigma_c)^n \qquad (2.10)$$

where σ_f is the failure stress, σ_c and n are the creep parameters defined in Equation 2.6, and $\dot{\varepsilon}$ is the applied strain rate. This implies that the two parameters σ_c and n should be equivalent for constant strain rate and constant stress creep tests. Some authors (Goughnour, 1967; Bragg, 1980) experimentally found that the constant strain rate strengths of frozen sands were considerably higher than the corresponding strengths in creep tests. Goughnour (1967) attributes this disagreement to the possibility that higher plastic strain energies would be consumed in strain-controlled (constant strain rate) tests than would be consumed in stress-controlled (creep) tests, considering the stress-strain curve. Other experimental data on polycrystalline ice at -7°C (Hawkes and Mellor, 1972) indicated that no significant difference existed between the results of constant stress creep tests and constant strain rate tests at low strain rates.

2.3 Pile Tests in Ice:

As a result of ice adhesion a floating ice cover can develop substantial vertical loads on a structure to which it is frozen, due to changes in water level. In the analysis of vertical ice loads on

piles, Lofquist (1951) assumed that ice has a viscoelastic behavior with deformation proportional to the cube root of time. A means for predicting vertical load was given, but no direct field or laboratory measurements were available to confirm the prediction. An almost similar analysis was made by Sanger (1969), giving average values for the ultimate adfreeze bond strength for saturated fine sands, saturated silts with ice lenses, and ice. Sanger cautioned that the strength values should be checked by field tests for final design.

Stehle (1970) has reported that short-term tangential adfreeze bond strengths of about 290 psi were observed for wooden piles (2.75-in. diameter) in ice. The bond stength varied linearly with pile settlement rate on a log-log scale suggesting a power law similar to that in Equation 2.5. Measurement of vertical ice loads developed on instrumented piles have also been reported by Doud (1978). A maximum load of 18 kips on a 14 in. diameter steel pile was developed by a 13.7-in. thick ice cover.

Frederking (1979) carried out laboratory tests to study the effect of ice thickness, pile diameter and displacement rate on downdrag loads developed on a vertical wood pile. These model piles, with diameters ranging from 2-in. to 6-in., were used with ice thicknesses from 1 to 8 inches. The pile load was observed to increase with increasing displacement rate. Unit pile load also increased with increasing ice thickness and decreased with increasing pile diameter as shown in Figure 2.8. Observations of the failure process for that test series showed that a combination of flexural and shear behavior was present in all cases. The relative contribution varied with test

cond

shea

Fred

ice

rate

to e

diam

Displ

[10^

inclu

of ac

that

the a

adfre

the d

tests

Preli

adfre

smoot

proba

ice i

the c

conditions, flexure predominating for the thinner ice sheets and shear for the thicker ice. Combining the effects of all test variables, Frederking (1979) formulated a composite empirical equation for the ice adhesive strength to wooden model piles as a function of displacement rate, ice thickness, and pile diameter.

Parameswaran (1981) conducted constant displacement rate tests to evaluate the adfreeze strength of wood, concrete, (both 3-in. in diameter) and steel H-section (4-in. wide flange) piles in ice at -6°C. Displacement rates ranged between 4×10^{-6} and 4×10^{-3} in./min. (10^{-4} to 10^{-1} mm/min.). The test results, summarized in Figure 2.9, include the three pile types. These curves show an almost linear variation of adfreeze strength with displacement rate leading to the conclusion that a power law, similar to Equation 2.5, can be derived relating the adfreeze strength to the displacement rate. Note that the adfreeze strength of smooth concrete piles in ice was independent of the displacement rate.

To check this behavior Parameswaran (1981) carried out a few tests using a smooth painted steel cylindrical pile in ice. Preliminary results from these tests showed a rate independent of adfreeze strength. For these piles (concrete and painted steel with smooth surfaces) Parameswaran (1981) suggested that the adfreeze strength probably is decided by the first major crack developed at the pile-ice interface. Parameswaran (1981) used his test results to estimate the contribution of ice adhesion to the total adfreeze strength of

va

2.

tw
at
de
mo
no
19
19
in

and
Uni
pos
The
hav
Vya
and
test
adfr
in i
segr
cu.

various piles in frozen sand, as described in the following section.

2.4 Pile Tests in Frozen Soils:

The shearing resistance developed at the pile-soil interface has two components: ice adhesion to the pile; and soil grain friction at the pile-soil interface. End bearing is normally excluded from design considerations because of the greater movement required to mobilize end bearing resistance in comparison with much smaller movements for adfreeze bond failure (Crory, 1963; Nixon and McRoberts, 1976, Nixon, 1978; Phukan and Andersland, 1978; Morgenstern, et al., 1980; Weaver and Morgenstern, 1981 b). This point will be discussed in more detail later.

Although measurements of the adfreeze strength between piles and frozen ground have been taken since 1930, mainly in the Soviet Union, sufficient information is not yet available to make it possible to design for different foundation materials in various soils. The results of early work in the Soviet Union from short-term tests have been given by Tsytovich and Sumgin (1959), Tsytovich (1975), and Vyalov (1965). Crory (1963), Crory and Reed (1965), Sanger (1969), and Nixon and McRoberts (1976) have reported the results of pile load tests in the permafrost regions of North America. Most of the available adfreeze strength for piles were obtained from field tests of piles in ice-rich soils (i.e. soils which possess a continuous network of segregated ice, and usually with bulk densities less than 106 lbs./cu. ft., as categorized by Weaver and Morgenstern, 1981 a).

Long-term pile creep tests were conducted in ice-rich frozen soils

by se
data
facto
and i
appli
loadi
facto
steam
gives
of the

V
taking
of ins
holes
diamet
increa

O
of ful
pipe
a diame
pile an
moistur
Figure
that cl

by several investigators. An independent comparison of the published data is difficult because the pile behavior depends on a number of factors, the more important including pile type, type of frozen soil and its temperature, method of installation, and the rate of load application. Vyalov (1959) performed a large number of full-scale loading tests in which he studied the effects of most of the above factors. For timber piles (6-in. diameter) hand-driven into pre-steamed holes, in both silty sandy loam and agrillaceous loam, Vyalov gives the following empirical formula for the temperature dependence of the long-term adfreeze strength, τ_{lt}:

$$\tau_{lt}\ (kg/cm^2) = \sqrt{1.65\ \theta(°C)} - 0.3 \qquad (2.11)$$

Vyalov (1959) also proposed a series of correction factors, taking into account the effect of different soil types and methods of installation. For example, for piles driven into dry-augered holes having a diameter 10 to 40 percent smaller than the pile diameter, he recommended that τ_{lt} values from Equation 2.11 be increased by 30 to 50 percent.

On the other hand, Crory (1963) reports on the results of a series of full scale tests carried out in Alaska on 8-in. (20 cm) diameter pipe piles installed in frozen silty sand in dry-augered holes having a diameter about 2-in. greater than the pile. The gap between the pile and the soil was filled with a silt-water slurry (40 to 80 percent moisture content). The adfreeze strength of this slurry is shown in Figure 2.10 as a function of temperature. Crory (1963) also reported that clay-water slurries have adfreeze strengths which approach that

of f
silt
In c
that
stre

by J
at t
site
about
clay
incre
year,
secon
pile
diffe
all t
by Jo
defor
plast
in Fi

A
shear
homoge
length

of ice, and have an ultimate strength of approximately half that of silt. The behavior of a frozen dry sand backfill was like thawed sand. In contrast, Crory reports that low-temperature pile tests disclose that a well-graded sand slurry, vibrated in place, has an adfreeze strength 50 percent higher than its silt counterpart at the same temperature.

Long-term creep tests were also carried out on grouted rod anchors by Johnston and Ladanyi (1972). A power auger (6-in. diameter) was used at the Thompson site, whereas a hammer drill was used at the Gillam site to make holes for the anchors. The grouted lengths ranged from about 8.5 ft. to 10.5 ft. In both sites, the soil was ice-rich varved clay and silt at temperatures from $-0.11^{\circ}C$ to $-.28^{\circ}C$. Step-wise increasing loads, applied for time periods from 1 hour to more than a year, permitted observation of all three stages of creep (i.e. primary, secondary, and tertiary). The piles failed by slip along the soil-pile interface. The slip failure occurred at different times under different loads, but the total displacement was of the same order for all tests. A theoretical analysis of the test results was also made by Johnston and Ladanyi (1972). In their analysis, the frozen ground deformation around a pile shaft was idealized as shearing of a visco-plastic half space medium around an elastic cylindrical rod as shown in Figure 2.11, thus following the work of Nadai (1963).

Also, the analysis involved several assumptions including uniform shear stress distribution over the rod (pile) length, weightless and homogeneous soil, and a constant temperature over the embedded rod length. Using a cylindrical coordinate system (r, θ, and z), and

assum

strai

due t

under

of a

define

$\dot{\gamma}$ as (

(1972)

$\dot{\gamma}$

in whi

creep

2.11,

then i

gives:

$\dot{u}$

N

before

2.13 s

creep

For a

materia

Johnsto

reduces

$\dot{\gamma}$ =

assuming a vertically loaded pile as shown in Figure 2.11, the strains around the pile in the tangential θ-direction will be zero due to symmetry. Consequently each element of frozen soil deforms under plain strain by simple shear. If u denotes vertical displacement of a particle at radius r, the corresponding shear distortion γ was defined (Nadai, 1963) as (-du/dr), and similarly the shear strain rate $\dot{\gamma}$ as (-d$\dot{u}$/dr). In order to solve the problem, Johnston and Ladanyi (1972) introduced the following stress-strain relationship:

$$\dot{\gamma} = \dot{\gamma}_c(\tau/\tau_c)^n \qquad (2.12)$$

in which τ_c and n are creep parameters determined in a simple shear creep test, and $\dot{\gamma}_c$ is an arbitrary shear strain rate. From Figure 2.11, substituting (-d$\dot{u}$/dr) for $\dot{\gamma}$ and τ_a(a/r) for τ in Equation 2.12, then integrating, and noting that at r=a, $\dot{u}=\dot{u}_a$, and at r=∞, $\dot{u}$=o, gives:

$$\dot{u}_a = \dot{\gamma}_c \; a(\tau_a/\tau_c)^n/(n-1) \qquad (2.13)$$

Note that if there is no slip between the rod and the soil, i.e. before failure, then $\dot{\delta}=\dot{u}_a$, where $\dot{\delta}$ is the rod displacement rate. Equation 2.13 shows how the time-dependent rod displacement is related to average creep properties of frozen soil obtained from a simple shear test. For a general state of stress and a plastic (incompressible) von Mises material subjected to simple shear, under plane strain conditions, Johnston and Ladanyi (1972) showed that the generalized creep equation reduces to:

$$\dot{\gamma} = 3^{(n+1)/2} \dot{\varepsilon}_c \; (\tau/\sigma_{cu\theta})^n \qquad (2.14)$$

where

tests

one f

This

estim

for t

with

same

creep

(in w

creep

the p

the t

in rea

Use of

to-gra

conser

the tw

tests,

b) sug

seconda

these

where the proof stress $\sigma_{cu\theta}$ is obtained from uniaxial compression creep tests at a constant temperature θ. Comparing Equations 2.12 and 2.14, one finds that if $\sigma_{cu\theta}$ is chosen equal to τ_c, then:

$$\dot{\gamma}_c = 3^{(n+1)/2} \dot{\varepsilon}_c \qquad (2.15)$$

This analysis assumes a constant n-value for a particular soil. The estimated long-term adfreeze strength, based on this analysis, computed for the rod anchors at the Thompson and Gillam sites compared well with experimental data (Johnston and Ladanyi, 1972). Following the same analysis, Nixon and McRoberts (1976) proposed a two-term power creep law for adfreeze strength of piles in ice and ice-rich soils (in which secondary creep dominates). The authors used existing creep tests from many different sources to obtain the constants in the power law.

Nixon and McRoberts (1976) and later Nixon (1978) showed that the theoretical predictions provided by the two-term power law were in reasonable agreement with test results from other published data. Use of the same law for dense ice-poor soils (soils for which grain-to-grain contact may influence soil behavior) would be overly conservative, since in such soils primary creep dominates whereas the two-term creep law was based on steady-state (secondary) creep tests, with two deformation mechanisms.

Morgenstern et al. (1980) and Weaver and Morgenstern (1981a and 1981 b) suggest that in ice-poor soils displacement rates would not reach secondary creep under loads normally encountered in the field. Since these loads are probably smaller than the long-term strength of dense

frozen soils, soil creep would stay within the primary stage, region I in Figure 2.3. Therefore, Weaver and Morgenstern (1981 b) used the primary creep law (Equation 2.3) and adopted the same approach as that suggested in Figure 2.12, in order to recommend the following relationship:

$$\delta / at^{b} = 3^{(c+1)/2} \, (\tau / \omega(\theta+1)^{k})^{c} / (c-1) \qquad (2.16)$$

where $b=\lambda/m$, $c=1/m$, k, m, λ, and ω are the soil parameters defined in Equation 2.3. In their analysis, Weaver and Morgenstern (1981 b) assumed constant values for b, c, k, and ω of 0.263, 1.32, 1.0, and 21.0, respectively, based on experimental data available in the literature (Sayles, 1968)for frozen Ottawa sand. Using these values in Equation 2.16, the two authors have suggested a design chart for friction piles in frozen Ottawa sand.

Direct simple shear tests were also conducted on a variety of reconstituted frozen soils and ice (Weaver and Morgenstern, 1981 a) to investigate the load transfer process associated with adfreeze bond to piles. Tests were performed at -1°C for durations up to 45 days to explore ultimate creep rates. These experimental data on frozen soils show how creep rate tends to decrease with increasing soil density except for dirty ice (ice with very low solid concentrations and typical bulk densities between 59.0 and 62.4 lbs./cu. ft.) which displays creep rates slightly higher than those observed for pure ice (Weaver and Morgenstern, 1981 a).

Weaver and Morgenstern (1981 b) later extended procedures developed previously for predicting settlement and adfreeze strength

of pi

that

long-

rough

both

expre

τ

where

a roug

assume

normal

reduce

typica

1.2 b)

A

betwee

the in

concre

an inn

(1.2 m

"frost

increas

increas

(1978 a

piles o

of piles in ice-rich soils to include ice-poor soils. They proposed that the adfreeze strength of a frozen soil, τ, is related to the long-term shear strength, τ_{lt}, by $\tau=\kappa\tau_{lt}$, where κ is primarily a roughness parameter. The long-term shear strength τ_{lt} consists of both frictional, ϕ_{lt}, and cohesive, c_{lt}, components and can be expressed by the Mohr-Coulomb relationship, so that τ becomes:

$$\tau = \kappa(c_{lt} + \sigma \tan \phi_{lt}) \qquad (2.17)$$

where σ is the normal stress on the shear plane and κ is primarily a roughness-dependent parameter. Weaver and Morgenstern (1981 b) assumed that the frictional component may be neglected, since the normal stress is typically less than 14.5 psi. Hence, Equation 2.17 reduces to $\tau=\kappa c_{lt}$. Using published data the authors suggest typical values for κ ranging from o.6 for plain steel piles (Figure 1.2 b) to 1.0 for corrugated pipe piles (Figure 1.2 c).

A systematic laboratory measurement of the adfreeze strength between piles and frozen soils is not available. Laba (1974) measured the instantanuous adfreeze force (frost grip) between frozen sand and concrete under laboratory conditions. Frozen sand was pushed from an inner cylindrical cavity in a concrete block at a rate of 0.0472 in. (1.2 mm) per minute. These results indicate, in general, that "frost grip" decreased rapidly with increasing porosity, that it increased with increasing ice content in the sand and that "frost grip" increased with decreasing temperature. Recently, Parameswaran (1978 a, 1978 b, 1979) conducted laboratory experiments on cylindrical piles of wood, concrete, and steel(cylindrical and H-section)in frozen

Ottawa sand (14 percent moisture content). Each cylindrical pile was 3-in. in diameter. The H-section pile was a wide flange steel H-beam with a 4-in. depth of section and 12-in. in length. Test results indicate that the load dependence for steady-state creep rate of piles in frozen sand agrees with the displacement rate dependence of the adfreeze strengths determined by extrapolation of the results of constant rate tests. In general, maximum adfreeze strength developed with natural B.C. fir, and the minimum with creosoted B.C. fir. Based on a linear variation of adfreeze strength with either the creep or displacement rate on a log-log scale, Parameswaran (1979) deduced a simple power law similar to that suggested by Johnston and Ladanyi (1972).

More recently, Parameswaran (1981) estimated the contribution of ice adhesion to the total adfreeze strength of similar piles in frozen sand. Returning to Figure 2.9, Parameswaran reduced the values for ice adfreeze strength by the ratio of the volume of water present in sand, packed round the pile to a 7.5-in. height, to the volume of water filled to the same height. This reduction factor (0.2377) was used because the ice in a later study (Parameswaran, 1981) was of a different structure from that of the polycrystalline ice normally present in soil pores. Figure 2.12 shows the adfreeze strength of piles in frozen sand (solid lines) and the contribution to this strength by ice present in the sand (dashed lines). Note that the dashed lines are the same as the solid lines in Figure 2.9, but reduced by a factor of 0.2377. If the lines were not reduced

the adfreeze strength for the concrete piles in ice would have been much higher than that in frozen sand at displacement rates below $4.0X10^{-5}$ in./minute.

2.5 Circular Footing in Frozen Soils:

In permafrost regions deep circular footings and piles are the most frequently used foundation types (Ladanyi and Paquin, 1978). Loads applied to deep foundations or piles are partly carried by lateral shearing forces and partly by end bearing. The ratio of the two supporting forces depends on a number of factors including soil type, footing shape, method of installation, embeddment ratio, and the footing settlement. The complexity of the observed phenomena sometimes obscures the contribution from the two separate supporting forces and makes any clear comparison with theoretical predictions difficult. Some authors (Nixon and McRoberts, 1976; Nixon, 1978) show theoretically that for ice-rich soils with the creep parameter $1.5<n<3$, the ratio of end bearing to pile shaft load is approximately in the ratio of pile diameter to its length. Therefore, for a 20-ft. long and 1-ft. diameter pile, only 5 percent (1/20) of the total load would be due to end bearing.

A similar theoretical analysis made by Weaver and Morgenstern (1981 b) showed that even for ice-poor Ottawa sand and an 82-ft. long by 8-in. diameter pile the fraction of load supported in end bearing is only 1.1 percent. Note that these analyses are based on creep parameter data from published sources. In the literature several accounts have been made regarding field and laboratory pile load

test

labo

froz

inen

the

fiel

heli

of fr

The a

depth

sure

the d

dicte

(Hill

press

1973)

Gibso

was f

with

for va

1975;

predi

tests. However, very few data are available concerning field or laboratory tests on deep footings (including end bearing piles) in frozen soil. Only limited comparisons have been made between experimental data and theoretical predictions due to the complexity of the problem.

To help fill this gap, Johnston and Ladanyi (1974) conducted field tests on deep circular anchor plates in permafrost. Ten single helix screw anchors, Figure 1.2 (d), were power-installed in layers of frozen varved clay and silt with temperatures of $-0.1^{\circ}C$ to $-0.33^{\circ}C$. The anchors ranged in diameter from 8.15 in., and were installed at depths ranging from 8 to 14 ft. Although the observed anchor pressure varied non-linearly with displacement rate on a log-log scale, the data compared reasonably well with the theoretical values predicted by Ladanyi and Johnston (1974) using cavity expansion theory (Hill, 1950). The two authors used creep parameters determined from pressuremeter tests on frozen soil at the site (Ladanyi and Johnston, 1973).

Since the early work on bearing capacity of foundations by Gibson (1950) and Meyerhof (1951), where the cavity expansion model was first mentioned in the literature, the theory has been applied with success to the problem of bearing capacity of deep foundations for various soil types by several authors (Ladanyi, 1963, 1967, 1973, 1975; 1973). In frozen soils, the theory can be used for predicting creep settlements and time-dependent bearing capacity of

deep circular footings (Ladanyi and Johnston, 1974), strip footings (Ladanyi, 1975) and laterally loaded piles (Rowely et al., 1973, 1975). In the latter case, the solution was obtained by analogy with the strip footing case.

According to observations made by Vyalov (1959) on circular flat ended punches in undisturbed frozen silty clay and by Johnston and Ladanyi (1974) on the screw anchors, it appears that in frozen soils the Prandtl-Terzaghi bearing capacity model loses its experimetal justification since the formation of Prandtl type slip surfaces was not observed in those tests. There was, instead, a deformed zone or "cavity" clearly visible above the screw anchor's in the varved soil when the anchors were excavated. Note that the term "cavity" refers to an expanding spherical region which is formed as the circular punch (footing) advances continuously into the soil. As shown in Figure 2.13 (a) the cavity is always preceded and surrounded by a plastic front which may have a spherical shape(under a circular footing) or a cylindrical shape (under a long rectangular footing).

Also note that the penetration of a circular punch deep into the soil produces a state of stress and strain very similar to that resulting from the expansion of a spherical cavity in an elastic half space medium (Hill, 1950). For transformation of a cavity expansion to a deep footing problem, Ladanyi and Johnston (1974) assumed that during penetration of a footing into the soil, a rigid soil cone (circular footing) or wedge (strip footing) is formed at the footing base (Figure 2.13 b) with the angle α close to 45^{o}. Both,

for th

the pr

cohesi

indica

total

the au

settle

$V_s=V_u$

soil i

pressi

(for a

criter

(1974)

settlem

$s<$

where r

pressur

(for $\phi>$

$c=$

where c

f is th

Us

penetra

strengt

for the cone and the wedge, statical considerations at failure give the pressure q as a function of the cavity expansion pressure P_i, cohesion c, and the friction angle ϕ. Ladanyi and Johnston (1974) indicated that in frozen soils the ultimate load is reached at a total settlement close to 10 percent of the punch diameter B. Also, the authors transformed cavity-expansion displacements u_i into footing settlements s, by equalizing the displaced volumes in both cases, i.e. $V_s=V_u$ in Figure 2.13 (c). This assumption implies that the frozen soil inside the "cavity" or the cone is perfectly plastic (incompressible). Using the generalized stress vs. strain rate relationship (for an incompressible von Mises material), the Mohr-Coulomb failure criterion, boundary and equillibrium conditions, Johnston and Ladanyi (1974) deduced the following relationship between the footing creep settlement rate $\dot{s}^c$ and the applied pressure q:

$$\dot{s}^c = (\dot{\varepsilon}_c/2\sigma_{cu\theta}^n)(3/2n)^n(q-p_o-\eta c)^n \qquad (2.18)$$

where $\eta=10s/B$ if $s<0.10B$, and $\eta=1$ if $s>0.10B$, p_o is the confining pressure, and c is the triaxial test cohesion and is given by (for $\phi>0$):

$$c=\sigma_{cu\theta}(\varepsilon_f/\dot{\varepsilon}_c t_f)/2f^{\frac{1}{2}} \qquad (2.19)$$

where ε_f is the strain at failure, t_f is the time to failure, and f is the flow value and equals $(1+\sin\phi)/(1-\sin\phi)$.

Using the same theory, Ladanyi (1976) has shown that the static penetration test can also be used in frozen soils to determine their strength parameters. A series of quasi-static and static (or

incre
site
study
with
tip c
resis
leadi
of pe
with
(1978
soil
(Hoff
that
up to
numer
appea
compa

effect
soils.
availa
Sego,
settle
from C
that w

incremental loading) penetration tests were conducted at a permafrost site near Thompson, Monitoba (T=-0.10°C to -0.33°C). The field study included stress and penetration rate-controlled tests, performed with an electric penetrometer (1.4-in. dia.). The original conical tip of the penetrometer was replaced by a flat disc. The point resistance was plotted versus penetration rate on a log-log scale leading to a general power law relationship for the rate dependence of penetration resistance. The experimental data were in good agreement with the solution obtained from the cavity expansion theory. Nixon (1978) attempted two solutions; the Boussinesq solution for linear soil behavior, and a numerical solution based on Hoff's analogy (Hoff, 1954) to consider the soil non-linearity. Nixon (1978) showed that cavity expansion theory tends to over-predict settlement rates up to a factor of 2 for value of $1<n<3.5$, when compared with the numerical method. For values of $n>3.5$ the linear Boussinesq solution appears to over-predict settlement rates up to a factor of 3, in comparison to the two other methods.

The depth of embeddment of the footing appears to have a similar effect on the settlement and bearing capacity as that in unfrozen soils. Although no theoretical solution of this problem is yet available (Ladanyi, 1981b), experimental data (Vyalov et al. 1973; Sego, 1980) show that the depth of burial reduces the total creep settlement to about one half when the relative depth D'/B increases from 0 to 1.25 (Figure 2.14). On the other hand, Sego (1980) observed that when a punch settles more than about 5 percent of its diameter,

the

dept

buri

1980

1978

of l

sett

succ

load

2.14

test

Ladar

plat

a sa

rate

(Figu

tests

tests

settl

long

mobil

attai

loadi

then

the soil enters into a viscoplastic region and the effect of burial depth becomes much smaller. Under such conditions, no effect of burial depth was observed between D'/B = 0.5 and 3.3 in ice (Sego, 1980) and between D'/B = 5 and 15 in frozen sand (Ladanyi and Paquin, 1978).

Little information is available in the literature on the effect of loading history. Vyalov et al. (1973) presents information on the settlement of 6.3-in. (16 cm) diameter punches, loaded in five successive stages, on blocks of ice in Figure 2.14. In each stage the load was increased and kept constant for 10 days. Data in Figure 2.14 show that a steady-state settlement rate was attained in these tests after about 1 to 2 days. A similar conclusion was reached by Ladanyi and Paquin (1978) when analyzing the results of their deep plate (1.4-in. diameter circular punches) loading tests embedded in a saturated frozen sand. They observed that a constant settlement rate usually developed after 1 to 5 days under constant load (Figure 2.15). The instantaneous settlement was negligible in such tests. It was also negligible in Ladanyi's (1976) static penetration tests on frozen silt. Ladanyi and Paquin (1978) found that the settlement rate remains a function of the loading history only as long as the penetration resistance of the soil is not completely mobilized, which happens after the total accumulated settlement attains about 1/3 the footing diameter. Beyond that settlement, the loading history effect appears to be erased and the settlement rate then depends only on the applied load, as long as the soil remains

unc

2.6

resu
cons
in t
give
visc
1966
stud
abse
work
Jess
unde

Figu
1976
curve
on th
behav
was t
Prand
Mende
compu
Both

unchanged.

2.6 Frozen Soil Beam Tests:

To investigate the multiaxial stress state and to verify the results of analytical or numerical analyses based on properties or constitutive laws, it is convenient to simulate frozen soil structures in the laboratory. Examples of model piles and footings have been given in previous sections. Although analytical solutions for viscoelastic plain beams have been attempted (Hult, 1966; Odqvist, 1966) and also numerical solutions (Klein and Jessberger, 1978), model studies on frozen soil beams (plain or reinforced) are generally absent in the literature. An exception to this is the experimental work published by Meissner and Eckardt (1976), as quoted by Klein and Jessberger (1978), and more recently an experimental-analytical study undertaken by Soo (1983).

An experimental creep curve for Emscher-Marl at -6°C is shown in Figure 2.16 for a frozen simply supported beam (Meissner and Eckhardt, 1976). The dashed lines represent the theoretical creep deflection curves, for Emscher-Marl at -10°C and Karlsruher sand at -33°C, based on the finite element method of analysis. Identical stress-strain behavior was assumed in tension and compression. The uniaxial case was transformed to the multiaxial state of stress based on the Prandtl-Reuss equation and the von Mises flow rule (Hill, 1950; Mendelson, 1968). The finite element program was also used to compute the stress distribution across the beam depth, Figure 2.17. Both the deflection rates and the stress distribution were in close

agreement with the analytical solution proposed by Hult (1966) and Odqvist (1966). The stress distribution can be evaluated analytically by satisfying the moment equillibrium equation given below (Hult, 1966; Odqvist, 1966):

$$\int_0^{h'} \sigma\, z(b\, dz) = 0 \qquad (2.20)$$

where h', b, and z are defined in Figure 2.17, and for identical soil behavior in tension and compression the neutral axis is located at the cross-section centroid, i.e. at $z_1 = h/2$. Applying the elastic analog, in which the strain rate $\dot{\varepsilon}$ is made equal to the elastic strain ε, then σ can be expressed as:

$$\sigma = \sigma_{cu\theta}(\varepsilon/\dot{\varepsilon}_c)^{1/n} \qquad (2.21)$$

The assumption of identical soil behavior in tension and compression does not appear to be always valid. Short-term creep tests on frozen silt, at -10°C, showed that the ratio of its compressive to tensile strength, σ^c/σ^t, was about 4 (Vyalov, 1965) at one hours time to failure. The ratio was deduced from parabolic Mohr-Coulomb failure envelopes at different times to failure. For a 12-hour time to failure envelope, the ratio was reduced to about 3.5, thereafter remained almost constant. Hawkes and Mellor (1972) observed that the ratio σ^c/σ^t increased from unity at strain rates below 10^{-6} sec.$^{-1}$, in creep tests, to about 8 at higher rates, in constant strain rate tests on polycrystalline ice at -7°C. This is because for higher rates, tensile strength σ_t changed very slightly as the strain rate $\dot{\varepsilon}$ increased, while the compressive strength σ_c continued to increase (Ladanyi, 1981).

one

10⁻

3.5

(19

str

str

rec

obt

to

str

axi

at

sho

ove

Bra

whe

Sub

int

A s

ten

Haynes et al. (1975) reported that the ratio remained equal to one, for a frozen silt at -9.4°C, until the strain rates exceeded 10^{-3} sec.$^{-1}$. After that, the ratio started to increase up to about 3.5, with increasing brittleness in tension. Haynes and Karalius (1977) observed that the gap between the compressive and tensile strengths of frozen silt did not only increase with the increase in strain rate, but also with the decrease in temperatures. More recently, Bragg (1980) reported that the ratio σ^c/σ^t is about 5, obtained by extrapolation for frozen Wedron sand.

Based on the foregoing observations, a frozen soil beam subjected to external bending moment may fail because of a weakness in tensile strength. Therefore, it can no longer be assumed that the neutral axis is located at the centroid of the beam cross-section, especially at high strain rates. In this case, the position of the neutral axis should be determined by satisfying the force equillibrium condition, over the beam cross-section, given below (Hult, 1966; Odqvist, 1966; Bragg, 1980):

$$F_c = F_t \tag{2.22}$$

where F_c is the resultant force in the compression zone, and is given by:

$$F_c = \int_0^{z_1} \sigma_{cu\theta}(\varepsilon/\dot{\varepsilon}_c)^{1/n}(b\ dz) \tag{2.23}$$

Substituting z/R for ε, where R is the radius of beam curvature, and integrating gives:

$$F_c = (n\ b\ \sigma_{cu\theta}/\ 1+n)(1/\ R\ \dot{\varepsilon}_c)^{1/n}\ (z_1)^{1+1/n} \tag{2.24}$$

A similar expression may be derived, for the resultant force F_t in the tension zone, with z_1 replaced by $(h'-z_1)$ in Equation 2.24. The creep

par
pre
Equ
bot

and
sat
at
typ
a s
sum
lar
the
the
the
rat
rel
VI.

parameters n, $\sigma_{cu\theta}$, and $\dot{\varepsilon}_c$ may not be the same in tension and compression. Substituting for F_c and F_t by their corresponding expressions Equation 2.22 can be solved for z_1. Note that R would cancel from both sides of Equation 2.22.

Soo (1983) has included the effect of steel reinforcement (plain and deformed bars) in his experimental study. Frozen beams of saturated Wedron silica sand (64 percent sand by volume) were tested at -10°C under step loadings maintained for 7 to 20 hours. The two types of steel reinforcement used included plain rods and rods with a single lug at each end. Preliminary data from his tests are summarized in Figure 2.18. As expected, the plain beam showed the largest deflection when compared to the reinforced beams under almost the same load. Although the ultimate load carrying capacity of the beam with the deformed rod was larger than that of the beam with the plain rod, the latter showed a smaller deflection and deflection rate than the beam with a deformed bar. A discussion of these findings relative to the results from the present study are included in Chapter VI.


Ice Adhesive Strength, τ_{ii}, kg/cm^2

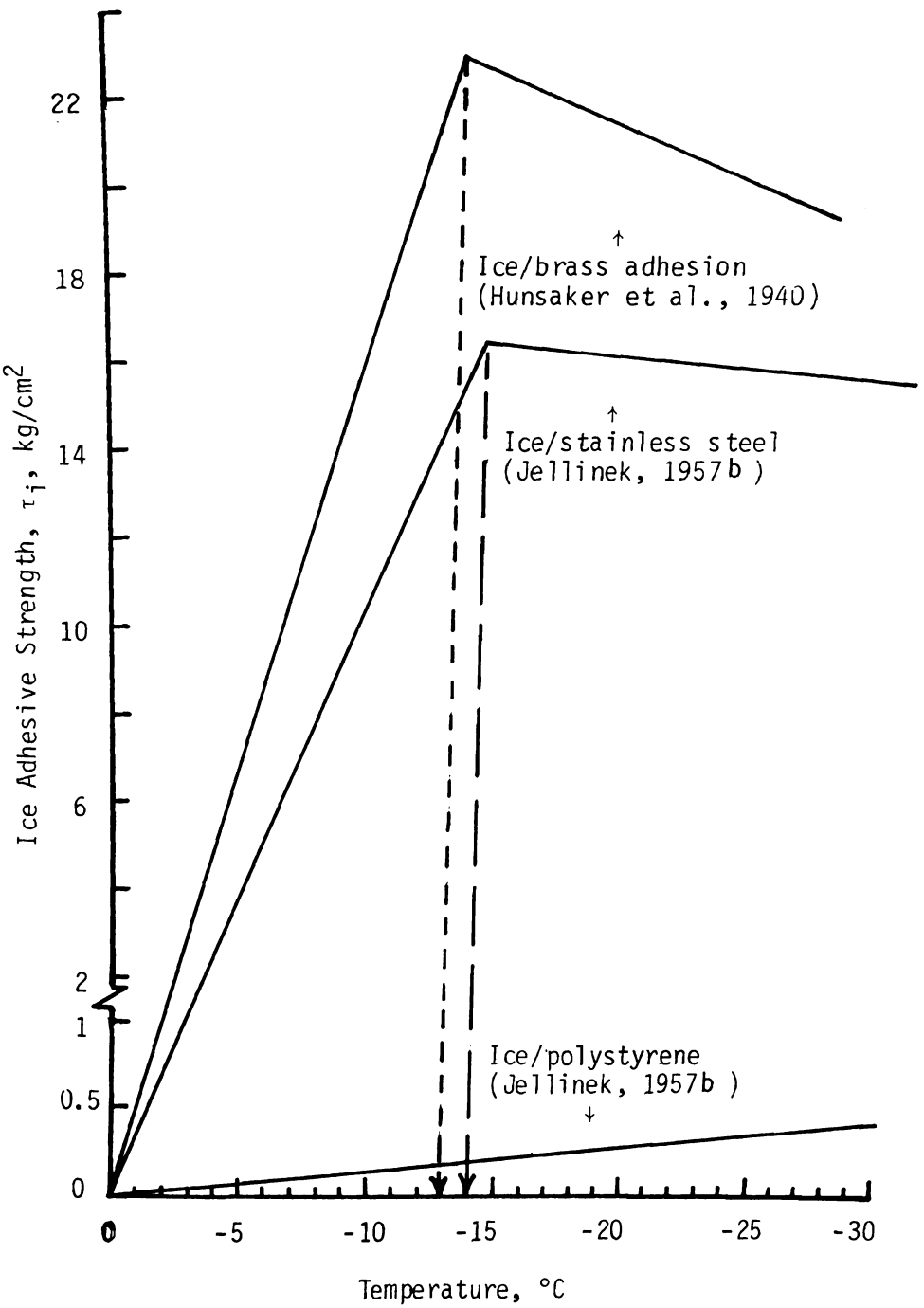

Figure 2.1: Adhesive strength of ice to different materials as a function of temperature.

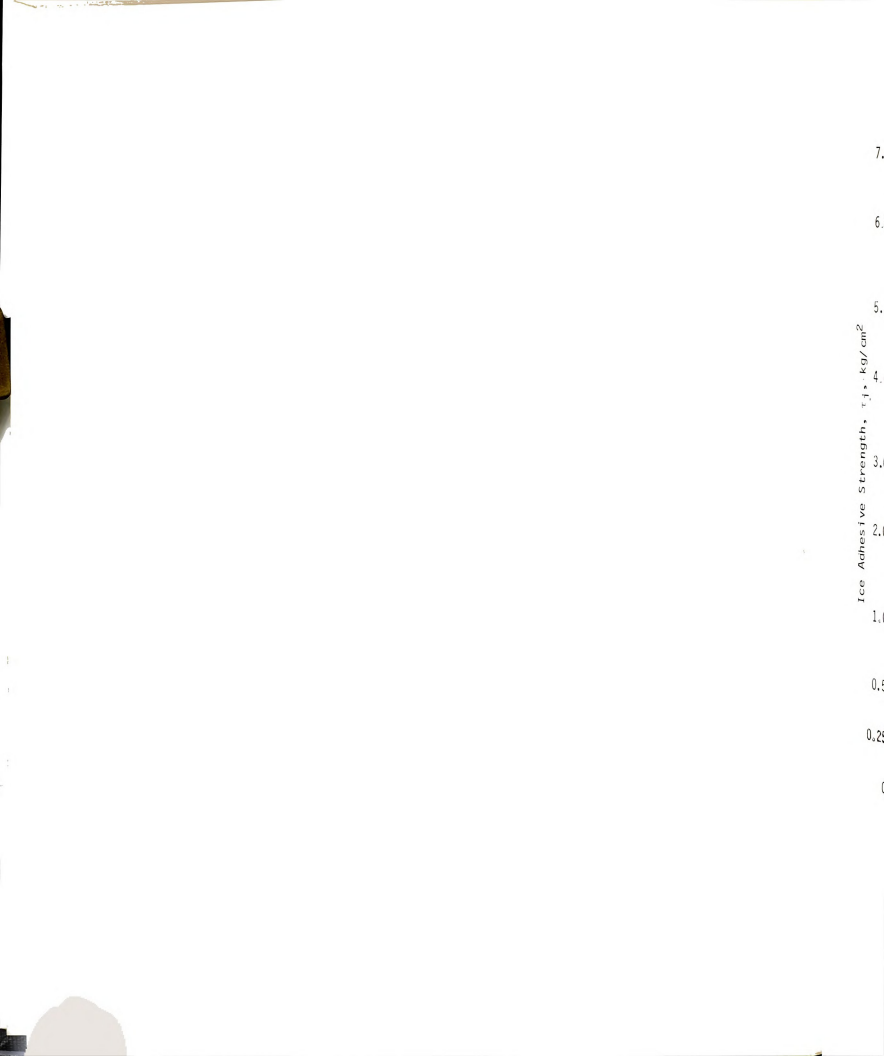
Ice Adhesive Strength, τ_j, kg/cm^2
7.
6.
5.
4.
3.
2.
1.
0.5
0.28

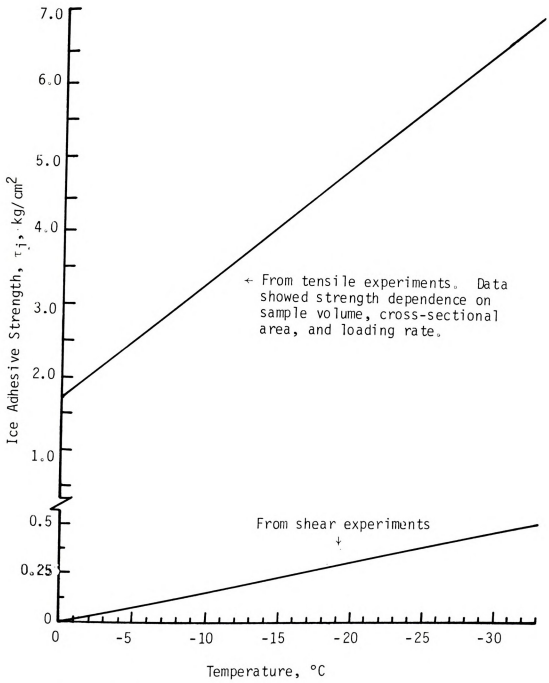

Figure 2.2: Effect of test type on the adhesive strength of ice to polystyrene surface (after Jellinek, 1957 b).

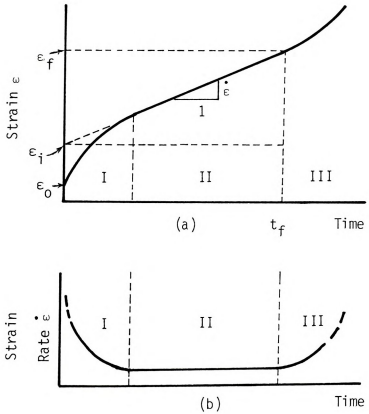

Figure 2.3: Constant-stress creep test: (a) basic creep curve; (b) true strain rate vs. time.


Test data (average)
12

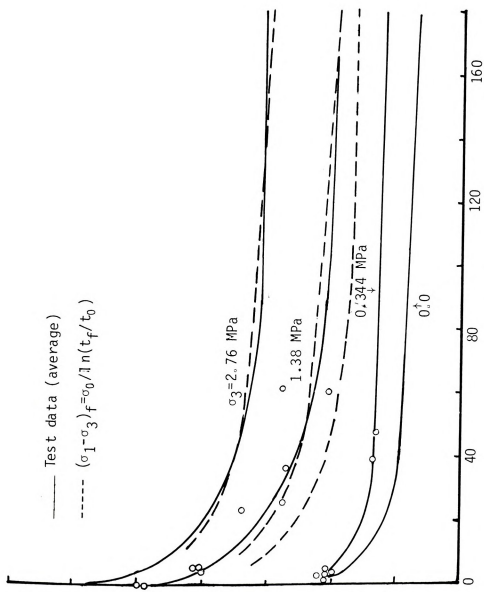

Figure 2.4: Creep strength vs. time to failure for frozen Ottawa sand at -3.85°C (after Sayles, 1973).


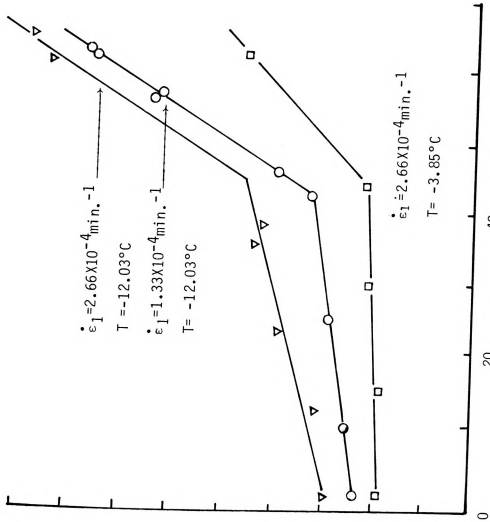

Figure 2.5: Volume concentration of Ottawa sand and peak strength (after Coughnour and Andersland, 1968).

$q=(\sigma_1+\sigma_3)/2.$ MPa

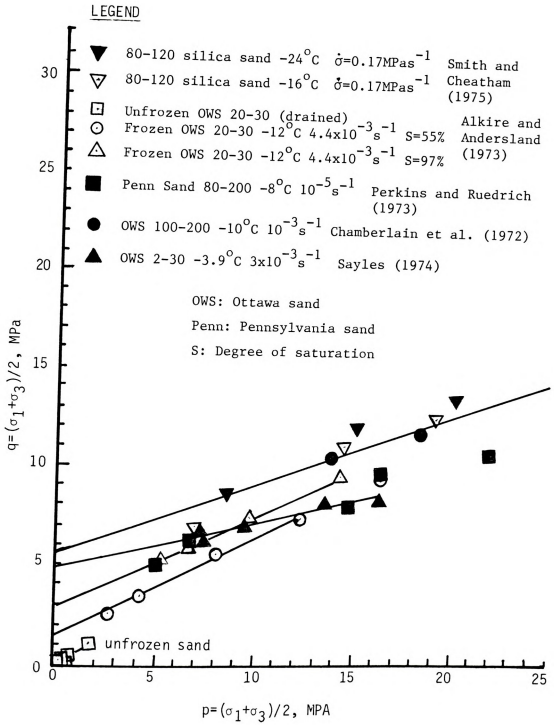

Figure 2.6: Results of strength testing on frozen soils at low confining stresses


30
I
II
LEGEND
Granular ice -11.5°C 5.4x10⁻⁴s⁻¹

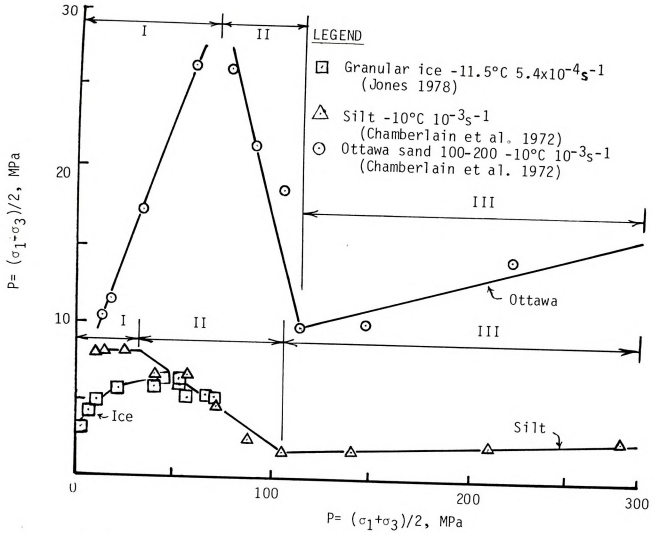

Figure 2.7: Effect of confining stress on the strength of ice and frozen soils.

Ice Thickness, H, mm

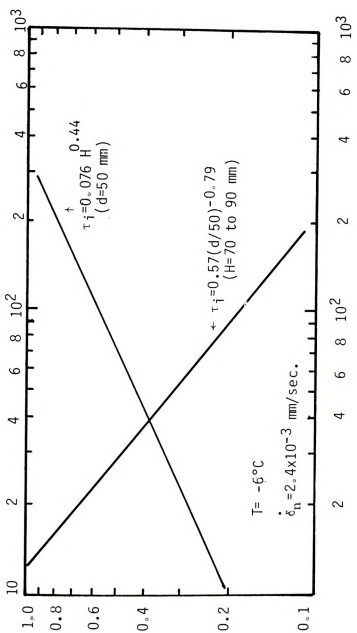

Figure 2.8: Effect of ice thickness and pile diameter on the ice adhesive strength (after Frederking, 1979).

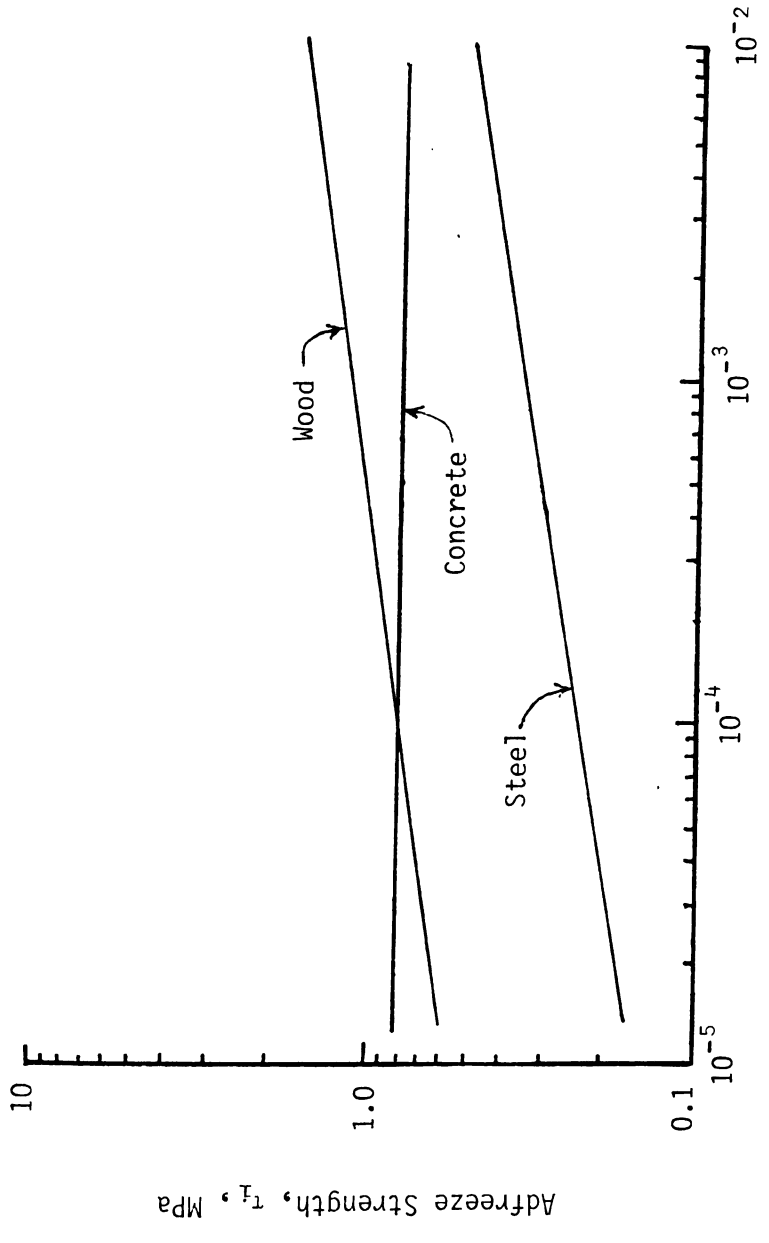

Figure 2.9: Adfreeze strength for piles in ice as a function of pile displacement rate (after Parameswaran, 1981)


Adfreeze Strength, psi

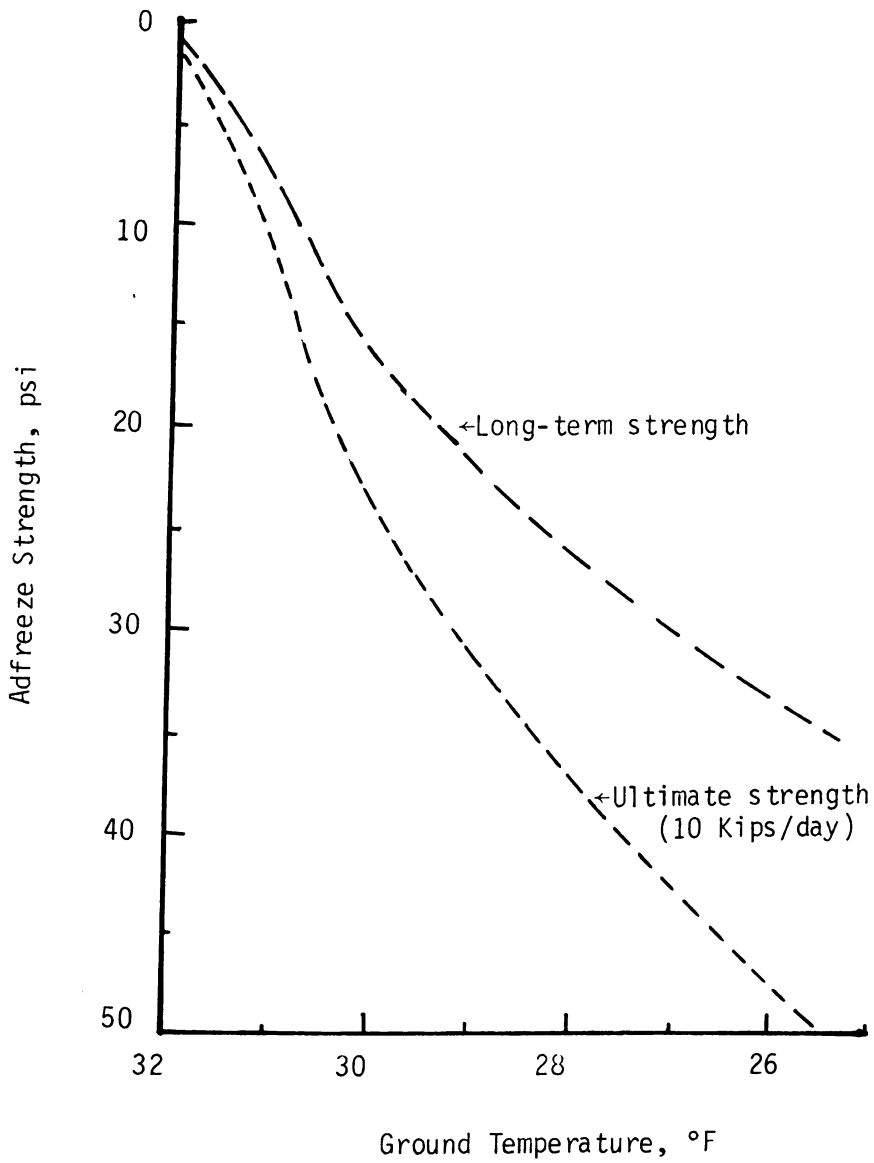

Figure 2.10: Adfreeze strength, of silt-water slurry to an 8-in. diamter steel pipe pile, versus temperature (after Crory, 1963).

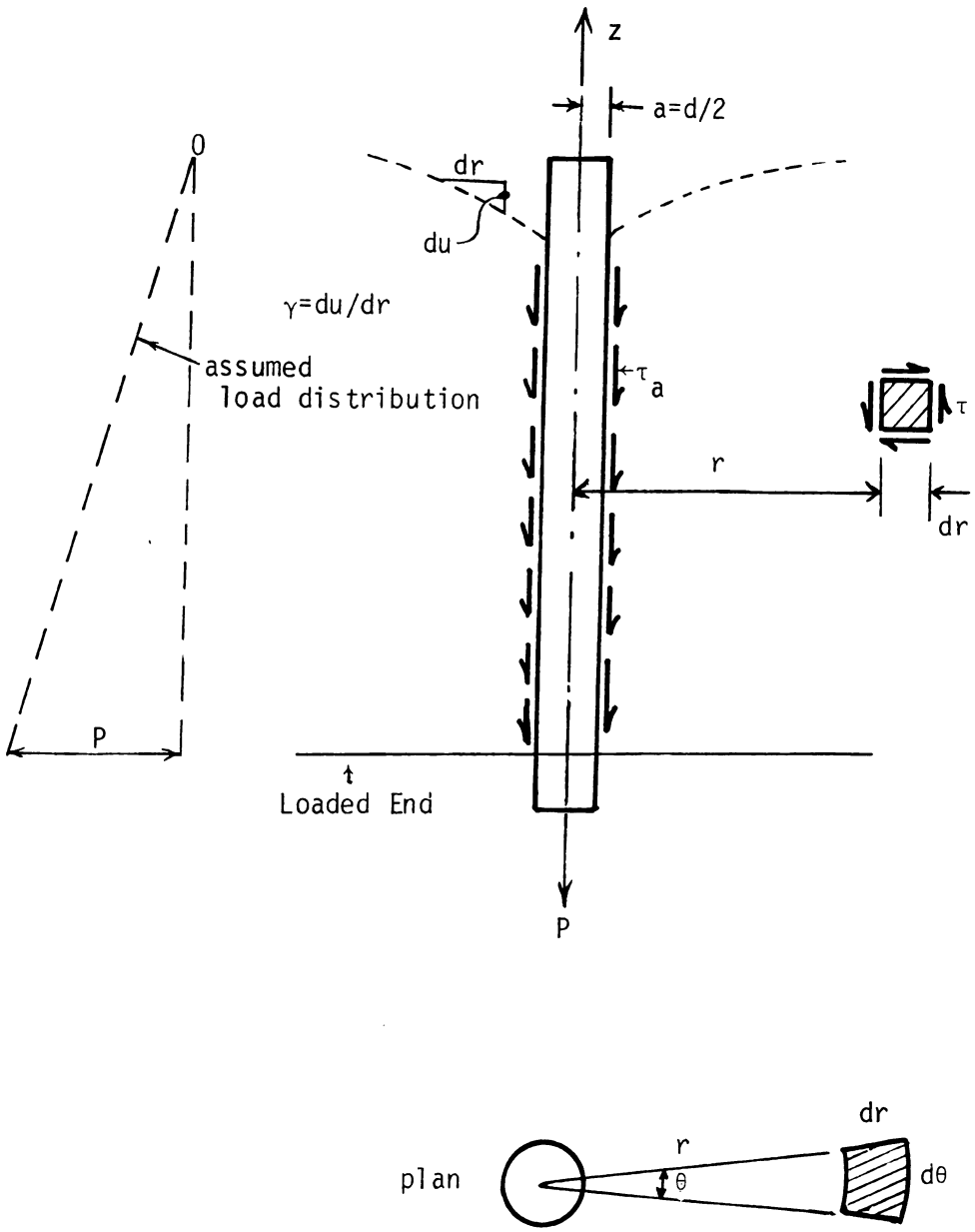

Figure 2.11: Definition of terms used in the bond analysis of a plain rod (pile) in frozen soil (after Johnston and Ladanyi, 1972).

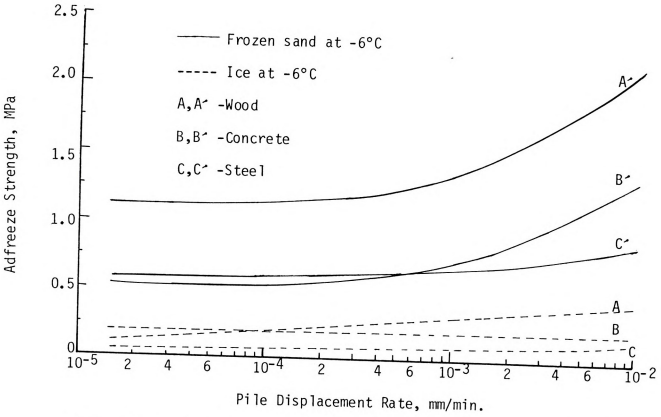

Figure 2.12: Variation of adfreeze strength of piles in frozen sand (solid lines) and contribution due to ice adhesion present in sand (dashed lines) with nominal pile displacement rate (after Parameswaran, 1981).

Figu

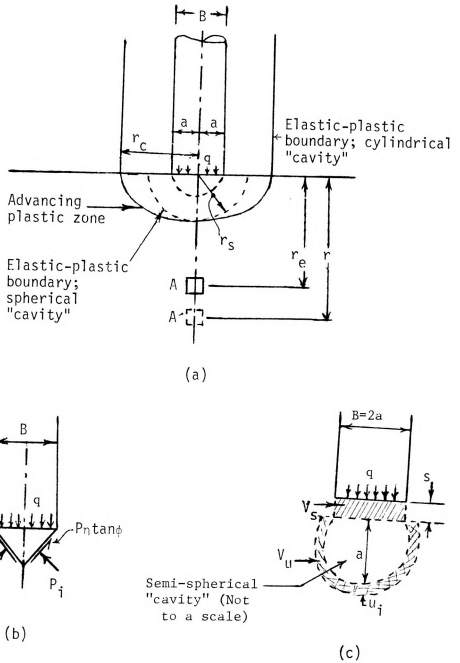

Figure 2.13: (a) Soil response to penetration by a flat circular punch, (b) and (c) notations for transformation of cavity expansion theory to a deep footing problem (after Ladanyi and Johnston, 1974).


0.0
q=0.2 MPa
q=0.3 MPa

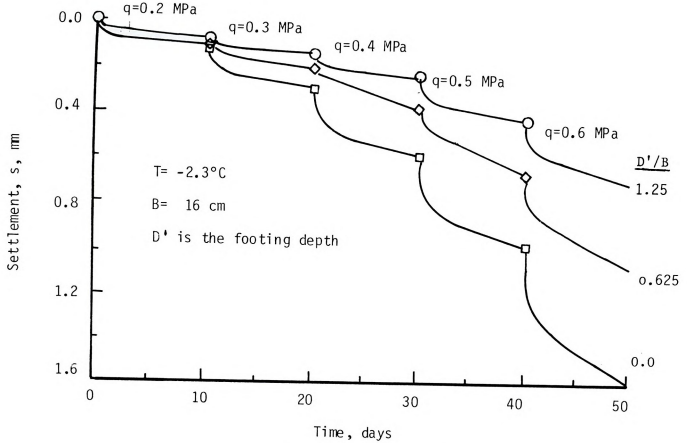

Figure 2.14: Effect of footing depth on settlement of circular test plates in ice at -2.3°C (after Vyalov et al., 1973)

Total Settlement, s, cm

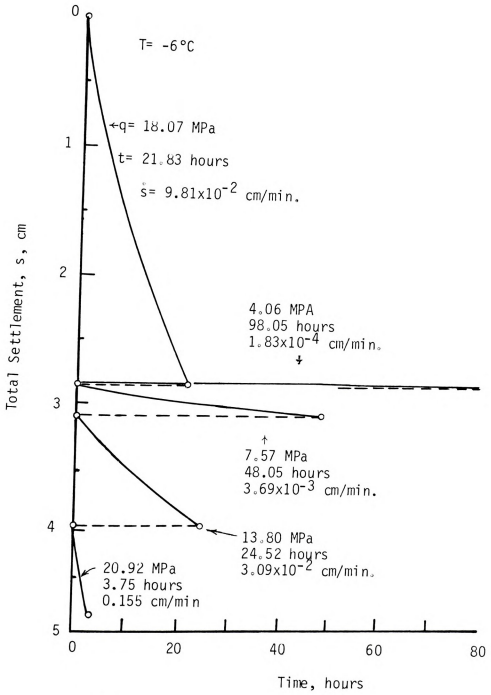

Figure 2.15: Results of a loading creep test on a circular plate (1.4 in. diameter, 18 in. deep) in frozen sand (after Ladanyi and Paquin, 1978).

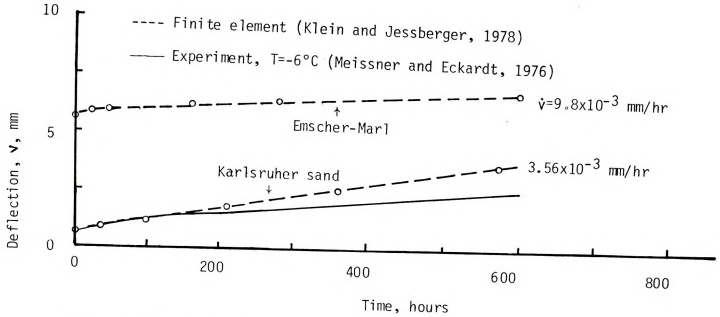

Figure 2.16: Creep deflection at the center of frozen sand beams (after Klein and Jessberger, 1978).

Distance from Neutral Axis, cm

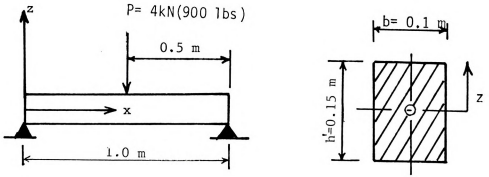

(a)

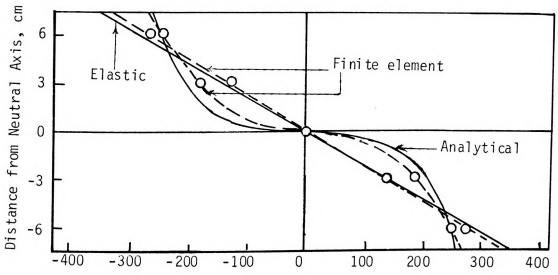

(b) Normal Stress at x=0.475m, σ_x, psi

Figure 2.17: Frozen Soil Beam; (a) Diagram of a Simply Supported Beam; (b) Stress Distribution (after Klein and Jessberger, 1978).

Beam Deflection, v, $x10^{-2}$ in.

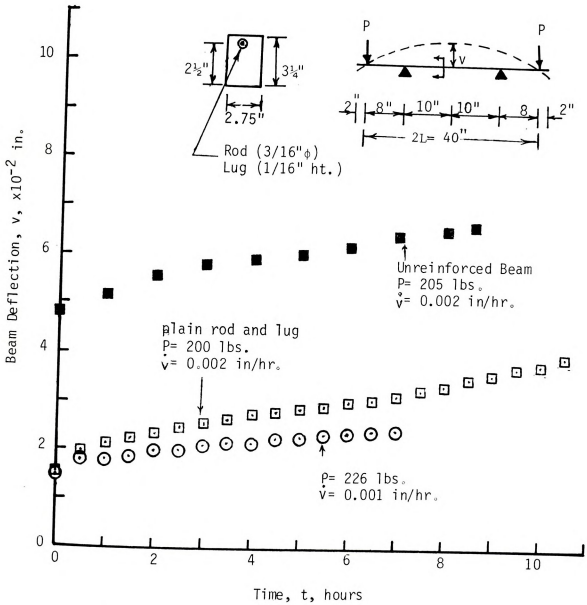

Figure 2.18: Deflection creep curves for simply supported beams of frozen sand at -10°C (after Soo, 1983).

CHAPTER III

MATERIAL PROPERTIES AND SAMPLE PREPARATION

3.1 Steel Rods:

For most ice samples, a plain cold-rolled steel rod, 5/8 in. diameter, was used. A few samples were tested with a 3/8 in. diameter rod for comparison. For sand-ice samples, several diameters ranging from 3/32, 6/32, 12/32, and 20/32 in. plain cold-rolled steel rods were used. All of these rods included a threaded portion at both ends which permitted easy attachment to an eye connector and hook at the bottom of the coolant bath and mounting of a displacement transducer at the upper rod end (Figures 3.1 and 3.2 a). Lugs welded to the 3/8 in. diameter rod, shown in Figure 3.2 b, included heights, h, of 1/16, 2/16, and 3/16 in. and a length of 1/2 inch. Lug heights were limited to 3/16 in. so as to avoid a tensile failure in the 3/8 in. steel rod. Plain rods with a single lug are referred to as deformed bars.

Lug face angles of 45 and 90 degrees, Figure 3.2 (c), were selected to provide preliminary information on wedging between the frozen sand and rod during pull-out. Rod surface roughness was considered by using three steel surface types: ground-finish steel with a roughness factor ρ of 90 percent, cold-rolled with ρ = 625%, and shot-blasted with ρ = 1489%. The latter type surface was prepared from the ground-finish steel by shot-blasting with commercially available, uniformly graded glass beads with all beads passing the No. 60 U.S. standard sieve and retained on

the No. 100 sieve (size range of 0.0058 in. to 0.0097 in.). Shot-blasting generally gave the steel surface a finely-textured grey color, whereas the ground-finish steel displayed an almost white, shiney and highly polished surface with minimum imperfections. The cold-rolled steel rod surface was dark grey with very fine spots due to some imperfections which originated during its manufacture. A standard deformed 3/8 in. diameter rod with lugs spaced at 0.3125 in. on centers was also used in several tests. The lug height for this rod was about 1/64 in. (0.015 in.).

3.2 Ice Samples:

Three ice types used in this study are referred to as Ice(1), Ice(2), and Ice(3). For the first type, ice samples were prepared by pouring distilled water directly into a cylindrical split steel mold with a 6 in. inside diameter and 7 in. height. The water was poured to a height of 6 in. ± 1/8 in., in four layers. Before that, the mold was first mounted on a 6 in. diameter by 1/2 in. high steel reaction plate. This plate was attached, by screws, to a rectangular aluminum reaction beam, 1 1/2 in. X 5 in. X 12 in., with a circular hole in the center to allow for the steel rod embedded in the pull-out specimens. Clearance between the rod and the hole for each rod size was maintained at 0.063 in. by use of a removable washer in the reaction plate.

To prevent leakage a commercial putty was used to seal the mold at the edges and to minimize ice adhesion to the mold it was lined with a thin sheet of plastic saran wrap. All samples were frozen and stored in a freezer at close to -20°C for at least 12 hours. Directional freezing took place from the base upward and from the sides radially to

the center. The sample top was covered with a one inch layer of styrofoam insulation to minimize sample damage due to delayed volume expansion caused by change of water to ice in the central core of the sample. Ice samples prepared in this way were clear with few or no entrapped air bubbles. After removal from the mold, rubber membranes (double thickness) were placed, as shown in Figure 3.1, to protect the ice sample during immersion in the circulating anti-freeze/water coolant mixture.

For Ice(2), samples were prepared by first cooling the mold in the freezer, placement of crushed ice in the mold, and pouring precooled (T=0°C) tap water over the crushed ice. Very little ice melted when combined with the precooled water. The crushed ice was also formed from ordinary tap water, with a hardness close to 450 parts per million as calcium carbonates. Ice(3) was prepared by placing dry natural fresh snow in the precooled mold and pouring precooled distilled water over the snow. The fresh natural snow was collected and stored in the freezer and later, before use, was sieved on a No. 4 U.S. standard sieve, with nominal grain diameter of 0.187 inch. Ice(2) and Ice(3) were cloudy due to entrapped air bubbles.

These two ice types are both polycrystalline, similar to that which forms in the pores of the frozen sand. The average density of all ice samples was close to 56.2 lbs/cu. ft. (0.90 gms./cu. cm) ± 1.2 percent difference depending on the temperature (Pounder, 1967). The prepared ice samples were transferred to a bath in which an anti-freeze/water coolant mixture at the test temperature circulates around the protected sample. All samples were cooled at least 10 hours before testing to permit temperatures to equalize throughout the sample. Constant displacement rate tests were carried out on ice samples labeled as

I-1 through I-32 in Appendix A. Constant load (creep) tests were conducted on ice samples labeled as CI in Appendix B.

3.3 Sand-Ice Samples:

A commercially available sand produced by the Wedron Division of the Pebble Beach Corporation of Wedron, Illinois, was used in this investigation. The Wedron sand consisted of sub-angular quartz particles with a specific gravity of 2.65. The sand gradation was uniform with all material passing the No. 30 U.S. standard sieve and retained on the No. 40 sieve (size range of 0.0232 to 0.0165 in.). The coefficient of uniformity was about 1.50. The pull-out samples were, 6 in. in diameter and 6 in. high, prepared in the same split mold used for ice samples.

A sand volume fraction of 64 percent was selected for samples, except those prepared for the study of sand concentration effect. This volume fraction is comparable to values normally encountered in the field and insured the development of dilatancy and interparticle friction in front of the lugs. The value of 64 percent sand by volume corresponds to a dry density of 105.8 lbs./cu. ft., void ratio of 0.5625, and ice saturation close to 97 percent. To insure this high degree of saturation, the mold was partially filled with a pre-determined amount of distilled water and sand was slowly poured into the water permitting air bubbles to escape to the surface. The sample was tamped with a steel rod (0.25 in. in diameter) to give the desired sand packing. The methods of sealing and lining the mold, freezing the sample and transferring it to the coolant bath for testing were similar to those described for the ice samples.

Preparation of frozen samples with sand particles in dispersed positions, i.e. with sand concentrations lower than 64 percent, involved

use of sand chilled to below freezing and then carefully mixed with dry natural snow (sieved through a No. 4 sieve). This sand-snow mixture was then placed into the cold mold and distilled water, precooled to 0°C, was poured over the mixture. Very little snow melted as a result of pouring ice water over the snow and sand mixture. The resulting sample contained uniformly dispersed sand particles. For each sample, a specified amount of air-dry sand was pre-determined to give the required sand concentration. After sample preparation, the excess sand was air-dried, weighed, and deducted from the pre-determined amount to give the weight of sand in the sample. Several sand concentration values, v_s, were considered; 64.0 percent, 52.8 percent, 48.6 percent, 44.5 percent, 32.3 percent, 17.5 percent, and 0 percent for the snow-ice sample.

Tests were also conducted on frozen sand samples of different heights (1 in., 2 in., 3 in., 4 in., 5 in., and 6 in.). These samples were prepared in the same manner, except that for samples with heights less than 6 in., styrofoam plates 6 in. in diameter and about 1 in. thick were added to the top of each sample to make a total height of 6 inches. Different diameter samples were prepared using available molds with diameters of 1.9375 in., 2.75 in., and 4 inches. These samples were prepared in the same manner as described for the 6 in. sample diameter.

Figur

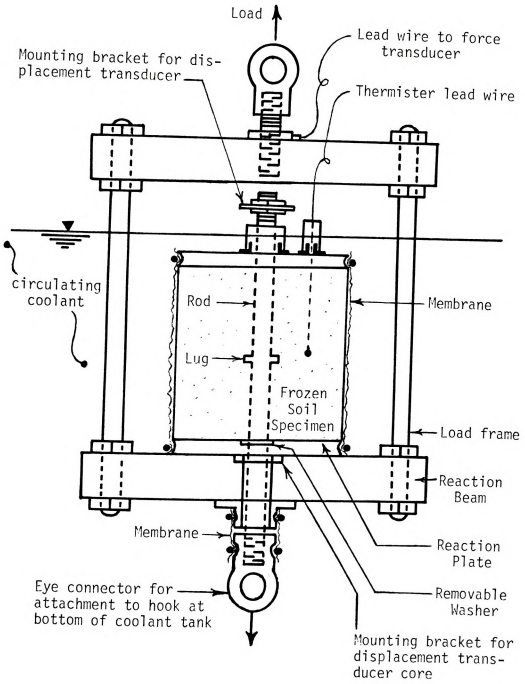

Figure 3.1: Equipment for pull-out tests including a frozen sand sample, steel rod with lug, and loading frame immersed in the circulating coolant.

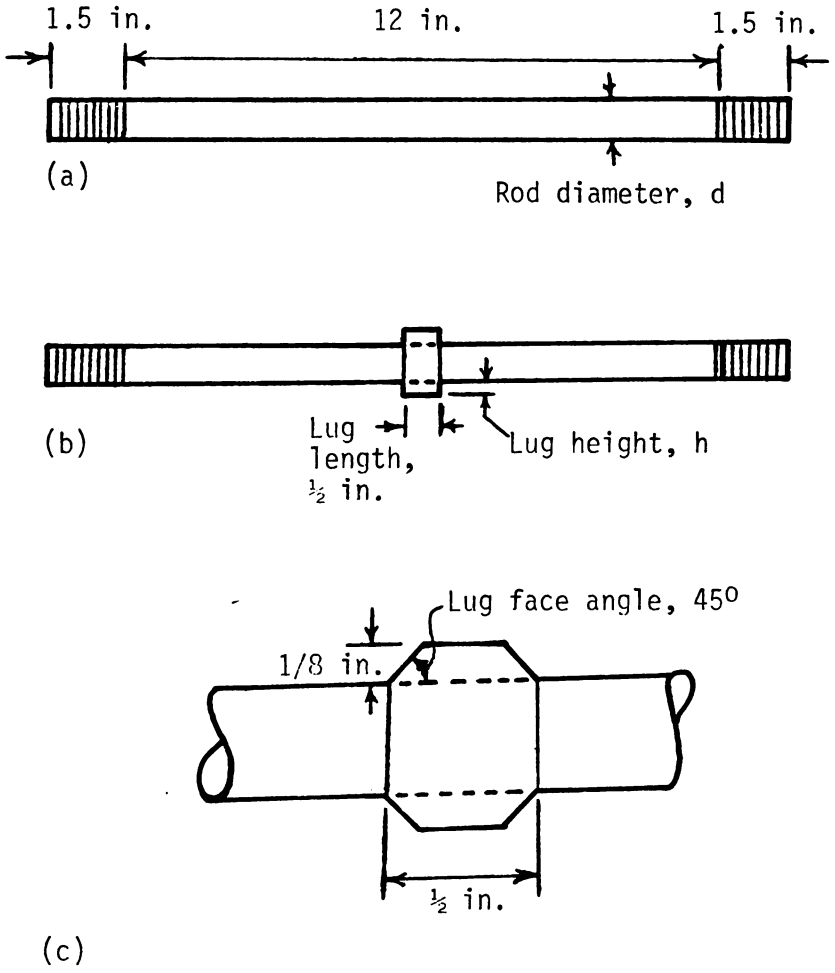

Figure 3.2: Bar configuration. (a) Plain rod. (b) Plain rod with 90 degree lug. (c) Lug with 45 degree face angle.

CHAPTER IV

EQUIPMENT AND TEST PROCEDURE

4.1 Equipment:

Constant displacement rate and constant load (creep) pull-out tests were conducted using the loading frame shown in Figure 3.1. The frame consists of a 6 in. diameter by 1/2 in. thick sample reaction plate; upper and lower 1.5 in. by 5 in. by 12 in. aluminum beams; two 5/8 in. diameter 16 in. long steel rods, for load transfer from the upper to the lower beam; and eye connectors at the top and bottom. The frame stiffness was assumed to be high compared to that of the reinforcement rods. Attached to the upper beam was a 10,000 pound capacity load cell (Strainsert Model FL10 -25PKT) for monitoring the applied load. Displacement of the steel rod relative to the base of the frozen sample was monitored using a Sanborn Linearsyn differential transformer (Model 585 DT-1000). This transducer was supported by a bracket mounted at the top of the steel rod (Figure 3.1). The LVDT core was supported by a small rod attached to the lower reaction beam.

An insulated steel rectangular coolant bath, 14 in. by 14 in. by 16 in., helped confine the coolant liquid surrounding the frozen sample. The anti-freeze/water coolant mixture circulates from a refrigeration unit to the bath as shown in Figure 4.1. Equal parts of water and ethylene glycol was close to the optimum combination for the coolant mixture. A one inch external covering of styrofoam insulation helped maintain the

sample and bath test temperatures. A Graham electric motor, with variable speed gear box, mounted on a 10,000 pound capacity Soiltest loading frame (Figure 4.1) provided the constant displacement rate pull-out loads. Displacement rates available from the variable speed gear box ranged from about 10^{-5} to 10^{-1} in./min. For constant load (creep) tests, a steel lever system (Figure 4.2) with arm ratio of 8:1 was attached to the Soiltest load frame. Dead weights, up to 550 lbs., were applied to give a maximum pull-out load of 4,400 pounds.

A Sanborn two-channel recorder (Model 7702B) with preamplifier (Model 8805A) was used to monitor loads and displacements for all tests. At maximum sensitivity, one millimeter stylus deflection on the displacement strip chart represented 0.0005 in. displacement for the transducer. This sensitivity limited the range of creep data obtainable for small displacements observed for ice adhesion to plain rods. For the load chart, at maximum sensitivity one millimeter of stylus deflection corresponded to 14 lbs. applied to the load cell. A Hewelett-Packard digital Logging Multimeter (Model 3467A) and thermistor was used for monitoring sample temperatures. The thermistor was embedded in the sample during preparation with the lead wire entering through an opening in the upper circular plate (Figure 3.1).

Measurement of the rod surface roughness was made using a Physicists Research motor (Mototrace Type V, No. 680) which moves a tracer (Model LA4-10) on the surface in question at constant speed of 0.221 in/sec.; a profilometer and DC input (Type O, Model 8, No. 538) with a dial gage for reading the maximum and minimum surface aspirity heights. At maximum sensitivity, a one micro-inch height of aspirity could be read on the gage.

was achieved or when excessive displacements were reached. For constant load (creep) tests, incremental step loads were added until either failure occurred, the ultimate load capacity of frame was reached (about 4,500 lbs.), or the displacement limits on the load frame was reached. Recorder strips were labeled and the data for each test was transcribed to test summary sheets.

For measurement of rod surface roughness, a duplicate surface for each steel type was prepared on a flat plate, for easy tracer movement on the surface. Measurements were made by connecting the tracer to the profilometer, and the latter to the DC recorder. After warm-up, the recorder stylus was adjusted to the chart center. Paper movement was selected at 10 cm/min. and the attenuation knob was adjusted to keep the trace on the recording paper for the highest asperity on all surfaces. As the tracer moved on each surface, the maximum and minimum asperity heights (in micro-inches) were read on the profilometer gage, while a continuous record of the surface irregularities was being made on the recorder strip chart. The corresponding aspirity heights (including the maximum and minimum) were given in millimeters on the chart. For each surface, these measurements were repeated several times for a better representation of the surface roughness. A roughness factor, defined by Wright (1955), was used as a criterion for the rod surface roughness. The data and method of calculating the roughness factor are presented in Chapter V.

A Sanborn one-channel chart recorder with DC input (Model 322) was used to make a continuous chart record of the surface irregularities.

4.2 Test Procedure:

After sample preparation, placement in the test loading frame, and cooling to the desired test temperature, several additional steps were required for completing the test. The transducers were connected to the recorder which was allowed to warm up for approximately 30 minutes prior to testing. After the warm-up period, the stylus needles were adjusted to a zero reading for load and displacement. For the constant displacement rate tests the loading ram of the Soiltest load frame was adjusted and attached to the upper eye connector in Figure 3.1, but with no applied load. The sample temperature was observed and recorded. During a constant load (creep) test, which normally took several days, the coolant refrigeration bath maintained test temperatures to within $\pm$ 0.10°C. Large room temperature variations did influence the coolant bath temperature. For test temperatures warmer than -10°C, the variation appeared to be within $\pm$ 0.05°C. In all cases, these temperatures variations did not appear to have affected the test results.

The gear box controls were adjusted to give the desired displacement rate, and the ram was engaged with upper eye connector. The strip chart paper movement was selected according to the loading rate. As the test progressed, the stylus needle deflections on the recorder was adjusted, as needed, to keep the trace on the recording paper. All constant displacement rate tests were continued until complete failure was observed by sudden rupture in the case of plain rods. When deformed rods (with lugs) were used, the test was stopped after an ultimate load

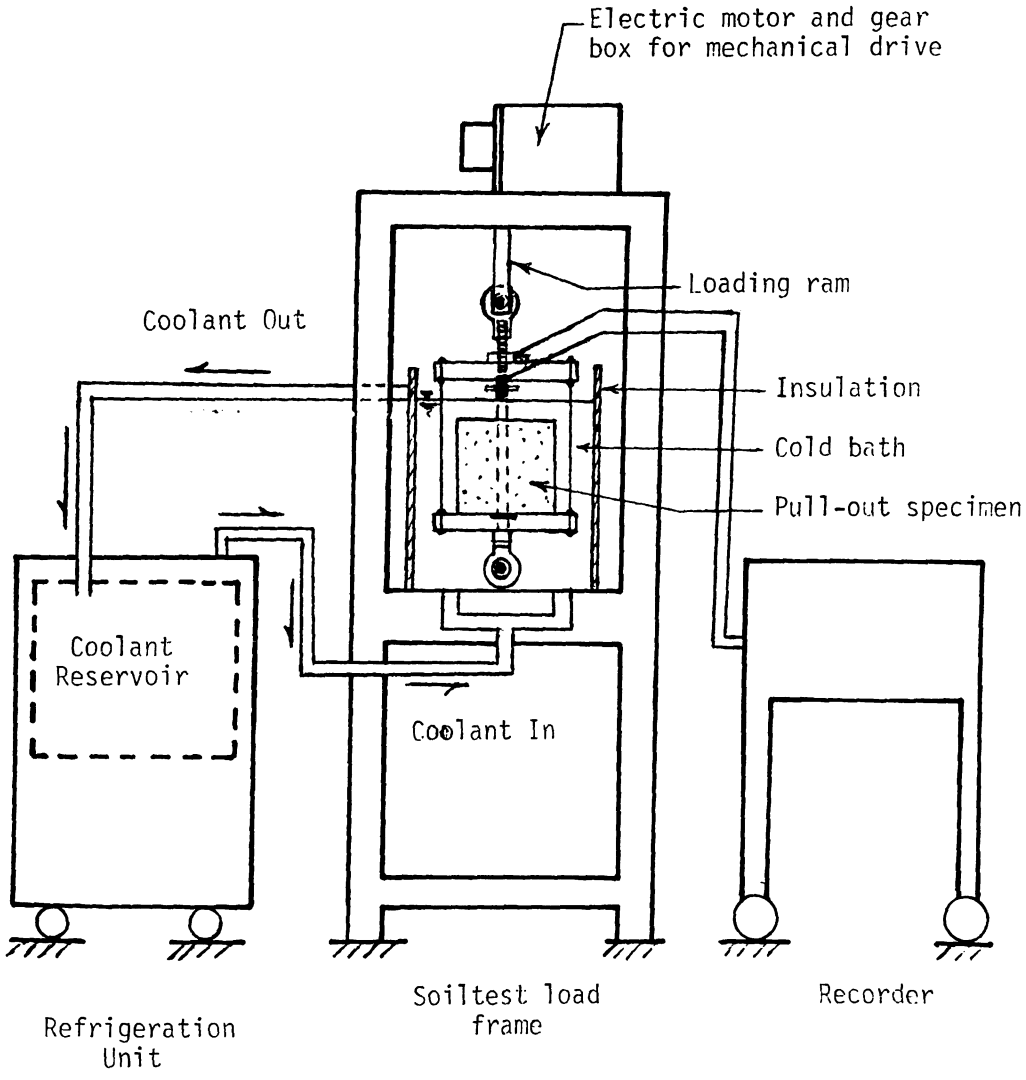

Figure 4.1: Diagram of test system for constant displacement rate tests.

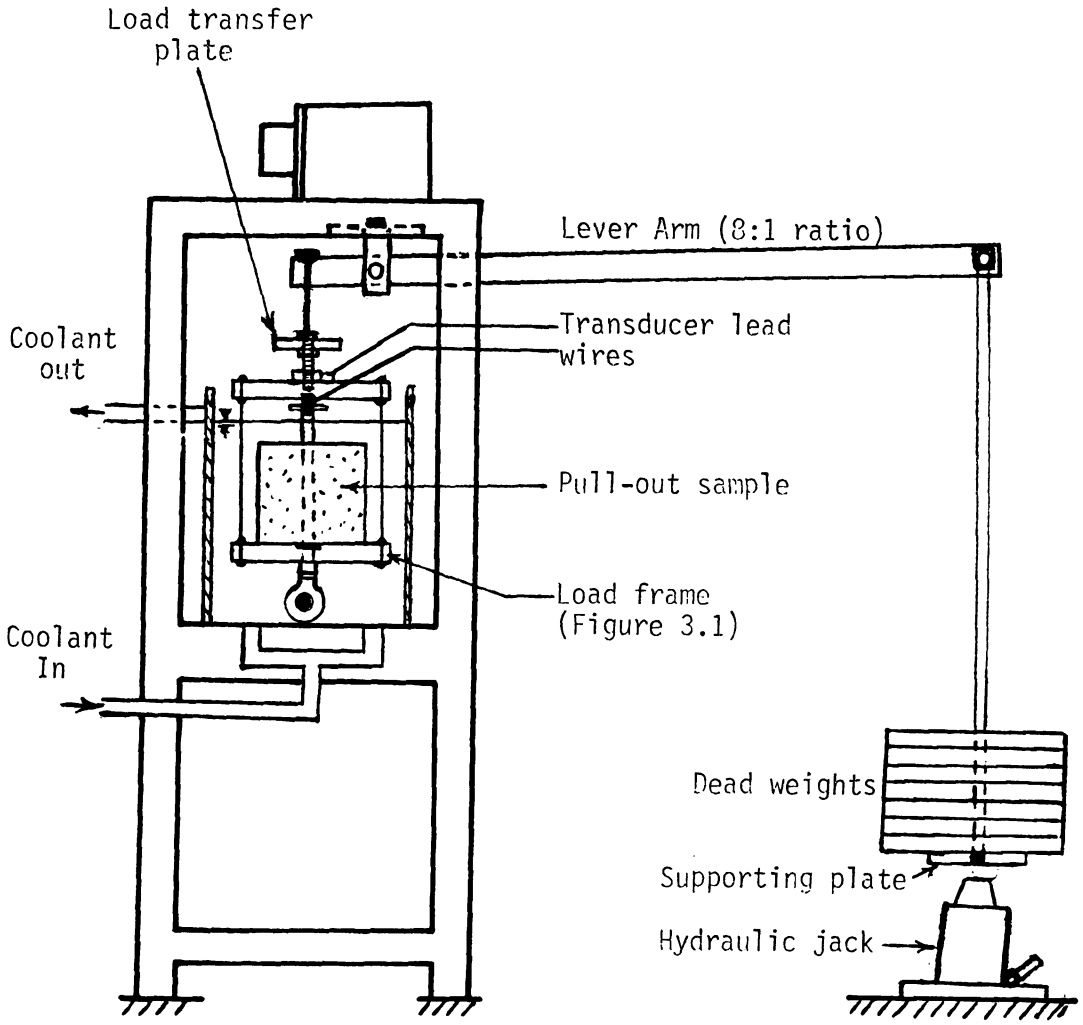

Figure 4.2: Diagram of test system for constant load (creep) tests.

CHAPTER V

EXPERIMENTAL RESULTS

A summary of experimental data along with a brief discussion of their implications are given in this chapter. The material is presented in two parts: constant displacement rate tests and constant load (creep) tests.

5.1 Constant Displacement Rate Tests:

In this section, results are presented for a series of constant displacement (or loading) rate pull-out tests conducted to determine the influence of displacement rate, temperature, bar size, sample height, water impurities, sand concentration, lug size and shape, and bar surface roughness on the adfreeze bond strength characteristics of frozen pull-out specimens. Physical properties of ice and sand-ice specimens, including the steel rods, are listed in Table 5.1. Test results for these samples are summarized in Table 5.2.

5.1.1 Displacement (and Loading) Rate Effects:

Pull-out tests were conducted on frozen sand samples with a sand volume fraction close to 64 percent (dry unit weight of 105.6 lbs./cu. ft.). The bar displacement rates ranged from about 0.0001 in./min. to 0.1 in./min. The corresponding loading rates ranged from about 2 lbs./min. to 20,000 lbs./min. The pull-out specimens were tested at temperatures ranging from -2°C to -26°C using two bar configurations; a

pla

wi

tim

sta

the

occu

some

elas

clea

"pre

reco

perm

(Fig

the

the

incr

(i.e

occu

and

obse

$\dot{\delta}_n$ do

rate

rods.

plain cold-rolled 5/8 in. diameter steel rod, and a 3/8 in. diamter rod with a single 1/8 in. high lug as shown in Figure 3.2 (b).

For the plain rods, typical load and displacement variations with time are shown on the recorder strip chart in Figure 5.1. As the test starts, the load increased with time at an almost constant rate while the displacement showed little or no increase until an initial slip occurred. At rupture a large reduction in the load was observed and in some cases zero values were noted. The displacement before rupture, the elastic portion, was in most cases too small (about 0.0005 in.) to be clearly shown on the recorder. Due to equipment limitations, the "pre-failure" displacements were estimated on the basis of very small recorded movement. During testing the bond resistance or stiffness permitted development of a nominal (machine) displacement rate $\dot{\delta}_n$ (Figure 5.1) only after rupture had occurred.

The observed behavior may be attributed partially to stiffness of the test system. In turn, the test system stiffness was dependent on the rigidity of all system components and connections. As the load increased, elastic strain energy was stored in the test system (i.e. the test frame, loading ram, loads cells, etc.). Once rupture had occurred and the loading rate decreased, the strain energy was released and the corresponding slip and increase in displacement rate were observed, as shown in Figure 5.1. Since the nominal displacement rate $\dot{\delta}_n$ does not correspond to the "pre-failure" loading stage, the loading rate $\dot{P}$, as defined in Figure 5.1, was used in place of $\dot{\delta}_n$ for the plain rods.

The time to failure for all plain rods ranged from a few seconds to

abou

temp

with

depe

rods

str

vs.

show

ice

adhe

for

(35

zati

alth

rate

that

rate

elas

figu

rod

alon

plot

log

p, o

the

about two hours depending on the loading rate, and to some extent on temperature. At colder temperatures the time was longer. For plain rods with lugs, the time to failure ranged from one hour to about 12 hours depending mainly on the lug size. It took longer to reach failure for rods with larger lug sizes. Data for each test, as given on the recorder strip (Figure 5.1), were transcribed to a data sheet from which a load-vs.-displacement curve was plotted. Typical load-displacement curves are shown for plain rods at different loading rates in Figure 5.2. Initially, ice adhesion combined with sand friction prevents slip. After the adhesion was broken and partial slip had occurred, a small residual value for adhesion and friction controls the pullout load. At the slow rate (35 lbs./min. in Figure 5.2) the "healing" effect due to ice recrystallization, was more pronounced than at the faster rate (1978.6 lbs./min.) although an increase in load was also observed after failure at the latter rate. The "healing" effect at slow rates may be attributed to the fact that more time permitted more ice refreezing as compared to the fast rates.

The change in loading rates illustrate two features; the faster rates produced a higher peak load and a larger initial slope within the elastic range of the curves in Figure 5.2. The right hand scale of this figure shows the bond stress, τ, calculated by dividing the load by the rod surface area. This calculation assumes a uniform stress distribution along the rod. The bond strength (ultimate value at failure, τ_u) is plotted versus the loading rate $\dot{P}$, at different temperatures, on a log-log plot in Figure 5.3. A consistent linear relationship between τ_u and $\dot{P}$, on a logarithmic scale, appears to exist at all temperatures. Using the least-squares fitting method, the relationship suggests a power law

of t

or

wher
para
chos
of m
temp

corr
betw
Figu
anal

or

wher
Thes

disp
The
Othe
prob

(or

of the form:

$$\tau_u = \tau_c \, (\dot{P}/\dot{P}_c)^m \tag{5.1}$$

or

$$\dot{P} = \dot{P}_c(\tau_u/\tau_c)^n \tag{5.2}$$

where n = 1/m is the strain-hardening parameter in compression tests. The parameter τ_c corresponds to the "proof" bond stress at an arbitrarily chosen loading rate, $\dot{P}_c$, taken equal to 1 lb./min. in this study. Values of m, n, and τ_c, listed in Table 5.3, indicate that these parameters are temperature dependent.

Despite the fact that the nominal displacement rate $\dot{\delta}_n$ does not correspond to the pre-failure stage, a general linear trend was observed between τ_u and $\dot{\delta}_n$ on a log-log scale at the same temperatures as shown in Figure 5.4. Thus, a power law may be established using the least-squares analysis, of the form:

$$\tau_u = \tau_c' \, (\dot{\delta}_n/\dot{\delta}_c)^{m'} \tag{5.3}$$

or

$$\dot{\delta}_n = \dot{\delta}_c \, (\tau_u/\tau_c)^{n'} \tag{5.4}$$

where m', n', $\dot{\delta}_c$, and τ_c' are equivalent to m, n, $\dot{P}_c$, and τ_c, respectively. These parameters also appear to be temperature dependent.

The large data scatter made it difficult to analyze the effect of displacement (and loading) rate on the adhesive strength of ice specimens. The scatter may be attributed to the large variability in the ice material. Other researchers (Jellinek, 1957 b; Gold, 1978) have noted the same problem.

For the 3/8 in. diameter rod with a single lug, the displacement (or loading) rate appears to have an effect on lug bearing capacity similar

to

cu

ca

Fi

mo

wa

on

co

fu

wa

in

mo

di

th

ul

th

an

po

la

to

di

bo

th

is

to that on adfreeze bond for plain rods in frozen sand. The load-displacement curves for two displacement rates, Figure 5.5, both indicate a significantly different failure mechanism from that for plain rods shown in Figure 5.2. Initially, adhesion combined with friction and a slight mobilization of bearing action on the lug prevents slip. After adhesion was broken and partial slip had occurred, bearing action of frozen sand on the lug restrained movement of the reinforcement bar and prevented complete rupture. However, some reduction in the load may occur before full mobilization of bearing action on the lug. This "initial yield" was more noticeable at the lower rates (Figure 5.5). As the displacement increased, the load was gradually transferred to the lug until full mobilization of the ultimate lug bearing, P_u, was reached at about 5 mm displacement. This observed lug performance shows a close similarity to the bearing capacity behavior of frozen soils.

The displacement and loading rates are both plotted versus the ultimate load P_u on a logarithmic scale in Figure 5.6. The data indicate that an approximate linear relationship may exist between P_u and $\dot{\delta}$, or P_u and $\dot{P}$ on a log-log scale. Using the least-squares fitting method, a power law of the form given in Figure 5.6 may be suggested for either relationship.

The two regression lines in Figure 5.6 appear to be almost parallel to each other, implying that the same failure mechanism governs both the displacement rate and the loading rate. This fact may be the result of both lines representing data from tests on the same samples. Note that the displacement rate $\dot{\delta}_n$ at which the specimens were loaded in Figure 5.6, is believed to be close to the true rate. The $\dot{\delta}_n$ value represents

the

occ

5.1

int

Ice

to

rod

in

rat

tur

sho

a s

sma

5.7

tha

by

plo

Fig

ave

set

of

rat

may

ave

the slope of the straight line portion after the "initial yield" has occurred, while the load was still increasing on the strip chart.

5.1.2 Temperature Effect:

The temperature effect on ice adhesion, sand friction, and mechanical interaction was determined for a sand volume fraction of 64 percent. Ice and sand-ice samples were tested at temperatures ranging from -2°C to -26°C, using plain and deformed rods (with a single lug). For plain rods typical load-displacement curves plotted at different temperatures in Figure 5.7 indicate a behavior similar to those at different loading rates (Figure 5.2). The bond strength τ_u increased with colder temperatures as it did with faster loading rates. The displacement curves also show the same initial behavior characteristics of smooth bars followed by a sudden drop in the load. The ultimate (peak) load developed at very small displacements, about 0.0005 to 0.001 inches. Also note in Figure 5.7 that the "healing" effect was more pronounced at temperatures colder than -15°C. At these temperatures several cycles of failure (represented by immediate rupture) and "healing" were observed.

Using the data in Figure 5.3, the ultimate bond strength τ_u can be plotted versus temperature T for different loading rates, as shown in Figure 5.8. The loading rate indicated on each curve in Figure 5.8 is the average of all loading rates for samples tested at the same machine setting with a nominal displacement rate. For example, the average value of 157.4 lbs./min. corresponds to samples tested at a machine displacement rate of 0.0029 in./min. The data scatter for some points in Figure 5.8 may be attributed to small difference in loading rate, with a common average value, $\dot{P}_{avg.}$, indicated for each curve.

th

te

co

ba

sl

mo

te

lo

de

wh

pl

n'

Re

in

of

sh

me

pl

At

ima

rap

par

Fig

To reduce data scatter, values of τ_u interpolated (Figure 5.3) to the given average loading rate shown in Figure 5.8 were plotted versus temperature in Figure 5.9. The data in this figure appear to be more consistent and the curves are improved. The bond strength for the plain bars, Figure 5.9, show a linear relationship with temperature at the slow (5.6 lbs./min.) loading rate. At higher rates strength increased more rapidly for the warmer temperatures, down to -5°C. At colder temperatures the increase in strength was similar to that for the slower loading rates. For the temperature range between -5°C and -20°C one may deduce, using the least-squares fitting, the following linear relationship:

$$\tau_u = a' + b' \Theta \qquad (5.5)$$

where $\Theta = -T$, a' and b' are constants which depend on the loading (and displacement) rates as indicated in Figure 5.9.

The temperature effect can be extended to include parameters n and n' (defined by Equations 5.2 and 5.4) for plain rods in frozen sand. Recall that the slopes of lines in Figure 5.3 were almost equal to those in Figure 5.4 at the corresponding temperatures. Therefore, if the values of n (Table 5.3) are plotted against the corresponding values of n' as shown in Figure 5.10, one may conclude that n is the same whether displacement rate or loading rate is used. For this reason values of n (or n') are plotted against temperature in Figure 5.11 giving a nonlinear relationship. At temperatures warmer than -15°C the relationship appears to be approximated by a straight line.

In general, values of n increased as temperatures decrease. The rapid increase in n as temperature goes below -15°C occurs because the n parameter is cotangent of the angle at which the regression lines in Figures 5.3 and 5.4 are inclined from the horizontal axis. A

semi-logarithmic plot of the n parameter versus temperature, shown in Figure 5.12, gives approximately a linear relationship. The least-squares fitting method gives

$$n = \exp (1.224 + 0.0886\ \theta) \qquad (5.6)$$

(for $-26^{o}C \leq T \leq -2^{o}C$)

where $\theta = -T$. The change in n value with temperature indicates a change in the mechanism which controls failure of plain rods in frozen sand at different temperatures.

Temperature effect on ice adhesive behavior was generally similar to that observed for sand-ice material in Figure 5.7. More data scatter was noted, as compared to the frozen sand, when the ultimate ice adhesive strength was plotted against temperature as shown in Figure 5.13. Sensitivity of ice adhesion to the same minor factors, mentioned earlier, appears to be the main cause of scatter (Jellinek, 1967; Barns et al., 1971; Gold, 1978). The data trend shown in Figure 5.13, despite the noticeable scatter, indicates an almost linear increase of adhesive strength with colder temperatures. This statement may be limited to temperatures in the range of $-5^{o}C$ to $-15^{o}C$. There was no data above $-5^{o}C$ and below $-15^{o}C$ the scatter was too large to give a reliable conclusion. The line segment shown in Figure 5.13 with dashed lines indicates limitations of the results. The linear relationship (solid line) given in the figure was obtained using the least-squares fitting, where $\theta = -T$.

The temperature influence on lug behavior appears to be similar to that for the displacement rate effect. Pullout sand-ice samples were tested at different temperatures, using a plain rod with a 1/8 in. height lug. Typical load-displacement curves are plotted in Figure 5.14. At low

te

le

in

in

re

mo

in

lo

wi

wa

po

to

re

(F

90

se

5.

fr

pl

th

we

Th

co

ba

temperatures, below -15°C, the load reduction due to "initial yield" was less noticeable than at warmer temperatures. Only a reduced rate of load increase was observed below -15°C. The curves generally show the same initial behavior characteristics as for plain bars, followed by a drop or reduced rate of load increase. Additional lug displacement continues to mobilize frictional and dilatancy strength components of the frozen sand in front of the lug leading to increased pullout loads. The ultimate load P_u, plotted against temperature in Figure 5.15, showed a linear increase with decrease in temperature at the given displacement rate. No adjustment was required to P_u values, since displacement rates for individual data points was close to the average displacement rate, $\dot{\delta}_{avg}$, for all points.

The "initial yield" loads, designated P_{iy} in Figure 5.14, also appear to vary with temperature. The data in Figure 5.15 show a nonlinear relationship between P_{iy} and T. The temperature effect on other lug shapes (Figures 3.2 b and c) was also considered for comparison with the present 90°-lug shape. Further discussion on this aspect will be made in a later section.

5.1.3 Bar Size and Sample Height Effects:

Experimental data presented in previous sections were based on frozen specimens 6 in. in diameter by 6 in. high with a 5/8 in. diameter plain rod. The diameter of all bars with lugs was 3/8 in. Starting with the effect of rod size on bond strength of plain bars, four bar diameters were selected for pull-out tests; 3/32 in., 3/16 in., 3/8 in., and 5/8 in. The tests were carried out at two temperatures; -10°C and -20°C, for comparative purposes. Note that all tests on plain rods, regardless of bar size, sample size or temperature, showed the same load-displacement

ch

di

in

ra

fo

al

al

re

ot

th

th

di

th

di

ca

po

(F

at

po

on

th

da

at

characteristics as summarized in Figures 5.2 and 5.7. Data from tests on different bar sizes, summarized in Figure 5.16, show a nonlinear increase in bond strength with increase in rod diameter, d. The dimensionless ration d/H, where H is the sample height, provided a convenient number for expressing the bar size effect on the bond strength. This ratio may also be related to the bar stiffness relative to the total load applied along a certain height H.

Data points with question marks in Figure 5.16 are those doubtful results caused by possible leakage of coolant fluid into the sample, or other equipment problems. For rod sizes larger than 3/8 in. (Figure 5.16) the rate of strength increase has decreased. There was some increase in the 5/8 in. rod strength (d/H = 10.4 percent) over that of the 3/8 in. diameter rod (d/H = 6.25 percent). When tested at different temperatures, these two rod diameters showed similar strengths (Figure 5.17). The difference in strengths was consistently small at all temperatures and can be neglected in comparison to the experimental scatter for some data points.

Plotting the data of Figure 5.16 on a semi-logarithmic scale (Figure 5.18) suggests a linear relationship between the ratio d/H and τ_u at both temperatures. Note that the colder temperature, -20°C, corresponds to a higher rate of strength increase with increase in d/H. Based on linear regression analysis two empirical expressions were deduced for the two temperatures as given in Figure 5.18. These equations represent data within the range of 2 percent < d/H < 10 percent.

The effect of varying sample height on bond strength of frozen sand, at -10°C, has been considered for two bar diameters; 3/8 in. and 5/8 in.

Te
sh
Th

5.

ti
wi
si
Th
3/
th
th
3/
Th
st
in

fo
we
cu
be
yi
bo
on
t
be

Test results are summarized in Figure 5.19 for both bar sizes. The data show that sample height appears to have a small effect on bond strength. The strength increased slightly as height was increased from 1 to 6 inches.

5.1.4 Lug Size and Shape Effects:

A 90 -lug with different heights was welded to each of three identical plain, 3/8 in. diameter, cold-rolled steel rods. A fourth rod, with no lugs (h = 0), permitted measurements to be made on four lug sizes. Tests were conducted at -10°C and -20°C for comparative purposes. The load-displacement curves for lug heights of 0, 1/16 in., 2/16 in., and 3/16 in., plotted in Figure 5.20, all show a typical behavior except for the plain rod (with no lugs). The latter showed a significant drop in the load after bond due to adhesion and friction was broken. A standard 3/8 in. diameter deformed bar was also tested in frozen sand at -10°C. The hot-rolled steel rod (usually more brittle than the cold-rolled steel) has lugs spaced at 0.3125 in. with equivalent lug height of 1/64 inch.

It was anticipated that the load would exceed the equipment capacity for a 6 in. sample height with standard deformed bar. Therefore, tests were carried out on sample heights of 2 and 3 inches. The load-displacement curves for these two samples, presented in Figure 5.21, show a different behavior from those in Figure 5.20. Generally, there was an "initial yield " as for other lugs, caused by rupture of adhesive and frictional bond, followed by an increase in the load as bearing forces were mobilized on the lugs. After a peak load was achieved, the load decreased monotonically with additional displacement as shown in Figure 5.21. This behavior appears to be more dependent on the lug height and spacing than

on the number of lugs in each sample. For comparison, the displacement curve for a plain rod is also shown in Figure 5.21.

The ultimate load P_u is plotted versus the ratio of lug area A_l to the rod cross-sectional area A_r in Figure 5.22 for all lug sizes. This ratio appears to give a more consistent variation of load than does the lug height. Although the relationship shown in Figure 5.22, for both temperatures, may not be linear, they can be reasonably approximated by a straight line. The small data scatter with large loads suggests good agreement between tests. It was convenient to represent two least-squares regression lines in Figure 5.22 by the linear relationships given in the figure for each temperature. The data points indicated by question marks in Figure 5.22 were not included in the regression analysis. These data are doubtful due to possible leakage of anti-freeze coolant into the sample. The two points indicated for a standard deformed bar were calculated as if they were a single lug, using the data from Figure 5.21. The method of calculation will be explained in Chapter VI. Since these two points are nearly identical with each other, and consistent with the general trend of the other data, they were included in the regression analysis.

Changing the lug shape from a 90 degree angle, Figure 3.2 b, to a 45 degree angle, Figure 3.2 c, did not appear to have a significant effect on the experimental results. Typical load-displacement curves for both types (Figure 5.23) show an almost similar behavior, although some relatively minor differences may be noted. These differences were not repeated when the two types are compared at several temperatures in Figure 5.24. For practical purposes, the ultimate loads, P_u, for both lug

shapes are close enough to be considered equal.

The same conclusion may be drawn for the "initial yield" loads, P_{iy} shown in Figure 5.24. Generally, an almost linear variation of ultimate loads, P_u, with temperature may be noted. The linear relationship shown in Figure 5.24 can be considered applicable to both lug shapes for temperatures ranging from -2^oC to -20^oC. The "initial yield" loads P_{iy} appear to change rapidly in a non-linear fashion at temperatures above -2^oC. Below -2^oC the loads appear to increase almost linearly with colder temperatures. An empirical least-squares equation of the form given in Figure 5.24 appears to be applicable to both lug shapes for temperatures ranging from -2^oC to -20^oC.

5.1.5 Bar Surface Roughness:

The terms smooth and rough are often used to describe a certain surface texture. Surface texture is considered as those aspects of fine surface topography, or small-scale irregularities, that might be neglected in comparison with any measurable lug height. Smoothness and roughness are relative terms that have not yet been well classified or precisely defined. Besides, there are no sub-divisions (or terms) to identify the intermediate conditions between the two limits of rough and smooth surfaces. These two characteristics depend to a large extent on the degree of magnification to which the surface is exposed. At a higher magnification there are greater irregularities, no matter how smooth the surface appears to the naked eye.

Several roughness criteria have been suggested in the literature by different authors. Each criterion appears to have its merits, and requires a certain measurement technique. The one favored in this

st

wh

to

va

ac

(8

fo

He

de

Ch

gr

ch

ea

ch

5.

do

su

st

di

fa

th

wi

study is the "roughness factor" ρ, defined by Wright (1955) as follows:

$$\rho = \frac{L_r - L_t}{L_t} \times 100 \qquad (5.7)$$

where L_r = length of the "roughness line" in Figure 5.25, and L_t = total length of the standard chords, L_c, forming the "unevenness line."

From Figure 5.25, note that as the chord length L_c decreases the value of L_t increases when the "unevenness line" comes closer to the actual surface. However, Wright (1955) tried different chord lengths (8 cm, 4 cm, 1 cm, 1/2 cm, 1/4 and 1/8 cm) and compared the value of L_t for each one with that of a series of four 8 cm chords, i.e. L_t = 32 cm. He recommended a standard chord 8 cm in length. Four standard chords are desired, whenever possible, to give L_t = 32 cm as shown in Figure 5.25.

In this study the profilometer and the DC recorder described in Chapter IV were used for measuring roughness of three steel surfaces; ground-finished, cold-rolled, and shot-blasted surfaces. The strip chart recorder output for each surface type is shown in Figure 5.26. For each surface represented in this figure, a single 8 cm standard chord was chosen for practical reasons, hence a value of 8 cm for L_t in Equation 5.7. Note that the chord length of 8 cm, measured on the strip chart, does not represent the actual tracer distance travelled on the steel surface. The chord length, and the "roughness line," both depend on the strip chart movement per unit of time, i.e. chart speed which was different from that of the tracer on the actual surface. The roughness factor ρ is a relative number which may be used only for discriminating the three surfaces. Tests were also carried out on three bars, each with a 45°-lug but having different surface roughnesses; ground-finished

cold-rolled, and shot-blasted as for bars with no lugs.

The load-displacement curves for the rods with no lugs (Figure 5.27) clearly indicate that the shot-blasted surface with the highest roughness factor) showed the highest ultimate load. The residual load P_r for this surface was also the highest compared to the other two surfaces. The ultimate loads are plotted versus roughness factor on a logarithmic scale in Figure 5.28. Since the data in this figure are almost linear, they were approximated by a straight line to give the power law given in Figure 5.28. Consideration of lug height as part of the roughness definition will be discussed in Chapter VI.

5.1.6 Water Impurities and Sand Concentration:

The effect of water impurities on the adfreeze bond strength of ice and frozen sand materials was included to provide a basis for comparison. The initial objective was to evaluate the contribution of ice adhesion to the total bond strength of frozen sand to plain steel rods. Samples of crushed ice saturated with distilled water, prepared and tested at several temperatures, provided a polycrystalline structure similar to the ice which forms between sand particles. The crushed ice prepared from ordinary tap water, contained about 450 parts per million (ppm) in hardness as calcium carbonates.

The experimental results for snow ice (distilled water), crushed ice (tap water), and ice layers (distilled water) are summarized in Figure 5.29. Data scatter makes comparisons difficult. Bands indicated by the lines show that water frozen in layers has a significantly lower strength as compared to crushed ice. The effect of bar size on bond strength has been neglected based on data shown in Figure 5.17.

Ice structure and water impurities represent the only difference between the three ice types shown in Figure 5.29. To separate the effect of ice structure from that of water impurities, several samples of fresh snow, saturated with distilled water, were frozen and tested. Test results for Ice (3) shown in Figure 5.29 appear to give the highest bond strengths. Comparing Ice (1) with Ice (3) only on the basis of structure and ignoring minor difference in water impurities, one may conclude that the polycrystalline ice possesses a higher adfreeze bond strength than monocrystalline ice. A comparison of Ice (2) with Ice (3), neglecting differences due to ice grain size, shows that water impurities reduce the ice adfreeze bond strength. To verify this conclusion, several frozen sand samples were fully saturated with tap water during preparation and were tested. Test results are compared with those from tests on samples saturated with distilled water in Figure 5.30. The data clearly indicate the effect of water impurities on bond strength of frozen sand to plain rods.

Constant displacement rate bond tests were also carried out on samples with different sand concentrations. Preparation of samples with a sand fraction less than 59% (by volume) was described in Chapter III. Test results, plotted in Figure 5.31, showed that the range in which strength varied significantly is limited to a sand concentration of 45 percent to 64 percent sand by volume. This conclusion has important implications relative to design and construction procedures for friction piles in permafrost. It is believed that the sand concentration in most naturally and artifically frozen soils would not fall below about 40 percent soil by volume. In addition, the scatter in test results for samples with $v_s < 45$ percent was large enough so that the bond strength

was not clearly defined.

5.2 Constant Stress (Creep) Tests:

In this part of the study, pull-out specimens were tested by applying a constant load while continuously monitoring the displacement until either failure occurred or the equipment displacement limit was exceeded. Most samples were tested by a step loading procedure. Each load increment was maintained for a time long enough to achieve a steady-state displacement rate (secondary creep). The effects of load, temperature, lug size and position, sample diameter, and sand concentration on the pull-out loads are considered in this section. Physical properties of all ice and frozen sand samples tested under constant load are listed in Table 5.4. Test results on these samples are summarized in Table 5.5.

5.2.1 Load Effect:

The data from Section 5.1 permitted a preliminary prediction of the initial load increment to be applied to each sample. Tests on plain rods did not show, in general, a clear indication of the actual creep behavior for the small displacements due to equipment limitations. The first four samples failed before any precise measurement of the creep displacement could be taken under each step loading. Transducer limitations ± 0.0005 in. prevented more accurate measurements for the small displacements associated with creep for the ice adhesion component of adfreeze bond. The failure displacement was often too small to be precisely measured with the available recorder at its maximum sensitivity.

However, some data was acquired by running additional tests on specimens with plain rods. These data were, in most cases, obtained on

the basis of visual judgement using a magnifying lense to enlarge the stylus movement on the strip chart. Typical creep curves for plain rods, in sand-ice specimens tested at -10°C, are shown in Figure 5.32 (a and b). For sample number CS-29, Figure 5.32 (a), an initial load increment of 250 lbs. did not appear to achieve the secondary creep stage. A second load increment, which brought the total load to 530 lbs., was then applied to the specimen. This load appeared to cause tertiary creep failure almost immediately in the sample. The duplicate sample, number CS-30 in Figure 5.32 (b), was tested under loads as indicated on the creep curves.

The displacements plotted versus time in both figures, were close to the actual values measured during the load application. The creep displacement rate $\dot{\delta}^c$ was defined as the slope of the straight line portion of each curve in Figure 5.32 (a and b). Data points with the large scatter, in this figure on plain rods and the subsequent tests, were approximated by straight lines. The total loads are plotted versus their corresponding displacement rates on a log-log scale in Figure 5.33. The four data points appear to be consistent with each other and give a straight line relationship. Based on data summarized in Figure 5.33 it appears that the creep displacement rate of plain rods in frozen sand increases with increase in applied load according to a power law similar to that given by Equation 5.4.

For rods with lugs, the loading effect was more clearly shown in contrast to that described for plain rods. The scatter in data points was far less. A creep curve for step loading, on a 3/8 in. diameter plain rod with a 90°-lug, is shown in Figure 5.34 (a). Several points

may be featured in this figure. The creep displacements at all loading stages were large enough to be measured on the recorder with reasonable accuracy. These displacements were the result of bearing action of frozen soil on the lug. The stress history appears to have some effect in reducing (or almost eliminating) the primary creep, for loading stages following the first load increment. On the other hand, the displacement rate does not appear to be much influenced by the stress history, for the continuous loading condition. To explain this, refer to Figures 5.34 (b) and (c), both of which show creep curves for two more duplicate samples step-loaded at the same temperature (-10°C). Comparing the displacement rate of 2.53×10^{-4} in/min. for the third load increment (P = 2780 lbs.) in Figure 5.34 (a) with that of 2.5×10^{-4} in./min. for the first load increment (same total load, P = 2780 lbs.) in Figure 5.34 (b), the small difference may be due to interpretations from the plot. Also, the same comparison would hold for the displacement rates corresponding to the last load (P = 3560 lbs.) in Figure 5.34 (b) and to the first load (P = 3560 lbs.) in Figure 5.34 (c), respectively. The difference of 1.7×10^{-4} in./min. (about 17 percent) may, again, be considered within a possible experimental scatter.

Tests on other duplicate samples, Table 5.5, confirmed the same behavior as shown for the previous three samples. However, when the sample was unloaded, the creep rate appeared to be far more influenced by the stress history than in the loading case. Sample CS-18 was step-loaded from 1220 lbs. to 2380 lbs. as shown in Figure 5.35. After that, and before total failure, the sample was unloaded back to 2100 lbs., 1540 lbs., and to the initial load increment of 1220 lbs. As shown in

Figure 5.35, only the 2100 lbs. unloading stage showed some creep at a constant rate of 4.25 X 10^{-5}in./min., which was reasonably close to the 5.09 X 10^{-5} in./min. value for the loading stage.

When the sample was unloaded from 2100 lbs. to 1220 lbs. in two steps, the final displacement remained almost constant with very negligible decrease after 22 hours. This behavior may be attributed to densification in front of the lug during the loading stages. It was also possible that the 22 hrs., of unloading from 2100 lbs. to 1220 lbs., may not have been long enough for the sample to reach complete recovery, and then to start creeping again. Had the recovery occurred, the creep rates then would have, probably, been slightly less than the corresponding rates of the loading stages. Creep curves for other duplicate samples were also plotted, with the creep rates summarized in Table 5.5. Creep data for these samples are given in Appendix B.

Using the data in Table 5.5, the total load P applied at each stage can be plotted against its corresponding creep rate $\dot{\delta}^c$ on a log-log scale, as shown in Figure 5.36. A linear trend on this plot describes the creep behavior, at least within the range of experimental data. A straight line was fitted to the data points, using the least-square analysis, and the empirical power law indicated in Figure 5.36 can be written. Note that the regression line in Figure 5.36 is ended with dashed lines as shown, due to the limited data available at both ends.

5.2.2 Temperature Effects:

The temperature effect has been considered on a 5/8 in. diameter plain rod, and on a 3/8 in. diameter rod with a single lug, both in frozen sand. A clear conclusion, again, can not be drawn for the plain

rod samples, because of difficulty with precise measurement of very small displacements. Three different temperatures; -6°C, -10°C, and -15°C, were selected for comparison. At each temperature two duplicate samples with the same plain rod (5/8 in. in diameter) were step-loaded until failure.

As observed for the two samples tested at -10°C (Figures 5.32 a and b) creep curves for step loading on samples at other temperatures showed the same behavior. Figures 5.37 (a) and (b) show a similar behavior at both temperatures with relatively small displacements (less than 0.002 in.) for all loading stages which was followed by a sudden rupture. The last segments of both curves appear to represent tertiary creep. Before failure, the colder temperature, -15°C, reduces creep displacements at all loading stages. It also reduces the total displacement at failure; for example, compare the value of 0.004 in. for P = 1040 lbs. at -15°C (Figure 5.37 b) with 0.012 in. for P = 640 lbs. at -6°C (Figure 5.37 a).

The total load P, applied at each loading stage was plotted against the corresponding displacement rate $\dot{\delta}^c$ on a log-log scale at -6°C, -10°C, and -15°C, in Figure 5.38. The data points at all temperatures show some scatter, especially at -6°C. Only two data points are plotted for -6°C, to remove any possible confusion in showing the temperature effect. For the other temperatures, -10°C and -15°C, the data are approximated by straight lines only for comparison. The general trend of these lines indicates, qualitatively, that a power law may govern the relationship between applied loads and the corresponding displacement rates. Note that other data points for -6°C may all be considered questionable, hence they were not shown in Figure 5.38. Further tests on duplicate samples did not appear worth while, because of equipment limitations for small

displacements.

The temperature effect on lug behavior remains to be covered. Identical pull-out frozen sand specimens were tested at $-2^{o}C$, $-6^{o}C$, and $-15^{o}C$. Creep curves for step loading on these samples, Figure 5.39 (a to c), showed a behavior similar to those at $-10^{o}C$ (Figures 5.34 and 5.35). The data for tests at $-2^{o}C$, $-6^{o}C$, and $-15^{o}C$ are compared to those plotted for $-10^{o}C$, in Figure 5.40. The creep displacement rates decreased at colder temperatures for a given applied load. Under small loads, the displacement rates appear to be overestimated at all temperatures. However, it is believed that when the applied load is smaller than the long-term strength, the steady-state (secondary) creep rate was not achieved within the few days available.

The data points in Figure 5.40 are approximated by a straight line for each temperature. The four lines are almost parallal to each other, implying that the failure mechanism, of bearing action on lugs, is the same at all temperatures. Assuming a linear relationship on a log-log scale also implies that a power law of the form defined in Figure 5.40, would govern the P versus $\dot{\delta}^{c}$ relationship. Since the lines were assumed parallel to each other, the parameter m in Figure 5.40 should be independent of temperature. Only the "proof" load $P_{c\theta}$ is a function of temperature. The value of $P_{c\theta}$ corresponds to an arbitrarily chosen displacement rate $\dot{\delta}_{c}$ of 5×10^{-4} in./min.

5.2.3 Lug Size and Position:

Creep pull-out tests were conducted on frozen sand specimens with 3/8 in. diameter rods having lugs heights of 1/16 in., 2/16 in., and 3/16 in. The creep behavior for different lug heights was similar to

that observed for the 2/16 in. lug height. For comparison the experimental data are summarized in Table 5.5 and are also plotted in Figure 5.41. Seven tests on duplicate samples with a 2/16 in. lug height and the corresponding data points gave a consistent linear trend as shown in Figure 5.41. Three samples with a 1/16 in. lug height and two samples with a 3/16 in. lug height were tested using step loading. No additional tests were conducted with the 3/16 in. lug height, since its maximum bearing load would exceed the equipment loading capacity.

All data plotted as straight lines in Figure 5.41. The dashed line in this figure was estimated from three data points for a creep test on a standard 3/8 in. diameter deformed bar, with lug height of 1/64 inch. The load P in Figure 5-42 was divided by 10 for transformation to a single lug load in Figure 5.41. This procedure assumes that the applied load was equally carried by all 10 lugs for the standard deformed rod in a 3 in. sample height. Although the regression lines in Figure 5.41 are not exactly parallel to each other, it appeared that the difference in slopes may have resulted from limited experimental data, especially for the 1/64 inch and 3/16 inch lug heights. The other two lines, for 1/16 in. and 2/16 in. lug heights, appear to closely parallel each other, implying that the bearing action mechanism of frozen soil on any lug size is the same.

A power law, relating the load and creep rate, was deduced for each lug size and it has the form given in Figure 5.41, where m was made the same as that for the 2/16 in. lug height, assuming that the lines are parallel. The "proof" load P_c is dependent on lug size, and its values are given in Figure 5.41.

Up to this point all lugs tested were positioned at the mid-sample

height, i.e. half-way between the loaded end and the free end of the sample such that z = H/2. The distance z equals 0 at the base plate (loaded end). The effect of possible lug interaction with the base plate on creep behavior was considered by placement of a single 2/16 in. lug at z = H/4 and z = 3H/4. The alternate lug locations were obtained by reversing the rod direction before sample preparation. Test results for these two lug positions, summarized in Table 5.5, did not show any significant difference in behavior when compared with that of the H/2 lug position shown in Figure 5.43. All data points in this figure appear to be close enough to neglect any minor differences.

The above results show that lug position does not have an important influence, if the z distance is maintained beyond a height H/4 from the base place. Since the data are consistent with each other, for all lug positions, they were included in one regression analysis in order to deduce a single empirical equation. This equation, shown in Figure 5.43, is a power law that is valid for the three lug positions.

5.2.4 Sample Diameter and Sand Concentration:

In concrete structures, a minimum cover requirement is considered necessary for development of the normal bearing action against lugs for deformed bars (Mains, 1951; Ferguson, 1966; Perry and Thompson, 1966). In pull-out tests used to evaluate the load transfer behavior a minimum cover requirement for the steel bars would seem necessary. In this investigation, the cover required to develop the bearing action on the lugs is represented by a minimum sample diameter relative to the rod size and lug height.

Three additional sample diameters; 1.938 in., 2.781 in., and 4 in. beside the 6 in. diameter were selected for this purpose. The choice of

diameters was based on availability of steel molds in the laboratory. Sample preparation depended to some extent on sample diameter but was similar to the standard procedure described in Chapter III. Creep behavior for the step loading technique on the different pull-out specimens did not differ from those mentioned earlier.

The pull-out load P is plotted against its corresponding creep rate $\dot{\delta}^c$ on a log-log scale in Figure 5.44, for tests on the different sample diameters. The influence of sample diameter appears to be more significant for diameters less than 4 inches. The loads, interpolated to creep rates of 10^{-4} in./min. and 10^{-5} in./min., are plotted in Figure 5.45 against a ratio λ defined as:

$$\lambda = (D-d)/2h \qquad (5.8)$$

where D is sample diameter, d is rod diameter, and h is lug height. This ratio is believed to be some measurement of the frozen sand cover. The load appears to increase nonlinearly as the ratio λ increases (Figure 5.45) until it reaches a value of about 13 where the load was no longer affected by sample diameter. The "critical" sample diameter corresponding to $\lambda = 13$ is about 4 in. This conclusion indicates that test results, obtained in this investigation on 6 in. diameter samples were not being affected by sample diameter.

Another factor, briefly described in Section 5.1.6 on plain rods, was sand concentration which is now considered in terms of lug behavior. All samples tested at sand fractions less than 64 percent by volume were prepared by mixing a pre-weighed quantity of dry precooled sand with dry fresh snow to give the desired sand concentration. Two samples of snow-ice (saturated with distilled water) included the zero sand fraction for

creep tests. Samples with sand fraction below 50 percent showed a different behavior from that observed for samples with 64 percent sand concentration.

Creep curves for step loading on these samples are presented in Figures 5.46 and 5.47, including the snow-ice samples. For the initial load increment of 520 lbs. note that the displacement for all of these specimens remained unchanged (almost zero reading on the recorder) for a period of time. This time period appears to be a function of the sand fraction; longer times for the lower sand concentrations. Thereafter, the displacement increased with time in the normal manner. Further discussion on this behavior is made in Chapter VI. The effect of sand fraction on lug bearing action was similar to that observed for adhesion and friction to plain rods (Figure 5.31) with constant displacement rate tests. Loads interpolated to two different creep rates; 10^{-4} in./min. and 10^{-5} in./min., using the load versus creep rate curves in Figure 5.48, showed that they vary significantly in the range of about 43 percent to 64 percent sand (by volume) as shown in Figure 5.49. In this range, frictional and dilatational strength components of frozen sand appear to be more effective. Below a sand fraction of 43 percent the change in strength was not significant.

To evaluate the amount of lug load reduction as sand fraction v_s was reduced from 64 percent to 51 percent (by volume), consider loads at selected creep rates. Loads for v_s equal to 64 percent ($P_{64\ percent}$) are plotted against loads for v_s equal to 51 percent ($P_{51\ percent}$) in Figure 5.50. An almost linear relationship between $P_{64\ percent}$ and $P_{51\ percent}$ is noted for the range of creep rates selected. This result implies

that the amount of load reduction due to decrease in sand fraction was almost constant and independent of the creep rate $\dot{\delta}^c$, at least within a range of creep rates. As shown in Figure 5.50, values of $P_{64\ percent}$ equal 1.75 times $P_{51\ percent}$, i.e. about 43 percent reduction in the loads occurred on reducing v_s from 64 percent to 51 percent.

le 5.1: Physical properties of ice, frozen sand specimens, and steel rods, for constant displacement rate tests.

ple o.	Material	Steel surface	V_s (%)	H (in.)	D (in.)	d (in.)	h (in.)
	Ice(1)*	CR**	0	5.866	5.677	5/8	0†
	"	"	0	5.750	5.875	5/8	0
	"	"	0	5.688	5.875	5/8	0
	"	"	0	5.438	5.938	5/8	0
	"	"	0	5.938	5.875	5/8	0
	"	"	0	5.938	5.969	5/8	0
	"	"	0	5.938	5.875	5/8	0
	"	"	0	6.125	5.938	5/8	0
	"	"	0	5.875	5.938	5/8	0
0	"	"	0	5.969	5.938	5/8	0
1	"	"	0	5.938	5.938	5/8	0
2	"	"	0	6.000	6.000	5/8	0
3	"	"	0	6.000	6.000	5/8	0
4	"	"	0	5.906	6.000	5/8	0
5	"	"	0	5.938	6.000	5/8	0
6	"	"	0	5.938	6.000	5/8	0
7	"	"	0	5.344	6.000	5/8	0
8	"	"	0	5.906	6.000	5/8	0
9	"	"	0	5.938	6.000	5/8	0
0	"	"	0	5.000	6.000	5/8	0
	"	"	0	6.000	6.000	5/8	0
	Ice(2)*	"	0	6.000	6.000	3/8	0
	"	"	0	6.500	6.000	3/8	0
	"	"	0	6.375	6.000	3/8	0
	"	"	0	6.125	6.000	3/8	0
	"	"	0	6.000	6.000	3/8	0
	"	"	0	6.000	6.000	3/8	0
	Ice(3)*	"	0	6.197	6.000	5/8	0
	"	"	0	6.000	6.000	5/8	0
	"	"	0	6.375	6.000	5/8	0
	"	"	0	6.375	6.000	5/8	0

(Continued)

ble 5.1: (Cont'd)

mple No.	Material	Steel surface	V_s (%)	H (in.)	D (in.)	d (in.)	h (in.)
32	Ice(3)	CR	0	6.500	6.00	5/8	0
1	FS(DW)*	CR	64.0	6.000	6.00	5/8	0
2	"	"	64.0	6.000	6.00	5/8	0
3	"	"	64.0	6.000	6.00	5/8	0
4	"	"	64.0	6.000	6.00	5/8	0
5	"	"	66.3	6.871	6.00	5/8	0
6	"	"	64.0	6.000	6.00	5/8	0
7	"	"	64.0	6.000	6.00	5/8	0
8	"	"	64.0	6.000	6.00	5/8	0
9	"	"	64.6	5.938	6.00	5/8	0
10	"	"	64.0	6.000	6.00	5/8	0
11	"	"	64.0	6.000	6.00	5/8	0
12	"	"	64.0	6.000	6.00	5/8	0
13	"	"	64.0	6.000	6.00	5/8	0
14	"	"	64.0	6.000	6.00	5/8	0
15	"	"	64.5	6.000	6.00	5/8	0
16	"	"	64.0	6.000	6.00	5/8	0
17	"	"	64.0	6.000	6.00	5/8	0
18	"	"	64.0	6.000	6.00	5/8	0
19	"	"	64.0	6.000	6.00	5/8	0
20	"	"	64.0	6.000	6.00	5/8	0
21	"	"	64.0	6.000	6.00	5/8	0
22	"	"	64.0	6.000	6.00	5/8	0
23	"	"	64.0	6.000	6.00	5/8	0
24	"	"	64.0	6.000	6.00	5/8	0
25	"	"	64.0	6.000	6.00	5/8	0
26	"	"	64.0	6.000	6.00	5/8	0
27	"	"	64.0	6.000	6.00	5/8	0
28	"	"	64.0	6.000	6.00	5/8	0
29	"	"	64.0	6.000	6.00	5/8	0
30	"	"	64.0	6.000	6.00	5/8	0
31	"	"	64.0	6.000	6.00	5/8	0
32	"	"	64.0	6.000	6.00	5/8	0
33	"	"	64.0	6.000	6.00	5/8	0
34	"	"	64.0	6.000	6.00	5/8	0
35	"	"	64.0	6.000	6.00	5/8	0
36	"	"	64.0	6.000	6.00	5/8	0
37	"	"	64.0	6.000	6.00	5/8	0
38	"	"	64.0	6.000	6.00	5/8	0
39	"	"	64.0	6.000	6.00	5/8	0
40	"	"	64.0	6.000	6.00	5/8	0
41	"	"	64.0	6.000	6.00	5/8	0
42	"	"	64.0	6.000	6.00	5/8	0
43	"	"	64.0	6.000	6.00	5/8	0
44	"	"	64.0	6.000	6.00	5/8	0
45	"	"	64.0	6.000	6.00	5/8	0
46	"	"	64.0	6.000	6.00	5/8	0
47	"	"	64.0	6.000	6.00	5/8	0
48	"	"	64.0	6.000	6.00	5/8	0
49	"	"	64.0	6.000	6.00	5/8	0
50	"	"	64.0	6.000	6.00	5/8	0
51	"	"	64.0	6.000	6.00	5/8	0
52	"	"	64.0	6.000	6.00	5/8	0
53	"	"	64.0	6.000	6.00	5/8	0
54	"	"	64.0	6.000	6.00	5/8	0
55	"	"	64.0	6.000	6.00	5/8	0
56	"	"	64.0	6.000	6.00	5/8	0
57	"	"	64.0	6.000	6.00	5/8	0
58	"	"	64.0	6.000	6.00	5/8	0
59	"	"	64.0	6.000	6.00	5/8	0
60	"	"	64.0	6.000	6.00	5/8	0
61	"	"	64.0	6.000	6.00	5/8	0
62	"	"	64.0	6.000	6.00	5/8	0
63	"	"	64.0	6.000	6.00	5/8	0
64	"	"	64.0	6.000	6.00	5/8	0
65	"	"	64.0	6.000	6.00	5/8	0
66	"	"	64.0	6.000	6.00	5/8	0
67	"	"	64.0	6.000	6.00	5/8	0
68	"	"	64.0	6.000	6.00	5/8	0
69	"	"	64.0	6.000	6.00	5/8	0
70	"	"	64.0	6.000	6.00	5/8	0
71	"	"	64.0	6.000	6.00	5/8	0
72	"	"	64.0	6.000	6.00	5/8	0
73	"	"	64.0	6.000	6.00	5/8	0
74	"	"	64.0	6.000	6.00	5/8	0
75	"	"	64.0	6.000	6.00	5/8	0
76	"	"	64.0	6.000	6.00	5/8	0
77	"	"	64.0	6.000	6.00	5/8	0
78	"	"	64.0	6.000	6.00	5/8	0
79	"	"	64.0	6.000	6.00	5/8	0
80	"	"	64.0	6.000	6.00	5/8	0
81	"	"	64.0	6.000	6.00	5/8	0
82	"	"	64.0	6.000	6.00	5/8	0
83	"	"	64.0	6.000	6.00	5/8	0
84	"	"	64.0	6.000	6.00	5/8	0
85	"	"	64.0	6.000	6.00	5/8	0
86	"	"	64.0	6.000	6.00	5/8	0
87	"	"	64.0	6.000	6.00	5/8	0
88	"	"	64.0	6.000	6.00	5/8	0
89	"	"	64.0	6.000	6.00	5/8	0
90	"	"	64.0	6.000	6.00	5/8	0
91	"	"	64.0	6.000	6.00	5/8	0
92	"	"	64.0	6.000	6.00	5/8	0
93	"	"	64.0	6.000	6.00	5/8	0
94	"	"	64.0	6.000	6.00	5/8	0
95	"	"	64.0	6.000	6.00	5/8	0
96	"	"	64.0	6.000	6.00	5/8	0
97	"	"	64.0	6.000	6.00	3/8	0
98	"	"	64.0	6.000	6.00	3/8	1/16†

(Continued)

able 5.1: (Cont'd)

ample No.	Mater-ial	Steel surface	Vs (%)	H (in.)	D (in.)	d (in.)	h (in.)
-32	FS(DW)	CR	64.0	6.00	6.00	3/8	2/16
-33	"	"	64.0	6.00	6.00	3/8	3/16
-34	"	"	64.0	6.00	6.00	3/8	3/16
-35	"	"	64.0	6.00	6.00	3/8	0
-36	"	"	64.0	6.00	6.00	3/8	1/16
-37	"	"	64.0	6.00	6.00	3/8	2/16
-38	"	"	64.0	6.00	6.00	3/8	3/16
-39	"	"	64.0	6.00	6.00	3/16	0
-40	"	"	64.0	6.00	6.00	3/32	0
-41	"	"	64.0	6.00	6.00	3/16	0
-42	"	"	64.0	6.00	6.00	3/32	0
-43	"	"	64.0	6.00	6.00	3/8	2/16
-44	"	"	64.0	6.00	6.00	3/8	2/16
-45	"	"	64.0	6.00	6.00	3/8	2/16
-46	"	"	64.0	6.00	6.00	3/8	2/16
-47	"	"	64.0	6.00	6.00	3/8	2/16
-48	"	"	64.0	6.00	6.00	3/8	2/16
-49	"	"	64.0	6.00	6.00	3/8	2/16
-50	"	"	64.0	5.00	6.00	3/8	0
-51	"	"	64.0	4.31	6.00	3/8	0
-52	"	"	64.0	6.00	6.00	3/8	0
-53	"	"	64.0	3.00	6.00	3/8	0
54	"	"	64.0	2.00	6.00	3/8	0
55	"	"	64.0	1.00	6.00	3/8	0
56	"	"	64.0	1.00	6.00	3/8	0
57	"	"	64.0	6.00	6.00	3/8	2/16
58	"	"	64.0	1.00	6.00	3/8	0
59	"	"	64.0	1.00	6.00	3/8	0
60	"	"	64.0	6.00	6.00	3/8	0
61	"	"	64.0	6.00	6.00	3/8	0
62	"	"	64.0	6.00	6.00	3/8	2/16
63	"	"	64.0	6.00	6.00	3/8	0

(Continued)

ble 5.1: (Cont'd)

mple No.	Mater-ial	Steel surface	V_s (%)	H (in.)	D (in.)	d (in.)	h (in.)
64	FS(DW)	CR	64.0	6.0	6.0	3/8	0
65	"	"	64.0	6.0	6.0	3/8	0
66	"	"	64.0	6.0	6.0	3/8	0
67	"	"	64.0	6.0	6.0	3/16	0
68	"	"	64.0	6.0	6.0	3/8	2/16
69	"	"	64.0	6.0	6.0	3/8	0
70	"	"	64.0	6.0	6.0	3/16	0
71	"	"	64.0	4.0	6.0	3/8	0
72	"	"	64.0	6.0	6.0	3/8	0
73	"	"	64.0	6.0	6.0	3/8	0
74	"	"	64.0	6.0	6.0	5/8	0
75	"	"	64.0	6.0	6.0	3/8	0
76	"	"	64.0	2.0	6.0	5/8	0
77	"	"	64.0	5.0	6.0	3/8	0
78	"	"	64.0	5.0	6.0	5/8	0
79	"	"	64.0	3.0	6.0	3/8	0
80	"	"	64.0	4.0	6.0	5/8	0
81	"	"	64.0	2.0	6.0	3/8	0
2	"	"	64.0	3.0	6.0	5/8	0
3	"	"	64.0	2.0	6.0	5/8	0
4	"	"	64.0	2.0	6.0	5/8	0
5	"	GF**	64.0	6.0	6.0	3/8	0
6	"	"	64.0	6.0	6.0	3/8	0
7	"	"	64.0	6.0	6.0	3/8	2/16 (45^o)†
8	"	SB**	64.0	6.0	6.0	3/8	0
9	"	CR	64.0	6.0	6.0	3/8	2/16 (45^o)
0	"	SB	64.0	6.0	6.0	3/8	2/16 (45^o)
	"	CR	64.0	6.0	6.0	3/8	2/16 (45^o)
	"	"	64.0	6.0	6.0	3/8	0
	"	"	64.0	6.0	6.0	3/8	2/16 (45^o)
	"	"	64.0	6.0	6.0	3/8	0
	"	"	64.0	6.0	6.0	3/8	0

(Continued)

ole 5.1: (Cont'd)

mple No.	Material	Steel surface	V_s (%)	H (in.)	D (in.)	d (in.)	h (in.)
96	FS(DW)	CR	64.0	6.00	6.0	3/8	1/8 (45°)
97	"	"	64.0	6.00	6.0	3/8	1/8 (45°)
98	"	"	64.0	2.00	6.0	5/8	0
99	"	"	64.0	4.00	6.0	5/8	0
100	"	"	64.0	3.00	6.0	5/8	0
101	"	"	64.0	5.00	6.0	5/8	0
102	"	"	64.0	6.00	6.0	5/8	0
103	"	"	64.0	2.00	6.0	5/8	0
104	"	"	64.0	0.50	6.0	5/8	0
105	"	"	64.0	5.00	6.0	5/8	0
106	"	"	64.0	2.00	6.0	5/8	0
107	"	"	64.0	5.00	6.0	5/8	0
108	"	"	64.0	3.00	6.0	5/8	0
109	"	"	64.0	6.00	6.0	5/8	0
110	"	"	64.0	4.00	6.0	5/8	0
111	"	"	64.0	5.50	6.0	3/8	0
112	"	"	64.0	5.62	6.0	3/8	0
113	"	"	64.0	6.00	6.0	3/8	0
114	"	"	64.0	6.00	6.0	3/8	0
115	FS(TW)*	"	64.0	6.00	6.0	3/8	0
116	"	"	64.0	6.00	6.0	3/8	0
117	"	"	64.0	6.00	6.0	3/8	0
118	"	"	64.0	6.00	6.0	3/8	0
119	FS(DW)	"	64.0	6.00	6.0	5/8	0
120	"	"	64.0	2.00	6.0	3/8	SDB†
121	"	"	64.0	3.00	6.0	3/8	SDB
122	"	"	64.0	6.00	6.0	3/8	1/16
123	F(SID)*	"	42.0	6.00	6.0	3/8	0
124	"	"	29.6	6.00	6.0	3/8	0
125	"	"	53.8	6.12	6.0	3/8	0
126	"	"	52.7	6.00	6.0	3/8	0

(Continued)

ble 5.1: (Cont'd)

mple No.	Material	Steel surface	Vs (%)	H (in.)	D (in.)	d (in.)	h (in.)
127	F(SID)	CR	30.3	6.0	6.0	3/8	0
128	"	"	44.2	6.0	6.0	3/8	0

Ice(1)- Ice layers (distilled water)
Ice(2)- Crushed ice (tap water) saturated with distilled water
Ice(3)- Snow ice saturated with distilled water
FS(DW)- Frozen sand (with distilled water)
FS(TW)- Frozen sand (with tap water)
F(SID)- Frozen sand (snow ice with distilled water)

CR- Cold-rolled steel surface
GF- Ground-finish steel surface
SB- Shot-blasted steel surface

Plain rods for h = 0
All 90^{o}-lugs, unless noted
(45^{o})- 45 degree lug
SDB- Standard deformed bar, with h = 1/64 in.

le 5.2: Summary of test results for constant displacement rate tests.

ple o.	T (^{o}C)	$\dot{\delta}_n$ (in./min.)	$\dot{P}$ (lbs/min)	P_{iy}† (or P_u) (lbs.)	P_u†† (or P_r) (lbs.)	δ_r ($\times 10^{-3}$ in.)
	-10.1	4.24×10^{-3}	140.0	930	190	0.90
	-15.1	4.50×10^{-3}	136.8	620	105	0.76
	-15.1	4.40×10^{-3}	130.0	607	200	1.50
	-15.1	4.90×10^{-3}	105.4	455	96	1.10
	- 6.1	*	*	*	*	*
	- 6.1	3.68×10^{-3}	89.6	112	56	0.40
	-20.0	3.90×10^{-3}	136.4	500	175	0.001
	-20.0	3.60×10^{-3}	115.7	216	130	0.28
	-10.0	3.55×10^{-3}	111.8	326	82	0.40
0	-10.1	3.32×10^{-3}	91.6	336	94	0.20
1	-10.1	3.43×10^{-3}	94.0	470	78	0.20
2	-26.1	9.00×10^{-4}	126.0	840	120	0.20
3	-26.7	4.00×10^{-3}	143.2	1480	180	0.24
4	-26.4	3.50×10^{-4}	4.9	440	320	2.00
5	-26.6	8.00×10^{-4}	22.5	990	140	0.80
6	-20.4	1.05×10^{-3}	27.0	1040	90	1.40
7	-15.5	3.52×10^{-4}	23.6	2830	200	5.70
8	-10.1	2.30×10^{-4}	28.5	890	80	0.75
9	- 6.6	not recoded	22.1	1940	300	4.40
)	-10.1	2.60×10^{-4}	26.4	1780	200	2.80
l	-20.1	6.15×10^{-4}	23.0	1740	210	0.80
?	-10.1	5.70×10^{-4}	21.6	540	30	0.20
3	-22.0	5.64×10^{-4}	20.1	624	50	0.40
	-20.0	5.10×10^{-4}	17.2	560	32	0.40
	-15.0	5.40×10^{-4}	20.0	670	40	0.10
	-6.0	5.65×10^{-4}	16.1	210	16	0.10
	- 2.0	5.80×10^{-4}	19.1	105	10	0.10
	-10.0	4.50×10^{-3}	183.5	1560	70	0.75
	-14.8	1.92×10^{-3}	233.3	1435	30	0.50
	-16.0	4.50×10^{-3}	280.0	880	50	0.25

(Continued)

ble 5.2: (Cont'd)

mple No.	T (^{o}C)	$\dot{\delta}_n$ (in./min.)	$\dot{P}$ (lbs/min)	P_{iy} (or P_u) (lbs.)	P_u (or P_r) (lbs.)	δ_r ($x10^{-3}$in.)
31	- 6.0	Fast rate	1290.0	430	Not recored	
32	-10.0	$4.61x10^{-3}$	258.0	1030	70	0.001
1	-10.0	$2.40x10^{-3}$	159.5	1075	135	0.16
2	-10.2	$5.00x10^{-4}$	32.5	1300	280	2.20
3	- 6.3	$6.97x10^{-4}$	29.7	860	400	1.60
4	-14.6	$3.67x10^{-4}$	30.7	2090	520	2.50
5	-20.0	$5.00x10^{-4}$	32.7	2810	575	1.80
6	-26.7	$6.38x10^{-4}$	37.5	2740	600	1.90
7	-26.8	$6.15x10^{-4}$	39.7	2800	450	0.80
8	-27.1	$1.32x10^{-3}$	208.7	3800	920	1.00
9	-20.0	$2.53x10^{-3}$	210.3	3260	580	0.80
10	- 6.3	$1.12x10^{-3}$	186.7	1400	200	1.80
11	-15.1	$3.86x10^{-3}$	204.6	2660	430	1.20
12	-10.0	$3.73x10^{-3}$	222.7	2450	970	2.60
13	- 6.0	$1.96x10^{-2}$	2133.3	1920	330	1.40
14	-15.2	$3.00x10^{-2}$	2033.3	3660	530	0.60
15	-10.0	$2.13x10^{-2}$	1978.8	2770	440	0.40
16	-25.6	$4.00x10^{-2}$	2210.0	4420	900	0.70
17	-20.0	$1.32x10^{-2}$	2240.0	3360	750	0.20
18	-25.0	$1.10x10^{-4}$	5.1	3440	1080	2.90
19	-10.0	$1.66x10^{-4}$	4.5	1630	1200	1.80
20	- 6.0	$1.00x10^{-4}$	4.4	720	380	0.50
21	-15.0	$1.86x10^{-4}$	6.5	2080	580	1.50
22	-20.0	$1.33x10^{-4}$	4.4	2770	1000	1.40
23	-10.0	$3.83x10^{-3}$	268.1	2480	540	1.50
24	- 2.0	$4.00x10^{-3}$	100.0	450	240	4.10
25	- 2.0	$3.71x10^{-2}$	1714.3	720	320	6.10
26	- 2.0	$8.60x10^{-5}$	2.1	210	190	3.60
27	- 2.0	$6.00x10^{-4}$	26.3	460	350	2.40
33	-20.0	$3.90x10^{-2}$	2478.3	3420	770	0.01

(Continued)

e 5.2: (Cont'd)

le	T	$\dot{\delta}_n$	$\dot{P}$	P_{iy} (or P_u)	P_u (or P_r)	δ_r
.	(^oC)	(in./min.)	(lbs/min)	(lbs.)	(lbs.)	($x10^{-3}$in.)
	-15.0	LVDT OFF	220.9	2540	660	LVDT OFF
	-10.0	$8.00x10^{-4}$	29.3	880	140	0.80
	-10.0	$5.20x10^{-4}$	29.7	1560	1040	1.20
	-10.0	$5.33x10^{-4}$	33.4	2040	1520	2.00
	-10.0	$5.82x10^{-4}$	32.0	2190	1830	2.00
	-10.0	$4.21x10^{-4}$	31.3	2320	4800	2.80
	-20.0	$6.94x10^{-4}$	138.7	1040	300	1.00
	-20.0	$5.10x10^{-4}$	32.8	1820	2660	0.01
	-20.0	$3.90x10^{-4}$	37.5	2360	3580	1.60
	-20.0	$4.10x10^{-4}$	35.8	3400	7020	0.60
	-10.0	$5.00x10^{-4}$	27.1	130	40	0.40
	-10.0	$4.32x10^{-4}$	5.3	80	20	1.20
	-20.0	$5.43x10^{-4}$	15.8	530	50	0.40
	-20.0	$4.50x10^{-4}$	7.4	152	80	0.20
	-10.0	$2.10x10^{-2}$	2220.0	2220	4320	3.00
	-10.0	$3.36x10^{-3}$	198.1	2080	4540	1.60
	-10.0	$7.00x10^{-5}$	4.8	1120	1000	2.00
	-15.0	$2.80x10^{-4}$	30.6	2080	3800	1.80
	-26.0	$5.02x10^{-4}$	33.0	2540	6080	2.00
	- 6.0	$5.70x10^{-4}$	32.4	1200	2080	2.60
	- 2.0	$3.28x10^{-4}$	17.0	440	1390	1.50
	-10.0	$5.63x10^{-4}$	28.4	610	120	0.40
	-10.0	$1.14x10^{-4}$	5.2	730	120	0.01
	-10.0	$1.40x10^{-4}$	6.3	940	140	0.01
	-10.0	$5.63x10^{-4}$	24.3	54	130	1.00
	-10.0	$6.50x10^{-4}$	20.4	224	64	0.10
	-10.0	$1.44x10^{-4}$	9.6	48	28	2.00
	-10.0	$3.00x10^{-4}$	14.4	144	64	0.16
	-10.0	$4.43x10^{-4}$	34.7	1560	2920	0.20
	-10.0	$6.00x10^{-4}$	10.4	188	40	0.40

(Continued)

le 5.2: (Cont'd)

ple o.	T (^{o}C)	$\dot{\delta}_n$ (in./min.)	$\dot{P}$ (lbs/min)	P_{iy} (or P_u) (lbs.)	P_u (or P_r) (lbs.)	δ_r ($x10^{-3}$in.)
9	-10.0	$6.80x10^{-4}$	13.7	96	40	0.16
0	-15.0	$1.25x10^{-4}$	33.8	760	200	0.10
1	-26.0	$6.31x10^{-4}$	24.1	880	400	1.00
2	-20.0	$4.65x10^{-4}$	29.0	1740	4580	0.10
3	- 2.0	$2.25x10^{-4}$	17.3	260	50	0.60
4	- 6.0	$9.50x10^{-5}$	18.2	520	100	0.30
5	-15.0	$6.31x10^{-4}$	22.6	880	220	0.10
6	-20.0	$6.47x10^{-4}$	23.9	800	320	0.40
7	-20.0	LVDT OFF	16.3	480	210	LVDT OFF
8	-20.0	$2.30x10^{-4}$	17.7	1220	4580	0.10
9	-25.4	$6.50x10^{-4}$	21.8	1060	420	0.05
0	-10.0	$5.87x10^{-4}$	12.3	344	120	0.40
1	-10.0	$6.10x10^{-4}$	19.5	495	95	6.00
2	-10.0	$5.50x10^{-4}$	12.0	520	160	0.80
3	-15.0	$4.67x10^{-4}$	25.5	1170	470	0.40
4	-20.0	*	*	*	*	*
5	- 6.0	$4.50x10^{-4}$	11.6	625	175	0.10
6	*	*	*	*	*	*
7	-10.0	$4.10x10^{-4}$	11.7	780	190	2.00
3	-10.0	*	*	*	*	*
9	-10.0	$4.75x10^{-4}$	13.7	540	140	1.40
)	-10.0	*	*	*	*	*
!	-10.0	$4.50x10^{-4}$	9.0	270	60	0.80
?	-10.0	*	*	*	*	*
3	-10.0	$3.10x10^{-4}$	6.8	290	80	0.60
:	-10.0	*	*	*	*	*
;	-10.0	$3.24x10^{-4}$	20.0	530	180	0.10
;	-10.0	$2.80x10^{-4}$	24.4	670	140	0.10
	-10.0	$5.93x10^{-4}$	23.2	2090	2730	0.40
	-10.0	$7.50x10^{-4}$	18.5	1740	730	3.20

(Continued)

e 5.2: (Cont'd)

le .	T (^{o}C)	$\dot{\delta}_n$ (in./min.)	$\dot{P}$ (lbs/min)	P_{iy} (or P_u) (lbs.)	P_u (or P_r) (lbs.)	δ_r ($\times 10^{-3}$ in.)
	-10.0	5.50×10^{-4}	25.0	1560	3380	0.10
	-10.0	5.39×10^{-4}	30.0	2160	3400	1.00
	-15.0	5.00×10^{-4}	23.0	2160	4360	1.50
	-15.0	6.25×10^{-4}	20.5	1250	280	0.80
	-20.0	5.20×10^{-4}	34.9	2720	4620	0.10
	-20.0	5.85×10^{-4}	18.0	1700	440	0.40
	-26.0	6.67×10^{-4}	22.2	1840	640	0.10
	- 6.0	5.60×10^{-4}	27.6	1380	2040	3.00
	- 2.0	5.67×10^{-4}	19.3	580	1520	4.50
	-10.0	5.73×10^{-4}	25.0	576	145	0.40
	-10.0	6.67×10^{-4}	36.9	1920	480	1.80
0	-10.0	5.60×10^{-4}	31.2	1280	290	0.80
1	-10.0	6.03×10^{-4}	44.2	3120	1220	2.00
2	-10.0	5.71×10^{-4}	41.7	3380	1180	1.50
3	-10.0	5.70×10^{-4}	28.1	980	260	2.40
4	-10.0	*	*	*	*	*
5	-10.0	*	*	*	*	*
6	-10.0	5.86×10^{-4}	25.0	576	120	1.60
7	-10.0	*	*	*	*	*
8	-10.0	5.80×10^{-4}	26.5	530	130	0.01
9	-10.0	5.00×10^{-4}	35.0	1960	480	2.00
0	-10.0	5.56×10^{-4}	28.2	500	120	0.80
1	-10.0	6.67×10^{-4}	20.0	560	40	0.50
2	-10.0	6.25×10^{-4}	21.2	640	80	0.10
3	-15.0	4.75×10^{-4}	25.2	1060	280	0.70
	-15.0	4.00×10^{-4}	25.8	1250	240	0.40
	-10.0	4.20×10^{-4}	17.3	580	30	1.00
	-10.0	4.84×10^{-4}	20.3	460	40	0.40
	-20.0	2.10×10^{-4}	24.6	1330	180	0.60
	-20.0	2.80×10^{-4}	22.0	810	170	0.10

(Continued)

Table 5.2: (Cont'd)

ample No.	T (^{o}C)	$\dot{\delta}_n$ (in./min.)	$\dot{P}$ (lbs/min)	P_{iy} (or P_u) (lbs.)	P_u (or P_r) (lbs.)	δ_r ($x10^{-3}$ in.)
-119	-10.0	$1.17x10^{-4}$	33.4	1370	240	0.90
-120	-10.0	$4.60x10^{-3}$	170.0	1420	2300	7.50
-121	-10.0	$4.50x10^{-3}$	235.0	2100	4025	4.40
-122	-10.0	$6.70x10^{-4}$	40.0	1600	1750	1.80
-123	-10.0	$8.20x10^{-4}$	22.0	375	120	0.50
-124	-10.0	$6.80x10^{-4}$	31.8	525	60	0.20
-125	-10.0	$7.001x10^{-4}$	20.8	225	75	0.10
126	-10.0	$8.40x10^{-4}$	44.0	710	145	0.40
127	- 9.9	$1.10x10^{-3}$	31.6	525	60	0.80
128	-10.0	$8.10x10^{4}$	30.0	320	40	0.50

P_{iy} for lugs, P_u for plain rods (both correspond to the small displacement δ_r)

P_u for lugs, P_r for plain rods (both at large displacements)

Data void (leakage of fluid or equipment defect)

ble 5.3: Temperature effect on the parameters used in Equations 5.1 to 5.4.

C)	τ_c* (psi)	m	n	τ_c'** (psi)	m'	n'
	16	0.1945	5.40	17	0.2220	4.50
	48	0.1585	6.31	62	0.1852	5.40
	113	0.1087	10.40	137	0.1404	9.35
	145	0.1000	11.40	167	0.1016	10.60
	213	0.0400	23.00	240	0.0436	22.90
	270	0.0314	31.00	308	0.0314	31.00

nterpolated from Figure 5.3 for $\dot{P}_c$ = 1 lb./min.

nterpolated from Figure 5.4 for $\dot{\delta}_c$ = 10^{-4} in./min.

e 5.4: Physical properties of ice, frozen sand specimens, and steel rods used in constant load (creep) tests. Sample height H = 6 in. and cold-rolled steel rods were used for all specimens.

le .	Material	V_s (%)	D (in.)	d (in.)	h (in.)	z (in.)
	Ice(1)*	0	6.00	3/8	1/8**	3.0†
	"	0	6.00	3/8	1/8	3.0
	FS(DW)*	64.0	6.00	5/8	0**	NA
	"	64.0	6.00	5/8	0	"
	"	64.0	6.00	5/8	0	"
	"	64.0	6.00	5/8	0	"
	"	64.0	6.00	3/8	2/16	3.0
	"	64.0	6.00	3/8	2/16	3.0
	"	64.0	6.00	3/8	2/16	3.0
	"	64.0	6.00	3/8	2/16	3.0
	"	64.0	6.00	3/8	1/16	3.0
0	"	64.0	6.00	3/8	2/16	3.0
1	"	64.0	6.00	3/8	3/16	3.0
2	"	64.0	6.00	3/8	2/16	3.0
3	"	64.0	6.00	3/8	1/16	3.0
4	"	64.0	6.00	3/8	2/16	3.0
5	"	64.0	6.00	3/8	1/16	3.0
6	"	64.0	6.00	3/8	2/16	3.0
7	"	64.0	6.00	3/8	3/16	3.0
3	"	64.0	6.00	3/8	2/16	3.0
9	"	64.0	6.00	3/8	1/16	3.0
)	"	64.0	6.00	3/8	2/16	4.5
:	"	64.0	1.938	3/8	2/16	3.0
?	"	64.0	6.00	3/8	2/16	4.5
;	"	64.0	1.938	3/8	2/16	3.0
	"	64.0	6.00	3/8	2/16	3.0
	"	64.0	1.938	3/8	2/16	3.0
	"	64.0	6.00	3/8	2/16	1.5
	"	64.0	2.781	3/8	2/16	3.0

(Continued)

Table 5.4: (Cont'd)

Sample No.	Material	V_s (%)	D (in.)	d (in.)	h (in.)	z (in.)
CS-28	FS(DW)	64.0	4.00	3/8	1/8	3.0
CS-29	"	64.0	6.00	5/8	0	NA
CS-30	"	64.0	6.00	5/8	0	"
CS-31	"	64.0	6.00	5/8	0	"
CS-32	"	64.0	6.00	5/8	0	"
CS-33	"	64.0	6.00	5/8	0	"
CS-34	"	64.0	6.00	5/8	0	"
CS-35	"	64.0	6.00	5/8	0	"
CS-36	F(SID)*	44.6	6.00	3/8	1/8	3.0
CS-37	"	32.3	6.00	3/8	1/8	3.0
CS-38	"	51.6	6.00	3/8	1/8	3.0
CS-39	"	48.6	6.00	3/8	1/8	3.0
CS-40	"	52.8	6.00	3/8	1/8	3.0
S-41	"	17.5	6.00	3/8	1/8	3.0
S-42	FS(DW)	64.0	1.938	3/8	1/8	3.0
S-43	"	64.0	4.00	3/8	1/8	3.0
S-44	"	64.0	6.00	3/8	SDB*	NA
S-45	"	64.0	6.00	3/8	1/8	3.0

See Table 5.1 for abbreviations.

* All 90 degree lugs, h = 0 for plain rods.

Lug position from reaction base plate

A-Not applicable

Note: For sample CS-44, H = 3 in.)

Table 5.5: Summary of test results for constant load (creep) tests.

Sample No.	T (^{o}C)	P (lbs.)	$\dot{\varepsilon}_c$ (in./min.)
CI-1	-10.0	520	2.88×10^{-3}
CI-2	-10.0	200	2.70×10^{-7}
		280	62.5×10^{-7}
		360	6.25×10^{-7}
		440	2.08×10^{-6}
		520	4.34×10^{-6}
CS-1	-10.0	1420	TC
CS-2	-10.0	1040	TC
CS-3	-10.0	750	4.41×10^{-6}
		910	2.00×10^{-5}
CS-4	-10.0	520	TC
CS-5	-10.0	2300	1.00×10^{-4}
		2500	1.68×10^{-4}
		2780	2.58×10^{-4}
		3020	3.75×10^{-4}
		3180	4.46×10^{-4}
CS-6	-10.0	2800	2.50×10^{-4}
		3080	4.36×10^{-4}
		3320	6.96×10^{-4}
		3560	8.30×10^{-4}
CS-7	-10.0	3560	1.00×10^{-3}
		3780	1.66×10^{-3}
		4000	2.00×10^{-3}
CS-8	-10.0	4000	2.86×10^{-3}
CS-9	-10.0	1400	4.67×10^{-4}
		1560	7.00×10^{-4}
		1800	1.04×10^{-3}
		2080	1.66×10^{-3}

(Continued)

Table 5.5: (cont'd)

Sample No.	T (^{o}C)	P (lbs.)	$\dot{\delta}_c$ (in./min.)
CS-10	-10.0	1580	8.33×10^{-5}
		1860	9.38×10^{-5}
		2140	1.33×10^{-4}
		2300	1.31×10^{-4}
CS-11	-10.0	2000	1.61×10^{-5}
		2480	4.05×10^{-5}
		3040	6.71×10^{-5}
		3600	9.07×10^{-5}
		4160	2.04×10^{-4}
CS-12	-10.0	4000	LVDT OFF
CS-13	-10.0	850	8.00×10^{-5}
		1200	2.12×10^{-4}
		1560	5.89×10^{-4}
		2600	7.18×10^{-3}
CS-14	-10.0	4500	9.75×10^{-3}
CS-15	-10.0	3000	2.50×10^{-2}
CS-16	-15.0	1560	1.88×10^{-5}
		2000	2.75×10^{-5}
		2500	5.39×10^{-5}
		3000	1.06×10^{-4}
		3500	2.45×10^{-4}
		4000	7.00×10^{-4}
CS-17	-10.0	2500	8.00×10^{-5}
		3500	1.00×10^{-4}
		2500 U	1.41×10^{-5}
CS-18	-10.1	1220	1.82×10^{-5}
		1540	1.77×10^{-5}
		1820	3.64×10^{-5}

(Continued)

Table 5.5: (cont'd)

Sample No.	T (^{o}C)	P (lbs.)	$\dot{\delta}^{c}$ (in./min.)
CS-18	-10.1	2100	5.09×10^{-5}
		2380	6.94×10^{-5}
		2100 U	4.25×10^{-5}
		1540 U	Negative value
		1200 U	0
CS-19	-10.0	1500	9.27×10^{-4}
CS-20	-10.0	1500	4.58×10^{-5}
		2000	1.11×10^{-4}
		2500	3.85×10^{-4}
		3000	9.30×10^{-4}
CS-21	-10.0	1000	3.20×10^{-5}
		1740	2.92×10^{-4}
CS-22	-10.0	1500	4.13×10^{-5}
		2000	6.25×10^{-5}
		2500	2.00×10^{-4}
		3000	5.22×10^{-4}
		3500	1.28×10^{-3}
CS-23	-10.0	1500	2.83×10^{-4}
CS-24	- 6.0	1020	1.97×10^{-5}
		1500	4.57×10^{-5}
		1980	1.21×10^{-4}
		2500	5.40×10^{-4}
		3000	2.88×10^{-3}
CS-25	-10.0	1500	1.69×10^{-4}
		1980	1.00×10^{-3}
CS-26	-10.0	1020	3.89×10^{-6}
		1500	3.75×10^{-5}

(Continued)

Table 5.5: (Cont'd)

Sample No.	T (^{o}C)	P (lbs.)	$\dot{\delta}_c$ (in./min.)
CS-26	-10.0	1940	3.75×10^{-5}
		2500	1.94×10^{-4}
CS-27	-10.0	1020	4.55×10^{-6}
		1500	1.13×10^{-5}
		2020	1.20×10^{-4}
		2500	4.64×10^{-4}
		3000	TC
CS-28	-10.0	1020	7.57×10^{-7}
		1500	2.96×10^{-6}
		1980	6.43×10^{-6}
		2500	2.30×10^{-5}
		3000	2.02×10^{-4}
CS-29	-10.0	250	0
		530	4.50×10^{-6}
CS-30	-10.0	250	5.71×10^{-7}
		410	2.05×10^{-6}
		570	4.93×10^{-6}
		730	TC
CS-31	-10.0	160	$\simeq 0$
		240	$\simeq 0$
		360	$\simeq 0$
		480	$\simeq 0$
		600	$\simeq 0$
		720	$\simeq 0$
		840	$\simeq 0$
		960	$\simeq 0$
		1080	TC

(Continued)

Table 5.5: (Cont'd)

Sample No.	T (^{o}C)	P (lbs.)	$\dot{\delta}_c$ (in./min.)
CS-32	-15.1	240	PC
		400	≃0
		600	≃0
		760	≃0
		900	≃0
		1080	≃0
		1280	TC
CS-33	-15.1	400	1.10×10^{-7}
		560	2.44×10^{-7}
		720	2.32×10^{-7}
		880	8.33×10^{-7}
		1040	4.96×10^{-6}
CS-34	- 6.1	160	4.36×10^{-7}
		280	4.10×10^{-7}
		400	1.25×10^{-6}
		520	5.00×10^{-7}
		640	TC
CS-35	- 6.0	280	7.58×10^{-7}
		400	5.80×10^{-7}
		520	1.00×10^{-6}
		640	8.30×10^{-7}
		720	1.00×10^{-6}
		800	9.60×10^{-7}
		920	2.20×10^{-6}
		1040	TC
CS-36	-10.0	520	1.66×10^{-5}
		1080	2.26×10^{-4}
		1560	1.22×10^{-3}

(Continued)

able 5.5: (Cont'd)

ample No.	T (^{o}C)	P (lbs.)	$\dot{\delta}_c$ (in./min.)
S-37	-10.1	520	7.05×10^{-5}
		1080	1.68×10^{-3}
S-38	-10.0	520	8.50×10^{-6}
		1080	2.44×10^{-5}
		1520	2.68×10^{-4}
		1980	TC
S-39	-10.0	520	9.52×10^{-6}
		1080	2.12×10^{-4}
		1560	1.25×10^{-3}
S-40	-10.0	520	5.38×10^{-6}
		720	7.00×10^{-6}
		1080	7.37×10^{-5}
		1240	7.30×10^{-5}
		1560	2.85×10^{-4}
S-41	-10.0	520	21.0×10^{-4}
		600	5.00×10^{-4}
		680	1.29×10^{-3}
S-42	-10.0	520	2.70×10^{-6}
		720	4.98×10^{-6}
		1080	2.80×10^{-5}
		1240	3.57×10^{-5}
		1560	8.29×10^{-5}
		1840	2.50×10^{-4}
		2120	1.28×10^{-3}
-43	-10.0	1080	1.27×10^{-5}
		1440	2.83×10^{-5}
		1840	5.00×10^{-5}
		2200	1.05×10^{-4}

(Continued)

able 5.5: (Cont'd)

ample No.	T (^{o}C)	P (lbs.)	$\dot{\delta}^{c}$ (in./min.)
S-43	-10.0	2560	2.35×10^{-4}
		2840	5.62×10^{-4}
S-44	-10.0	1080	5.60×10^{-6}
		1560	9.00×10^{-6}
		1980	3.60×10^{-5}
		2560	TC
S-45	- 2.0	520	1.10×10^{-5}
		800	2.70×10^{-5}
		1160	1.28×10^{-4}
		1560	1.04×10^{-3}

C Primary creep
C Tertiary creep
Unloading

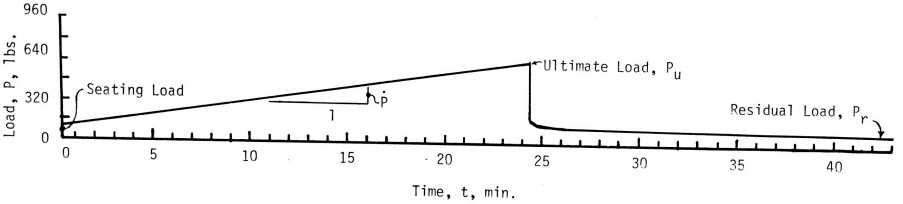

Figure 5.1: Typical strip chart load and displacement records for plain steel rods in ice and sand-ice specimens.

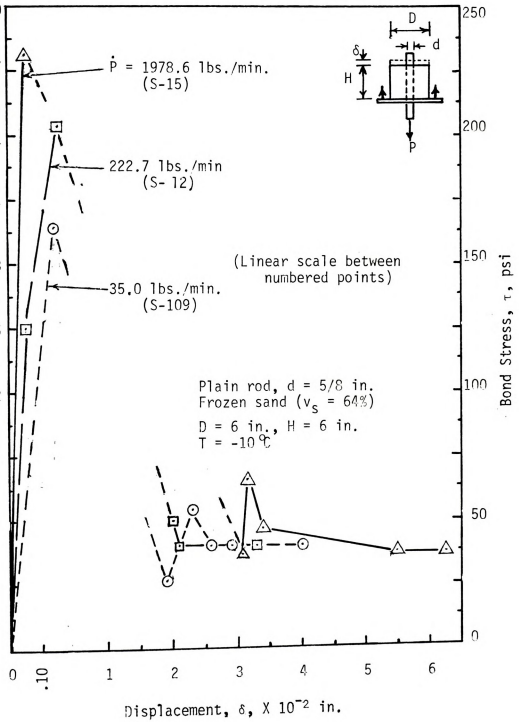

5.2: Typical load-displacement curves at different loading rates for the bond of frozen sand (v_s = 64%) to a plain steel rod.

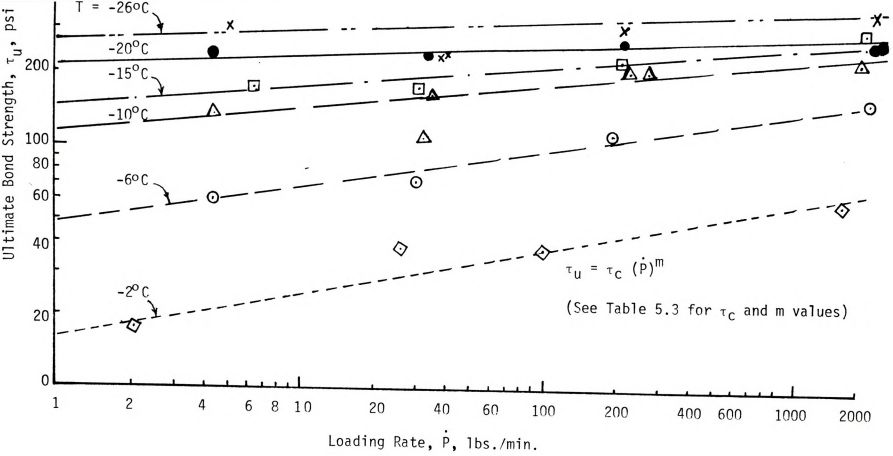

Figure 5.3: Effect of loading rate on the bond strength of frozen sand (v_s = 64%) to a 5/8 in. diameter plain steel rod at different temperatures.

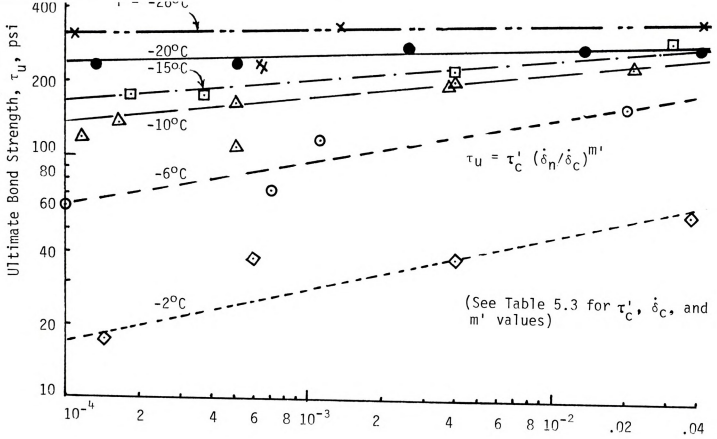

Figure 5.4: Effect of nominal displacement rate on the bond strength of frozen sand (v_s = 64%) to a 5/8 in. diameter plain rod.

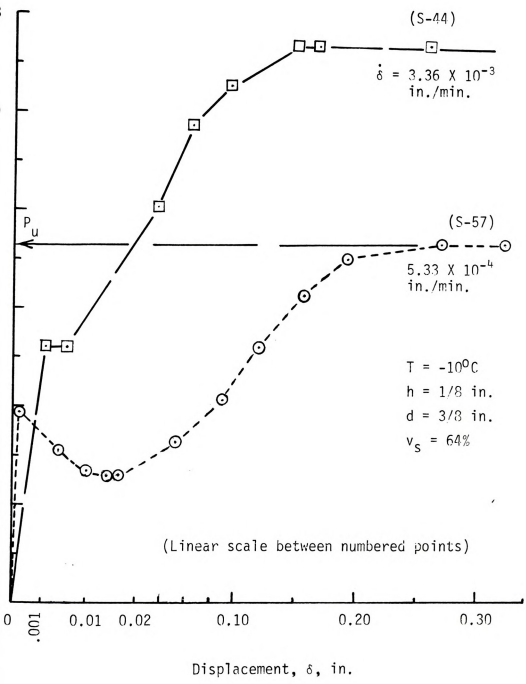

ure 5.5: Typical load-displacement curves at different displacement rates for a plain rod with a single lug in frozen sand (v_s = 64%).

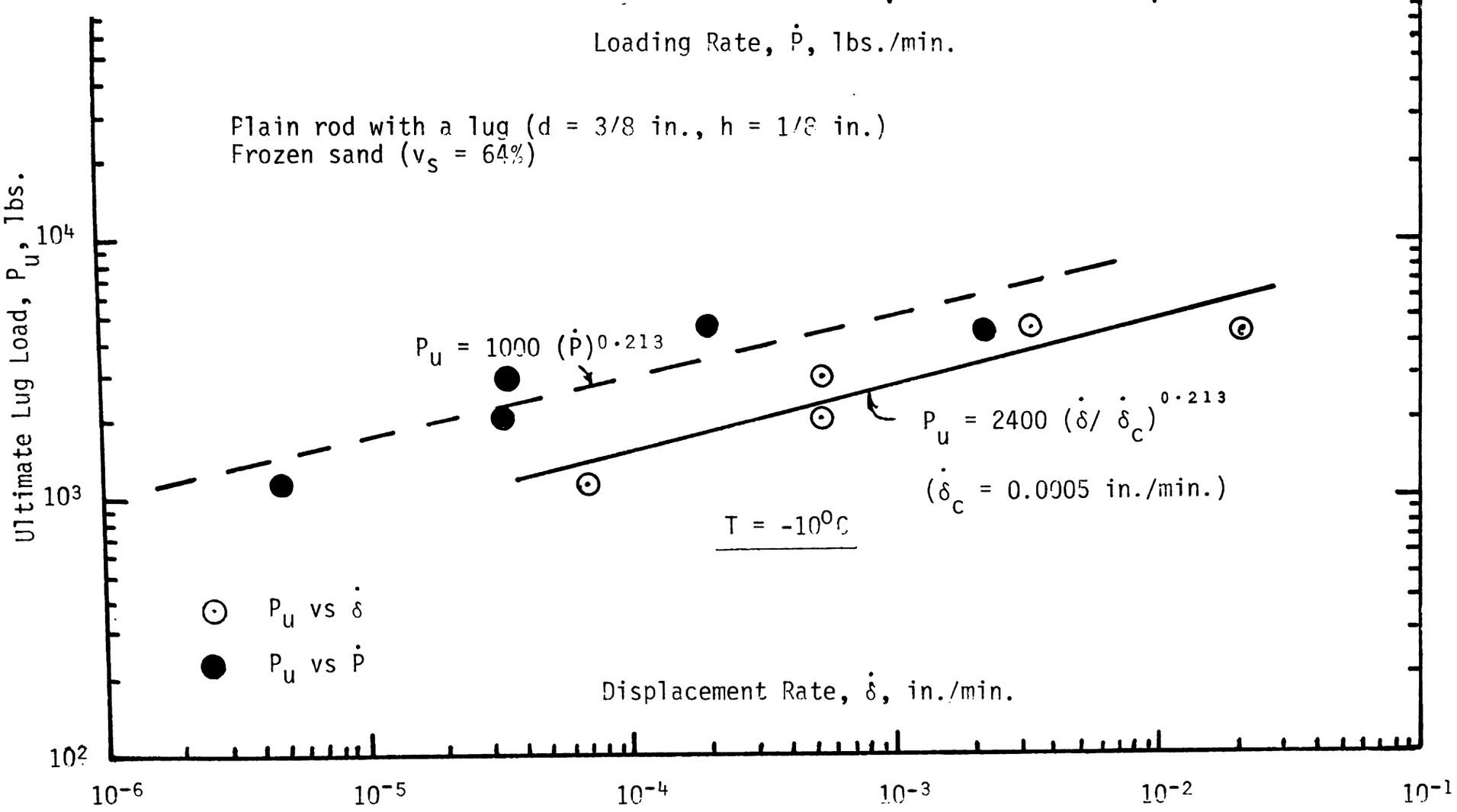

Figure 5.6: Effect of displacement and loading rates on the ultimate lug capacity in frozen sand (v_s = 64%) at -10°C.

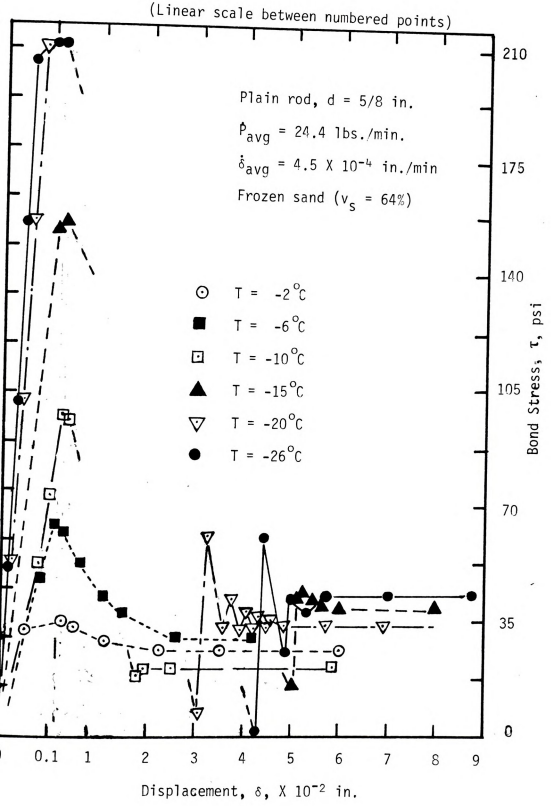

igure 5.7: Typical load-displacement curves at different temperatures for a plain rod in frozen sand (v_s = 64%).

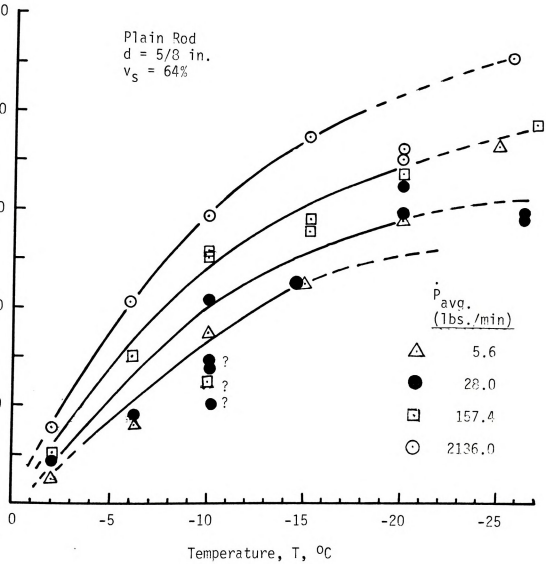

e 5.8: Temperature effect on the bond strength of frozen sand (v_s = 64%) to a plain steel rod, at several loading rates.

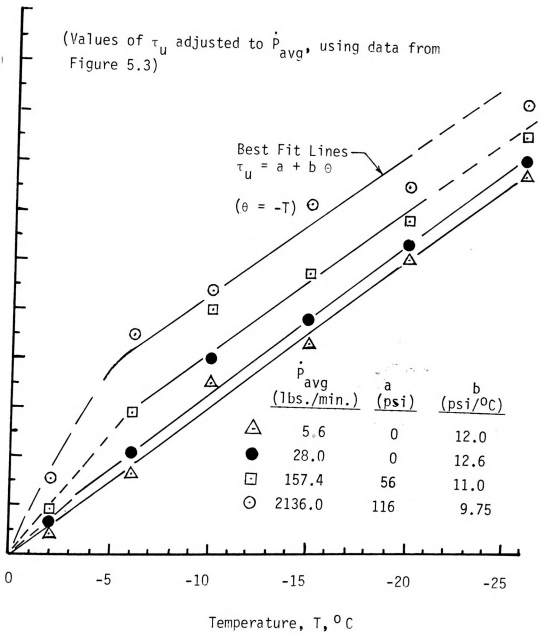

5.9: Relationship between temperature and bond strength of frozen sand (v_s = 64%) to a 5/8 in. plain rod, at several loading rates.

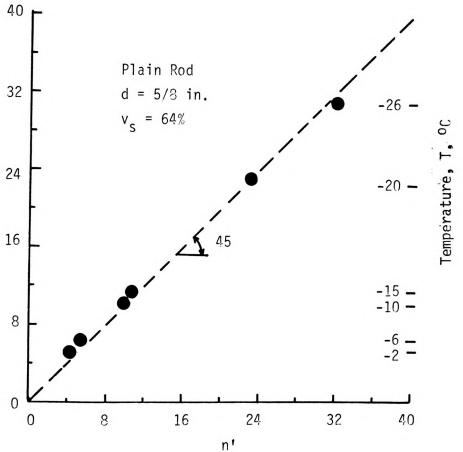

e 5.10: Comparison of strain hardening parameters, n based on constant loading rate and n' based on constant displacement rate, for 5/8 in. diameter plain rod in frozen sand (v_s = 64%).

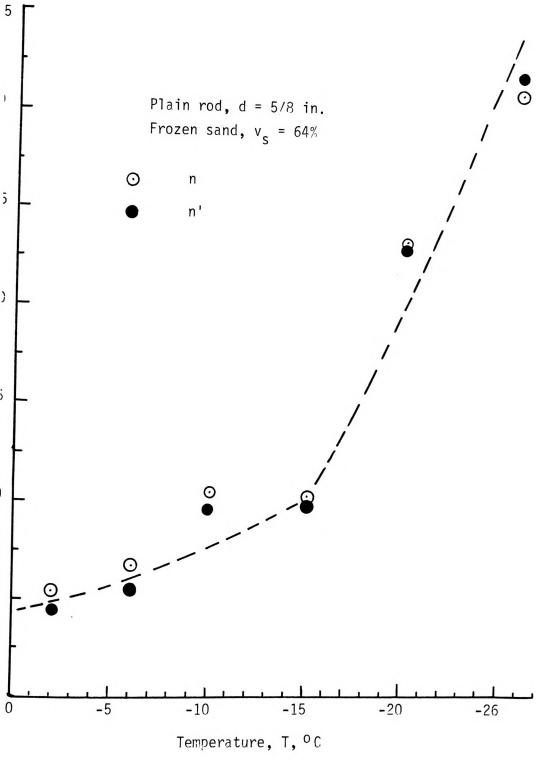

e 5.11: Temperature effect on the n parameter as defined by Equations 5.1 and 5.3.

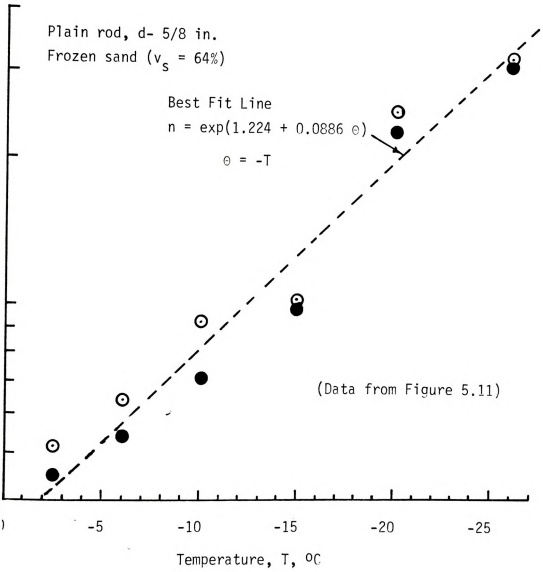

5.12: Relationship between temperature and the n parameter for a plain rod in frozen sand (v_s = 64%).

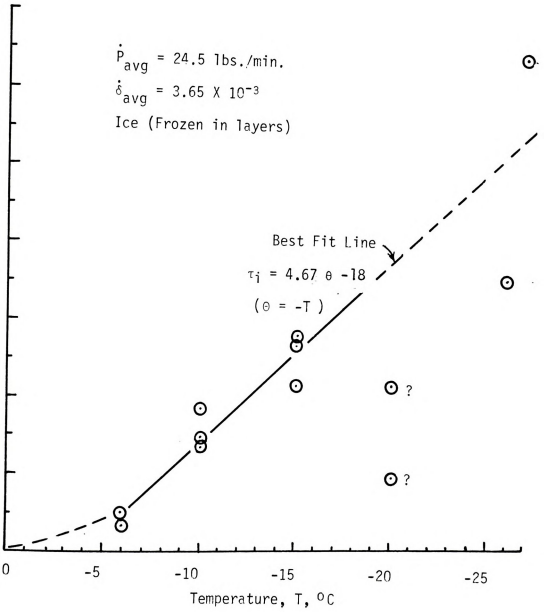

re 5.13: Temperature effect on ice adhesion to a 5/8 in. diameter plain rod.

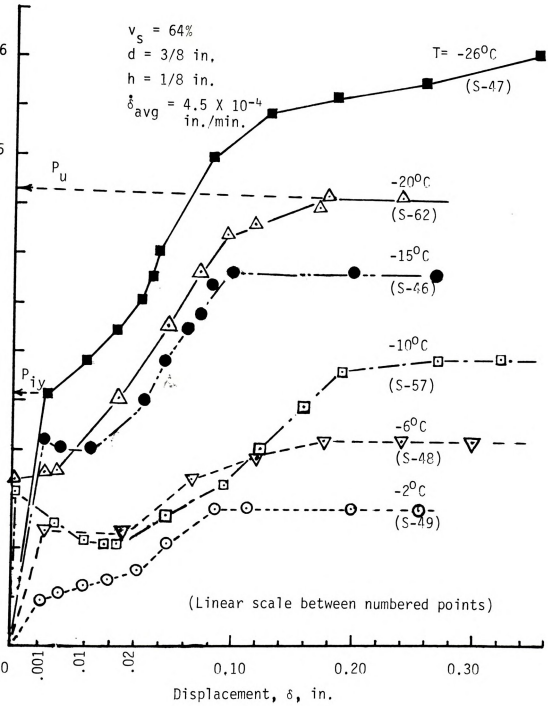

e 5.14: Typical load-displacement curves at different temperatures for a plain rod with lug in frozen sand (v_s = 64%)

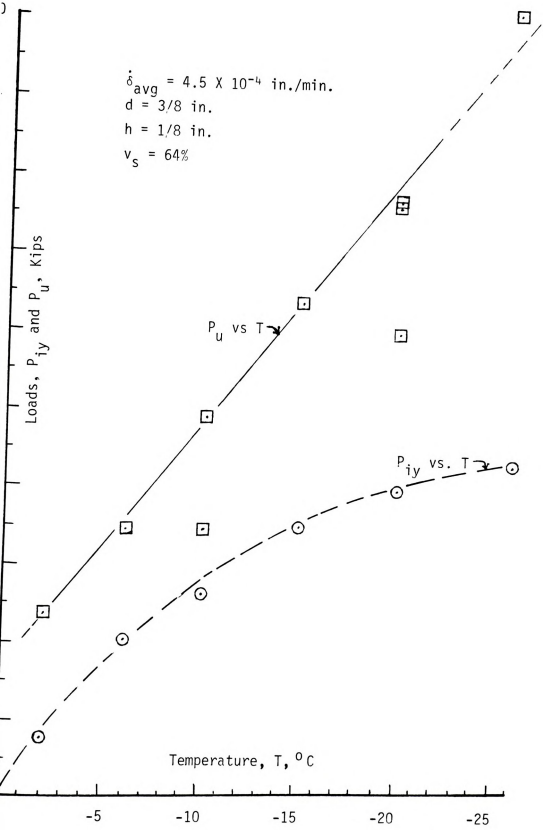

ure 5.15: Temperature effect on lug bearing, ultimate and "initial yield" loads, in frozen sand (v_s = 64%).

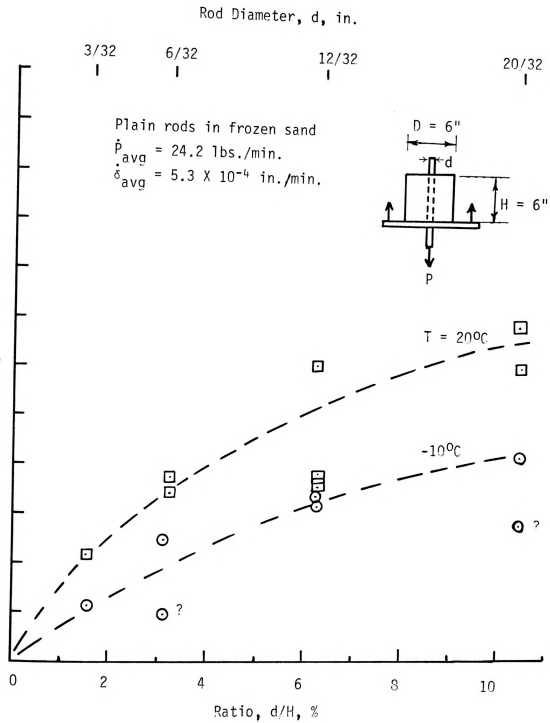

re 5.16: Effect of rod size (diameter) on the bond strength of frozen sand (v_s = 64%) to plain steel rods.

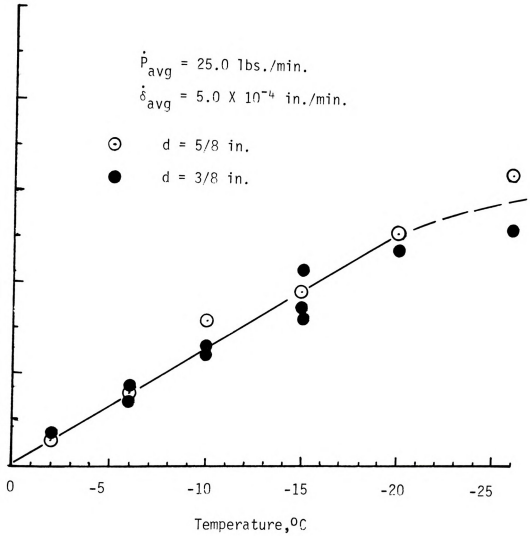

e 5.17: Comparison of bond strength for two plain rod diameters in frozen sand (v_s = 64%) at several temperatures.

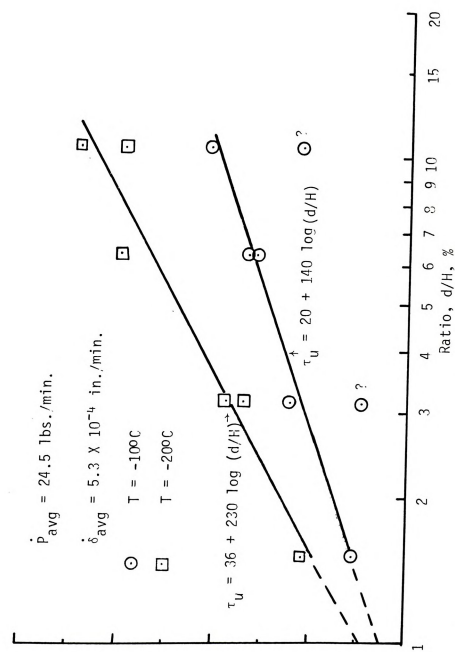

Figure 5.18: Relationship between the d/H ratio and bond strength of frozen sand (v_s = 64%) to plain rods.

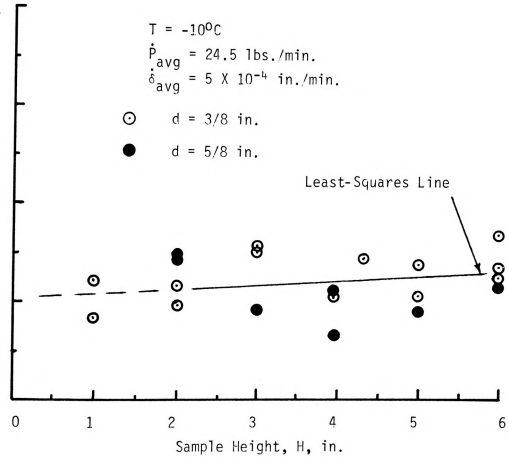

e 5.19: Effect of sample height on bond strength for plain steel rods in frozen sand (v_s = 64%).

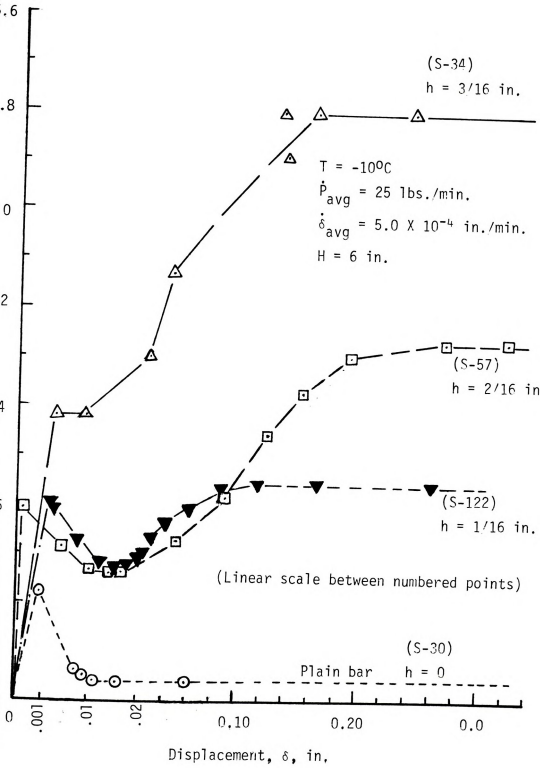

e 5.20: Load-displacement curves for a 3/8 in. steel rod with four lug sizes in frozen sand (v_s = 64%) at -10°C.

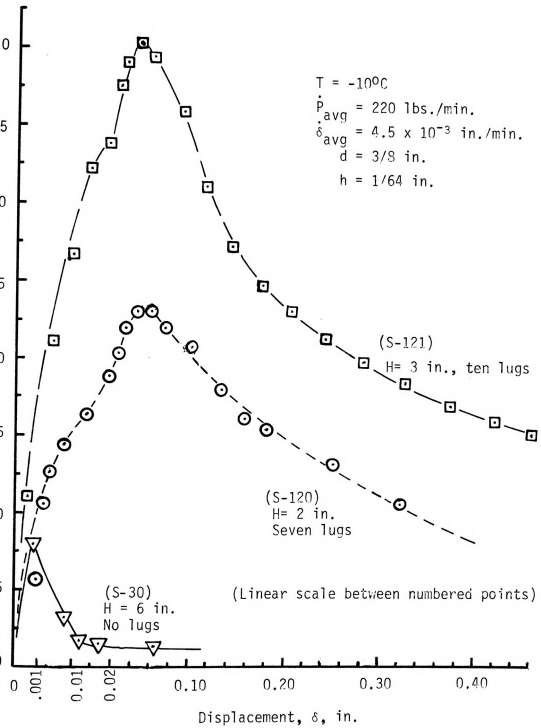

re 5.21: Load-displacement curves for a standard deformed No. 3 bar in frozen sand (v_s = 64%) at -10°C.

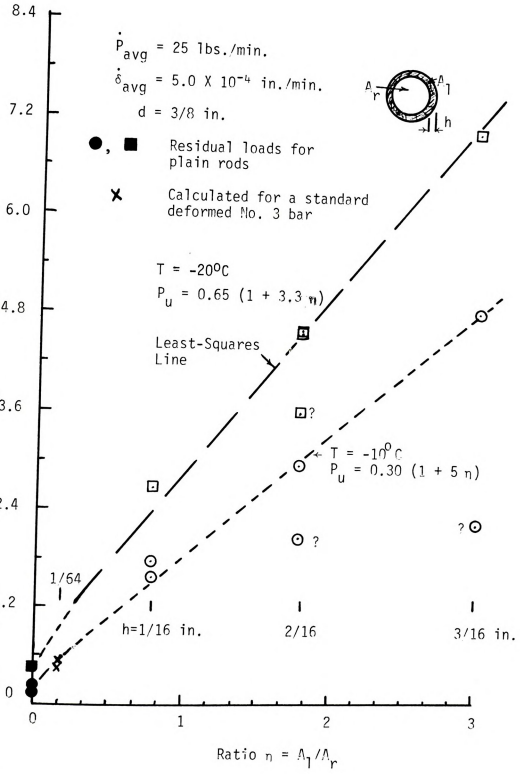

ure 5.22: Effect of lug size (height) on the ultimate lug capacity in frozen sand (v_s = 64%)

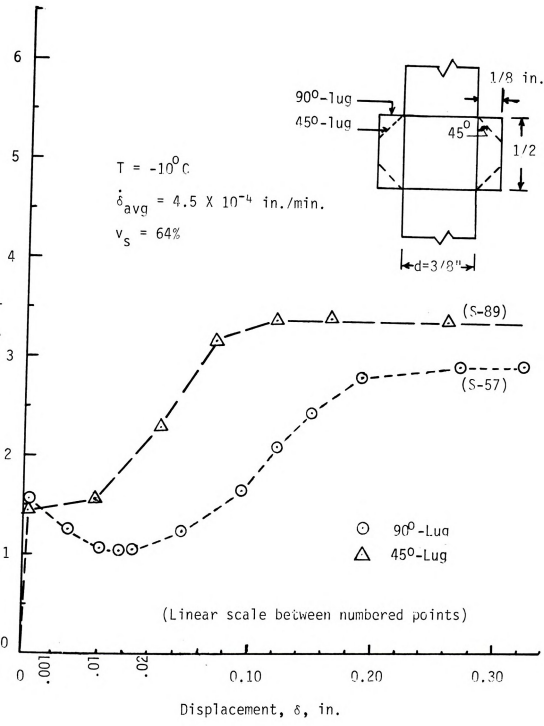

re 5.23: Typical load-displacement curves for plain rods with two lug types; 45°-lug and 90°-lug, in frozen sand (v_s = 64%).

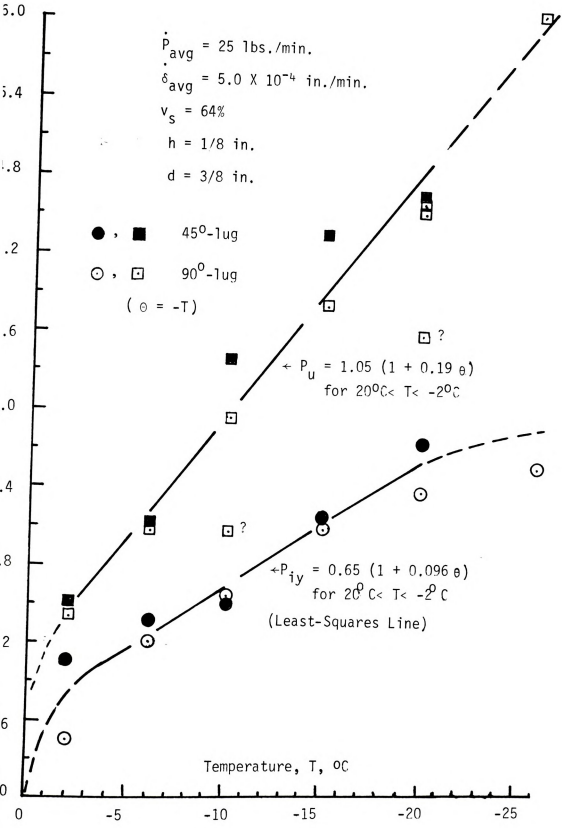

gure 5.24: Relationship between temperature and lug bearing capacity in frozen sand (v_s = 64%).

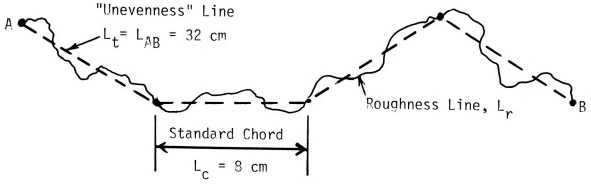

Figure 5.25: Roughness criterion (After Wright, 1955).

SURFACE	μin.	μin.	mm	mm	mh	ρ%
GF*	4.5	6.5	6.0	6.0	152	90
CR	22.5	55.0	10.0	18.0	580	625
SB	32.5	47.5	11.5	19.0	1271	1489

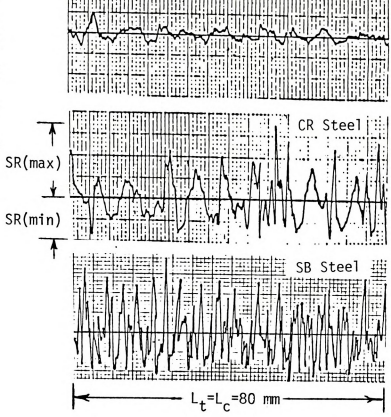

* GF: Ground-Finished steel surface
CR: Cold-rolled " "
SB: Shot-blasted " "

** SP(min) & SP(max) are minimum and maximum heights of aspirities as observed on the profilometer.

SR(min) & SR(max) are the corresponding heights as observed on the recorder strip chart, measured from the centerline.

L_c Length of a standard chord
L_t Total length of standard chords
L_r Length of "roughness" line
ρ is the roughness factor

Figure 5.26: Typical outputs for three types of steel surfaces as recorded on the strip chart, with a list of their properties.

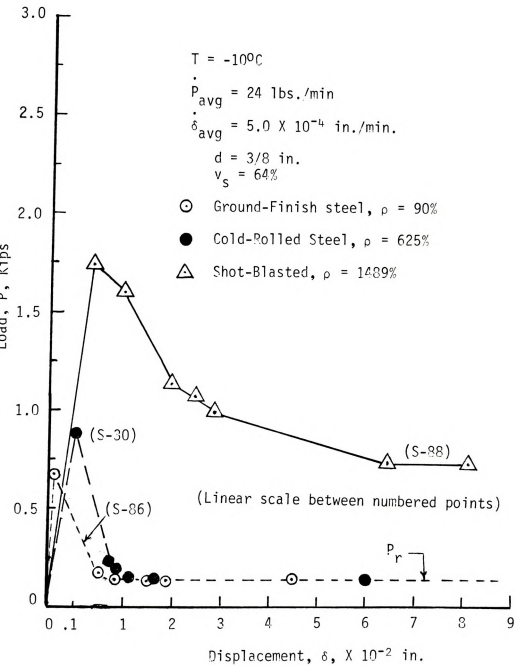

ıre 5.27: Load-displacement curves for three types of steel finish, in frozen sand (v_s = 64%) at -10°C.

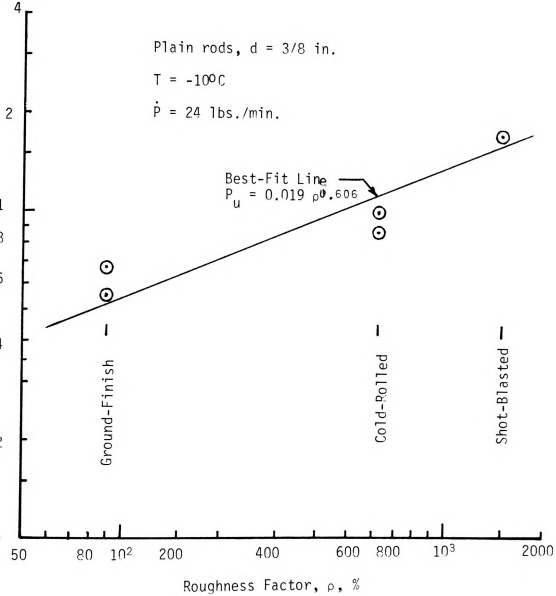

ure 5.28: Effect of surface roughness on the bond strength of frozen sand (v_s = 64%) to plain steel rods.

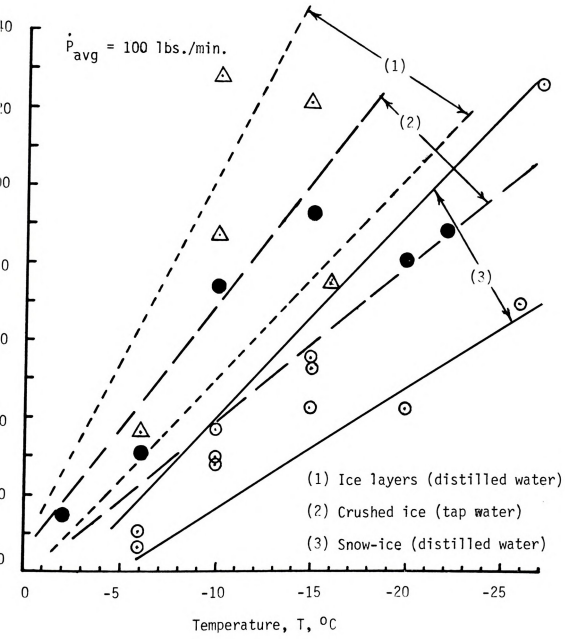

ure 5.29: Bond strength dependence on ice sample preparation method.

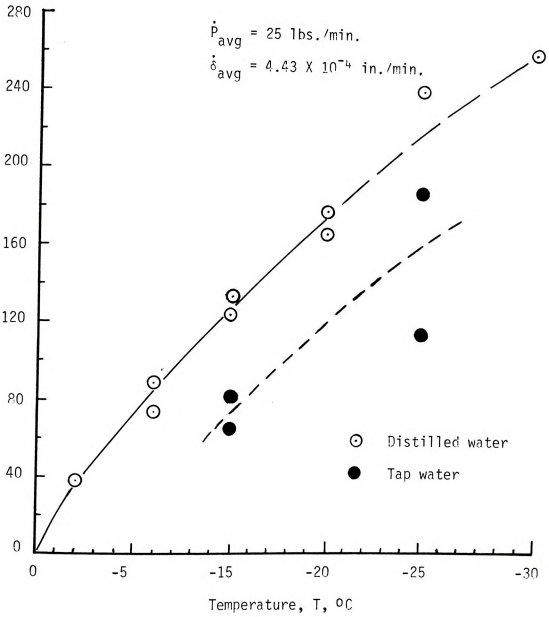

gure 5.30: Bond strength dependence on water impurities for a 3/8 in. diameter plain rod in frozen sand (v_s = 64%) at several temperatures.

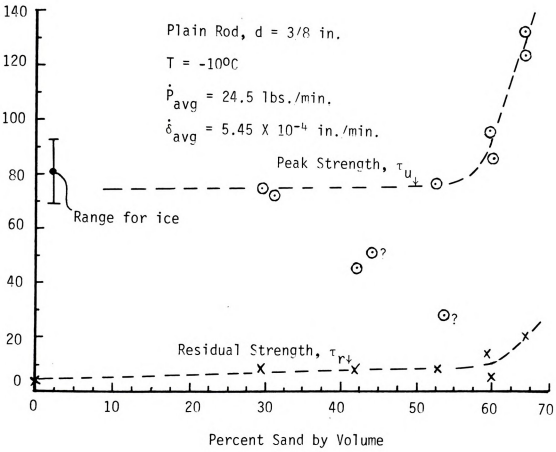

Figure 5.31: Effect of sand fraction on bond strength for plain rods, peak and residual at -10°C.

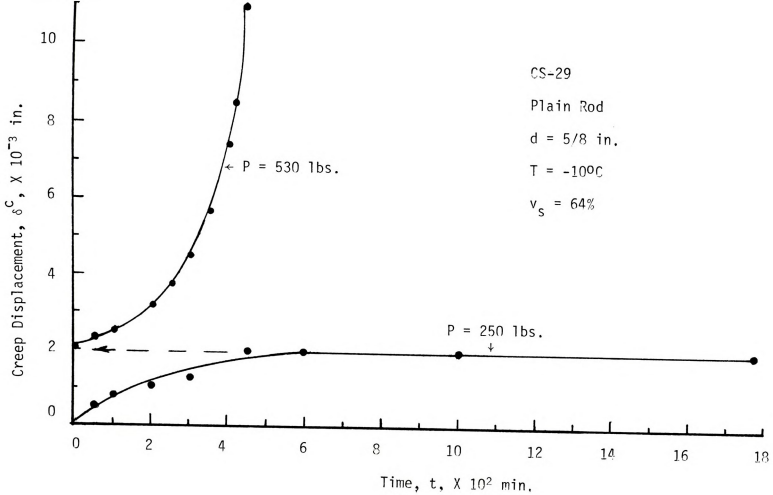

Figure 5.32: Creep curves based on step loading a plain rod in frozen sand (v_s = 64%) at -10°C. (a) Sample No. CS-29. (continued)

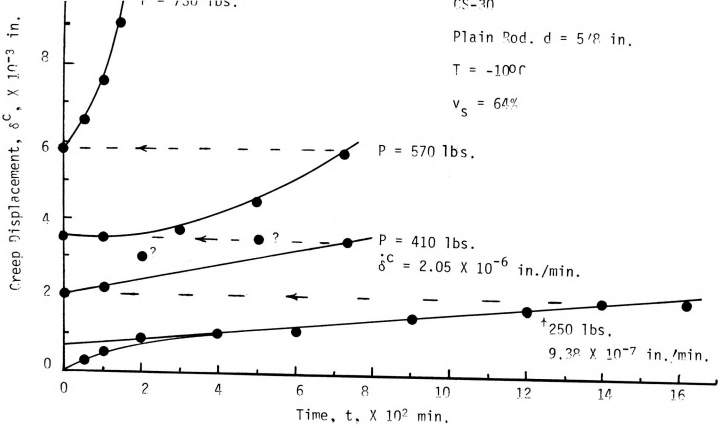

Figure 5.32 (continued): (b) Sample No. CS-30

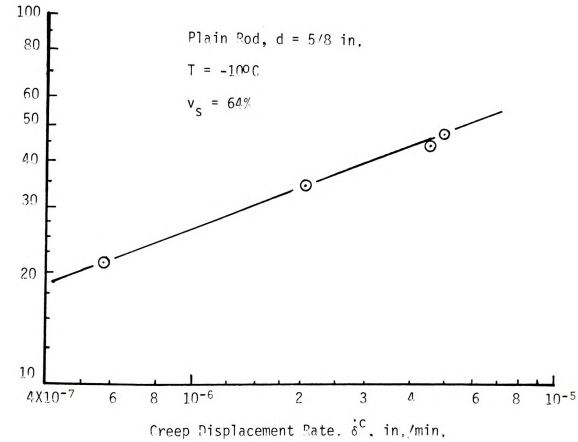

igure 5.33: Loading effect on the creep rate of a plain steel rod in frozen sand (v_s = 64%) at -1°C.

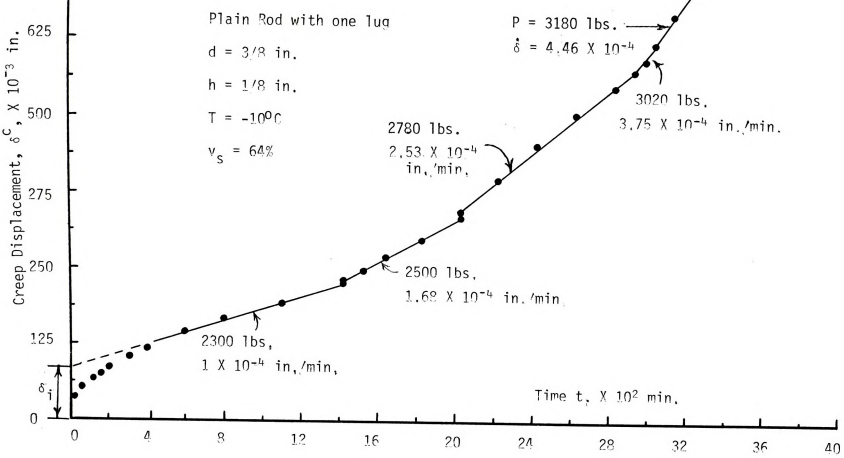

Figure 5.34: Creep curves for step loading of a plain 3/8 in. rod with a 1/8 in. lug height in frozen sand (v_s = 64%) at -10°C. (a) Sample No. CS-5. (Continued)

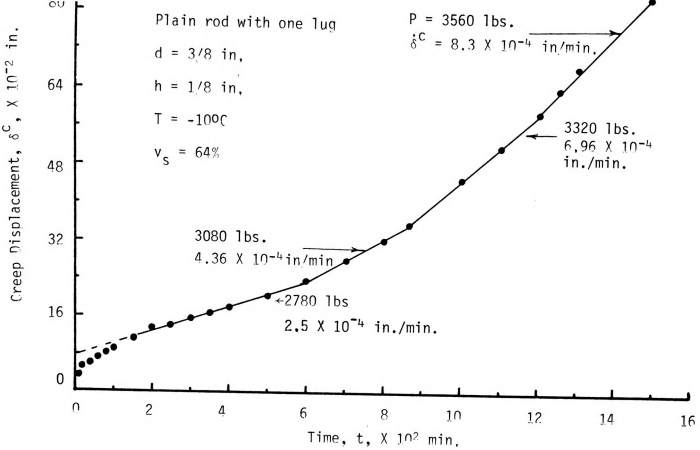

Figure 5.34 (Continued): (b) Sample No. CS-6

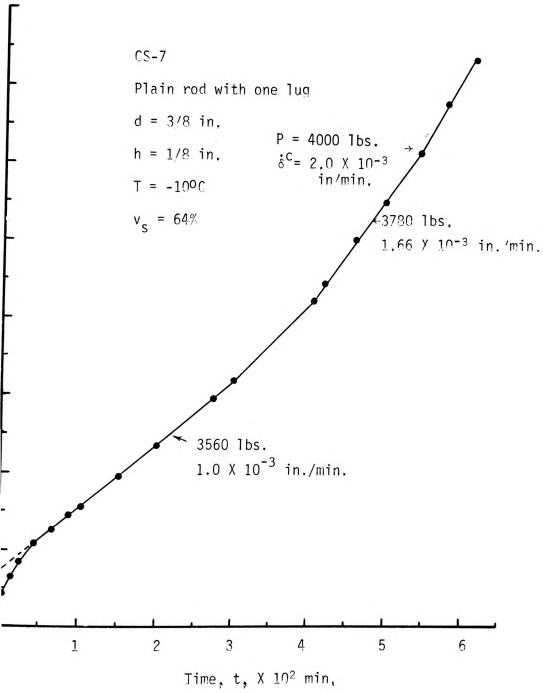

Figure 5.34 (Continued): (c) Sample No. CS-7.

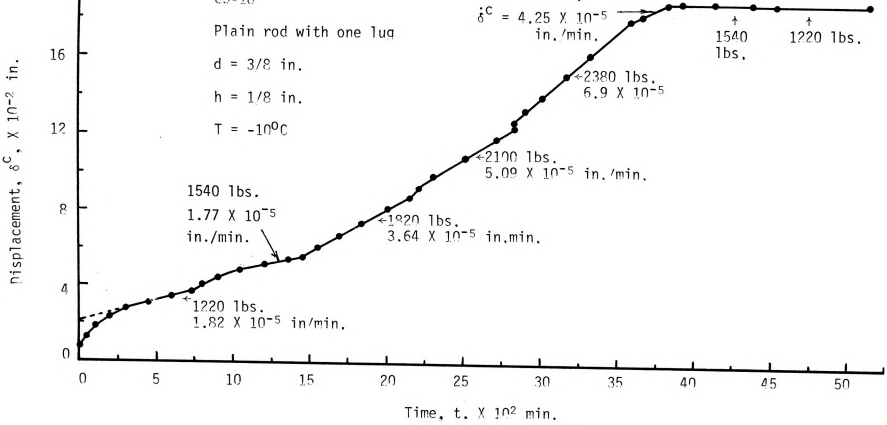

Figure 5.35: Creep curves for step loading followed by unloading a plain rod with one lug in frozen sand (v_s = 64%).

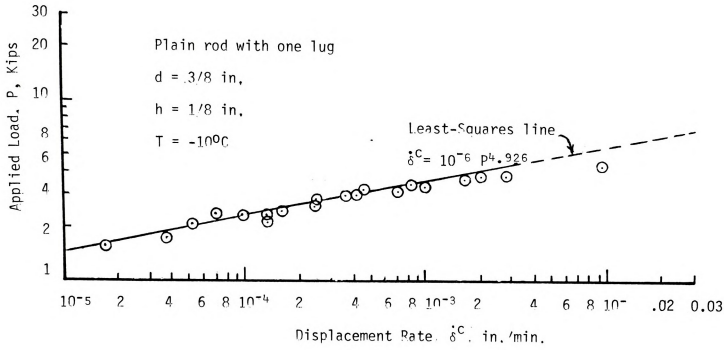

Figure 5.36: Loading effect on creep displacement rate of a plain rod with one lug in frozen sand (v_s = 64%) at -10°C.

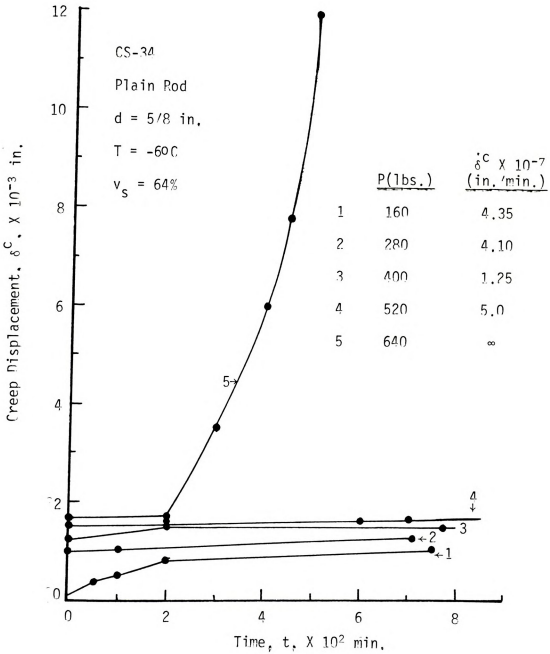

re 5,37: Creep curves for a plain rod in frozen sand (v_s = 64%). Step loading procedure, (a) Sample No. CS-34, at -60C. (Continued).

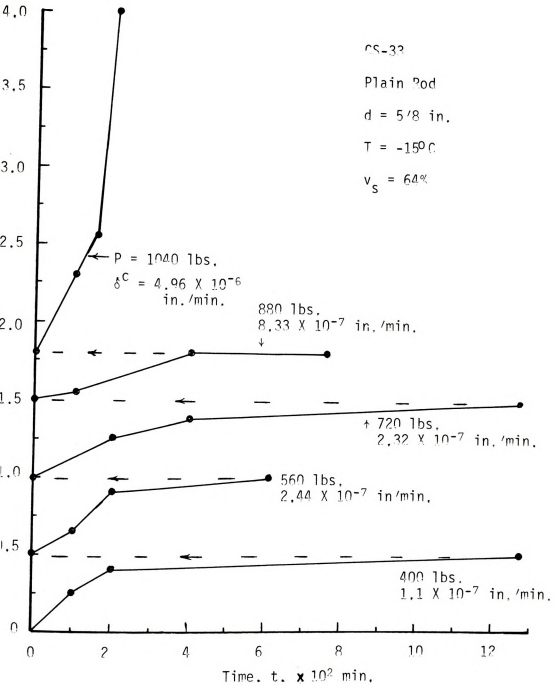

gure 5.37 (Continued): (b) Sample No. CS-33, -15°C.

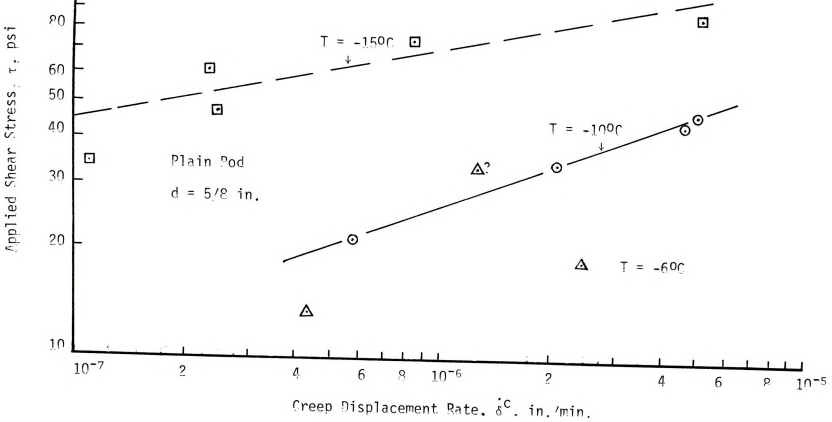

Figure 5.39: Temperature effect on creep rate of a plain rod in frozen sand (v_s = 64%)

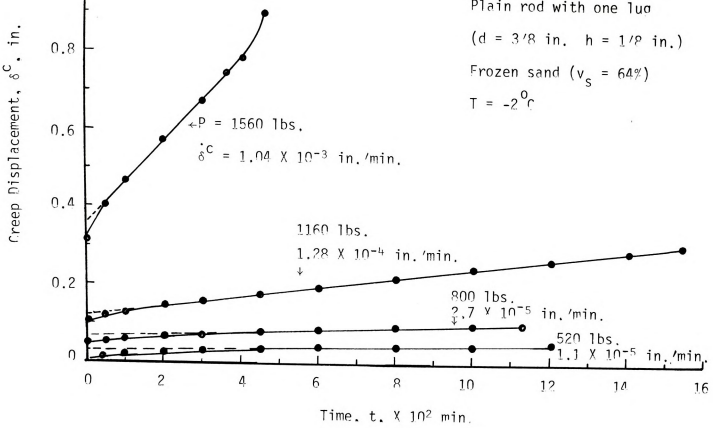

Figure 5.39: Creep curves for step loading a plain rod with one 90° lug in frozen sand (v_s = 64%). (a) Sample No. CS-85, at -2°C (Continued)

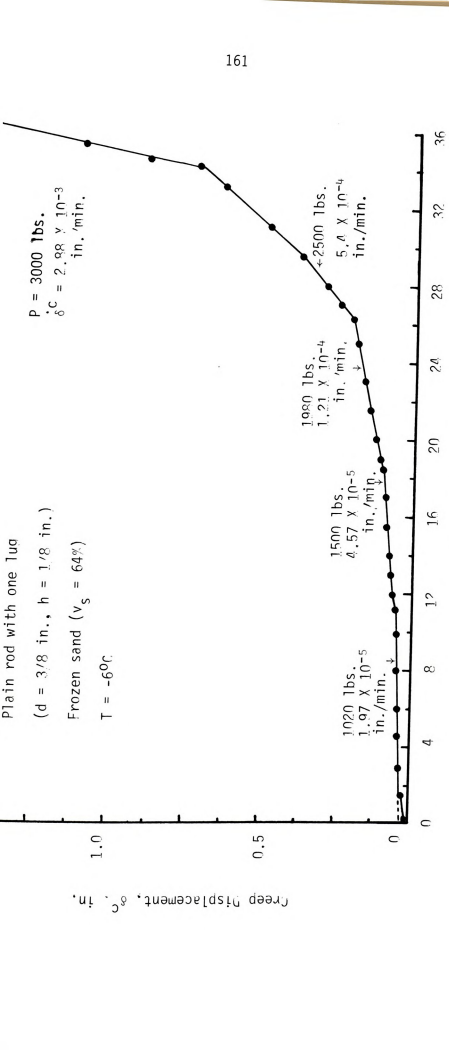

Figure 5.39 (Continued): (b) Sample No. CS-24, at -6°C.

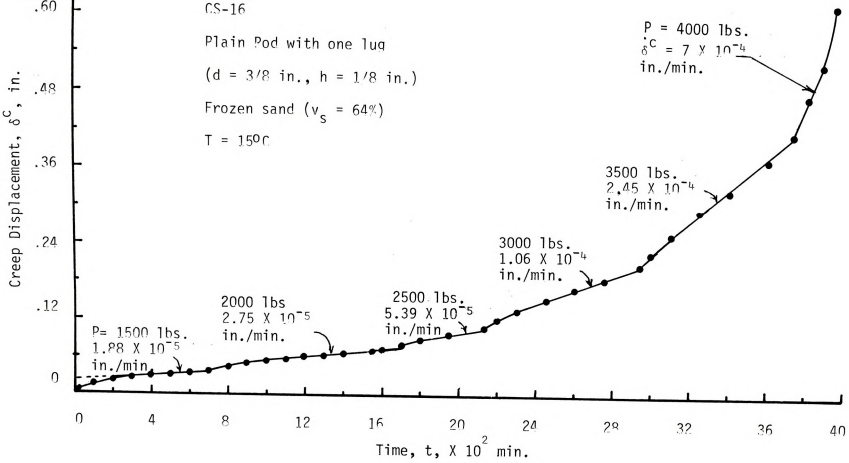

Figure 5.39 (Continued): (c) Sample No. CS-16, at -15°C.

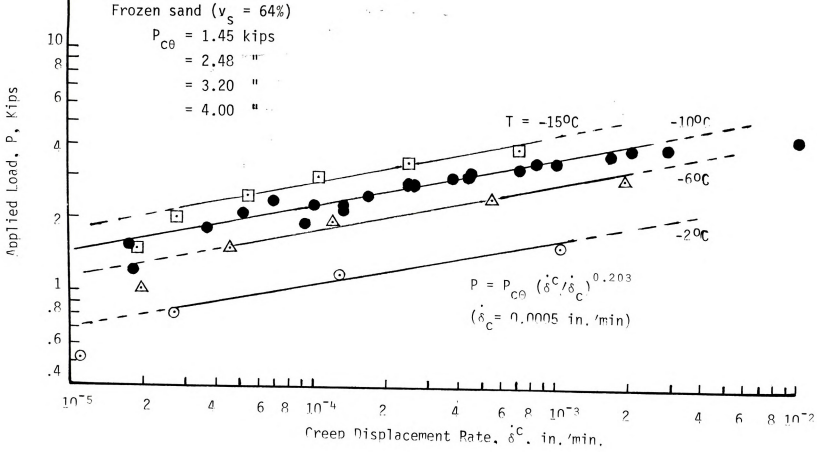

Figure 5.40: Creep displacement rates for a plain steel 3/8 in. rod with a 1/8 in. lug in frozen sand (v_s = 64%) at four temperatures.

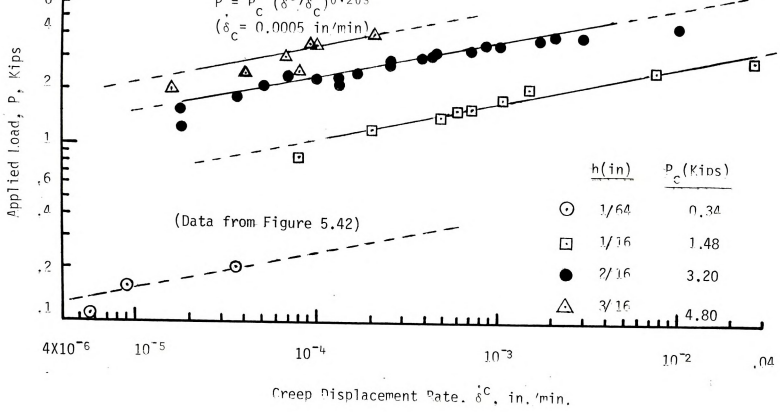

Figure 5.41: Effect of lug height on the creep behavior of a plain steel 3/8 in. rod with 90 lugs in frozen sand (v_s = 64%) at -10°C.

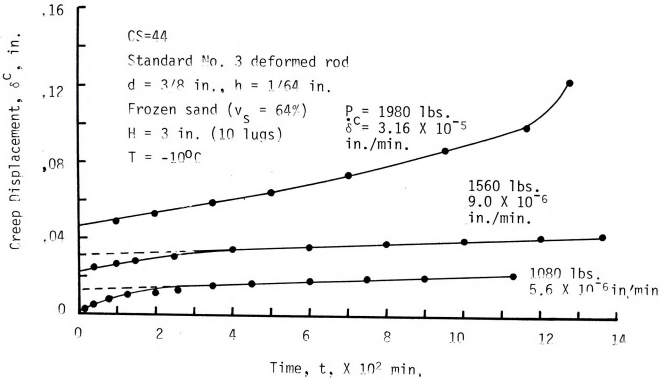

Figure 5.42: Creep curves for step loading a standard No. 3 bar in frozen sand (v_s = 64%) at -10°C.

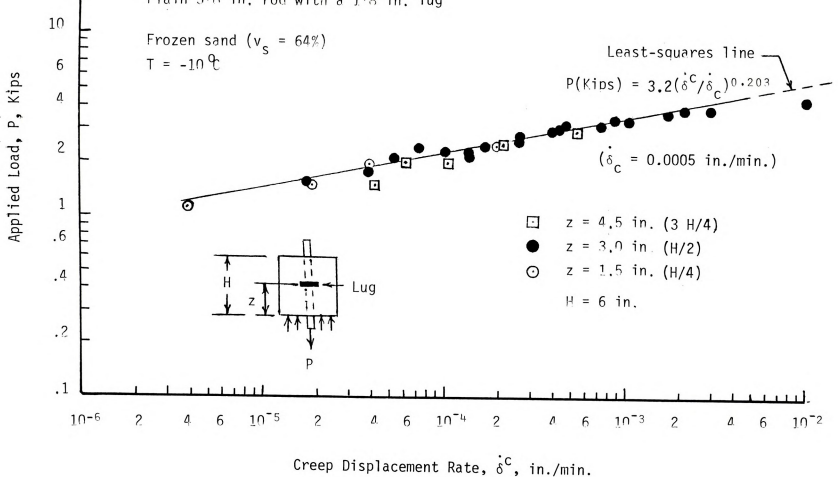

Figure 5.43: Load-displacement (creep) rate curve for a plain 3/8 in. steel rod with a 1/8 in. lug at different positions, in frozen sand (v_s = 64 %) at -10 °C.

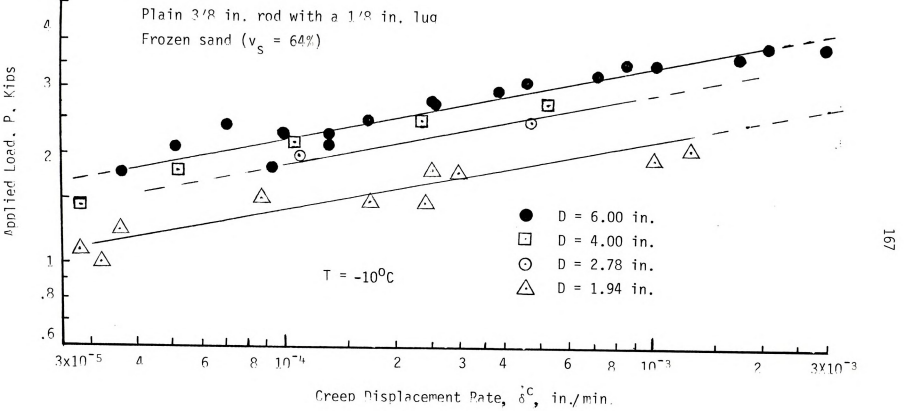

Figure 5.44: Effect of sample diameter on creep rate of a plain 3/8 in. steel rod with a 1/8 in. lug in frozen sand (v_s = 64%) at -10°C.

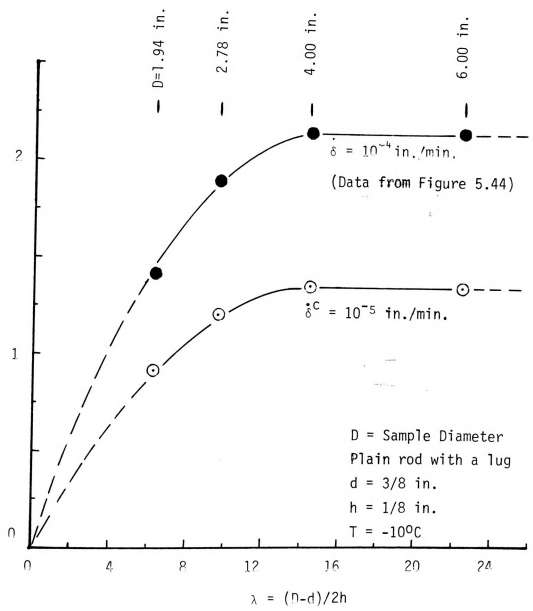

igure 5.45: Pull-out load dependence on soil cover for a plain steel 3/8 in. rod with a 1/8 in. lug in frozen sand (v_s = 64%)

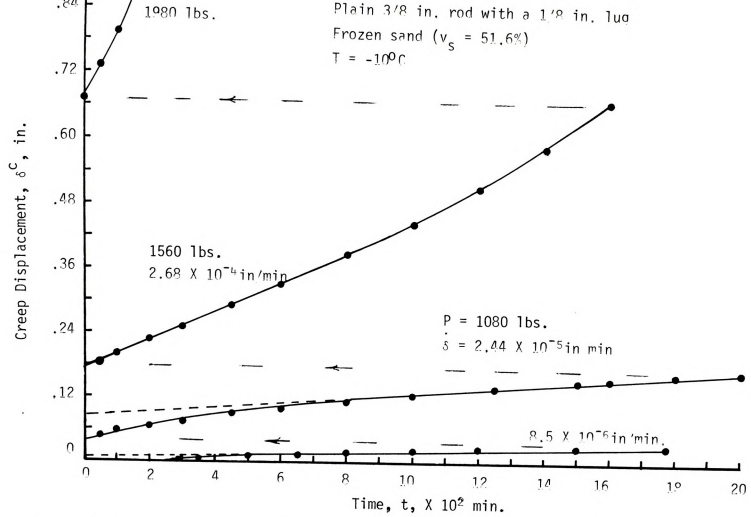

Figure 5.46: Creep curves for step loading plain bars with a 1/8 in. lug in frozen sand at -10°C (a) Sample No. CS-38 with v_s = 51.6% (Continued)

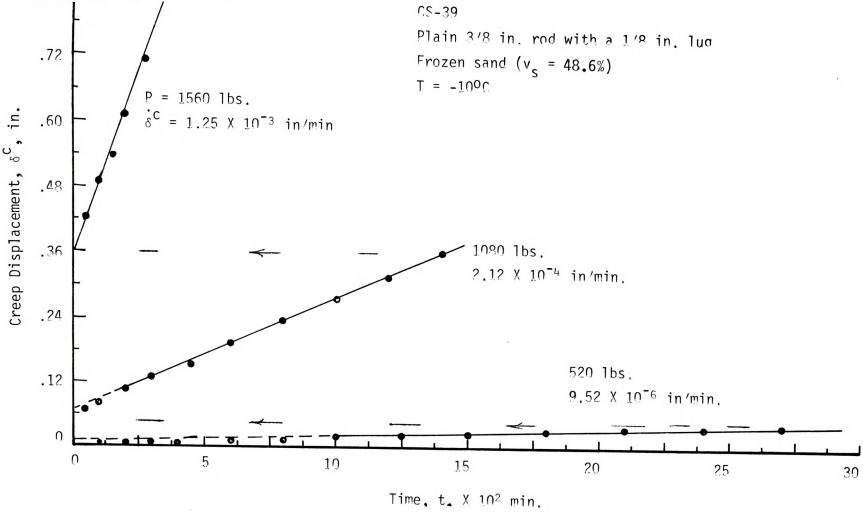

Figure 5.46 (Continued): (b) Sample No. CS-39 with v_s = 48.6%

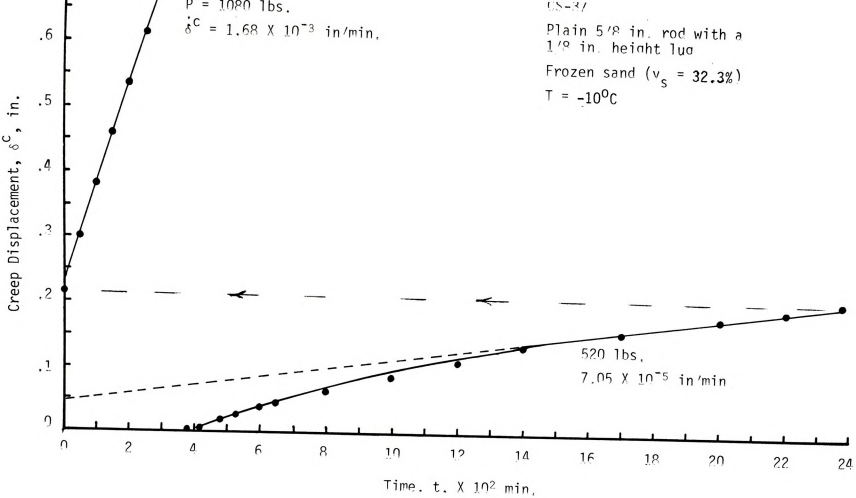

Figure 5.46 (Continued): (c) Sample No. CS-37 with v_s = 32.3 %.

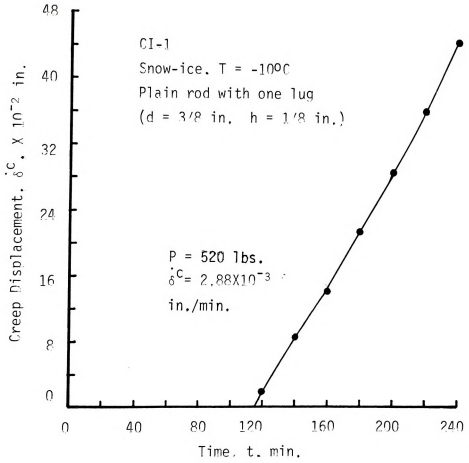

Figure 5.47: Creep curve for a plain 3/8 in steel rod with a 1/8 in. lug in snow-ice (v_s = 0) at -10°C.

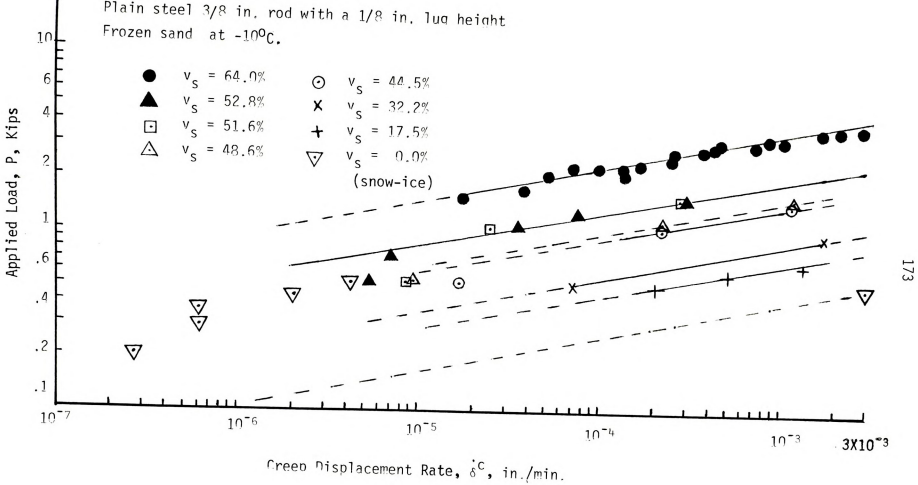

Figure 5.48: Creep displacement Rates for plain 3/8 in. steel rods with a 1/8 in. lug in frozen sand at -10°C and different sand volume concentrations.

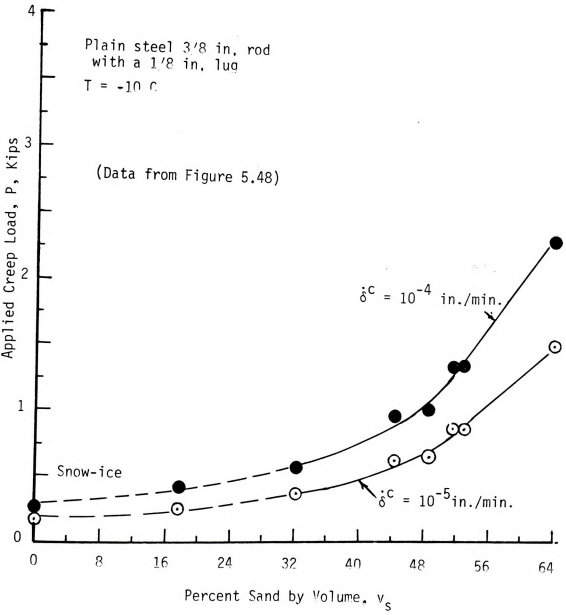

Figure 5.49: Load capacity dependence on sand concentration during creep for plain steel 3/8 in. rods with a 1/8 in. lug in frozen sands at -10°C

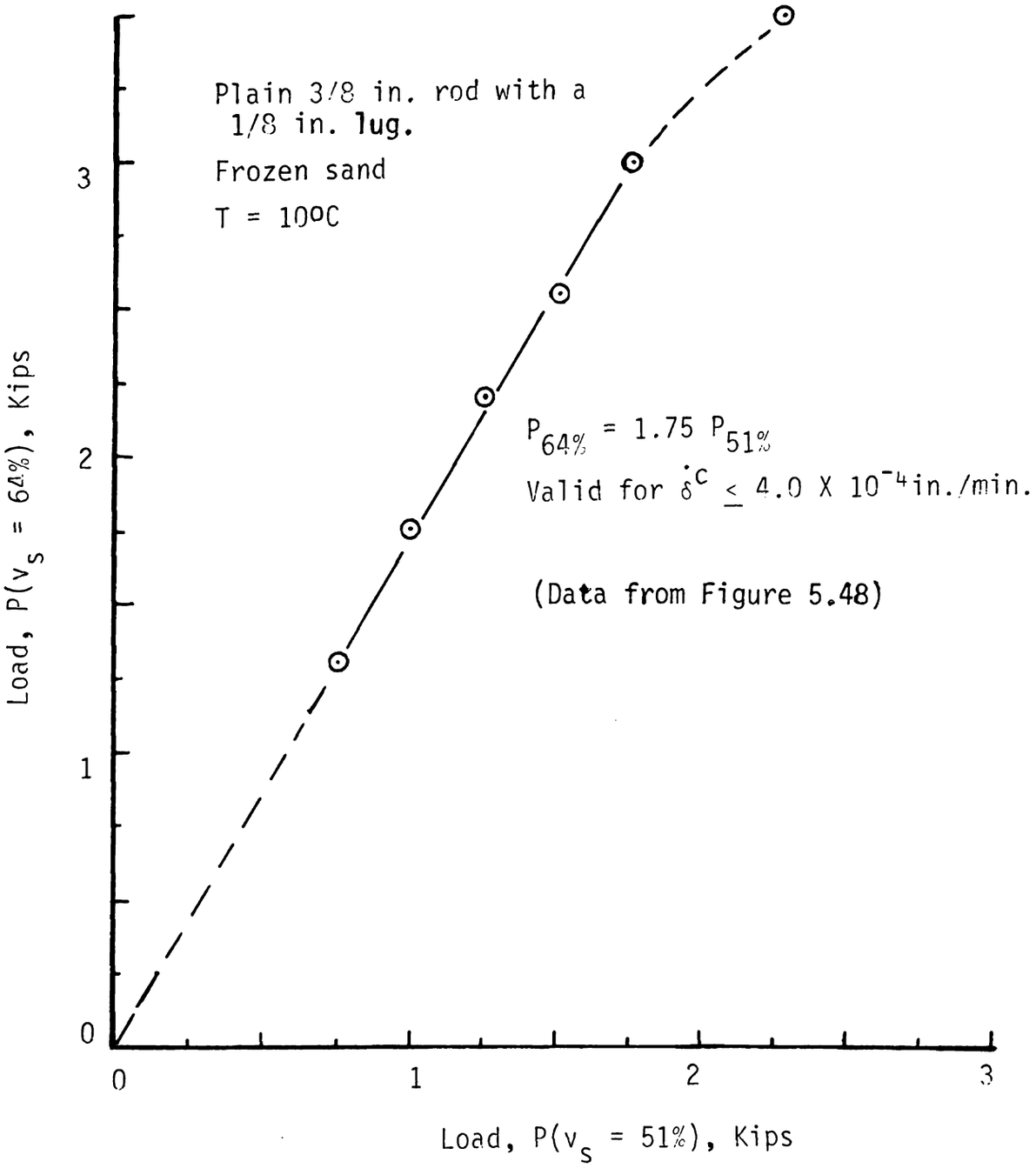

Figure 5.50: Comparison of lug loads at different sand concentration for frozen sand at $-10^{o}C$.

CHAPTER VI

ANALYSIS AND DISCUSSION

1 Load Transfer Mechanisms:

Shearing resistance at the rod-frozen sand interface develops as a sult of ice adhesion (or cohesion) and soil grain friction. When a ngle lug is added mechanical interaction caused by lug bearing against e frozen soil adds to load transfer between the rod and frozen soil. nce ice adhesion and particle friction appear to have a similar load ansfer behavior, it was convenient to consider them in the same section. g bearing will be discussed in a later section.

1.1 Ice Adhesion and Sand Friction:

These two adfreeze bond components provide shear resistance to l displacements relative to the frozen soil. Each components contribu- n to the total resistance has been considered separately throughout s study. Ice pullout specimens (prepared in different ways) were ted, using a 5/8 in. diameter plain cold-rolled steel rod. It was erved that ice adhesion was sensitive to many variables including perature, loading rate, ice structure, water impurities, stress and perature history, and other factors. Control of all these variables difficult due to the complexity of the load transfer phenomenon. lts of these tests, summarized in Figure 5.29, show the upper and r limits of ice adhesion for various conditions. Only a brief rpretation of these results will be given here, since adhesive

properties of ice deal with complex physico-chemical phenomena which are outside the scope of this investigation.

Starting with the temperature effect, the results show a general linear variation of ice adhesion with temperature (Figure 5.13) despite the large scatter. This is in agreement with work reported by other authors, as shown in Figures 2.1 and 2.2. Values of ice adhesion to plain wooden piles obtained by Tsytovich and Sumgin (1959), appear to vary almost linearly with temperature in the range of -7°C to -20°C (Figure 6.1). Although no displacement or loading rate was mentioned, these values are compared with Ice (1) in Figure 5.29. Ice (1) appears to be most similar to that reported by Tsytovich and Sumgin. Further comparisons with previous studies, unfortunately, are not as promising due to the diversity in test conditions, ice types, and contact surfaces. The increase in ice adhesion at colder temperatures has been attributed to a reduction in thickness of the liquid-like layer at the ice interface (Jellinek, 1957 b; Barnes et al., 1971).

Returning to Figure 5.29, the effect of water impurities on adhesive strength may be noted by comparing Ice (2) and Ice (3). Tap water often contains 1 p.p.m. or more flourine, in addition to about 450 p.p.m. in hardness as calcium carbonates. Jones and Glen (1969) observed a reduction of about 35% in ice shear strength at -70°C due to increase in flourine content from 0 to 0.05 p.p.m. and the reduction was about 60% when flourine content increased to 0.5 p.p.m. The two authors attributed the results to different types of physico-chemical defects and dislocations in ice crystals caused by the hydrogen fluoride (HF) molecule which enters the ice lattice.

The effect of water salinity on strength of ice and frozen soils have been investigated by many authors. Velli and Karpunina (1973) recommend that the adfreeze strength of frozen saline ground to concrete piles be taken with a factor of 0.75 of that of fresh water, based on several in-situ tests. In fact the reduction in adfreeze strength due to using tap water in Figure 5.30 was about 45 percent, which is far more than 25 percent. More recently, Ogata, et al. (1982) observed that a 3 percent increase in water salinity of alluvial sand over distilled water caused about 70 percent reduction in its unconfined compression strength at -20°C. They also observed that the rate of strength decrease with increase in salinity was largest for a low salt concentration, in the range of 1 percent. This was attributed to the increase in unfrozen water content due to the salt concentration. Creep deformation in the sand was also observed to be largely influenced by the increase in salt concentration. Similarly, Sego et al. (1982) showed that an increase in salinity of frozen sand caused a non-linear decrease in its proof strength, the exponent n from a power law, and a similar decrease in Young's Modulus, at -7°C.

Temperature history is believed to have some effect on ice adhesion. Its effect, when combined with the other factors, appears to be far less significant on the sand-ice behavior. More consistent data were obtained from pullout tests on frozen sand than those on ice. All specimens were frozen at about -24°C prior to testing. Ponomarjov (1982) experimentally showed that soil samples at first expand on freezing (due to phase change of water). The expansion continued to a maximum value at about -8°C (if the samples are fully saturated).

With a decrease of temperature below -8°C, thermal contraction reduces the sample back to its original size at about -55°C. Ponomarjov attributed this reverse deformation to the presence of gases and the possibility of deformation of ice crystals when the gases change in volume due to changes in temperature. Theoretical predictions made by Ponomarjov (1982) compared well with his experimental data.

Considering these possible changes in the pullout specimens, a 5/8 in. diameter circular hole (in the ice at -24°C) would expand* by 6.5×10^{-5} in. if the temperature were increased to -2°C. A steel rod of the same diameter, frozen in the ice, would contract by 1.5×10^{-5} in. The net effect would be a small gap of 8×10^{-5} between the ice and rod. If these assumptions are correct and the gap does exist due to temperature history, then the adfreeze bond would be weakened and the reinforcing effect due to surface "tension" would be less. This weakening may also occur during the test due to differences in Poisson's ratio of steel and ice. As the rod is pulled a slight reduction in its diameter will differ from that in the ice. The effect of temperature history and that due to differences in Poisson's ratio may not be as severe as they would first appear. The net result may be a cancellation of effects.

The load-displacement curves for plain rods in ice and frozen sand (Figure 5.2) are very similar. This behavior indicates a very small displacement leading to rupture at ultimate load followed by a small slip (Figure 5.1). Experimental work reported by Parameswaran (1978 b) on model piles in frozen Ottawa sand showed a similar

---

*See Michel (1978) for the coefficient of thermal expansion of ice.

load-displacement behavior. The Wedron sand appears to have properties similar to the Ottawa sand except for possibly grain shape. As shown in Figure 6.2, the ultimate adfreeze bond strength occurs at small displacements, followed by immediate rupture. The displacements in Figure 6.2 are normalized with respect to the rod (pile) diameter. The 25 percent difference in strength was probably due to a difference in soil types, rod surface roughness, and test conditions.

The creep behavior observed for plain rods in Figure 5.32 (a) and (b) was similarly reported in the literature. Vyalov, et al. (1973) stated that one of the model piles in ice (at -0.4°C) remained under a pulling stress of 4.26 psi for 1200 hours without any noticeable displacement, but then it suddenly pulled out.

The effect of rod diameter on frozen sand bond strength, Figure 5.18, does not agree with the findings reported by Frederking (1979) for wooden piles in ice (Figure 2.9). On the other hand, the results showing effect of ice thickness on bond strength in Figure 2.9, agree with a similar trend observed on frozen sand in Figure 5.19. The theoretical work of Mohaghegh and Coon (1973) also supports an increase in adhesive strength with increasing ice thickness for the case of thick circular plates. Although the effect of rod diameter does not agree with Frederking's findings, it would agree reasonably well with the general trend if one considers the combined effect of d and H in terms of the ratio d/H.

Combining Figures 5.18 and 5.19 on one plot, for T = -10°C, gives the relationship between τ_u and d/H shown in Figure 6.3. A ratio of d/H in the range of 6 percent to 10 percent appears to be an optimum

one in yielding the maximum bond strength. The dashed line represents both lines in Figure 2.9 plotted versus log (d/H) in Figure 6.3. Regardless of the numerical values, the general trend of decreasing bond strength with increasing d/H, in the range shown, is the same in both the present study and Frederking's study.

The temperature effect on bond strength of frozen sand appears to agree reasonably well with field tests conducted by Crory (1963) on 8 in. diameter steel pipe piles in frozen sand slurries (Figure 6.4). Data from Figure 5.3, interpolated to a loading rate of 7 lbs./min., is equivalent to the 10 kips/day indicated on the ultimate strength curve of Figure 2.11. In fact, Crory's dashed line in Figure 6.4 gives 50 percent higher values than those of the ultimate strength curve of Figure 2.11. This is explained by Crory's (1963) statement that a well-graded sand slurry, vibrated in place, has an adfreeze strength about 50 percent higher than its silt counterpart at the same temperature. Differences between Crory's values and those given in this study may be due to scale effect, test conditions, and dry densities (sand concentrations).

Small differences in dry densities makes a significant difference in the adfreeze strength, as shown in Figure 5.31. For sand concentrations greater than 50 percent (82.7 lbs. per cu. ft. dry density) the frictional component of adfreeze strength becomes more significant. The long-term adfreeze strength τ_{lt} proposed by Vyalov (1959) in Equation 2.11 for 6 in. diameter timber piles in frozen silty sandy loam is also plotted in Figure 6.4 for comparison. At warm temperatures (above $-3^{o}C$) the agreement between the three studies appears to be at its best.

At this point, it is convenient to distinguish between the two components, ice adhesion and sand friction, by plotting a typical load-displacement curve for a test on ice and one for a frozen sand. Figure 6.5 clearly shows the difference in ultimate and residual loads. Crushed ice was chosen to simulate the polycrystalline ice believed to exist in the frozen soil. Although the initial (at rupture) displacement, δ_r, for frozen sand in Figure 6.5 is slightly larger than that for ice, the difference is only part of the experimental scatter. Both materials, ice and frozen sand, showed essentially the same average initial displacement, about 0.002 in., considering the difficulty with precise displacement measurements on the recorder. Also, the initial displacement for all plain rods in ice and frozen sand specimens appeared to be independent of temperature and loading rate. A slight decrease in the displacement was observed at loading rates higher than 200 lbs./min., especially in ice specimens.

The initial displacement includes elastic bond displacement, rod extension, deflection of the reaction beam shown in Figure 3.1, and deformation of the frozen specimen. The latter was estimated to be about 8.0×10^{-6} in. for a maximum load of 3000 lbs. applied to plain rods in frozen Wedron sand. Data from previous work (Bragg, 1980) was used in the calculations. The corresponding rod extension was estimated to be 3.26×10^{-4} in. using Hook's law and a steel elastic modulus of 30×10^{6} psi. The reaction beam deflection (as a simply supported beam) was estimated to be 3.0×10^{-5} inch. The total deflection due to the system stiffness (about 3.5×10^{-4} in.) appears to be negligible in comparison to the average 0.002 in. initial displacement. This

displacement increased with increasing rod surface roughness as shown in Figure 5.27. The increase was probably due to interaction between sand particles and steel surface roughness, and which requires larger displacements for mobilization.

The greater adfreeze bond strength for frozen sand, compared to ice, develops because the presence of rigid sand particles adjacent to the steel requires that a large volume of the ice matrix be involved in the failure process. Another comparison between ice adhesion and sand friction can be made using data for frozen sand in Figure 5.17 and data for crushed Ice (2) in Figure 5.29. The best-fit lines for data from both figures are reproduced in Figure 6.6 with residual loads for ice and frozen sand (from Table 5.2) plotted against temperature. At ultimate loads the frictional component τ_{uf} contributes about 50 percent to 60 percent of the total adfreeze strength for the frozen sand. The frictional component becomes more significant for residual loads, τ_{rs}. The frictional contribution τ_{rf} to residual loads ranges from 78 percent to 84 percent. Note that these percentages are somewhat high due to the presence of water impurities in the crushed Ice (2), which was formed from ordinary tap water.

The choice of crushed ice, for comparison in Figure 6.6, was made instead of the snow-ice because the latter had the highest data scatter as shown in Figure 5.29. Also, the crushed ice strength values in Figure 5.29 are intermediate between the two extreme types, Ice (1) and Ice (3). The error, of under-estimating the adhesive strength for polycrystalline ice (in sand pores), is believed to be compensated by ignoring the contact area between sand grains and steel

rod. However, Lambe and Whitman (1969) reported that measurements of the contact area between sand particles (about 0.06 mm in. diameter) showed that typically it is approximately 0.03 of the total area. For quartz, with a hardness of about 1100 kg/mm^2, the stress on an asperity (in contact with the steel rod) must exceed 1,500,000 psi to produce plastic deformation. The frictional component is, therefore, only slightly affected by neglecting the contact area of sand grains in the calculation.

The adhesion and friction components also vary with the displacement rate at a given temperature along with surface (or pile) type as shown in Figure 2.13. In this figure, Parameswaran (1981) showed that the frictional contribution varied from about 84 to 93 percent of the total adfreeze strength of frozen sand to steel piles. This over-estimated percentage (at ultimate loads) was made when Parameswaran under-estimated the percentage of ice contribution. He simply multiplied the ultimate values of ice adfreeze strength (solid lines in Figure 2.9) by the porosity of frozen sand (0.2377) in order to obtain the dashed lines in Figure 2.12. In doing so, he had attempted to simulate the polycrystalline ice which exists in the sand pores. The ice represented in Figure 2.9 may not be polycrystalline ice since it was prepared by freezing the distilled water which had been poured around the pile to the required height.

5.1.2 Lug Bearing:

The addition of a single lug, by welding, to a plain 3/8 in. diameter rod permits bearing action of frozen sand on the lug to contribute to the total pull-out load. To illustrate the relative

contribution of each component, load-displacement curves for ice and frozen sand, both with a plain rod, and a third curve for frozen sand with a plain rod and single lug, are plotted in Figure 6.7. Two stages considered for comparison include the "initial yield" (failure) and the ultimate load (large displacement) conditions. The lug contribution has now been added to the ice adhesion and sand friction discussed earlier. The displacement curves for specimens with lugs show initial behavior characteristics similar to those observed with plain rods. After the initial rupture, mobilization of lug bearing prevents the load from dropping to the residual value.

When the "initial yield" loads, P_{iy}, for rods with lugs are compared with the ultimate loads, P_u, for plain rods at different temperatures (Figure 6.8) the lug contribution ranged from about 25 percent at -26°C to about 75 percent at -2°C. Considering the ultimate condition at large displacements where the total load was transferred almost entirely to the lug (Figure 6.7) the adhesion and friction become negligible. Comparing the ultimate lug loads P_u with the residual loads P_r for frozen sand from Figure 6.6, the lug contribution (P_l in Figure 6.9) ranges from 90 percent at -26°C to 100 percent of the total load at 0°C. Similar conclusions can be drawn on comparing lug contribution with the residual load for different lug sizes (Figure 6.10). In Figure 6.10 lug contribution increased from an average of 85 percent of the total load for h = 1/64 in. to 95 percent for h = 3/16 in. at temperatures of -10°C and -20°C.

It is of interest to compare the pull-out loads for plain rods and lugs with the uniaxial compressive strength σ_u for frozen sand. To

do so, strength data from Bragg (1980) are compared with the ultimate lug pull-out capacity P_u, the "initial yield" loads P_{iy}, and the ultimate bond strength τ_u in Table 6.1. Values for the uniaxial compressive strength correspond to an average strain rate $\dot{\varepsilon}_{avg.}$ of 3 X 10^{-6} per sec. in Bragg's (1980) Figure 5.9. This strain rate corresponds to a nominal machine displacement rate $\dot{\delta}_n$ of 5.0 X 10^{-4} in./min., calculated by multiplying $\dot{\varepsilon}_{avg.}$ times ℓ_o (= 2.82 in.), where ℓ_o was the length of uniaxial test samples in Bragg's (1980) study.

Note that comparisons based on equal displacement rates in both types of test (bond and uniaxial comparison tests) do not mean equal strain rates. Differences in sample size, test conditions such as applied confining pressures, and other factors would not yield equal strains in both tests. Equal displacement rates were chosen only to make the comparisons under similar conditions. There is some similarity in both tests because frozen soil experiences compression under the lug and also in the uniaxial compression test. Comparisons are made for lug movement at the same rate as the loading ram in the compression test (neglecting any differences due to machine stiffness). The data in Table 6.1 are plotted in figure 6.11. Although the relationships are not linear, they are approximated by straight lines which pass through the origin, except for the τ_u-vs-c relationship. By analogy to Equation 2.17 the ratio of bond strength, including lug bearing, to the frozen sand cohesion ($c = \sigma_u/2$) ranges from 0.190 for plain rods to 0.390 for lugs. Values of κ suggested by Weaver and Morgenstern (1981 b) in Equation 2.17 ranged from 0.6 for plain piles to 1.0 for corrugated piles, with c-values evaluated on a long-term basis. No standard definition for "corrugated" piles was mentioned by Weaver and Morgenstern

(1981 b).

For comparison purposes the cohesion ($c = \sigma_u/2$) was defined on the basis of a horizontal Mohr-Coulomb envelope ($\phi = 0$). Should this envelope be inclined to the horizontal at an angle ϕ, values of c would be slightly reduced, thus increasing the values of κ for this study. A comparison also can be made between the lug bearing capacity q_1 (lug contribution P_1, in Figures 6.9 and 6.10, divided by the lug area A_1) and the uniaxial compressive strength σ_u. Such a comparison, shown in Figure 6.12, was based on equal displacement rates for both tests. As shown in Figure 6.12 the relationship is not linear but can be approximated by a straight line. This relationship indicates that the ultimate lug bearing capacity is about seven times the uniaxial compressive strength of frozen sand.

6.1.2.1 Lug Behavior in Frozen Sands:

Lug behavior in frozen sand may be considered analogous to a deep plate (or footing) in frozen ground. Experimental work reported by Ladanyi and Paquin (1978) using a standard penetrometer (1.4 in. diameter) in a frozen quartz sand ($e_o = 1.034$, $v_s = 49.15$ percent, $C_u = 2.27$) provides comparative data for use with the lugs. The penetrometer placed at a depth of 18 in. can be classified as a deep footing. Data summarized in Figure 2.15 have been transformed into punch stress versus creep rate on a log-log scale in Figure 6.13 and compared with data from Figure 5.40 for a 1/8 in. height lug (equivalent punch diameter equals $d + 2h = 0.625$ in.). Both tests were conducted at -6°C. Both relationships are almost linear, especially for the penetrometer. The two lines are almost parallel indicating that a similar mechanism

appears to control the creep rates in both cases.

The main reason for a difference in creep rates (or strength) is believed due to the difference in void ratios (or sand fractions) of the two sands. The importance of sand fraction on lug bearing loads has been shown in Figure 5.49. A reduction in the sand fraction from 64 percent to 49 percent at -10^{0}C resulted in a load reduction close to 49 percent for creep rates of 10^{-4} in./min. or 10^{-5} in./min. A larger reduction would be anticipated at warmer temperatures such as -6^{0}C. Additional factors responsible for the difference in applied stress shown in Figure 6.13 involve the punch diameter, 0.625 in. for the lug versus 1.4 in. for the penetrometer. The significance of this difference in diameters is shown in Figure 5.41 and from Vyalov et al. (1973). When the P-values (in pounds) from Figure 5.41 were normalized with respect to the lug area A_1 to give $q_1 = P/A_1$ (as punch pressure in psi) the solid lines in Figure 6.14 were obtained to help explain the difference between curves in Figure 6.13. These lines clearly show that creep rate increases with an increase in lug size for the same stress level. This result is also supported by the experiments conducted by Vyalov, et al. (1973) on punches of three different sizes loaded in ice at -2.3^{o}C. For comparison the results of those experiments are included in Figure 6.14. Their data indicates that as the punch diameter was increased from 1.26 in. to 12.6 in. (10 times larger) the punch pressure decreased about 50 percent to 70 percent.

For the present study, increase in lug height from 1/16 in. (0.50 n. equivalent punch diameter) to 3/16 in. (0.75 in. punch diameter) aused a reduction in pressure of about 17 percent to 20 percent,

depending on the stress level. The difference in punch sizes indicated in Figure 6.13 may, therefore, have contributed about 25 percent to the total reduction in strength shown. Note that the comparisons made in Figure 6.13 are valid for the range of creep rates indicated, which do not necessarily coincide with the same range of strain rates at which the uniaxial compression tests on both sands were conducted.

Ladanyi and Paquin (1978) indicated that when trying to relate the behavior of a deep footing (punch) with that of a representative soil sample under triaxial test conditions, the problem most difficult to solve is usually that of selecting the strain rate in the test that would be representative of the average strain rate of the soil during penetration. Since the strain rate around a footing decreases continuously with distance, various interpretations are possible. The one considered by Ladanyi and Paquin (1978), relates the penetration rate of a circular footing with the time to failure of a soil element located below the base in the line of penetration, by a semi-empirical expression, the same as proposed by Ladanyi (1976). Based on that expression the two authors estimated that a range of penetration rates, from about 2×10^{-6} to 1.1×10^{-3} in./min., for their punch size of 1.4 in. diameter (Figure 6.13), would be equivalent to a strain rate of about 1.8×10^{-8} to 8.3×10^{-6} per second. In fact, both ranges are lower than the lowest applicable creep or strain rates in their experiments.

The difference in depths of punch embeddment in Figure 6.13, do not appear to be a significant factor. As noted in Section 2.5, when a punch settles more than about 5 percent of its diameter, the soil enters into viscoplastic region and the effect of burial depth becomes negligible.

Under such conditions, no effect of burial depth was observed for depth to diameter ratio D'/B between 3.3 and 5.0 in ice (Sego, 1980) and between 5 and 15 in frozen sand of Ladanyi and Paquin (1978). The decrease in creep rate, noted in Figure 2.16, with the increase of burial depth is, probably, due to the fact that the settlement did not exceed 1 percent of the footing diameter.

Since the lug penetration, or displacement, δ, exceeded the equivalent footing diameter (more than 200 percent) the burial depth did not appear to have any effect on the lug creep rate. This may be observed from Figure 5.43, where the lug position z was changed from 1.5 in. (D'/B= 4.5/0.635 = 7.2) to 4.5 in. (D'/B= 2.4). The equivalent depth of embeddment D' was measured from the sample top surface (at z = 6 in.). It is believed that some reinforcing effect by the steel rod to which the lug is welded, may be involved in eliminating the effect of burial depth on the lug creep rate. The steel rod would prevent any side tilting of the lug, which might occur at shallow depths. Lug position was also studied relative to possible interaction between the lug and the base plate. Data summarized in Figure 5.43 also imply that with the lug position as close as 1.25 in. (1.50 less 0.25 in. of total creep displacement) to the base plate, the creep rate was not affected. Due to equipment limitations, the distance z was not made smaller than 1.25 in. This minimum distance, which showed no interference between the lug and reaction base plate, corresponds to a D'/B ratio of 7.6 (= 4.75/0.625) and to a z/B ratio of 2 (= 1.25/0.625).

6.1.2.2 Lugs versus Standard Deformed Bars:

The measured peak loads for a standard deformed bar (d = 3/8 in., h = 1/64 in., lug spacing = 0.3125 in.) shown in Figure 5.21 were transformed into single lug loads as indicated in Figure 5.22. For example, the peak load for the 3 in. sample height (about 4000 lbs. in Figure 5.21) was divided by the number of lugs (10) after subtracting the residual load of 60 lbs. (= 120 X 3 in./6 in.) for the corresponding plain rod, i.e. P = (4000 - 60)/10 = 396 pounds. The latter was then added to the 120 lbs. residual load, giving a total of 516 lbs. load for a 6 in. sample height with a single lug. Similar calculations were applied to the 2 in. sample height in Figure 5.21 in order to obtain the two data points indicated in Figure 5.22. Although these points agree well with experimental data points for other lug heights, there is a difference in the load-displacement behavior for the standard deformed bar (compare Figure 5.20 with 5.21). The decrease in load after about 0.04 in. displacement (Figure 5.21) appears to be due to : (1) the lug interaction effect, and (2) the small ratio of lug height (0.015 in.) to the maximum particle size (0.023).

Little or no interaction between the reaction base plate and the nearest lug was anticipated because of adequate clearance between the deformed rod and removable washer in the support plate. Besides, if the lug spacing to lug height ratio were to be considered it would be large enough (0.3125/0.125 = 21) to prevent any interaction between the lugs. The interaction should, therefore, be explained in terms of the ratio of lug spacing to equivalent punch width, which is in this case less than one (0.3125/0.405). Such lug interference is illustrated in Figure 6.15. As shown in this figure, when the soil stress under the

top lug (No. 1) is q_o, the stress under the second lug would be $1.27q_o$ using Boussinesq's stress distribution. Soil stresses under successive lugs can be evaluated in a similar manner as shown in Figure 6.15. It has been estimated that a maximum stress of $1.37\ q_o$ occurrs under the sixth lug, where its value remains constant for subsequent lugs.

If the above assumption is reasonable, failure would initiate in the soil under the bottom lug and move upwards, due to lug interaction. As the lug penetrates into the soil, it leaves a gap equal to the displacement, thus weakening the support for the next lug. When the ultimate load is reached, the gap would have reached its limiting size, the soil support would decrease and hence the load for any further displacement (beyond 0.04 in.) as shown in Figure 5.21. In addition to lug interaction effect, when the lug height is smaller than the particle size the frictional and dilatational components may not be fully mobilized in front of the lug. A creep test on the 3/8 in. diameter standard deformed rod (Figure 5.42) indicated a reasonable agreement with tests on other lug heights as shown in Figure 5.41. In general, standard deformed rods tolerate smaller displacements at failure than single lugs (compare 0.04 in. in Figure 5.21 with 0.30 in. in Figure 5.20).

6.1.2.3 Long-Term Lug Bearing Capacity:

The data shown in Figure 2.4 suggest that frozen soil strength decreases exponentially with time to failure. The relationship described by Equation 2.1 indicates that the long-term strength (when t_f goes to infinity) is zero. Vyalov (1963) pointed out that after some long period of time the additional strength reduction is so insignificant

that it can be neglected in engineering calculations. The same conclusion applies to the lug behavior in frozen sand. A plot of load versus time to failure was prepared, for all creep tests on single lugs at -10°C, and is shown in Figure 6.16. In this figure, the time to failure t_f was defined as the time required to achieve a certain displacement since complete tertiary creep failure was observed only on the last load increment.

Excessive displacements (such as 0.25 in. or 1.0 in. as shown in Figure 6.16) may be considered as the basis for defining failure. Values of t_f corresponding to a certain load increment were obtained by extrapolation. The displacements 0.25 in. (or 1.0 in.) were divided by the creep rate corresponding to that load increment, after subtracting the "pseudo" instantaneous elastic displacement δ_i and values of t_f are listed in Table 6.2 for different load increments on a 3/8 in. rod with a 1/8 in. lug height in frozen sand at -10°C. The data summarized in Figure 6.16 indicate that the long-term load capacity was about 32 percent of the instantaneous capacity for 0.25 in. allowable displacement, and about 38 percent for a 1.0 in. maximum allowable displacement. Thus, assuming about 4500 lbs instantaneous strength for both cases, any load less than about 1800 lbs. in Figure 5.40 would not reach a secondary creep rate stage within the experimental times used.

Creep rates for loads below the long-term strength would continue in the primary stage and attenuate until the rate approached zero at infinite time. Creep rates for initial loads below 1800 lbs. in Figure 5.40 would be over-estimated if they were considered as secondary creep rates, even though they were measured at the end of that step loading. Also, at the small initial loads the adhesion and friction

contribution along the rod was significant (Figure 6.8), thus giving some errors in creep measurements, especially at colder temperatures (below -10^{o}C). However, at large displacements the lug contribution becomes far more significant (Figure 6.7) and neglecting the residual loads would not cause significant errors.

6.1.2.4 Sample Size and Sand Concentration:

The effect of sample diameter on the creep behavior of lugs in frozen sand has been considered in Figures 5.44 and 5.45. Note that sample diameters greater than about 4 in. would not affect the pull-out capacity for the bar and lug sizes used in this study. The reduction in strength at diameters smaller than 4 in. may be attributed to (1) the contribution of sample deformation to the total creep, and (2) the increased effect of stress concentration under the lug area.

For sample diameters greater than 2 in., it was estimated that sample deformations under a 4000 lbs. load would be negligible in comparison to soil creep under the lug. Therefore, stress concentration under the lug area is believed to be the main factor in reducing the load for sample diameters less than 4 inches. For these smaller diameters, visual inspections of samples after failure indicated that rupture had occurred on planes inclined at about 60^{o} from the horizontal, thus suggesting that the soil samples may have failed due to stress concentration. The latter also produces high tensile stresses in the tangential θ-direction with possible failure in tension.

The effect of sand concentration on lug bearing, summarized in Figures 5.48 and 5.49, may be compared with similar effects on the uniaxial compressive strength summarized in Figure 2.5 for Ottawa sand.

The average grain size of Ottawa sand used by Groughnour (1967) was 0.0306 in., slightly larger than that of the Wedron sand used here (about 0.0138 in.). Besides, the Ottawa sand grains were well-rounded compared to the sub-angular shaped Wedron sand grains. Other properties are believed to be almost the same for both sands. To make possible a closer comparison, one curve has been chosen from Figure 2.5; that corresponding to -12.03°C and a strain rate of 1.33×10^{-4} per min. This rate appears to correspond to a nominal (machine) displacement rate of about 3×10^{-4} in./min., based on a sample length of 2.26 in. used by Goughnour (1967). Load values were interpolated from Figure 5.48, for $\dot{\delta}^c$ of 3×10^{-4} in./min. and different sand concentrations. These loads were increased by about 13.5 percent to allow for the decrease in temperature from -10°C to -12.03°C. Using Figure 6.9 the ultimate loads in Figure 5.24 were reduced by 240 lbs. to account for the residual shear loads along the rod. A residual load of 90 lbs. at -12°C for the ice sample ($v_s = 0$) was considered in the calculations.

The adjusted loads were divided by the lug area to obtain the lug bearing pressure q_l. Values of q_l are plotted versus sand concentration v_s in Figure 6.17. The unconfined compressive strengths σ_u, show bi-linear relationships with v_s. Although the lug bearing may not vary linearly with sand concentration (Figure 5.49) it was approximated by two straight lines whose intersection point gives a critical sand concentration close to 43 percent sand by volume. This point, which is quite close to the 42 percent observed by Goughnour (1967), appears to indicate a change in the failure mechanism for frozen sands. This sand concentration corresponds to a porosity of 0.580 which is close to

0.476 for the loosest possible packing of uniform spheres (in cubical array) listed by Harr (1962). Therefore, at the critical volume concentration, sand grains just begin to make contact as the soil behavior becomes dependent on the closeness of adjacent sand particles.

Goughnour (1967) reported that samples of frozen Ottawa sand with more than 42 percent sand by volume showed a more rapid initial volume decrease (under compression tests) followed by a volume increase which progressed at an increasing rate, and was similar to the volume increase of dense unfrozen sand (Bishop and Henkel, 1962). Goughnour suggests that three mechanisms may serve to strengthen samples made with sand and ice versus those of pure ice. The first is associated with sand volume concentration in the sample and is probably caused by virtually all ice plastic deformation. This mechanism may explain the behavior represented by the first line segments in Figure 6.17.

The second mechanism is associated with grain to grain contact and is the result of friction at these contacts. The third mechanism is associated with volume increase of dense samples and has a counterpart in unfrozen sand. The sample volume increase is impeded by the ice matrix. Thus the ice matrix effectively exerts a confining pressure on the sand particles. The effect of this ice exerted pressure is to increase the effective stress on the sand skeleton, thus increasing its resistance to deformation similar to unfrozen soil. This "equivalent" confining pressure continues to increase until dilatancy levels off at a critical void ratio or the limiting ice cohesion is overcome.

6.1.2.5 Lug Bearing in Ice:

The lug behavior observed under the initial load increment in Figures 5.46 and 5.47, for samples with a sand fraction below 50 percent, appears to support Goughnour's (1967) first mechanism. He suggested that virtually all of the plastic deformation is accomodated by the ice matrix. This appears possible only when the sand friction and dilatancy do not significantly contribute to the total resistance. As shown in Figure 6.17 these components begin to develop at a sand fraction close to 42 percent. There may be some reinforcing effect by the sand grains which would impede the deformation mechanism of pure ice. Below the critical sand concentration (about 42 percent), the lug behavior appears to be mainly influenced by the ice deformational characteristics. In this case, seven deformation mechanisms have been identified by Gold (1963) in observing surface features of ice during deformation. These include slip bands, grain boundary migration, kink bends, distortion of grain boundaries, crack formation, cavities, and recrystallization.

Since ice creeps under very small stresses (Vyalov, 1963) the behavior observed in Figure 5.47 cannot be attributed to these seven mechanisms. The initial delay in the creep of snow-ice under pressure appears to be caused by bond (shear resistance) along the rod. This bond was mobilized at much smaller displacements as compared to lug bearing. The delay time observed in Figures 5.46 and 5.47 for the 520 lbs. initial load increment can be considered as the time to failure of the bond resistance under that load. Since the creep displacement at bond failure would have been too small to measure

with the available equipment, no precise correlation can be made between the sand fraction and time to failure (or the initial delay time).

From a careful consideration of the snow-ice behavior shown in Figure 5.48 one may conclude that a residual bond resistance of about 200 lbs. along the bar may have caused higher loads in some of the snow-ice samples as compared to the sand-ice samples. Otherwise, there is no reason why the data points would not be consistent with the dashed line extrapolated from the data point of test number CI-1 (Figure 5.47). This data point appears to be a coincidental point in which the residual bond resistance may have been the least.

For snow-ice and sand-ice (sand fraction below 50 percent) samples prepared by pre-cooling the mold and the rod below 0°C a thin layer of ice was observed around the rod soon after adding pre-cooled distilled water. For those samples the bond resistance along the rod may be due mainly to ice adhesion. That is probably why the initial delay time was not much affected by the sand fraction. Since the snow-ice was expected to have the lowest lug bearing compared to the sand-ice, the bond contribution in the latter may also be less significant than in the snow-ice. No correction for the residual bond (due to ice adhesion) was made in Figure 5.48, since it should be negligible in sand-ice and no accurate measurements for its value in snow-ice was possible due to equipment limitations.

6.2 Creep versus Constant Displacement Rate Tests:

Comparison of strength data from constant strain rate tests and data from creep tests was made by several authors (Goughnour, 1967; Hawkes and Mellor, 1972; Bragg, 1980). In this study, the adfreeze bond

strength for plain rods in frozen sand from constant displacement rate tests has been compared with the strength from creep tests as shown in Figure 6.18. There appears to be a reasonable agreement between the results from both tests. Assuming that the observed displacement rates ($\dot{\delta}_n$ and $\dot{\delta}^c$) are representative, there appears to be a transition from creep data (slow rates) to constant displacement rate (high rates). The change in slopes of the lines in Figure 6.18, at about 10^{-4} in./min., indicates a change in the strength mechanism upon transition from slow creep rates to the fast displacement rate for both temperatures.

For lugs, the displacement rates for both test types were approximately in the same range (Figures 5.6 and 5.36). The lug capacity from creep tests is plotted against lug capacity from constant displacement rate tests, at different temperatures, lug sizes, and creep rates, as shown in Figure 6.19. The data in Figure 6.19 indicate that creep tests produce lug capacities which are slightly higher than those obtained from constant displacement rate tests. It is believed that this higher strength was a result of some densification and stiffening of the frozen sand in front of the lug during creep. The difference is, however, small and might be neglected for practical purposes.

6.3 Correlation of Experimental Results:

The empirical equations deduced in Chapter V are combined in this section in order to give a composite equation which relates the lug capacity to the test variables. A similar equation has also been derived for the adfreeze bond strength of plain rods.

6.3.1 Plain Rods:

The ultimate bond strength τ_u of frozen sand (64 percent sand by volume) with a plain steel rod (5/8 in. diameter) was observed to depend on the nominal displacement rate $\dot{\delta}_n$ (machine speed) as shown in Figure 5.4 (and Equation 5.3). Bond dependence on the loading rate $\dot{P}$ was illustrated in Figure 5.3 and expressed by Equation 5.1, where τ_c and m (= 1/n) are the temperature dependent parameters shown in Figures 5.11 and 5.12, respectively. Since measurements of loading rates were more reliable than the displacement rates, it seemed reasonable to use loading rates for further correlations. Substituting 10.5 θ for τ_c in Equation 5.1 (Figure 5.9) and with $\dot{P}_c$ = 1 lb./min. gives the following relationship:

$$\tau_u \text{ (psi)} = 10.5\ \theta\ \dot{P}^m \qquad (6.1)$$

where m = 1/n = exp - (1.224 + 0.0886 θ) as shown in Figure 5.12, and θ = -T. Since Equation 6.1 was derived for a 5/8 in. diameter rod (d), 6 in. sample height (H), rod roughness ρ of 625 percent, and sand fraction v_s of 64 percent, these parameters may also be included in this equation.

To do so, consider the combined effect of the ratio d/H using the data in Figure 5.18. The two regression lines are combined by plotting τ_u/θ versus d/H on a log-log scale. This eliminates the temperature effect and gives the empirical relationship shown in Figure 6.20. This procedure implies that at a given ratio d/H the bond strength τ_u is a linear function of temperature θ. This assumption appears to be true for all loading rates $\dot{P}$ below 6.0 lbs./min. as shown in Figure 5.9. Assuming that the optimum ratio of d/H is 10 percent (Figure 6.3) and neglecting the effect for d/H $\geq$ 10 percent, the value of τ_u in Equation

6.1 can be multiplied by $(d/10H)^s$, where s = 0.692 if d/H $\leq$ 10 percent and s = 0.0 if d/H $\geq$ 10 percent. The roughness factor ρ can be included by multiplying Equation 6.1 by $(\rho/625)^{0.354}$, using the relationship in Figure 5.28.

The sand fraction v_s was included in Equation 6.1 by replotting the data in Figure 5.31 on a log-log scale. An experimental power law of the form shown in Figure 6.21 can be deduced, applicable for $v_s \geq 45$ percent. Combining all test variables into one equation leads to

$$\tau_u \text{ (psi)} = 10.5(\dot{P})^m (\rho/625)^{0.354}(v_s/64)^{2.246} (d/10\ H)^s \theta \quad (6.2)$$

where $m = \exp - (1.224 + 0.0886\ \theta)$; $\theta = -T$, ^oC; $\dot{P}$ = loading rate, lbs./min.; ρ = roughness factor, percent; s = 0.692 for d/H $\leq$ 10 percent and 0.0 for d/H $\geq$ 10 percent; v_s = sand fraction, percent.

Equation 6.2 would be limited to test conditions used in this study, i.e.

$2^oC \leq \theta \leq 26^oC$

1 lb./min. $\leq \dot{P} \leq$ 2000 lbs./min.

2 percent $\leq$ d/H $\leq$ 40 percent

45 percent $\leq v_s \leq$ 64 percent

$\rho \leq$ 1500 percent

Equation 6.2 appears to compare reasonably well with experimental data as shown in Figure 6.22. A comparison of Equation 6.2, derived from constant displacement rate test data, with creep displacements of plain rods could not be made because of equipment limitations. More experimental work is needed on creep of plain rods using equipment capable of displacement measurements to at least $\pm 10^{-5}$ inches.

6.3.2 Deformed Rods:

Test variables affecting lug behavior can also be combined into one Equation. The relation between load and creep rate shown in Figure 5.36 gives the expression:

$$q\ (psi) = q_{c\theta}\ (\dot{\delta}^c/\dot{\delta}_c)^{0.203} \qquad (6.3)$$

where $q_{c\theta}$ is the temperature dependent lug pressure, corresponding to an arbitrarily chosen creep rate $\dot{\delta}_c$ of 0.0005 in./min., and can be expressed as:

$$q_{c\theta} = q_{co}\ (1 + \theta/\theta_o)^{0.6} \qquad (6.4)$$

where q_{co} = 3718 psi at 0°C, and θ_o is a reference temperature equal to 1°C. Equation 6.4 was derived by plotting values of $P_{c\theta}$ from Figure 5.40 and values of P_u from Figure 5.24 against the temperature function $(1 + \theta/\theta_o)$ on a log-log scale as shown in Figure 6.23. For small temperature intervals, the exponent in Equation 6.4 can be made equal to unity, and the power law reduces to the linear expression given in Figure 5.24. The power law (Equation 6.4) will be used instead since it is applicable over larger temperature ranges (Vyalov, 1963; Ladanyi, 1972). Substituting $P_{c\theta}$ from Equation 6.4 and 0.0005 in./min. for $\dot{\delta}_c$ into Equation 6.3 gives:

$$q\ (psi) = 3718\ (1 + \theta)^{0.6}\ (\dot{\delta}^c/0.0005)^{0.203} \qquad (6.5)$$

Next consider the effect of lug size. Note that the load P_u (pounds) in Figures 5.22 and 5.41 increases with an increase in the ratio A_l/A_r (or in the lug size). Also note that, when the same load was normalized with respect to the lug area A_l for each lug size (lug pressure q_l in psi), the effect was reversed as shown in Figure 6.14. The applied lug pressure in Figure 6.14 appears to increase with a reduction in lug

height. Since the rod area A_r is constant (d = 3/8 in. for all lugs) the ratio A_l/A_r (data from Figures 5.22 and 5.41) may be plotted versus lug pressure q_l on a log-log scale, as shown in Figure 6.24.

Using the least-squares line on Figure 6.24 gives:

$$q \text{ (psi)} = 15600 \, (A_l/1.78 \, A_r)^{-0.191} \qquad (6.6)$$

Note that Equations 6.5 and 6.6 were derived for frozen sand with 64 percent sand by volume. Frozen sands with less than this percentage of sand give lower lug pressures as shown in Figure 5.49. Equations 6.5 and 6.6 can be modified to include the sand fraction. Recall that for a sand fraction below about 42 percent (Figure 6.17), the soil would be in a very loose condition and would represent an ice-rich permafrost. The emphasis here has been placed on sand fractions above 42 percent where a small change in the sand content would result in a significant change in the frozen strength.

It was shown in Figure 5.50 that the ratio of $P_{51\%}$ to $P_{64\%}$ is almost constant, about 0.571. This has two implications: (1) the reduction in lug bearing (about 43 percent) was almost independent of creep rate and (2) the rate of change of lug bearing with change in sand concentration, i.e. slope of the lines for $v_s > 42$ percent in Figure 5.49, is dependent on the creep rate. The latter condition complicates the solution. It means that for every value of creep rate a certain empirical equation must be used to account for the sand concentration effect. Although several procedures can be made to avoid this complication, plotting the load P versus sand fraction v_s on a log-log scale appears to be the simplest procedure.

Choosing an arbitrary creep rate, say 0.0005 in./min., the load

P can be interpolated from Figure 5.48, and plotted against the corresponding v_s values on a log-log scale as shown in Figure 6.25. The linear relation suggests a power law of the form:

$$q\ (psi) = 15790\ (v_s/64)^{2.654}$$

(valid for $v_s \geq 45$ percent sand by volume) (6.7)

The overall effect of different factors may be considered by combining Equations 6.5, 6.6, and 6.7 to give the following composite empirical equation:

$$q\ (psi) = 0.2288\ (1 + \theta)^{0.6}\ (\dot{\delta}^c)^{0.203}\ (A_1/A_r)^{-0.191}\ v_s^{2.654} \quad (6.8)$$

The range of experimental data limits Equation 6.8 to the following conditions:

$2^oC \leq \theta \leq 20^oC$

10^{-5} in./min. $\leq \dot{\delta}^c \leq 10^{-2}$ in./min.

$0 \leq A_1/A_r \leq 3$

$v_s \geq 45$ percent sand by volume

The remaining question involves a relationship between the applied lug bearing pressure q and time to failure t_f. Most creep curves for sand-ice specimens did not reach tertiary creep within a relatively short time period, say less than 24 hours, except at large loads (more than 4000 lbs.). In constant displacement rate tests, the time to failure varied from a few hours up to about 36 hours. Besides, the failure was clearly defined by two peaks (see Figure 5.20). In creep tests, it appears reasonable to use a certain limiting creep displacement δ_f as a basis for creep failure criterion in the frozen sand. This has the advantage of limiting the total displacement to acceptable values

in the design.

From the displacement behavior for a constant stress creep test (first load increment in Figure 5.34) it follows that:

$$\delta_f = \delta_i + t_f \dot{\delta}^c \tag{6.9}$$

where δ_i is the pseudo-instantaneous displacement. A small part of this displacement is elastic, which may be neglected, and the major part is plastic (irreversible). Equation 2.6 shows that the plastic strain (second term) is related to the applied stress by a power law. By analogy, a similar power law may be deduced by plotting the measured displacements δ_i versus the applied lug load P (Figure 6.26). Dividing the empirical equation shown in this figure by the lug area gives:

$$\delta_i = 8.3 \times 10^{-8} \quad q^{1.429} \tag{6.10}$$

By rearrangement of variables in Equation 6.8 and some calculations, the creep displacement rate $\dot{\delta}^c$ is given by:

$$\dot{\delta}^c = 8980 \ (1 + \theta)^{-2.95} \ (A_l/A_r)^{0.941} \ v_s^{-13.07} \ q^{4.93} \tag{6.11}$$

Substituting for δ_i and $\dot{\delta}^c$ from Equations 6.10 and 6.11, respectively, into Equation 6.9, and rearrangement of terms gives the time to failure t_f:

$$t_f = \frac{\delta_f - (8.3 \times 10^{-8}) \ q^{1.429}}{8980 \ (1 + \theta)^{-2.95} \ (A_l/A_r)^{0.941} \ v_s^{-13.07} \ q^{4.93}} \tag{6.12}$$

To compare Equation 6.12 with some of the experimental data, the "failure" or limiting displacement δ_f should be defined. Values of 0.25 in. and 1.0 in. were earlier selected as convenient limiting displacements, δ_f. The time to failure t_f was observed for these limiting displacements and the corresponding applied load was noted. For step

loading creep curves, an extrapolation procedure was used to estimate some values of t_f. The data are summarized in Table 6.3 and plotted in Figure 6.16. This figure shows that lug bearing pressure decreased with time until it reached a finite value q_{lt} after a fairly long time. Neglecting δ_i, Equation 6.12 predicts that the lug bearing capacity will go to zero as t_f approaches infinity. Figure 6.16 suggests that the long-term lug bearing capacity, q_{lt}, does exist since infinity is far beyond the usual service life. Note that when the applied lug pressure is lower than q_{lt}, the secondary creep rate becomes practically zero. For these reasons, it appears reasonable to replace q in Equation 6.12 by $(q-q_{lt})$. In this case the lug bearing capacity q would tend to a finite value q_{lt} as t_f tends to infinity.

The data in Figure 6.16 may now be compared with Equation 6.12. Only data points corresponding to 1.0 in. limiting displacement are replotted in Figure 6.27 on a log-log scale. Experimentally derived data and failure times predicted by Equation 6.12 (dashed lines) are in reasonable agreement.

6.4 Theoretical Predictions:

This experimental study has been primarily concerned with pull-out loads for a steel bar embedded in a small frozen sand sample. A model pile or anchor section is preferred when they save money and when questionable assumptions are required for analytical methods. There are some limitations imposed on straight-forward application of the results from model tests to full-scale structures. Rocha (1957) suggests that the following conditions must be fulfilled; the geometry, stresses, strains, displacements, time required, Poisson's ratio, modulus of

elasticity and other properties of the model should be proportioned to those of the field structure. The main purpose here is to adopt some of the analytical methods, using the basic creep parameters of frozen Wedron sand (Bragg, 1980) and the available theories, in order to predict the pull-out capacity of plain and deformed rods. The failure mechanisms of plain rods are different from those of lugs. The two cases are, therefore, treated separately. A theoretical attempt has also been made to relate both cases to the roughness criterion defined in Equation 5.7.

6.4.1 Bond for Plain Steel Rods:

The stress and displacement analysis for frozen soil surrounding a plain rod (Figure 2.12) reviewed in Chapter II may now be adopted for comparison with the present experimental data. Equation 2.13 suggests that creep parameters from simple shear tests can be used to predict the bond vs. displacement rate relationship for a plain rod in frozen soil. Since some data (Bragg, 1980) from unconfined compression tests on frozen Wedron sand are available, the shear strain rate $\dot{\gamma}_c$ from Equation 2.15 may be used, with the proof stress τ_c replaced by $\sigma_{cu\theta}$, in Equation 2.13 to give:

$$\dot{\delta} = a\ \dot{\varepsilon}_c\ 3^{(n+1)/2}\ (\tau_a/\sigma_{cu\theta})^n/(n-1) \qquad (6.13)$$

For given values of a, n, $\dot{\varepsilon}_c$, and $\sigma_{cu\theta}$ the relationship between τ_a and $\dot{\delta}$ can be established for a given temperature. Consider, for example, the experimental lines in Figure 6.18 for the -10°C, and a 5/8 in. diameter plain rod (radius a = 5/16 in.). Using the available data (Bragg, 1980) on frozen Wedron sand, with n = 11.765, $\dot{\varepsilon}_c$ = 6.0 X 10^{-5}

min.$^{-1}$, and $\sigma_{cu\theta}$ = 1875 psi at -10°C, Equation 6.13 was plotted on a log-log scale in Figure 6.28. The theoretical solution provided by Equation 6.13 significantly over-predicts the bond strength in comparison with the experimental lines in Figure 6.28. This large difference between the predicted and experimental strength values may be partly attributed to the difficulty with precise measurement of small rod displacements due to equipment limitations. Also, the difference between the predicted and experimental values appears to depend on the proper choice of $\sigma_{cu\theta}$ and $\dot{\varepsilon}_c$ for use in Equation 6.13. For example, using $\sigma_{cu\theta}$ = 7067 psi and $\dot{\varepsilon}_c$ = 60 min.$^{-1}$, as given by Bragg (1980), in Equation 6.13 would reduce the predicted bond strength by about 13.5 percent.

Equation 6.13 was derived (Johnston and Ladanyi, 1972) for piles in permafrost ground with boundary conditions slightly different from those applicable to the pull-out specimen. For example, the effect of soil stresses at the base plate on the strains around the rod were ignored. Derivation of Equation 6.13 clearly implies that the n-value for bond and compression tests is the same, thus assuming the same failure mechanism for both tests. Experimental data (Table 6.4) showed that the n-value from creep bond tests is about 31 percent of that from compression tests, and its value from bond tests with constant displacement rates is about 88 percent of that from compression tests, as shown in Figure 6.29. Therefore, the failure mechanism on the rod-soil interface is not the same as that on a shearing surface within the frozen soil.

Jellinek (1957 b) observed that at temperatures warmer than -14°C (Figure 2.1) the adhesive strength of ice was smaller than its cohesive strength. At temperatures colder than -14°C he observed that all the breaks were cohesive, i.e. within the ice crystal, thus indicating

that the adhesive strength of ice to stainless steel at these temperatures was higher than its cohesive strength. In sand-ice materials, sand friction becomes a contributing factor to the total bond strength. The introduction of sand friction would make it difficult to assume whether or not the adhesive and cohesive mechanisms in sand-ice are the same, without further experimental work.

It may be of interest to compare Weaver and Morgenstern's (1981 b) Equation 2.16 with some of the creep data on plain rods shown in Figure 6.30. Information on the time t, elapsed after load application, and the corresponding creep displacement δ_c for use in Equation 2.16 were obtained from the creep curves in Figure 5.32(a and b). Weaver and Morgenstern (1981 b) assumed constant values for the creep parameters b, c, k, and ω on the basis of available data on frozen Ottawa sand. As shown in Figure 6.30, the predicted (dashed) line considerably under-estimates the strength for frozen Wedron sand. This might be attributed to differences in particle surface features of Wedron and Ottawa sands. Also, calculations show that a slight change in the value of c, according to Equation 2.16, would significantly affect the results. No primary creep data on frozen Wedron sand are available, to show whether or not the c-value remains constant with temperature as assumed by Weaver and Morgenstern (1981 b).

6.4.2 Load Prediction Based on Cavity Expansion Theory:

Lug bearing forces can be predicted on the basis of cavity expansion theory. The solution proposed by Ladanyi and Johnston (1974) for frozen soils (Equation 2.18) was based on an analogy for an expanding spherical cavity in a linear elastic-plastic infinite medium (Hill,1950).

The theory uses experimentally determined creep parameters for frozen soils, thus modifying the model to be used for a non-linear viscoelastic-plastic medium. With this procedure it appears that creep settlement and bearing capacity of frozen soils under deep circular footings may be predicted.

A comparison between the experimental data (Figure 5.40) for the lug behavior and Equation 2.18 can now be made. The lug area may be considered as the difference between two concentric circular footings. The inner circle corresponds to the rod cross-sectional area. The outer one corresponds to a footing with diameter d + 2h (or B), where h is the lug height. For given values of $\dot{\varepsilon}_c$, $\sigma_{cu\theta}$, n, p_o, and η the relationship between q and $\dot{\delta}^c$ can be established for a certain temperature. To apply Equation 2.18 unconfined compression test data from previous work (Bragg, 1980) on frozen Wedron sand was used. Bragg (1980) observed that the failure strain ε_f was almost constant throughout the tests. At strain rates below 10^{-5} sec^{-1}, its value was about 0.045 independent of temperature. At higher rates the value of ε_f at all temperatures decreased slightly with strain rate indicating a more brittle behavior. For comparison, a constant ε_f value equal to 0.045 was assumed for use in Equation 2.19 at all temperatures. Values of $\sigma_{cu\theta}$, c, n are temperature-dependent according to Bragg (1980). Using the condition of $\eta = 1$ if $\delta^c \geq 0.1$ B, the value of η was assumed to be 1.0, since the lug settlement δ in all creep tests was larger than 0.1 B. The value of p_o was set equal to zero in all calculations, since no confining pressure was applied to the pull-out specimens.

Results from these comparisons are summarized in Figure 6.31. The

predicted loads, P in this figure, were obtained by multiplying q, calculated from Equation 2.18 for each case, by the lug area. Note that the friction angle ϕ was assumed to be constant, and equal to 30° for all temperatures and strain rates. This assumption seems reasonable since Ladanyi (1981) reported that the friction angle for most frozen soils is almost equal to that of the corresponding unfrozen soil. The predicted loads (dashed lines) in Figure 6.31, generally, over-estimate the loads at creep rates below about 10^{-4} in./min. and appear to under-estimate the loads at higher rates. The reason appears to be a difference between n-values from compression tests and those from bond tests. If values of n from bond tests, were used in Equation 2.19 the predicted loads would be significantly improved.

Since the experimental lines in Figure 6.31 are parallel to each other, they clearly indicate that the failure mechanism for a deep lug (or footing) in frozen sand is the same for all temperatures from -2°C to -15°C. A single value of n (4.93) can be assumed for these lines. Other reasons for a difference between the predicted and experimental lines in Figure 6.31 may include a difference between the actual lug shape and the assumed circular footing in the theory, or the presence of the rod which may prevent the formation of a complete semi-spherical plastic "cavity" zone under the lug. Assuming a perfectly plastic (incompressible) material within the cavity may not be entirely compatible with the observed behavior. Uniaxial creep compression tests on frozen sand reported by Bragg (1980) showed that the volumetric strain increased with the creep strain. It was not clear whether reducing the dilatancy by application of confining pressure would have any effect on the volumetric strain. Visual inspections after thawing of all

pull-out specimens lead to the conclusion that continuous crushing of sand particles had occurred as the lug continued to penetrate through the soil.

Crushing of sand grains was clearly shown by the observation of a thin layer of powdered quartz radially pushed into the frozen soil all along the deformed zone behind the lug (Figure 6.32). It appeared that prior to crushing of grains complete melting of frozen water must have occurred under the high pressure (estimated at 25,000 psi for sample CS-14). The condition in front of the lug may correspond to stage II in Figure 2.7. Pressure melting may have occurred locally around the lug as the lug continued to penetrate into the soil. A sudden failure was not characteristic of the sample behavior, hence global pressure melting did not occur.

The cavity expansion theory assumes a maximum limit for the footing displacement δ^c of 0.1 to 0.2 B. The experimental lines were based mostly on the step loading procedure. Under the initial load increments creep rates often did not reach the steady-state, as shown earlier in Figure 5.40, thus under-estimating the strength. Under the same loads the total displacements did not exceed 0.2 B (Figures 5.39 a to c). At higher loads (over 2500 lbs.) the displacements far exceed 0.2 B without reaching tertiary creep (or failure), thus violating the assumption of a maximum δ of 0.2 B in the theory.

6.4.3 Roughness Criterion for Steel Rods:

The pull-out capacity of plain rods increased with increasing rod surface roughness as shown in Figure 5.28. If the roughness factor defined in Equation 5.7 is modified, lugs can be considered a part of the rod surface roughness, as a large-scale asperity. In this case,

the question arises as to how much roughness a single lug will add to the plain rod. To help explain the procedure used to define a single lug "roughness" the actual heights of asperities SP (in micro-inches) observed on the profilometer for different steel surfaces have been listed in Figure 5.26. Also listed are the corresponding heights SR as measured on the strip chart recorder (in millimeters). The latter record was used as a basis for measuring the roughness factor of plain rods.

To consider the lug as a large-scale asperity on the rod surface, a correlation was made between values of SP, minimum and maximum in Figure 5.26, with the corresponding values of SR as shown in Figure 6.33. The relationship in this figure was linearly extrapolated to include the actual lug height h, which is equivalent to SP in micro-inches on the profilometer and to SR in millimeters on the recorder. For example, if h = 1/8 in., the equivalent roughness SP = 125000 micro-inches on the profilometer and SR = 52090 mm on the recorder based on the relationship in Figure 6.33. This procedure is also illustrated in Figure 6.34. The information in this figure was calculated for a cold-rolled steel rod with a single lug (h = 1/8 in.) frozen into a 6 in. high sample.

Assuming that the tracer stylus could be moved 6 in. along the rod, the equivalent length L_t in Figure 5.25 would be 2720 mm (Figure 6.34) on the recorder strip chart. This length was calculated in proportion to the standard chord L_c of 80 mm used earlier for plain rods. A chord length of 80 mm on the strip chart was observed to correspond to 0.1767 in. on the actual surface. The observation was based on a tracer speed of 0.221 in./sec. on the surface roughness, and a corresponding strip

chart recorder speed of 10 cm/second. The total "roughness line" length L_r in Figures 5.25 and 5.26 equals (2 X 5209 + 272 X 58/8) or 12,390 cm for the cold-rolled steel rod in Figure 6.34.

The roughness factor ρ, based on Equation 5.7, equals {(12390 - 272) X 100/272} or 4455 percent. In the same manner, the roughness factor for rods with surface irregularities, including lugs, can be estimated. The effect of lug height on the ultimate loads shown in Figure 5.22, can be transformed in terms of roughness effect. Values of roughness factor ρ which correspond to different lug heights are listed in Table 6.5, with their ultimate loads. The data, plotted on a log-log scale in Figure 6.35, show a reasonable agreement with the data summarized in Figure 5.28. At small values of ρ, below 100 percent, the ultimate load appears to be less influenced by surface roughness. This behavior was attributed to the fact that bond strength of frozen soil does not totally depend on mechanical interaction between the soil grains and rod surface roughness. Even on a perfectly smooth surface, ρ = 0 percent, there will be some ice adhesion which may give a finite value for the ultimate load. For this reason, the best fit line was extrapolated as shown by the dashed curve in Figure 6.35.

6.5 Applications:

Design of frozen soil structures, which involve reinforcement, piles, or anchors, requires that suitable criteria be available for selection of allowable adfreeze bond stresses and displacements. Bond strength and creep rates are dependent on the frozen soil material properties, temperature, and surface properties (type and roughness) of the reinforcement member, pile, or anchor. To allow for complex geometry

within the structure and that stresses and strains may vary with time and temperature, a non-linear viso-plastic finite element analysis appears to be the most effective method.

In this section, a simplified analysis is explored for a reinforced frozen soil beam, under pure bending moment. The analysis is based on certain assumptions which require further verification by means of beam tests. Also, a preliminary analysis considers some of the experimental pull-out test results for application to piles and anchors in permafrost.

6.5.1 Frozen Soil Reinforcement:

There is general agreement that the behavior of frozen soil in tension is quite different from that in compression at strain rates higher than 10^{-5} sec.$^{-1}$ (Vyalov, 1962; Hawkes and Mellor, 1972; Haynes et al., 1975; Haynes and Karalius, 1977; Bragg; 1980; Eckardt, 1981). For frozen Wedron sand, it was observed that the ratio of compressive to tensile strength, σ^c/σ^t, was about 5. Therefore, a frozen soil beam may fail because of a weakness in tensile strength. Also, it was noted in Figure 2.18 that beam deflections can be greatly reduced with reinforcement.

For a simple beam subjected to pipeline load as shown in Figure 1.1 (c), or the laboratory beam model in Figure 2.18, the analysis can be simplified by neglecting tensile resistence of the frozen soil. Consider, for example, the beam in Figure 2.18 which failed under a total load increment P of 433.1 lbs., when reinforced with a 3/16 in. diameter plain rod (Soo, 1983). The corresponding external bending moment was calculated to be 5630 inch-pounds. It is of interest to compare this bending moment with that estimated from an analytical procedure. A cross-section for this beam is shown in Figure 6.36 (a). Using

Bernoulli's theorem (a plane section remains plane after bending) a linear strain distribution was assumed throughout the beam depth as shown in Figure 6.36 (b). Assuming the equillibrium condition shown in Figure 6.36 (c) and neglecting the soil resistance in tension, the position of the neutral axis z_1 can be determined using Equation 2.22.

Now calculate the resultant force F_c in the compression zone using Equation 2.24 and available data on frozen Wedron sand (Bragg, 1980). For a temperature of -10°C these data include the proof stress $\sigma_{cu\theta}$ = 1875 psi at $\dot{\varepsilon}_c = 6 \times 10^{-5}$ per minute, and n = 11.765. The radius of curvature R can be replaced by z_1/ε_c, where ε_c is the compression strain at the outer fiber. Substituting these parameters into Equation 2.24, the compressive force F_c can be expressed in terms of z_1 and ε_c (with b = 2.75 in.) as follows:

$$F_c = 10858\ z_1\ \varepsilon_c^{0.085} \qquad (6.14)$$

The resisting force in the tension zone is controlled by the steel tensile strength or by the bond resistance. In reinforced concrete, where creep is almost negligible in comparison to frozen soil creep, it is normally designed such that bond slip does not occur and failure is governed by the steel tensile strength (Hughes, 1976). In frozen soil, where there is no generally accepted design philosophy, bond creep is significant and it cannot be neglected. Interaction between the adfreeze bond and tension of steel rods depends on different factors including time, temperature, and rod surface roughness. While the bond resistance varies significantly with these factors, the tensile resistance remains almost constant for a given rod cross-section. Based on the available experimental data, the following calculations show that adfreeze bond resistance for the 3/16

in. diameter plain rod (Figure 6.36 a) controls and that it was small in comparison to tensile resistance in the rod.

The bond resisting force F_b (Figure 6.36 c) is given by:

$$F_b = \pi \, L \, d \, \tau_c \, (\delta_f / t_f \, \dot{\delta}_c)^m \qquad (6.15)$$

where L = 20 in. is the bond development length (Figure 2.18), d = 3/16 in. is the rod diameter, δ_f = 0.06 in. is the bond displacement of the rod at failure (Figure 5.32 b), and t_f = 5040 min. is the time to failure for the beam test (Soo, 1983). The creep parameter τ_c, $\dot{\delta}_c$, and m, obtained from Figure 5.33 include values of 26.5 psi, 10^{-6} per min., and 0.37, respectively. Substituting these values into Equation 6.15, gives F_b = 333 pounds. Comparing this value with that due to the rod tensile resistance of 1100 lbs. (based on 40000 psi yield stress) suggests that bond failure would be more probable than tensile failure. Equillibrium requires that $F_b = F_c$, and hence:

$$10858 \, z_1 \, \varepsilon_c^{0.085} = 333 \qquad (6.16)$$

According to Equation 6.16, the value of z_1 = 0.082 in. for $\varepsilon_c = 10^{-5}$, and z_1 = 0.04 in. for ε_c = 0.045 (failure strain based on Bragg's (1980) data). In both cases the value for z_1 is small compared to the depth d' of 2.5 in. in Figure 6.36 (a). Therefore, any value for ε_c in the range of 10^{-5} to 0.045 would not result in any significant error. With an average value of 0.06 in. for z_1, and $(d' - z_1)$ = 2.44 in. (Figure 6.36 b), the internal resisting moment would be 812.5 in.-lbs (= 2.44 in. X 333 lbs.). It is clear that the adfreeze bond would be inadequate to counter act the applied bending moment of 5630 inch-pounds. For this particular beam, a significant soil contribution must exist in the tension

zone.

It was anticipated that introduction of the frozen soil tensile resistance T_s would shift the neutral axis upward, as shown in Figure 6.36 (d), thus further complicating the analysis. For beams reinforced with deformed rods, which appear to tolerate larger displacements than plain rods (Figure 5.20), the strain ε_r at the reinforcement level (Figure 6.36 b) would be large enough to cause failure of frozen soil in tension before bond failure occurs. In this case, neglecting any soil tensile forces may introduce less error than the case of using plain rods. More experimental data on the beam behavior is needed before proceeding with the analysis.

6.5.2 Pile or Anchor Capacity:

Pile installation in permafrost often involves dry augered holes with a mixture of soil and water used to fill the annulus around the pile (Figures 1.2 b and c). Piles and anchors develop their load supporting capacity when the soil-water slurry is solidly frozen in place (Andersland et al., 1978). Pile capacity is primarily dependent on the long-term adfreeze bond strength of the frozen slurry, the pile type and surface roughness. There appears to be a general agreement that pile design in ice-rich soils should be based on limiting creep deformations, and in ice-poor soils design should be based on allowable adfreeze strengths (Weaver and Morgenstern, 1981 b). End-bearing at the pile tip is normally neglected, particularly in ice-rich soils.

Steel rods embedded in frozen sand specimens can be viewed as a section of a model pile. It appears reasonable to consider the experimental data herein in terms of potential field behavior of piles in permafrost.

Consider the following example involving a steel pipe pile (1 ft. diameter and 25 ft. length) to be used as a vertical support in a warm permafrost with an average temperature of -2°C. A sand slurry backfill, carefully controlled as to density, is placed around the pile as shown in Figure 1.2 (b). The permissible pile displacement is limited to 1 in., and the maximum active layer thickness is predicted to be 5 ft. during a 20 year service life for the structure. The allowable axial load is required for the pile (cold-rolled steel surface). The pile capacity is to be based on limiting creep deformation to 1 inch. For the 20 year service life and pile deformation the creep rate will be 8.5×10^{-8} in./min. This rate corresponds to the slow rate range in Figure 6.18. Since very limited creep data are available in this range, it will be assumed that the constant displacement rate power law (Equation 5.3) is applicable.

Using the data in Table 5.3, Equation 5.3 bcomes $\tau_u = 12\ \theta\ (10000\ \dot{\delta}_n)^{0.222}$. Since no loading rate $\dot{P}$ was given, Equation 6.2 could be written in terms of the displacement rate $\dot{\delta}_n$ as follows:

$$\tau_u\ (\text{psi}) = 12\ (10000\ \dot{\delta}_n)^{0.222} (\rho/625)^{0.325}\ (v_s/64)^{2.246}\ (d/10H)^s\ \theta \qquad (6.17)$$

Substituting d/H = 5.0 percent (1/20), s = 0.692, v_s = 60 percent, ρ = 625 percent (cold-rolled steel), $\dot{\delta}_n = 8.5 \times 10^{-8}$ in./min., and θ = 2°C into Equation 6.17, the adfreeze strength τ_u = 5.436 psi gives an allowable axial pile load of 49183 pounds. Note that the effective embeddment depth H was taken as 20 ft by neglecting the top 5 ft (the active layer). Also, any downdrag loads, were ignored in the example.

Corrugations (lugs) have been used on pipe piles (Figure 1.2 c) to increase load capacity on the trans-Alaska gas pipeline project (Thomas

and Luscher, 1980). The lugs were spaced at 1 ft, with a lug height h = 3/4 inch. If similar lugs are used on the 25 ft. piles, there would be 21 lugs in the effective 20 ft. embeddment. Load-displacement curves reported by Thomas and Luscher (1980) for corrugated piles showed a behavior similar to that observed for the lugs (Figure 5.14) with no "initial failure" and no drop in load at the ultimate condition (Figure 5.21). This behavior appears to indicate no lug interaction, described in Figure 6.15 for the standard deformed rods. Using Equation 6.8, with v_s = 60 percent, A_1/A_r = 0.2656, $\dot{\delta}^c$ = 8.5 X 10^{-8} in./min., and θ = 2^oC, gives q = 7105 psi for a single lug on a corrugated pile, and the pile load becomes 213,445 lbs. per single lug. The total allowable axial load for 21 lugs through the 20 ft. depth bearing layer would be 4,482,339 pounds. This load compared with the 49183 lbs. for plain piles is about 91 times higher. Such a load, however, would exceed the ultimate compressive strength (about 550000 lbs) for a pile cross-section with a 3/8 in. wall thickness. The lug height can be reduced and the spacing can be increased and still obtain a load capacity equal to that of the steel pipe. Note that the confining lateral earth pressure was neglected in the analysis. Had the confining pressure been considered, higher loads (for plain and corrugated piles) would be obtained.

Anchors are also used in permafrost for resisting uplift forces in various types of structures. The adfreeze strength of grouted rod anchors, or pile anchors, may be estimated from pull-out tests on plain rods in the same manner described for the pipe piles, using Equation 6.2. Screw anchors of the type shown in Figure 1.2 (d) can be simulated by the lug behavior observed in this study. The bearing capacity of a single helix (screw) anchor can be estimated using Equation 6.8.

The foregoing examples indicate that the scale effect (due to data transformation from a small-scale laboratory model to a large-scale field structure) can be eliminated by applying the dimensionless ratios d/H and A_1/A_r. However, when considering the load-displacement curves, the pull-out load can be normalized with respect to the rod surface area, to give a nominal bond stress, and the corresponding displacement can be normalized with respect to the rod radius to give the average shear strain, assuming a uniform stress and strain distribution along the rod length. Further model studies and dimensional analysis are required in order to make possible a multiple regression analysis for further applications.

Table 6.1: Comparison of frozen sand cohesion with the bond and lug bearing capacity.

T (^{o}C)	σ_u^* (psi)	$c=\sigma_u/2$ (psi)	q_l (psi)	$P_u/\pi H\ d$† (psi)	$P_{iy}/\pi Hd$† (psi)	τ_u†† (psi)
- 2	1100	550	7200	200	113	27
- 6	1700	850	10692	297	174	78
-10	2100	1050	15012	417	230	127
-15	2500	1250	19872	552	297	191

---

* Data from Bragg (1980), values of σ_u correspond to $\dot{\varepsilon}_{avg} = 3.0x10^{-6}$ sec.$^{-1}$ (Bragg's Figure 5.9).

† d = 3/8 in., H = 6.0 in.

†† For a 3/8 in. diameter plain rod.

(Other data from Table 5.2 for $\dot{\delta}_{avg} = 5.0x10^{-4}$ in./min. and $\dot{P}_{avg}$ = 25 lbs./min.)

Table 6.2: Effect of lug size on creep rate and lug bearing in frozen sand at -10°C.

Sample No.	h (in.)	A_l (sq.in.)	q_l (psi)	$\dot{\delta}^c \times 10^{-5}$ (in./min.)
CS-9	1/16	0.08590	16298	46.7
			18161	70.0
			20954	104.0
			24214	166.0
CS-13	1/16	0.08590	9895	8.0
			13970	21.2
			18161	58.9
			30268	718.0
CS-15	1/16	0.08590	34924	2500.0
CS-5	2/16	0.19635	11714	10.0
			12732	16.8
			14158	25.8
			15381	37.5
			16196	44.6
CS-6	2/16	0.19635	14158	25.0
			15686	43.6
			16909	69.6
			18131	83.0
CS-7	2/16	0.19635	18131	100.0
			19251	166.0
			20372	200.0
CS-8	2/16	0.19635	20372	286.0
CS-10	2/16	0.19635	8047	8.3
			9473	9.4

(Continued)

Table 6.2: (Cont'd)

Sample No.	h (in.)	A_1 (sq.in.)	q_1 (psi)	$\dot{\delta}^c \times 10^{-5}$ (in./min.)
CS-10	2/16	0.19635	10899	13.30
			11714	13.10
CS-14	2/16	0.19635	22918	975.00
CS-18	2/16	0.19635	6213	1.82
			7843	1.77
			9269	3.64
			10695	5.09
			12121	6.94
CS-11	3/16	0.33134	6036	1.61
			7485	4.05
			9175	6.71
			10865	9.07
			12555	20.40
CS-17	3/16	0.33134	7545	8.00
			10563	10.00

Table 6.3: Values of "psuedo" instantaneous displacement δ_i and time to failure t_f at different creep loads for a 1/8 in. lug in frozen sand, (δ_f is the assumed failure displacement).

Sample	P	δ_i	t_f(min.) for:	
No.	(lbs.)	(in.)	δ_f= 1.0 in.	δ_f= 0.25 in.
CS-5	2300	0.081	9188	1688
	2500	0.088	5431	967
	2780	0.097	3270	605
	3020	0.100	2400	400
	3180	0.106	2004	322
CS-6	2780	0.080	3680	680
	3080	0.084	2100	380
	3320	0.088	1310	233
	3560	0.092	1094	190
CS-7	3560	0.084	916	166
	3780	0.090	548	96
	4000	0.093	454	77
CS-8	4000	0.081	320	59
CS-10	1580	0.028	11669	2665
	1860	0.032	10314	2319
	2140	0.034	7263	1624
	2300	0.035	7366	1641
CS-14	4500	0.120	95	13
CS-18	1220	0.022	53736	12527
	1540	0.029	54859	12486
	1820	0.036	26483	5879
	2100	0.038	18978	4243
	2380	0.039	13876	3069

Table 6.4: Comparison of the n parameter from unconfined compression tests with that from bond tests.

T (^{o}C)	n_c	n_b	n_b'	n_b''
- 2	3.30	5.40	4.50	--
- 6	8.70	6.70	5.40	--
-10	11.67	10.40	9.35	2.70
-15	12.19	11.40	10.60	4.80

n_c From compression tests (Bragg, 1980)

n_b From bond tests, Figure 5.3

n_b' From bond tests, Figure 5.4

n_b'' From creep bond tests, Figure 5.38

Table 6.5: Variation of ultimate load with rod surface roughness, including lugs.

Type of steel	Lug** shape	h (in.)	ρ (%)	P_u (lbs.)
CR*	45^o	1/64	1085†	1050
CR	90^o	1/16	2540	1740
CR	90^o	2/16	4455	2920
CR	90^o	3/16	6370	4800
GF	45^o	2/16	3920	2730
CR	45^o	2/16	4455	3380
SB	45^o	2/16	5319	3400

* CR: Cold-rolled steel surface
GF: Ground-finish steel surface
SB: Shot-blasted steel surface

** For description of lug shapes, see Figure 3.2

† Data for a 3/8 in. standard deformed bar reduced to a single 1/64 in. lug. The 6 in. rod length was assumed to have the same roughness as that of the cold-rolled steel surface.

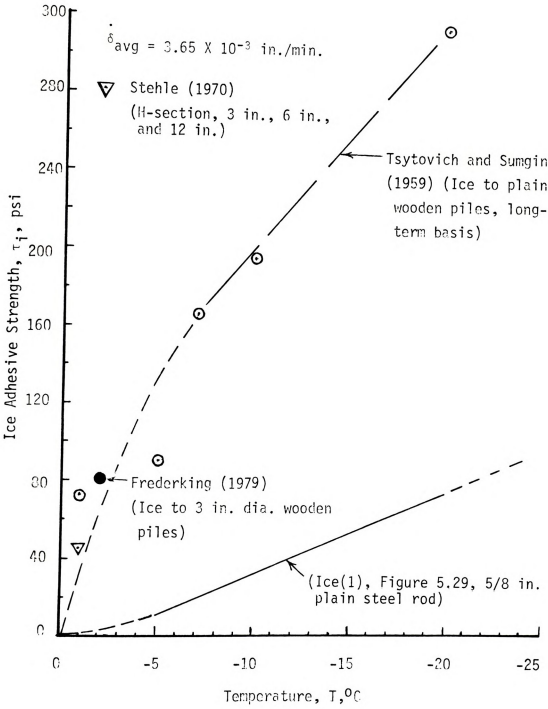

igure 6.1: Temperature effect on ice adhesion to different materials.

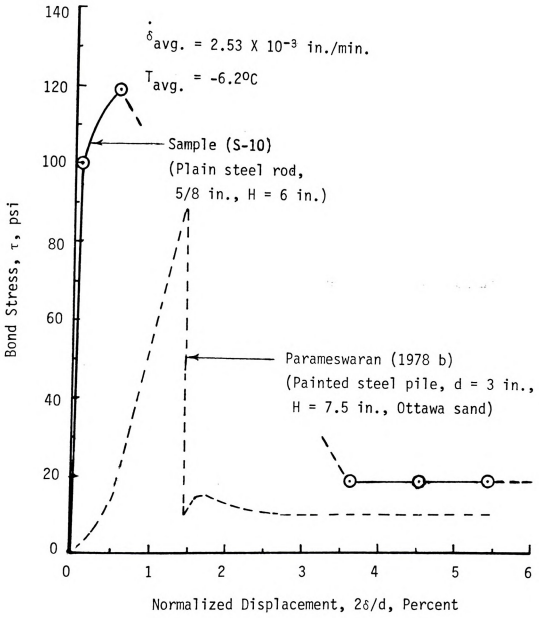

Figure 6.2: Typical bond stress versus displacement curves for plain steel piles (rods) in frozen sands.

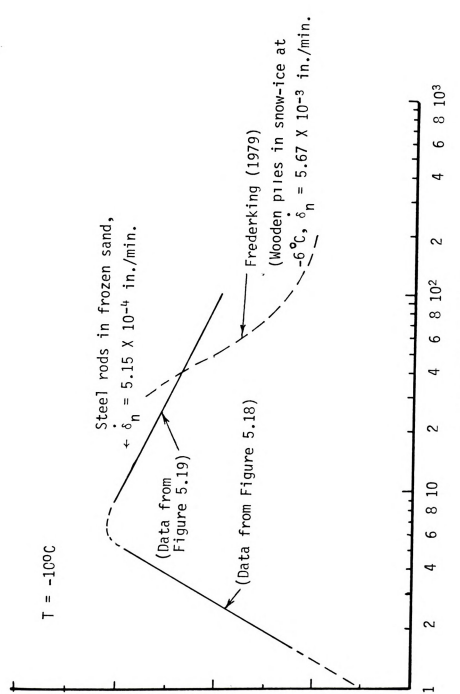

Figure 6.3: Variation of bond strength with the ratio d/H for ice and frozen sand (to piles of different materials).

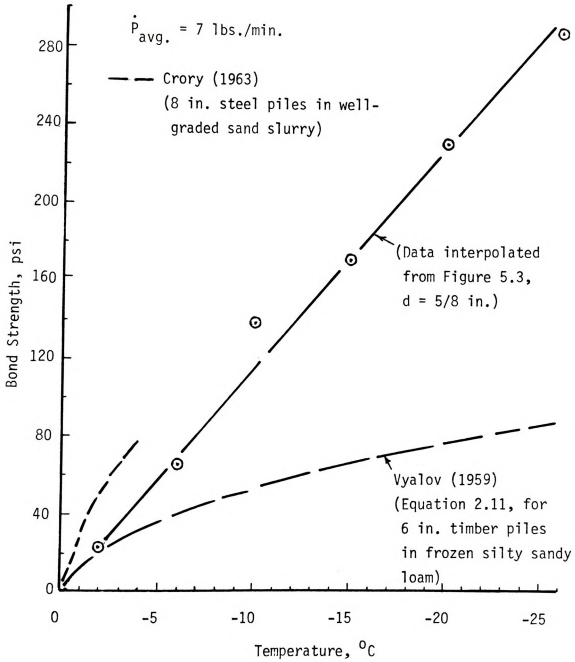

gure 6.4: Comparison of bond strength for different pile types in frozen sandy soils.

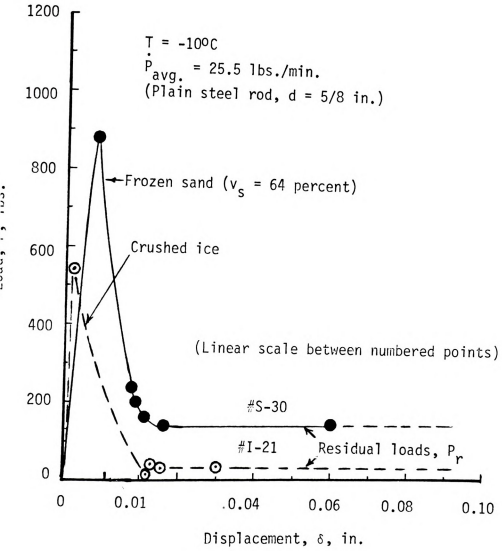

e 6.5: Comparison of load-displacement curves for a plain steel rod in ice and frozen sand.

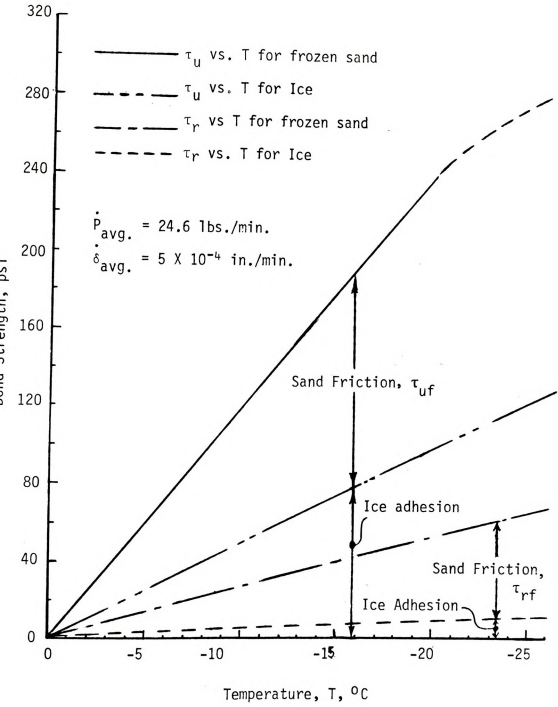

re 6.6: Comparison of ice adhesion and sand friction for a 3/8 in. plain steel rod embedded in ice and frozen sand.

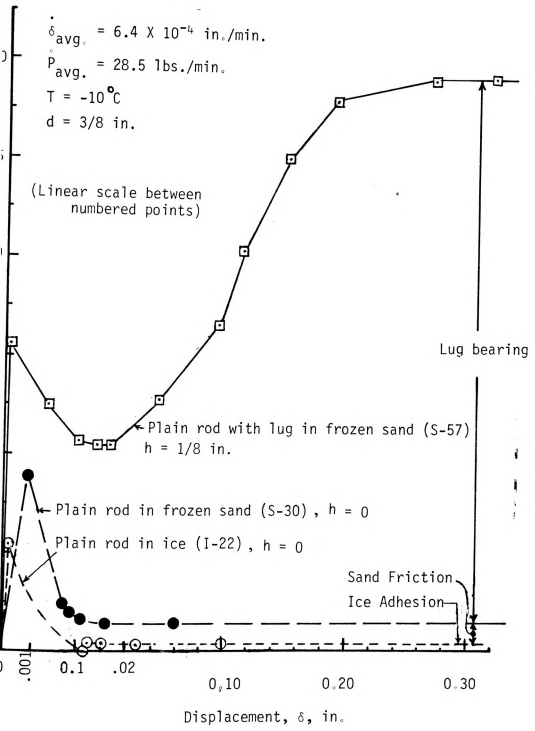

e 6.7: Comparison of lug bearing, sand friction, and ice adhesion effects on the load-displacement curves for steel rods.

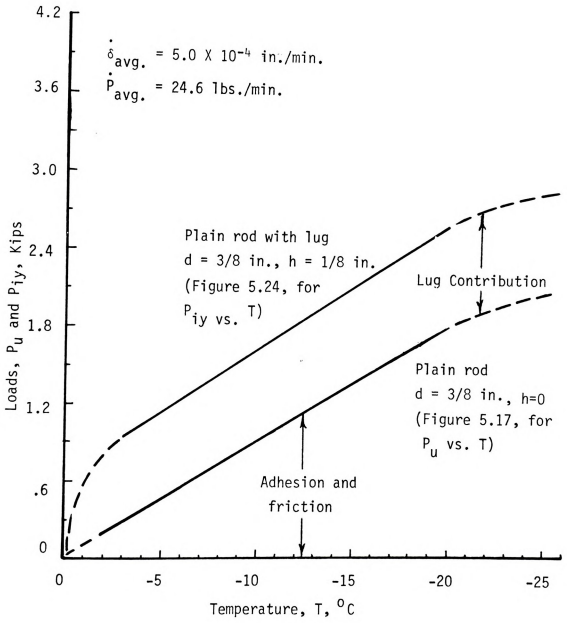

gure 6.8: Lug contribution for the initial bond rupture condition at different temperatures.

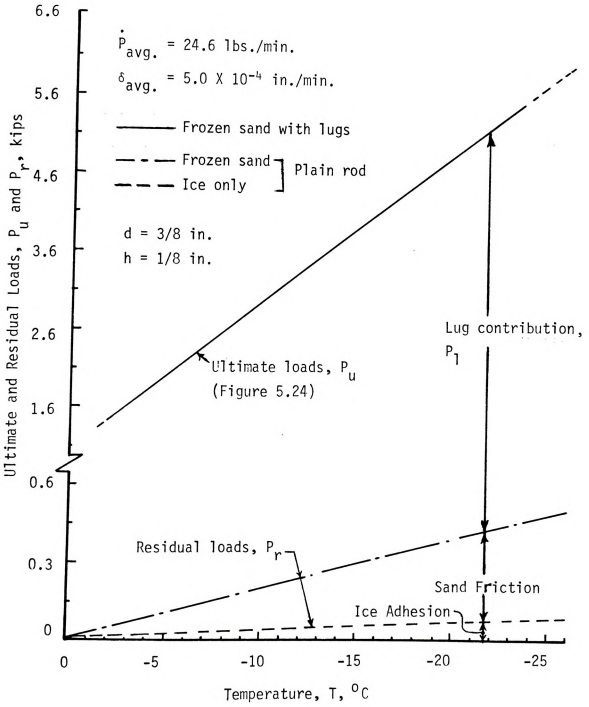

Figure 6.9: Comparison of ice adhesion, sand friction, and lug contribution for steel rods at different temperatures and ultimate conditions.

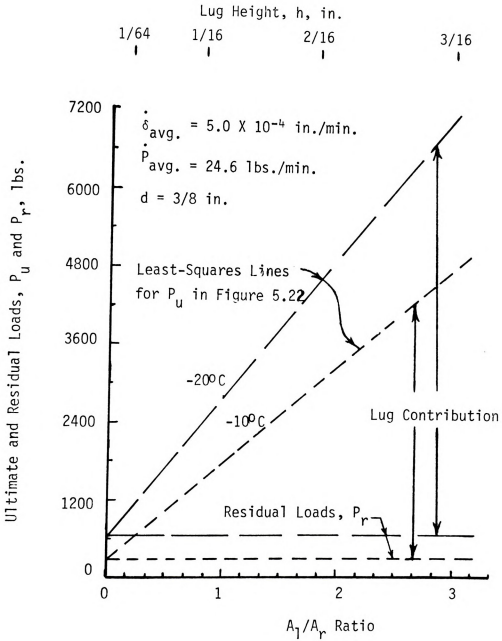

re 6.10: Lug contribution to the ultimate pull-out capacity of a plain rod, with a single lug with different lug heights, in frozen sand.

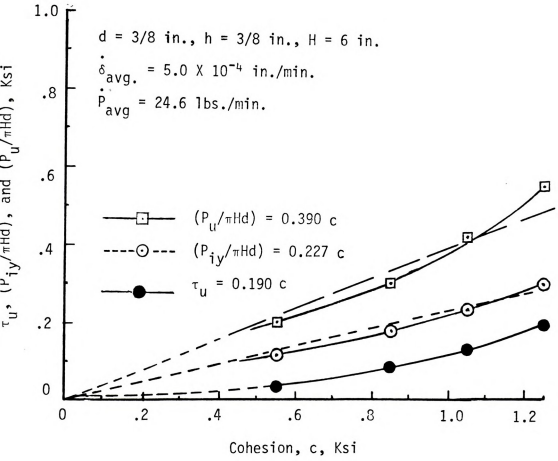

re 6.11; Comparison of frozen sand cohesion (at different temperatures) with the bond and lug bearing capacity.

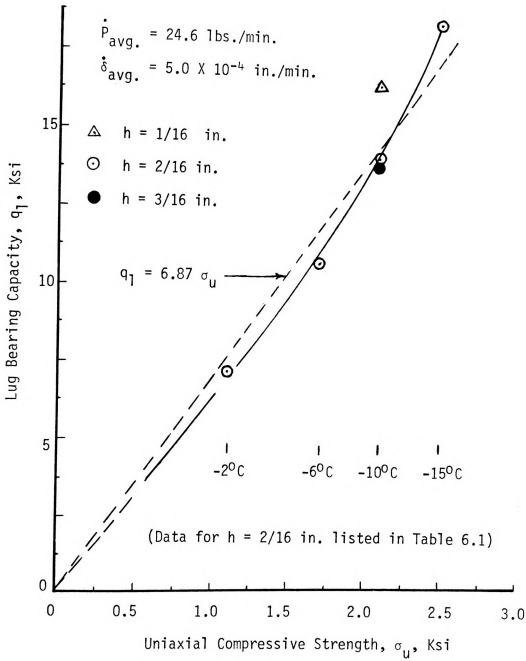

Figure 6.12: Relationship between lug bearing capacity and uniaxial compressive strength for frozen Wedron sand.

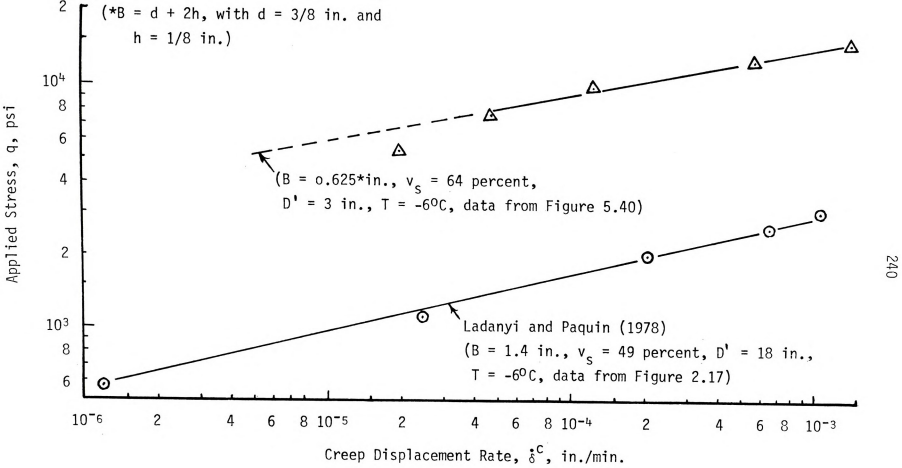

Figure 6.13: Comparison of lug behavior in frozen Wedron sand with that of a 1.4 in. diameter penetrometer in frozen quartz sand at -6°C.

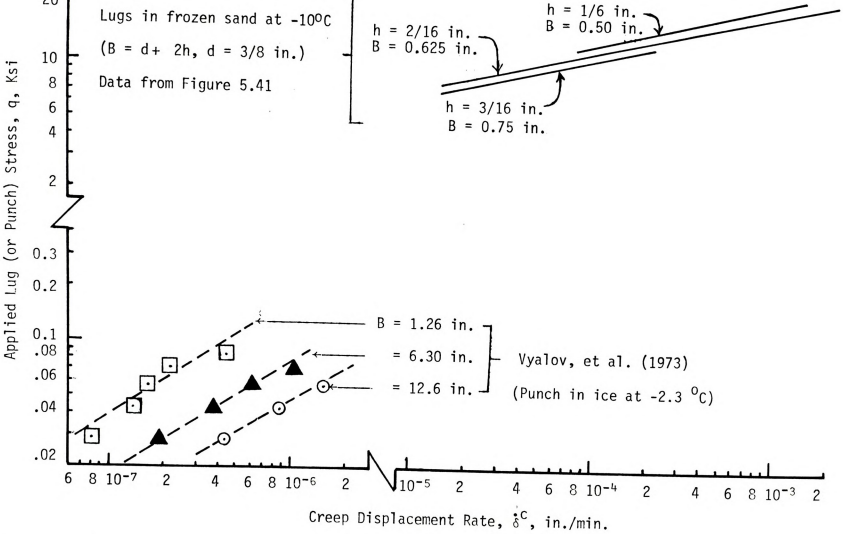

Fiigure 6.14: Creep rate dependence on size (area) for lugs and circular footings (punch).

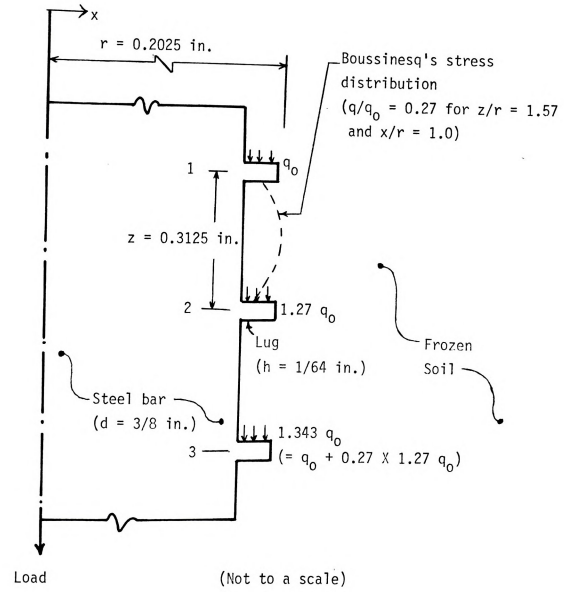

re 6.15: Pressure bulb overlap for consecutive lugs on a 3/8 in. diameter deformed bar.

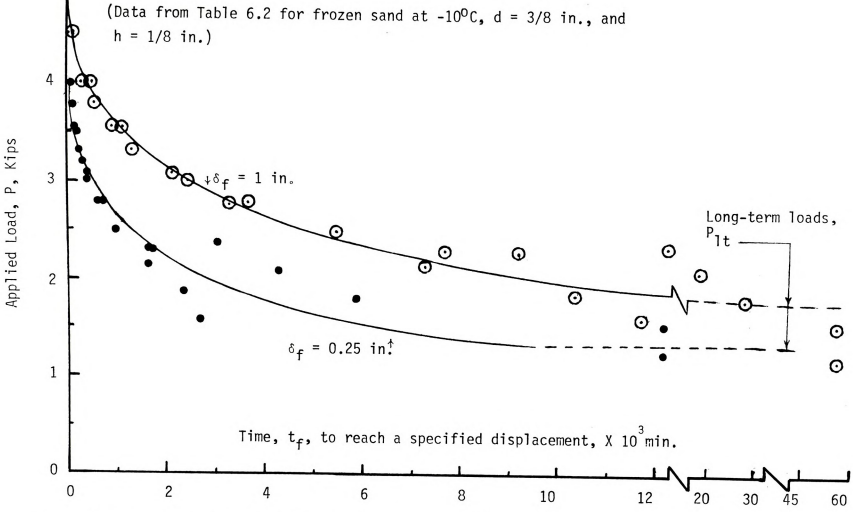

Figure 6.16: Time dependence of load relative to specified creep displacements, δ_f, at -10°C for a 3/8 in. rod with a 1/8 in. lug in frozen sand, (v_s = 64%).

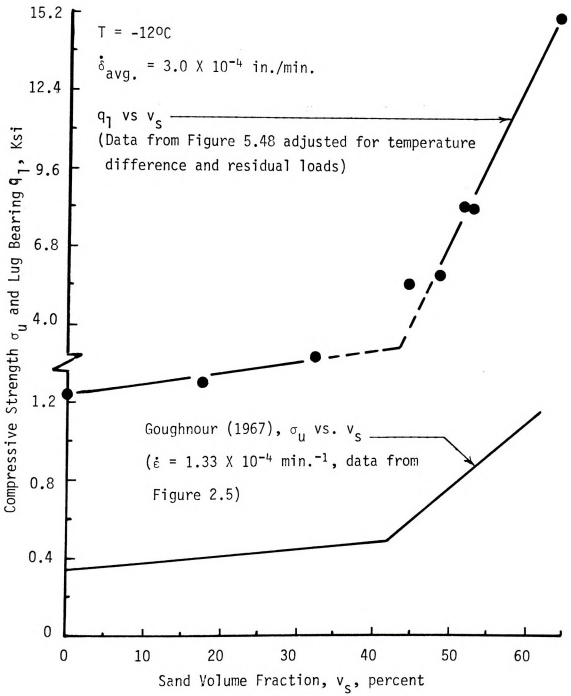

igure 6.17: Sand Volume fraction effect on the unconfined compressive strength of frozen Ottawa sand and the lug bearing capacity of frozen Wedron sand.

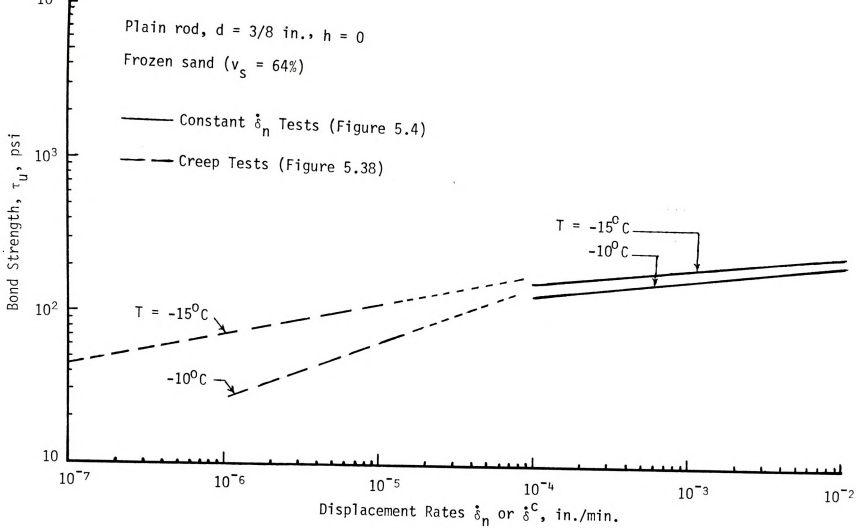

Figure 6.18: Bond strength for a plain rod in frozen sand, as a function of displacement rates, for creep tests and constant displacement rate tests.

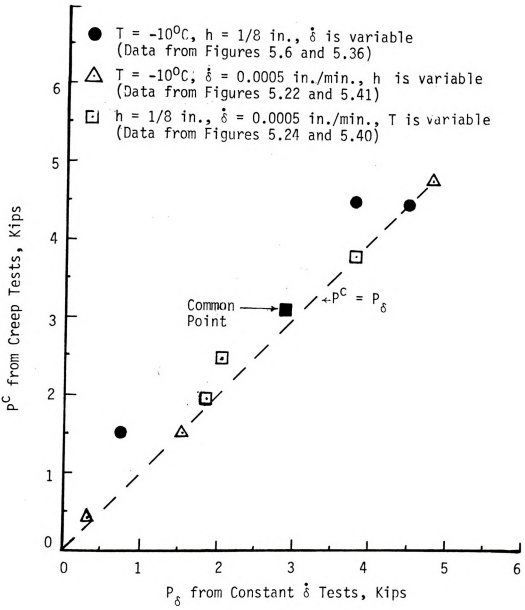

Figure 6.19: Lug capacity comparisons, creep tests versus constant displacement rate tests, for different test conditions.

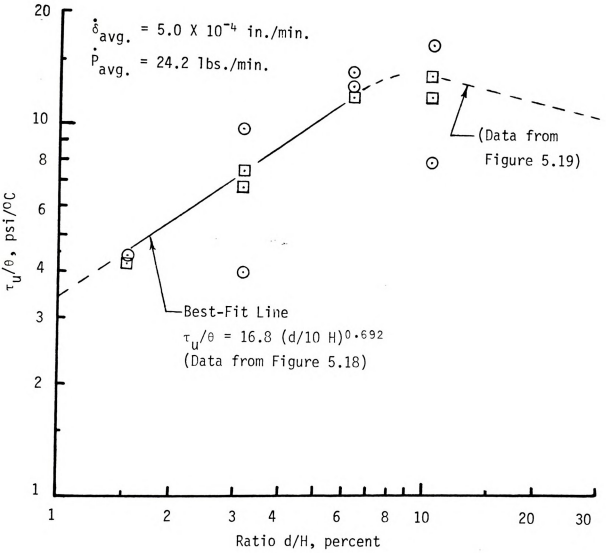

Figure 6.20: Modified relationship between bond strength and the ratio d/H for plain steel rods in frozen sand, (v_s = 64%).

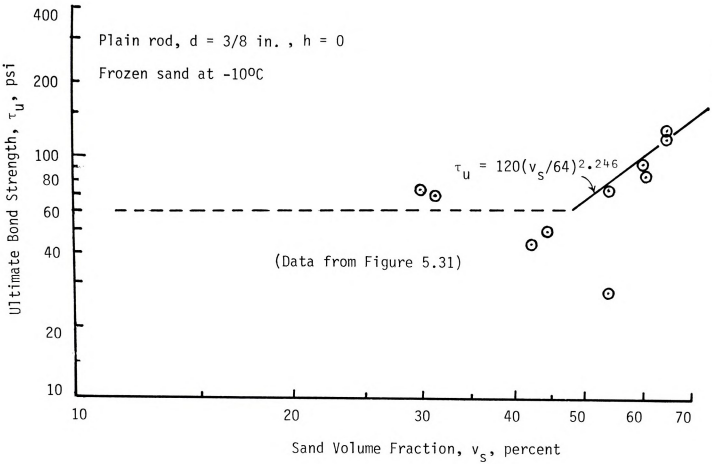

Figure 6.21: Bond strength of plain steel rods in frozen sand at -10°C as a function of sand fraction.

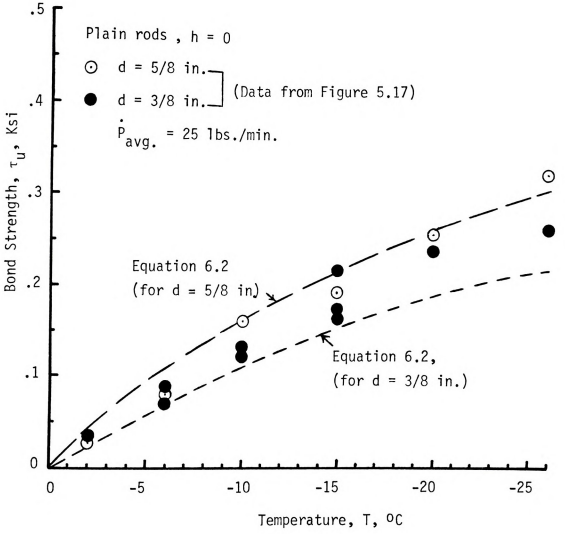

Figure 6.22: Comparison of Equation 6.2 with experimental data, for bond of plain rods in frozen sand (v_s = 64%)

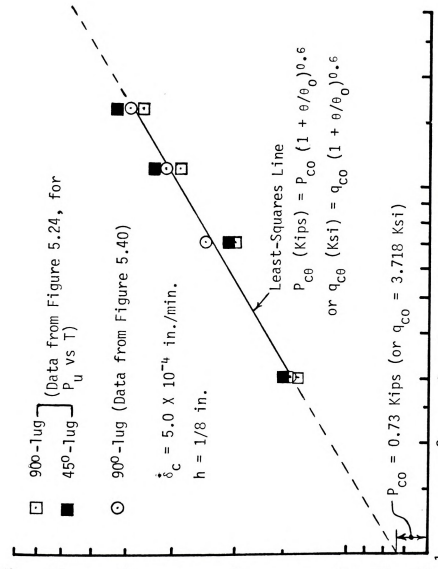

Figure 6.23: Lug pull-out capacity as a function of temperature for a displacement rate of 5 X 10^{-4} in./min.

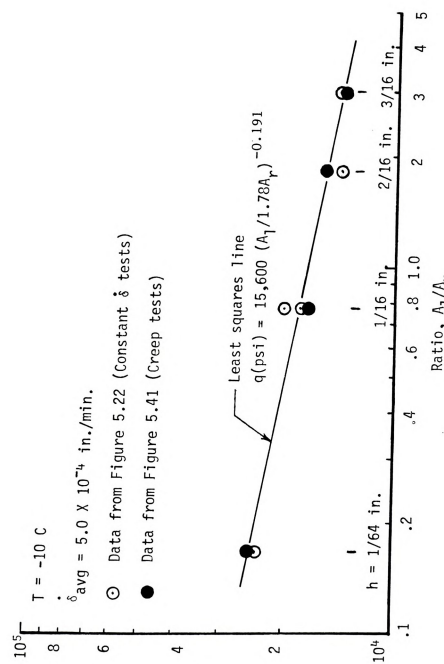

Figure 6.24: Effect of lug size (area) on bearing pressure.

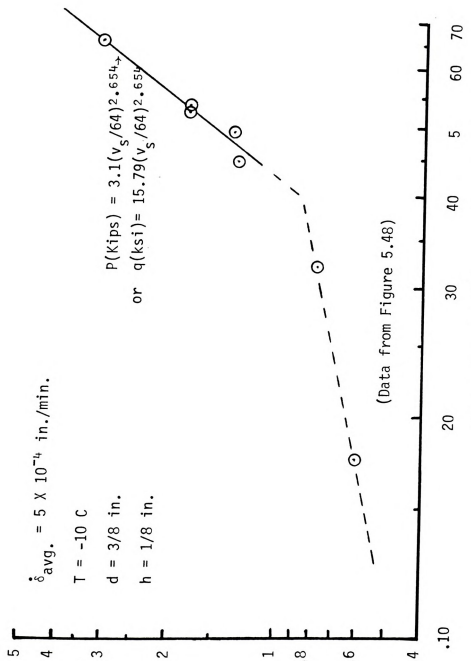

Figure 6.25: Lug capacity as a function of sand volume fraction, for a creep rate of 5 X 10^{-4} in./min.

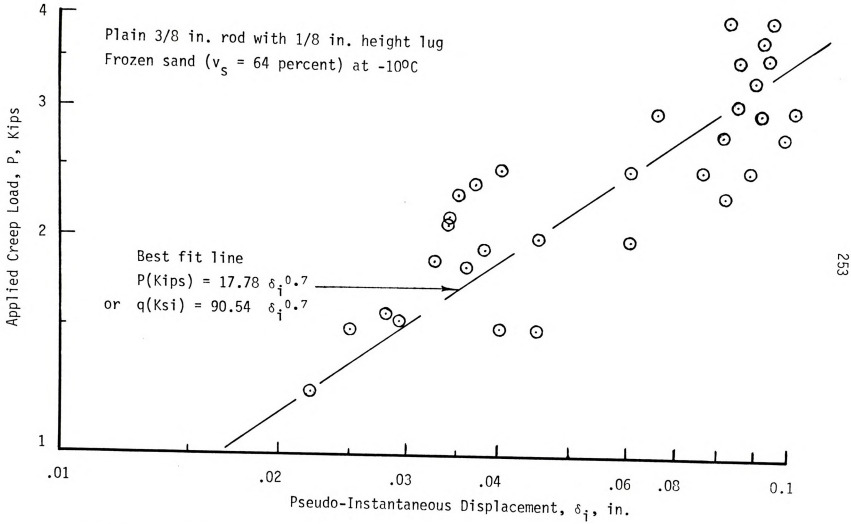

Figure 6.26: Creep load versus pseudo instantaneous displacement $^{o}\delta_i$ for a 3/8 in. diameter rod with a 1/8 in. lug in frozen sand (v_s = 64 %) at -10°C.

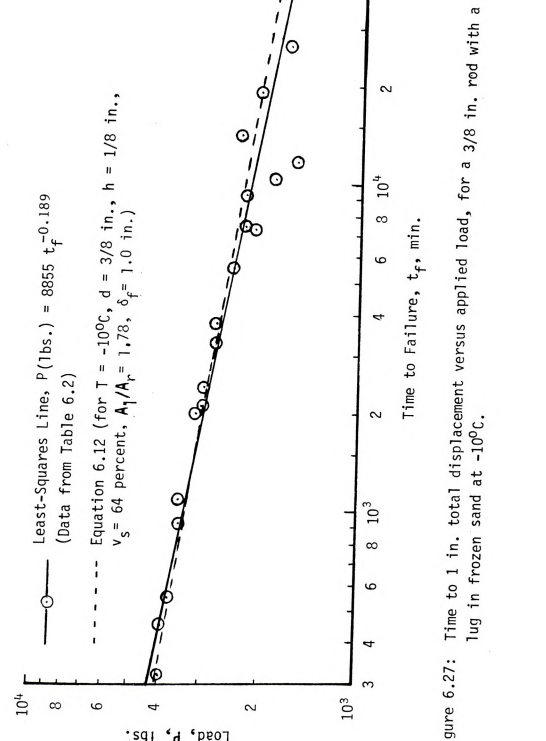

Figure 6.27: Time to 1 in. total displacement versus applied load, for a 3/8 in. rod with a 1/8 in. lug in frozen sand at -10°C.

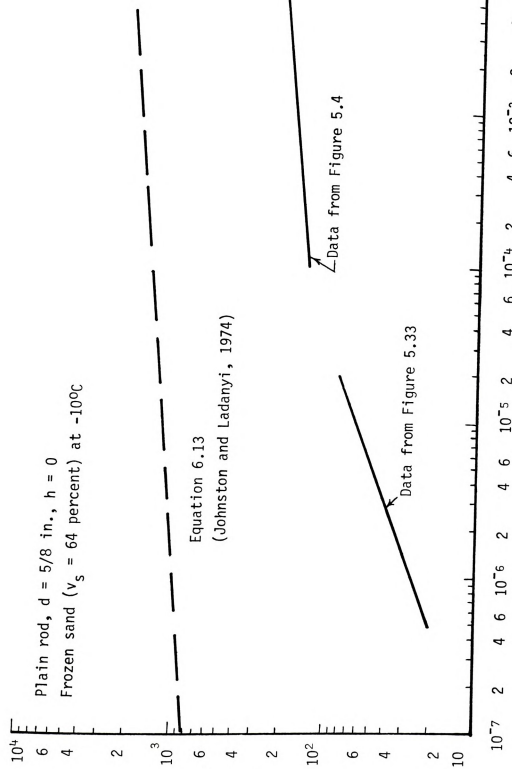

Figure 6.28: Comparison of experimental bond strength with the theoretical predictions for a plain 5/8 in. diameter rod in frozen sand (V_s = 64 percent) at -10°C.

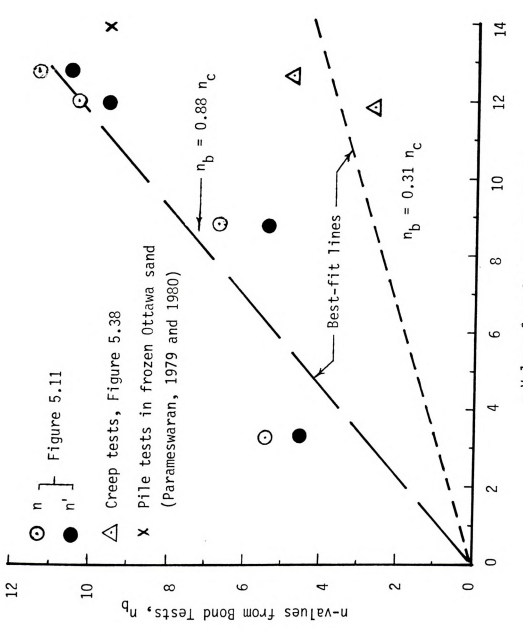

Figure 6.29: Comparison of n-values for bond tests with compression tests on frozen Wedron sand.

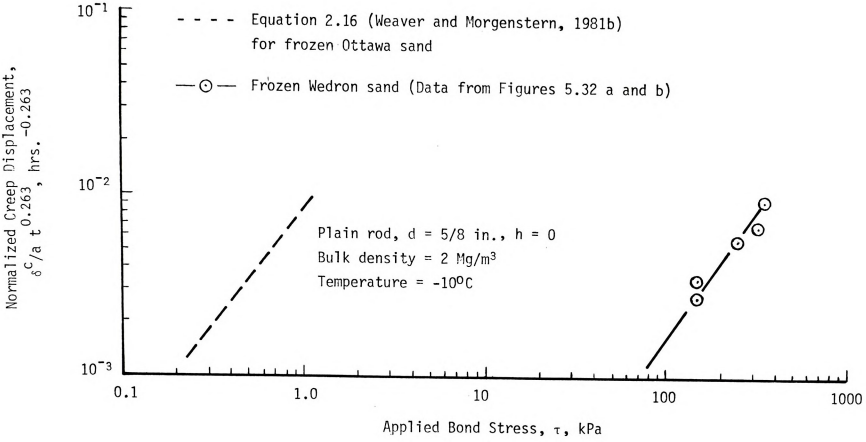

Figure 6.30: Comparison of Equation 2.16 with experimental bond strength for a plain 5/8 in. diameter rod in frozen sand (v_s = 64 percent) at -10°C.

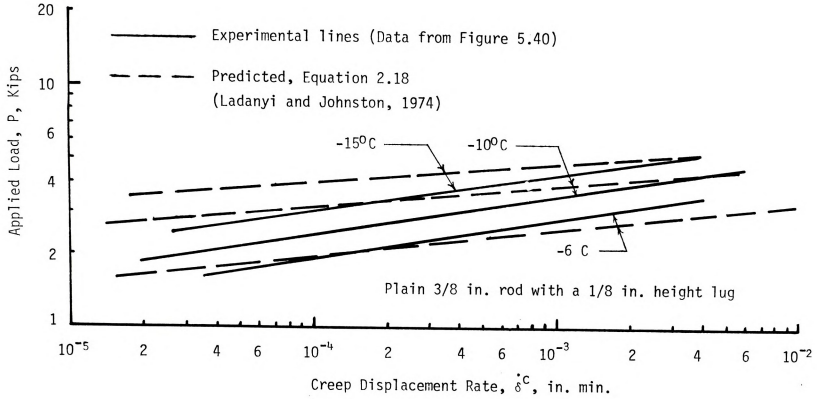

Figure 6.31: Load predictions based on cavity expansion theory for a single lug in frozen sand (v_s = 64 percent).

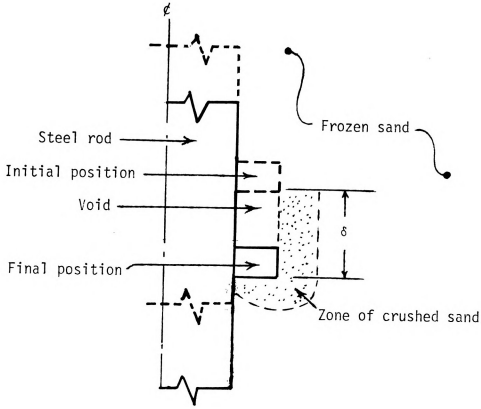

Figure 6.32: Zone of crushed sand observed around the lug, at the end of creep tests.

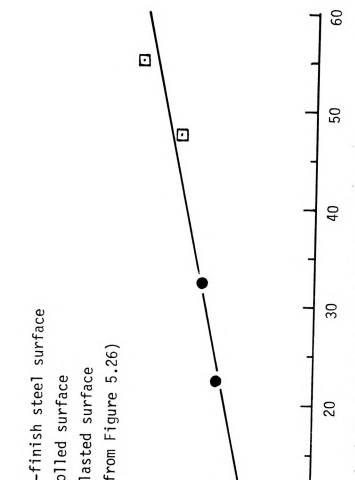

Figure 6.33: Correlation between profilometer and strip chart readings of aspirity heights for different steel surfaces.

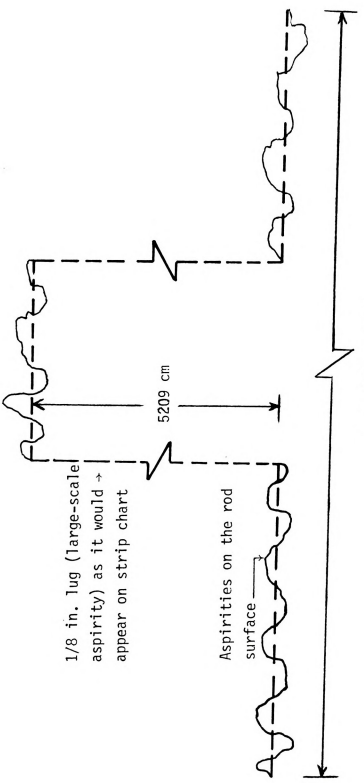

Figure 6.34: Roughness criterion (Figure 5.25) for a cold-rolled steel bar extended to include a 1/8 in. lug.

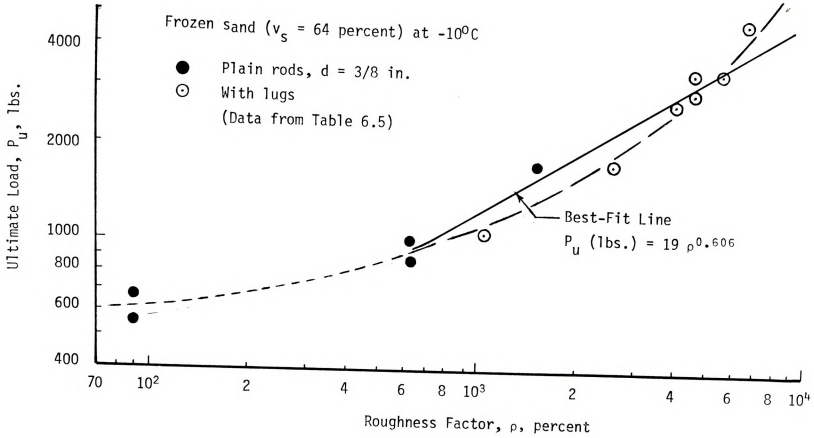

Figure 6.35: Ultimate pull-out capacity of steel rods in frozen sand (v_s = 64 percent) as a function of rod surface roughness.

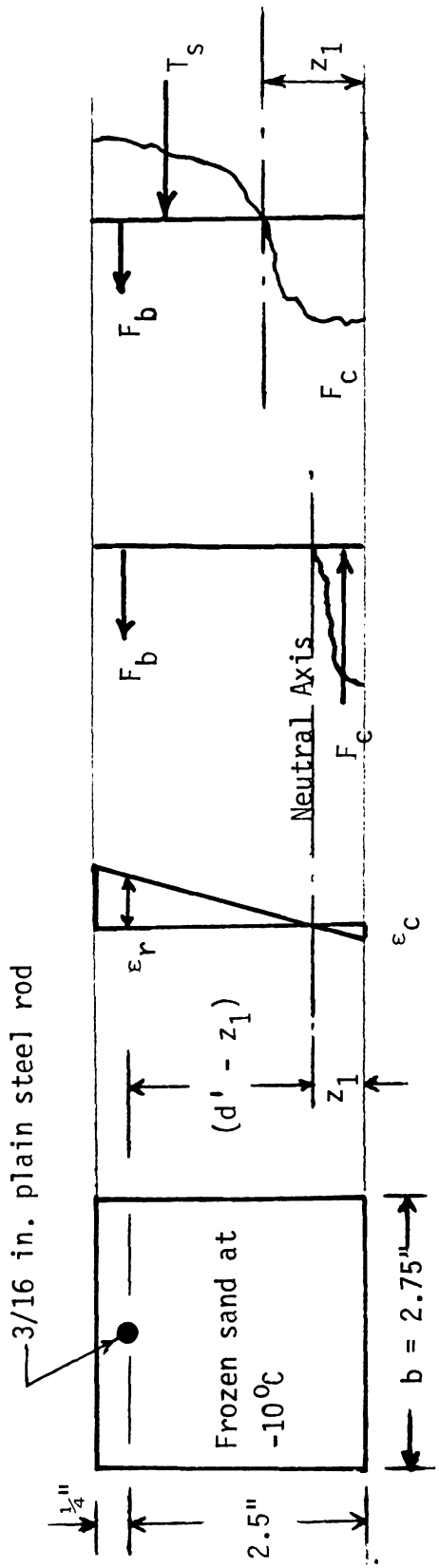

Figure 6.36: Conditions of equilibrium for a frozen sand beam reinforced with a plain steel rod.

CHAPTER VII

SUMMARY AND CONCLUSIONS

The results and conclusions based on this investigation are summarized in the following sections: test methods; load transfer mechanisms; applications-- reinforcement, piles, anchors; and recommendations for future work.

7.1 Test Methods:

Measurement of adfreeze bond between frozen sand and steel bars has involved use of constant displacement rate and constant load (creep) pull-out tests. Test temperatures included the range of -2 ^{o}C to -26 ^{o}C and were closely controlled ($\pm$ 0.05 ^{o}C) by immersion of protected samples (membrane enclosed) in a circulating and refrigerated coolant liquid. A specially constructed load frame supported the frozen sample while one end of the steel bar was attached to an eye connector and hook at the bottom of the coolant tank. An external loading system permitted pull-out of the bar at a constant displacement rate or bar creep movement relative to the frozen soil for a constant pull-out load. The following conclusions refer to sample preparation methods and test procedures:

1. Small rod displacements prior to bond failure and slip requires a high sensitivity for measurement equipment. Transducer sensitivity of at least $\pm$ 10^{-5} in. is desirable to show elastic movement prior to rupture in constant displacement rate tests and creep movement in constant load tests.

2. Loads selected for creep pull-out tests are limited by the high immediate bond failure stress and a lower long-term bond strength. Smaller loads do not develop steady-state creep rates needed for prediction of bar pull-out capacity. Vyalov's (1963) equation may be used for prediction of the long-term bond strength corresponding to a specified rod displacement.

3. The step loading procedure provided creep rate data for several pull-out loads on each sample. The initial time interval and load must satisfy long-term strength requirements to insure development of steady-state creep.

4. The ultimate load capacity of plain rods was dependent on rod and sample size as represented by the ratio of rod diameter to sample height, d/H. An optimum d/H ratio, on the order of 6 to 10%, appeared to give the largest adfreeze bond strengths for plain rods in frozen sand.

5. For 3/8-in. diameter rods with 1/8-in. high lugs, frozen soil diameters of 4 in. or more were required to avoid any influence of sample diameter on lug bearing capacity. Lug height h, rod diameter d, and sample diameter D may be used to define a ratio $\lambda = (D-d)/2h$ for which values should be at least 13 in order to avoid any influence of sample diameter on lug bearing and pull-out loads.

7.2 Load Transfer Mechanisms:

Adfreeze bond between frozen sand and embedded structural members (reinforcement, piles, or anchors) include: (1) ice adhesion, (2) friction with sand particles, and (3) mechanical interaction of frozen soil with surface roughness of the structural member. These bond components involve different load transfer mechanisms. Ice adhesion is the result

of increased attraction between water molecules and the surface of the structural member at freezing temperatures. Surface type (steel, wood, paint, etc.) and contaminants (salts, minerals, etc.) in the ice significantly influence adhesion forces at the interface and cohesive forces in the ice. Friction with soil particles is dependent on the friction angle between the soil particles and structural member, and is proportional to the normal stress that is pushing the particles against the member. Surface roughness of the structural member introduces particle dilatancy and reorientation effects adjacent to the surface. An increase in surface roughness by the introduction of lugs on the surface permits bearing forces to interact with frozen soil. The result was a significant increase in load transfer as surface movement mobilized mechanical interaction forces. The following conclusions refer to load transfer mechanisms:

1. Ice adhesion was mobilized at very small displacements with rupture typically at less than 0.002 inches. The presence of sand particles increased the ice matrix volume involved in rupture and thereby increased the adfreeze bond. An increase in surface roughness by use of lugs added significantly to the adfreeze bond with no observed change in displacements required for initial rupture.

2. Friction between sand particles and the structural member was negligible as shown by the small residual loads. Unconfined frozen sand samples contribute little normal stress on sand particles adjacent to the structural member.

3. An increase in surface roughness, by the addition of a single lug, gave load-displacement curves showing the initial rupture of ice adhesion followed by mobilization of bearing forces on frozen soil. Residual ice

adhesion and friction for larger displacements were negligible in contrast to the larger bearing forces.

4. Use of multiple lugs, a deformed steel bar as used for concrete reinforcement, showed an increase in the ultimate pull-out load in a direct ratio to the number of lugs after residual adhesion and friction loads were subtracted. A modified load-displacement curve suggested a possible relationship between ultimate load, lug size and spacing, and maximum particle size.

5. Sand density (or sand volume fraction) significantly influenced the adfreeze bond strength for a given creep rate, bar and lug size. For ice-rich samples (sand volume fraction < 42 %) the pull-out load depends primarily on plastic deformation of the ice matrix. For ice-poor samples (sand volume fraction > 42 %) the adfreeze bond and pull-out load increased abruptly with mobilization of sand dilatancy and particle reorientation effects along with soil bearing forces on the lugs.

6. Colder temperatures (range of -2 ^{o}C to -20 ^{o}C) and larger displacement rates both increased the adfreeze bond components. Experimental relationships were developed which account for temperature, bar displacement (or creep) rate, and other test variables.

7. A roughness factor defined by Wright (1955), provided excellent correlation with increased bond or pull-out loads for plain rods. An increase in surface roughness, the addition of lugs, extended this correlation suggesting possible future design applications.

7.3 Applications-- Reinforcement, Piles, Anchors:

Structural members (reinforcement, piles, anchors) are embedded in frozen soil to take tensile forces or to transfer and distribute compre-

ssive loads in such a way that stability of the structure is maintained. In all cases load transfer between the frozen soil and the structural member involves the adfreeze bond and possible slip at their common interface. Installation in frozen ground commonly involves dry augered holes with a mixture of sand and water used to fill the annulus around the pile or anchor. Load supporting capacity develops when the sand-water slurry is solidly frozen in place. Load capacity is dependent on the long-term adfreeze bond strength of the frozen sand in the zone adjacent to the structural member. Several conclusions can be made relative to design considerations for placement of these structural members:

1. The dry density (or sand volume fraction) of the sand-water slurry should be as high as possible to insure a high adfreeze bond strength. Vibration of the slurry during placement to insure a relatively high dry density appears to be a desirable requirement in construction specifications.

2. The use of multiple lugs on the structural member will significantly increase the long-term pull-out load. The lugs increase both the initial ice adhesion and friction and are responsible for development of bearing forces on the lugs at larger displacements

3. Lug spacing should be such that forces which develop in front of the lugs do not overlap with pressure zones from adjacent lugs. A preliminary analysis based on Boussinesq's equations suggests that a lug spacing should be at least twice the lug width (d+2h). The design should also allow for formation of a void space behind the lug with length equal to the allowable pile or anchor displacement.

4. Constant load (creep) pull-out tests using pile and soil materials

of the same type as proposed for a project will help an engineer to account for the many variables which affect adfreeze bond strength. Field tests are needed to correlate test results on model pile sections with full size piles.

7.4 Recommendations for future work:

Additional research is needed on several aspects related to the bond and slip of steel bars in frozen sand. Several specific problems are outlined below:

1. The influence of confining pressure on bond components should be investigated. The available predictions are mostly based on the assumption of soil incompressibility or volume constancy. The effect of confining pressure on the volumetric strain of frozen sand (which characterizes the dilatational behavior of soil in front of the lug) does not appear to have received the attention it warrants.

2. Use of standard deformed bars for reinforcement appears to provide a significant capacity at fairly small displacements. Further tests are needed on these bars in order to provide design information on the most appropriate lug spacing and lug size.

3. In order to precisely evaluate the bond stress along steel bars, it will be necessary to monitor the stress distribution along the bars during pull-out tests. Redistribution of stresses with time, during creep tests, is also anticipated. Measurement of stresses and strains along the bar can be achieved by using a split rod which accommodates a number of strain gages.

4. Laboratory investigation of the performance of reinforced beams would provide valuable information on the time dependent interaction bet-

ween the reinforcement and the frozen sand beam. Properly instrumented beams would help define the strain distribution in the beam. Such information would be a significant contribution to developing design procedures for field applications of reinforced frozen earth structural elements.

4. Further model studies and dimensional analysis are required in order to make possible a multiple regression analysis for further applications.

BIBLIOGRAPHY

BIBLIOGRAPHY

Reference Code:

ASCE: American Society of Civil Engineers

CGJ: Canadian Geotechnical Journal

HRB: Highway Research Board

ICP: International Conference on Permafrost

ISGF: International Symposim on Ground Freezing

JACI: Journal of the American Concrete Institute

JSMFD: Journal of the Soil Mechanics and Foundations Division

NAS: National Academy of Sciences, Washington, D.C.

NRC: National Research Council

RR: Research Report

SR: Special Report

USA CRREL: U.S. Army Cold Regions Research and Engineering Laboratory

USA SIPRE: U.S. Army Snow, Ice and Permafrost Research Establishment

BIBLIOGRAPHY

Alkire, B.D.; and Andersland, O.B. (1972) "The Effect of Confining Pressure on the Mechanical Properties of Sand-Ice Materials," Journal of Glaciology, Vol. 12, No. 66, pp.469-481

Andersland, O.B. (1963), Discussion-Session 6-Physicomechanical Properties of Frozen Soil, Proc. 1st ICP, Lafayette, Ind., NAS-NRC Publ. 1287, pp. 338-339.

Andersland, O.B.; and Akili, W. (1967) "Stress Effects on Creep Rates of Frozen Clay Soil," Geotechnique, London, Vol. 17, No. 1, pp. 27-39

Andersland, O.B.; and AlNouri, I. (1970) "Time-Dependent Strength Behavior or Frozen Soil," JSMFD, ASCE, Vol. 96, No. SM4, pp. 1249-1265.

Andersland, O.B.; and Douglas, A.G. (1970) "Soil Deformation Rates and Activation Energies," Geotechnique, London, Vol. 20, No. 1, pp. 1-16.

Andersland, O.B.; Sayles, F.H.; and Ladanyi, B. (1978) "Mechanical Properties of Frozen Ground," Chapter 5 in Geotechnical Engineering For Cold Regions (ed. by O.B. Andersland and D.M. Anderson), McGraw-Hill Book Co., New York.

Barnes, P.; Tabor, D.; and Walker, J. (1971) "The Friction and Creep of Polycrystalline Ice," Proc. Royal Society of London, A324, pp. 127-155.

Bishop, A.W.; and Henkel, D.J. (1962) "The Measurement of Soil Properties in the Triaxial Test," Edward Arnold (Publishers) Ltd., London, England.

Bragg, R.A. (1980) "Material Properties for Sand-Ice Structural Systems," Ph.D. Thesis, Michigan State University, East Lansing, Michigan.

Bragg, R.A.; and Andersland, O.B. (1980) "Strain Rate, Temperature, and Sample Size Effects on Compression and Tensile Properties of Frozen Sand," 2nd ISGF, Trondheim, Norway, pp. 34-47.

Braun, B.; Shuster, J.; and Burnham, E. (1979) "Ground Freezing for Support of Open Excavations," Engineering Geology, Special Issue on Ground Freezing (ed. by H.L. Jessberger) Elsevier Scientific Publ. Co., Vol. 13, pp. 429-453.

Chamberlain, E.; Groves, C.; and Perham, R. (1972) "The Mechanical Behavior of Frozen Earth Materials Under High Pressure Triaxial Conditions," Geotechnique, London, Vol. 22, No. 3, pp. 469-483.

Crory, F.E. (1963) "Pile Foundations in Permafrost," 1st ICP, Lafayette, Ind., NAS-NRC Publ. 1287, pp. 467-476.

Crory, F.E.; and Reed, R.E. (1965) "Measurements of Frost Heaving Forces on Piles," Technical Report 145, USA CRREL, Hanover, N.H.

Dillon, H.B.; and Andersland, O.B. (1966) "Predicting Unfrozen Water Contents in Frozen Soils," CGJ, Vol. 3, No. 2, pp. 53-60.

Doud, J.O. (1978) "Ice Sheet Loads on Marine Piles," CGJ, Vol. 15, No. 4, pp. 599-604.

Eckardt, H. (1982) "Creep Tests with Frozen Soils Under Uniaxial Tension and Uniaxial Compression," Roger J.E. Brown Memorial Volume. Proceedings of the 4th Canadian Permafrost Conference Calgary, Alberta, March 2-6, 1981. H.M. French (ed.), NRC of Canada, Ottawa, pp. 365-373.

Eckardt, H. (1979) "Creep Behavior of Frozen Soils in Uniaxial Compression Tests," Engineering Geology, Special Issue on Ground Freezing (ed. by H.L. Jessberger), Vol. 13, pp. 185-195, Elsevier Scientific Publ. Co., New York.

Eyring, H. (1936) "Viscosity, Plasticity and Diffusion as Examples of Absolute Reaction Rates," J. Chem. Physics, Vol. 4, No. 4, pp. 283-291.

Faraday, M. (1859) "On Regelation," Philosophical Magazine, 4th Ser., Vol. 17, p. 162.

Faraday, M. (1860) "Note on Regelation," Proc. Royal Society, London, Vol. 10, p. 440.

Ferguson, P.M. (1966) "Bond Stress-The Sate of the Art," JACI, Proc. Vol. 63, No. 11, pp. 1161-1188.

Frederking, R.M.W. (1979) "Laboratory Tests on Downdrag Loads Developed by Floating Ice Covers on Vertical Piles," Div. of Build. Res., NRC of Canada, Ottawa, DBR Paper No. 874, pp. 1098-1110.

Gibson, R.E. (1950) Discussion, J. of Institute of Civil Engineering, Vol. 34, p. 382.

Glasstone, S.; Laidler, K.J.; and Eyring, H. (1941) "The Theory of Rate Processes," McGraw-Hill Book Co., New York.

Glen, J.W. (1955) "The Creep of Polycrystalline Ice," Proc. Royal Society, London, A228, pp. 519-538.

Gold, L.W. (1970) "Process of Failure in Ice," CGJ, Vol. 7, No. 4, pp. 405-413.

Gold, L.W. (1978) "Ice Pressure and Bearing Capacity," Chapter 10 in Geotechnical Engineering For Cold Regions (ed. by O.B. Andersland and D.M. Anderson), McGraw-Hill Book Co., New York.

Goughnour, R.R. (1967) "The Soil-Ice System and the Shear Strength of Frozen Soils," Unpublished Ph.D. Thesis, Michigan State University, East Lansing, Michigan.

Goughnour, R.R.; and Andersland, O.B. (1968) "Mechanical Properties of a Sand-Ice System," JSMFD, ASCE, Vol. 94, No. SM4, pp. 923-950.

Harr, M.E. (1962) "Ground Water and Seepage," McGraw-Hill Book Co., New York.

Hawkes, I.; and Mellor, M. (1972) "Deformation and Fracture of Ice Under Uniaxial Stress," Journal of Glaciology, Vol. 11, pp. 103-130.

Haynes, F.D.; and Karalius, J.A. (1977) "Effect of Temperature on the Strength of Frozen Silt," RR 350, USA CRREL, Hanover, N.H.

Haynes, F.D.; Karalius, J.A.; and Kalafut, J. (1975) "Strain Rate Effect on the Strength of Frozen Silt," RR 350, USA CRREL, Hanover, N.H.

Hill, R. (1950) "The Mathematical Theory of Plasticity," Clarendon Press, Oxford, England.

Hoekstra, P. (1969) "The Physics and Chemistry of Frozen Soils," SR-103, HRB, pp. 78-90.

Hoff, N.J. (1954) "Approximate Analysis of Structures in the Presence of Moderately Large Creep Deformations," Quart. Appl. Math., Vol. 12, pp. 49-55.

Hooke, R. LeB.; Dahlin, B.B.; Kauper, M.T. (1972) "Creep of Ice Containing Dispersed Fine Sand," Journal of Glaciology, Vol. 11, No. 63, pp. 327-336.

Hori, T. (1956) "On the Super-cooling and Evaporation of Thin Water Films," Translation 62, Ser. A, Vol. 15, p. 34, USA SIPRE, Corps of Engineers, Wilmette, Ill.

Hosler, C.L.; Jensen, D.C.; and Goldslak, L. (1957) "On the Aggregation of Ice Crystals to Form Snow," Journal of Meterology, Vol. 14, pp. 415-420.

Hughes, B.P. (1976) "Limit State Theory of Reinforced Concrete Design," Van Nostrand Reinhold Co., New York.

Hult, J.A.H. (1966) "Creep in Engineering Structures," Blaisdell Publ. Co., Waltham, Mass.

Hunsaker, J.C.; Keyes, F.G.; Houghton, H.G.; Johnson, C.A.; and Dotson, J.V. (1940) "An Investigation of Methods for the De-Icing of Aircraft," Progress Report to NAS, Massachusetts Institute of Technology, Report No. 1.

Jellinek, H.H.G. (1957 a) "Tensile Strength Properties of Ice Adhering to Stainless Steel," RR 23, USA SIPRE, Corps of Engineers, Wilmette, Ill.

Jellinek, H.H.G. (1957 b) "Adhesive Properties of Ice, Part 1," RR38, USA SIPRE, Corps of Engineers, Wilmette, Ill.

Jellinek, H.H.G. (1960 a) "Bonding of Flat Ice Surfaces--Some Preliminary Results," RR 61, USA SIPRE, Corps of Engineers, Wilmette, Ill.

Jellinek, H.H.G. (1960 b) "Adhesive Properties of Ice, Part 2," RR 62, USA SIPRE, Corps of Engineers, Wilmette, Ill.

Jellinek, H.H.G. (1960 c) "Some Frictional Properties of Thin Water Films," SR 37, USA SIPRE, Corps of Engineers, Wilmette, Ill.

Jellinek, H.H.G. (1967) "Liquid-Like (Transition) Layer on Ice," Journal of Colloidal and Interface Science, Vol. 25, pp. 192-205.

Jellinek, H.H.G. (1970) "Ice Adhesion and Abhesion: A Survey," Proc. Int'l Symp. on Snow Removal and Ice Control Research, NRC-HRB SR115, pp. 46-76.

Jensen, D.C. (1956) "On the Cohesion of Ice," M.S. thesis, Pennsylvania State University, University Park, Pennsylvania.

Jessberger, H.L. (1980) "State-of-the-Art-Report, Ground Freezing: Mechanical Properties, Processes and Design," The 2nd ISGF, Trondheim, Norway, pp. 1-33.

Johnston, G.H., and Ladanyi, B. (1972) "Field Tests on Grouted Rod Anchors in Permafrost," CGJ, Vol. 9, No. 2, pp. 176-194.

Johnston, G.H.; and Ladany, B. (1974) "Field Tests of Deep Power-Installed Screw Anchors in Permafrost," CGJ, Vol. 11, No. 3, pp. 348-358.

Jones, S.J. (1978) "Triaxial Testing of Polycrystalline Ice," Proc. 3rd ICP, Edmonton, Alberta, pp. 671-674.

Jones, S.J.; and Glen, J.W. (1969) "The Effect of Dissolved Impurities on the Mechanical Properties of Ice Crystals," Philosophical Magazine, Vol. 19, pp. 13-24.

Klein, J.; and Jessberger, H.L. (1978) "Creep Stress Analysis of Frozen Soils Under Multiaxial States of Stress," Proc. 1st ISGF, Bochum, Germany, pp. 217-226.

Laba, J.T. (1974) "Adfreezing of Sands to Concrete," NRC, Transportation Research Board, Record No. 497, pp. 31-39.

Ladanyi, B. (1963) "Expansion of a Cavity in a Saturated Clay Medium," JSMFD, ASCE, Vol. 89, No. SM4, pp. 127-161.

Ladanyi, B. (1967) "Deep Punching of Sensitive Clay," Proc. 3rd Pan Amer. Conf. Soil Mech. Found. Eng., Caracas, Vol. I, pp. 535-546.

Ladany, B. (1972) "An Engineering Theory of Creep of Frozen Soils," CGJ, Vol. 9, No. 1, pp. 63-80.

Ladanyi, B. (1973) "Bearing Capacity of Deep Footings in Sensitive Clays," Proc. 8th Int'l Conf. Soil Mech. Found. Eng., Moscow, Vol. 2, pp. 159-166.

Ladanyi, B. (1975) "Bearning Capacity of Strip Footings in Frozen Soils," CGJ, Vol. 12, No. 3, pp. 393-407.

Ladanyi, B. (1976) "Use of the Static Penetration Test in Frozen Soils," CGJ, Vol. 13, No. 2, pp. 95-110.

Ladanyi, B. (1981 a) "Mechanical Behavior of Frozen Soils," Mechanics of Structured Media (ed. by A.P.S. Selvadurai) Elsevier Scientific Publ. Co., New York, pp. 205-245.

Ladanyi, B. (1981 b) "State-of-the-Art: Determination of Creep Settlement of Shallow Foundation in Permafrost," Presented at the October 26-30, 1981, ASCE Annual Convention and Exposition, held at St. Louis, Missouri, pp. 1-26.

Ladanyi, B; and Arteau, J. (1979) "Effect of Specimen Shape on Creep Response of a Frozen Sand," Engineering Geology, Special Issue on Ground Freezing (ed. by H.L. Jessberger), Vol. 13, pp. 207-222, Elsevier Scientific Publ. Co., New York.

Ladanyi, B.; and Johnston, G.H. (1973) "Evaluation of In-Site Creep Properties of Frozen Soils with the Pressuremeter," Proc. 2nd ICP, N. American Contribution, Yakutsk, U.S.S.R., pp. 310-318.

Ladanyi, B.; and Johnston, G.H. (1974) "Behavior of Circular Footings and Plate Anchors in Permafrost," CGJ, Vol. 11, No. 4, pp. 531-553.

Ladanyi, B.; and Paquin, J. (1978) "Creep Behavior of Frozen Sand Under Deep Circular Load," Proc. 3rd ICP, Edmonston, Alberta, pp. 680-686.

Lambe, T.W.; and Whitman, R.V. (1969) "Soil Mechanis," J. Wiley and Sons Inc., New York.

Lofquist, B. (1951) "Lifting Force and Bearing Capacity of Ice Sheet," Technical Transaction TT-164, NRC of Canada, Ottawa.

Mains, R.M. (1951) "Measurement of the Distribution of Tensile and Bond Stresses Along Reinforcing Bars," JACI, Proc. Vol. 48, No. 3, pp. 225-252.

Martin, R.T. (1960) "Adsorbed Water on Clay: A Review," Clays and Clay Minerals, Vol. 9, pp. 28-70.

Meissner, H.; and Eckardt, H. (1976) "Biegebalken aus gefrorenem Erdstoff mit konstanten Temperaturgradienten," Sechste Europaische Konferenz fur Bodenmechanik und Grundbau, Proceedings 1.1, Wien.

Mendelson, A. (1968) "Plasticity: Theory and Application," McMillan Publ. Co., New York.

Meyerhof, G.G. (1951) "The Ultimate Bearing Capacity of Foundations," Geotechnique, London, Vol. 1, pp. 301-331.

Michel, B (1978) "Ice Mechanics," Les Presses De L'Universite' Laval, Quebec.

Mitchell, J.K. (1976) "Fundamentals of Soil Behavior," J. Wiley and Sons Ice., New York.

Mitchell, J.K.; Campanella, R.G.; and Singh, A. (1968) "Soil Creep as a Rate Process," JSMFD, ASCE, Vol. 94, No. SM1, pp. 231-253.

Mohaghegh, M.M.; and Coon, M.D. (1973) "Plastic Analysis of Thick Circular Plates," Int. J. Mech. Sci., Vol. 15, pp. 935-942.

Morgenstern, N.R.; Roggensack, W.D.; and Weaver, J.S. (1980) "The Behavior of Friction Piles in Ice and Ice-Rich Soils," CGJ, Vol. 17, No. 3, pp. 405-415.

Nadai, A. (1963) "Theory of Flow and Fracture of Solids," Vol. 2, McGraw-Hill Book Co., New York.

Nakaya, U.; and Matsumoto, A. (1953) "Evidence of the Existence of Liquid-Like Film on Ice Surfaces," RR 4, USA SIPRE, Corps of Engineers, Wilmette, Ill.

Nerseova, Z.A.; and Tsytovich, N.A. (1963) "Unfrozen Water in Frozen Soils," Proc. 1st ICP, Lafayette, Ind., NAS-NRC Publ. 1287, pp. 230-233.

Nixon, J.F. (1978) "Foundation Design Approaches in Permafrost," CGJ, Vol. 15, No. 1, pp. 96-112.

Nixon, J.F.; and McRoberts, E.C. (1976) "A Design Approach for Pile Foundations in Permafrost," CGJ, Vol. 13, No. 1, pp. 40-57.

Odqvist, F.K.G. (1966) "Mathematical Theory of Creep and Creep Rupture," Oxford Mathematical Monograph, Oxford University Press, London.

Ogata, N.; Yasuda, M.; and Kataoka, T. (1982) "Salt Concentration Effects on Strength of Frozen Soils," Proc. 3rd ISGF, Hanover, N.H., pp. 3-10.

Parameswaran, V.R. (1978 a) "Laboratory Studies of the Adfreeze Bond Between Small-Scale Model Piles and Frozen Sand," Proc. 3rd ICP, Edmonton, Alberta, pp. 714-720.

Parameswaran, V.R. (1978 b) "Adfreeze Strength of Frozen Sand to Model Piles," CGJ, Vol. 15, No. 4, pp. 494-500.

Parameswaran, V.R. (1979) "Creep of Model Piles in Frozen Soil," CGJ, Vol. 16, No. 1, pp. 69-77.

Parameswaran, V.R. (1980) "Deformation Behavior and Strength of Frozen Sand," CGJ, Vol. 17, No. 1, pp. 74-88.

Parameswaran, V.R. (1981) "Adfreeze Strength of Model Piles in Ice," CGJ, Vol. 18, No. 1, pp. 8-16.

Parameswaran, V.R.; and Jones, S.J. (1980) "Triaxial Testing of Frozen Sand," Journal of Glaciology, Vol. 26, pp. 601-612.

Perkins, T.K.; and Ruedrich, R.A. (1973) "The Mechanical Behavior of Synthetic Permafrost," J. Soc. Petroleum Engineers, Vol. 13, No. 4, pp. 211-220.

Perry, E.S.; and Thompson, J.N. (1966) "Bond Stress Distribution on Reinforcing Steel in Beams and Pullout Specimens," JACI, Proc. Vol. 63, No. 8, pp. 865-874.

Phukan, A.; and Andersland, O.B. (1978) "Foundations for Cold Regions," Chapter 6 in Geotechnical Engineering For Cold Regions (ed. by O.B. Andersland and D.M. Anderson), McGraw-Hill Book Co., New York.

Ponomarjov, V.D. (1982) "Temperature Deformations of Frozen Soils," Proc. 3rd ISGF, Hanover, N.H., pp. 125-129.

Pounder, E.R. (1967) "The Physics of Ice," Pergamon Press, Oxford, England.

Rocha, M. (1957) "The Possibility of Solving Soil Mechanics Problems by the Use of Models," Proc. 4th Int'l. Conf. Soil Mech. Found. Eng., London, Vol. I, pp. 183-188.

Rowely, R.K.; Watson, G.H.; and Ladanyi, B. (1973) "Vertical and Lateral Pile Load Tests in Permafrost," Proc. 2nd ICP, N. American Contribution, Yakutsk, U.S.S.R., pp. 712-720.

Rowely, R.K.; Watson, G.H.; and Ladanyi, B. (1975) "Prediction of Pile Performance under Lateral Load," CGJ, Vol. 12, No. 4, pp. 510-523.

Sanger, F.J. (1969) "Foundations of Structures in Cold Regions," Monograph III-C4, USA CRREL, Hanover, N.H.

Sanger, F.J.; and Sayles, F.H. (1978) "Thermal and Rheological Computations for Artificially Frozen Ground Construction" Ground Freezing, Developments in Geotechnical Engineering, Vol. 26, pp. 311-337, (Edited by H.L. Jessberger) Elsevier Scientific Publ. Co., New York.

Sayles, F.H. (1966) "Low Temperature Soil Mechanics," Technical Note 143, USA CRREL, Hanover, N.H.

Sayles, F.H. (1968) "Creep of Frozen Sand," Technical Report 190, USA CRREL, Hanover, N.H.

Sayles, F.H. (1973) "Triaxial and Creep Tests on Frozen Ottawa Sand," Proc. 2nd ICP, North American Contribution, Yakutsk, U.S.S.R., pp. 384-391.

Sayles, F.H. (1974) "Triaxial Constant Strain Rate Tests and Triaxial Creep Tests on Frozen Ottawa Sand," Tech. Rept. 253, USA CRREL, Hanover, N.H.

Sayles, F.H.; and Epanchin, N.V. (1966) "Rate of Strain Compression Tests on Frozen Ottawa Sand and Ice," Technical Note 158, USA CRREL, Hanover, N.H.

Sego, D. (1980) "Deformation of Ice Under Low Stresses," Ph.D. Thesis, University of Alberta, Edmonton, Alberta.

Sego, D.C.; Shultz, T.; and Banasch, R. (1982) "Strength and Deformation Behavior of Frozen Saline Sand," Proc. 3rd ISGF, Hanover, N.H., pp. 11-17.

Smith, L.L.; and Cheatham, J.B. (1975) "Plasticity of Ice and Sand Ice Systems," J. of Engineering for Industry, Vol. 97, No. 2, pp. 479-484.

Soo, S. (1983) "Experimental and Numerical Analysis of Frozen Sand Structures," Ph.D. thesis (in preparation), Michigan State University, East Lansing, Michigan.

Stehle, N.S. (1970) "Holding Strength of Piles in Ice," Technical Report 700, U.S. Naval Civ. Eng. Lab., Port Hueneme, California.

Thomas, H.P., and Luscher, U. (1980) "Improvement of Bearing Capacity of Pipe Piles by Corrugation," Building under Cold Climates and on Permafrost, collection of papers from U.S.-Soviet Joint Seminars, Leningrad, U.S.S.R., pp. 229-234.

Tsytovich, N.A. (1958) "Bases and Foundations on Frozen Soil," HRB SR 58.

Tsytovich, N.A. (1966) "Bases and Foundations and Structures on Perennially Frozen Soils," Design Standards, SNiP II-B, p. 6-66.

Tsytovich, N.A. (1975) "Mechanics of Frozen Ground," McGraw-Hill Book Co., New York.

Tsytovich, N.A.; and Sumgin, M.I. (1959) "Principles of Mechanics of Frozen Ground," Translation 19, USA SIPRE, Corps of Engineers, Wilmette, Ill.

Velli, Y.Y.; and Karpunina, A.A. (1973) "Saline Permafrost as Bearing Ground for Permafrost," Proc. 2nd ICP, USSR Contribution, Yakutsk, USSR, Pp. 545-550.

Vesić, A.S. (1973) "Analysis of Ultimate Loads of Shallow Foundations," JSMFD, ASCE, Vol. 99, No. SMI, pp. 45-73.

Vyalov, S.S. (1959) "Rehological Properties and Bearing Capacity of Frozen Soils," Translation 74, USA CRREL, Hanover, N.H.

Vyalov, S.S. (1963) "Rheology of Frozen Soils," Proc. 1st ICP, Lafayette, Ind., NAS-NRC Publ. 1287, pp. 332-337.

Vyalov, S.S., ed., (1965) "The Strength and Creep of Frozen Soils and Calculations for Ice-Soil Retaining Structures," Translation 76, USA CRREL, Hanover, N.H.

Vyalov, S.S.; Dokuchayev, V.V.; Sheynkman, D.P.; Gaydayenko, Y.I.; and Goncharov, Y.M. (1973) "Ground Ice as the Bearing Stratum for Construction," Proc. 2nd ICP, USSR Contribution, Yakutsk, USSR, pp. 537-545.

Weaver, J.S.; and Morgenstern, N.R. (1981 a) "Simple Shear Tests on Frozen Soils," CGJ, Vol. 18, No. 2, pp. 217-229.

Weaver, J.S.; and Morgenstern, N.R. (1981 b) "Pile Design in Permafrost," CGJ, Vol. 18, No. 3, pp. 357-370.

Wright, P.J.F. (1955) "A Method of Measuring the Surface Texture of Aggregate," Magazine of Concrete Research, Vol. 7, No. 21, pp. 151-160.

APPENDICES

APPENDIX - Data:

A. Constant Displacement Rate Tests.
B. Constant Stress (Creep) Tests.

Table A-1: Ice Samples I-1 to I-21 (Ice 1)

Ice (1) samples were formed from distilled water in four layers (6 in. sample height). Average density equals 56.1 lb./cu.ft. A 5/8 in. diameter plain steel rod was used with samples I-1 to I-21.

Sample I-1:

$T = -10.1^{\circ}C$
$H = 5.866$ in.
$D = 5.677$ in.
$L = 5.685$ in.
$\dot{P} = 140$ lbs./min.
$\dot{\delta}_n = 4.24 \times 10^{-3}$ in./min.

t (sec.)	P (lbs.)	δ ($\times 10^{-3}$ in.)
225	430	o.24
295	630	0.25
340	760	0.50
360	820	0.60
400	930	0.90
400	360	10.00
406	310	11.00
412	290	12.00
418	270	12.75
436	250	14.00
460	240	15.50
475	230	16.50
670	200	30.00
895	190	46.50

Sample I-2:

$T = -15.0^{\circ}C$
$H = 5.750$ in.
$D = 5.875$ in.
$L = 5.625$ in.
$\dot{P} = 136.4$ lbs./min.
$\dot{\delta}_n = 4.50 \times 10^{-3}$ in./min.

t (sec.)	P (lbs.)	δ ($\times 10^{-3}$ in.)
2	40	0.010
20	85	0.025
65	150	0.080
110	200	0.135
170	360	0.210
230	510	0.282
272	620	0.760
272	220	7.640
278	185	9.110
290	165	10.580
305	152	11.900
350	130	15.440
395	120	19.120
575	105	32.350

Sample I-3:

$T = -15.1^{\circ}C$
$H = 5.688$ in.
$D = 5.875$ in.
$L = 5.719$ in.
$\dot{P} = 130.0$ lbs./min.
$\dot{\delta}_n = 4.40 \times 10^{-3}$ in./min.

t (sec.)	P (lbs.)	δ ($\times 10^{-3}$ in.)
60	52	0.04
120	187	0.07
180	330	0.11
255	557	0.77
280	607	1.50
286	370	5.91
292	310	7.75
300	270	8.85
315	250	10.16
375	230	14.75
435	218	19.31
495	210	23.72
615	200	32.32

Sample I-4:

$T = -15.1^{\circ}C$
$H = 5.438$ in.
$D = 5.938$ in.
$L = 5.375$ in.
$\dot{P} = 105.4$ lbs./min.
$\dot{\delta}_n = 4.90 \times 10^{-3}$ in./min.

t (sec.)	P (lbs.)	δ ($\times 10^{-3}$ in.)
220	390	0.37
259	455	1.10
259	220	9.20
265	170	11.26
280	150	13.32
295	135	15.10
310	126	16.46
370	110	21.72
430	100	26.65
505	96	32.53

Note: At t=0, P=0 and δ=0, unless noted.

Table A-1: (Cont'd)

Sample I-5:

(Leakage, data discarded)

Sample I-6:

$T = -6.1^{o}C$
$H = 5.938$ in.
$D = 5.969$ in.
$L = 5.969$ in.
$\dot{P} = 89.6$ lbs./min.
$\dot{\delta}_n = 3.68 \times 10^{-3}$ in./min.

t(sec.)	P(lbs.)	δ ($\times 10^{-3}$in.)
60	90	0.037
75	112	0.404
81	95	1.03
87	82	1.765
93	77	2.500
135	67	5.300
195	63	9.120
255	60	12.870
315	58	16.690
435	56	23.900

Sample I-7:

$T = -20.0^{o}C$
$H = 5.938$ in.
$D = 5.900$ in.
$L = 5.812$ in.
$\dot{P} = 136.4$ lbs./min.
$\dot{\delta}_n = 3.90 \times 10^{-3}$ in./min.

t (sec.)	P(lbs.)	δ ($\times 10^{-3}$in.)
220	500	0.001
220	278	5.000
235	253	6.786
250	240	8.214
280	222	11.785
325	207	15.000
385	195	19.285
590	175	32.142

Sample I-8:

$T = -20.0^{o}C$
$H = 6.125$ in.
$D = 5.938$ in.
$L = 6.125$ in.
$\dot{P} = 115.7$ lbs./min.
$\dot{\delta}_n = 3.60 \times 10^{-3}$ in./min.

t (sec.)	P (lbs.)	δ ($\times 10^{-3}$in.)
100	200	0.04
112	216	0.28
118	196	1.08
124	172	2.01
130	160	2.60
160	144	4.80
220	140	8.80
380	135	18.00

Sample I-9:

$T = -10.0^{o}C$
$H = 5.875$ in.
$D = 5.938$ in.
$L = 5.834$ in.
$\dot{P} = 111.8$ lbs./min.
$\dot{\delta}_n = 3.55 \times 10^{-3}$ in./min.

t (sec.)	P (lbs.)	δ ($\times 10^{-3}$in.)
75	112	0.01
120	216	0.20
175	326	0.40
175	100	6.00
240	90	10.60
330	84	16.80
450	82	23.00

Sample I-10:

$T = -10.1^{o}C$
$H = 5.969$ in.
$D = 5.938$ in.
$L = 5.938$ in.

(Continued)

Table A-1: (Cont'd)

Sample I-10: (Cont'd)

$\dot{P}$ = 91.64 lbs./min.

$\dot{\delta}_n$= 3.32×10^{-3} in./min.

t (sec.)	P (lbs.)	δ ($\times 10^{-3}$ in.)
90	134	0.01
165	240	0.12
220	336	0.20
220	120	5.60
250	112	8.80
310	100	13.60
415	94	19.40

Sample I-11:

T = -10.1°C
H = 5.938 in.
D = 5.938 in.
L = 5.938 in.

$\dot{P}$ = 94.0 lbs./min.

$\dot{\delta}_n$= 3.43×10^{-3} in./min.

t (sec.)	P (lbs.)	δ ($\times 10^{-3}$ in.)
250	370	0.01
270	424	0.08
300	470	0.20
300	145	6.00
320	105	10.00
350	90	12.00
380	85	14.00
455	78	18.00

Sample I-12:

T = -26.1°C
H = 6.0 in.
D = 6.0 in.
L = 6.0 in.

$\dot{P}$ = 126 lbs./min.

$\dot{\delta}_n$= 0.9×10^{-3} in./min.

t (sec.)	P (lbs.)	δ ($\times 10^{-3}$ in.)
110	165	0.08
400	840	0.20
400	140	5.60
580	120	8.20

Sample I-13:

T = -26.7°C
H = 6.0 in.
D = 6.0 in.
L = 6.0 in.

$\dot{P}$ = 143.2 lbs./min.

$\dot{\delta}_n$= 4.0×10^{-3} in./min.

t (sec.)	P (lbs.)	δ ($\times 10^{-3}$ in.)
90	170	0.01
430	1040	0.08
620	1480	0.24
620	190	40.00
640	220	42.14
645	220	42.54
730	195	43.10
840	200	45.00
940	180	65.00

Sample I-14:

T = -26.4°C
H = 5.906 in.
D = 6.000 in.
L = 5.910 in.

$\dot{P}$ = 4.9 lbs./min.

$\dot{\delta}_n$= 3.5×10^{-4} in./min.

t (min.)	P (lbs.)	δ ($\times 10^{-3}$ in.)
0.0	0	0.0
84.8	2140	3.6
84.8	320	38.6
90.0	440	42.0
90.5	330	43.0
96.0	420	44.0
96.5	325	45.4
101.7	400	46.2
102.2	320	47.4
106.5	390	48.2
107.7	320	49.0
111.4	375	49.8
113.0	320	50.4
116.0	355	51.0
118.4	320	51.8

Table A-1: (Cont'd)

Sample I-15:

$T = -26.6^{\circ}C$
H = 5.938 in.
D = 6.0 in.
L = 5.938 in.
$\dot{P}$ = 22.5 lbs./min.
$\dot{\delta}n = 8.0 \times 10^{-4}$ in./min.

t (min.)	P (lbs.)	δ ($\times 10^{-3}$ in.)
18	340	0.40
32	680	0.45
44	990	0.80
44	160	12.80
70	140	33.60

Sample I-16:

$T = -20.4^{\circ}C$
H = 5.938 in.
D = 6.0 in.
L = 5.938 in.
$\dot{P}$ = 27 lbs./min.
$\dot{\delta}n = 1.05 \times 10^{-3}$

t (min.)	P (lbs.)	δ ($\times 10^{-3}$ in.)
10.0	320	0.8
25.0	680	1.2
38.5	1040	1.4
38.5	100	20.0
48.0	90	30.0

Sample I-17:

$T = -15.5^{\circ}C$
H = 6.344 in.
D = 6.0 in.
L = 6.344 in.
$\dot{P}$ = 23.60 lbs./min.
$\dot{\delta}n = 3.52 \times 10^{-4}$ in./min.

t (min.)	P (lbs.)	δ ($\times 10^{-3}$ in.)
10.0	180	1.40
17.5	320	1.60
31.5	665	1.62
44.7	1010	1.68
57.8	1350	1.90
71.0	1710	2.22
84.2	2060	2.62

(Continued)

Sample I-17: (Cont'd)

t (sec.)	P (lbs.)	δ ($\times 10^{-3}$ in.)
97.7	2380	3.34
102.2	2480	3.48
119.8	1830	5.70
119.8	200	18.00
125.2	300	18.80
127.3	200	20.80
131.5	250	21.60
134.5	200	23.20

Sample I-18:

$T = -10.1^{\circ}C$
H = 5.906 in.
D = 6.0 in.
L = 5.906 in.
$\dot{P}$ = 28.5 lbs./min.
$\dot{\delta}n = 2.3 \times 10^{-4}$

t (min.)	P (lbs.)	δ ($\times 10^{-3}$ in.)
7.5	360	0.40
24.5	750	0.42
31.2	890	0.75
31.2	80	8.80
40.3	80	10.80

Sample I-19:

$T = -6.6^{\circ}C$
H = 5.938 in.
D = 6.0 in.
L = 5.969 in.
$\dot{P}$ = 22.1 lbs./min.
$\dot{\delta}n$ = **

t (min.)	P (lbs.)	δ ($\times 10^{-3}$ in.)
43.0	1030	0.2
62.0	1470	0.4
80.0	1890	1.6
82.0	1920	2.0
84.0	1940	3.0
85.5	1890	4.4
85.5	300	18.4

** Not recorded due to lack of recording paper.

Table A-1: (Cont'd)

Sample I-20:

$T = -10.1^{\circ}C$
$H = 5.0$ in.
$D = 6.0$ in.
$L = 5.0$ in.
$\dot{P} = 26.4$ lbs./min.
$\dot{\delta}_n = 2.6 \times 10^{-4}$ in./min.

t (min.)	P (lbs.)	δ ($\times 10^{-3}$ in.)
60.0	1300	0.4
76.5	1720	1.2
79.0	1760	1.6
81.0	1780	2.8
83.0	60	19.0
100.0	245	20.6
108.0	200	26.0

Sample I-21:

$T = -20.1^{\circ}C$
$H = 6.0$ in.
$D = 6.0$ in.
$L = 6.06$ in.
$\dot{P} = 23.0$ lbs./min.
$\dot{\delta}_n = 6.15 \times 10^{-4}$ in./min.

t (min.)	P (lbs.)	δ ($\times 10^{-3}$ in.)
43.0	810	0.4
75.5	1740	0.8
75.5	100	17.8
84.0	200	17.8
95.8	450	18.6
96.0	220	22.4
100.0	260	23.2
104.0	220	25.0
112.0	210	28.6

Table A-2: Ice Samples I-22 to I-27 (Ice 2)

Ice (2) samples were formed from crushed ice (tap water) and saturated with distilled water. Average density equals 56.1 lb./cu.ft. A 3/8 in. diameter plain steel rod was used with samples I-22 to I-27.

Sample I-22:

$T = -10.0^{\circ}C$
H = 6.0 in.
D = 6.0 in.
L = 6.0 in.

$\dot{P}$ = 21.6 lbs./min.

$\dot{\delta}_n = 5.7 \times 10^{-4}$ in./min.

t (min.)	P (lbs.)	δ ($\times 10^{-3}$ in.)
25	540	0.2
25	0	11.6
29	40	12.4
34	30	15.2
60	30	30.0
183	30	99.0

Sample I-23:

$T = -22.0^{\circ}C$
H = 6.5 in.
D = 6.0 in.
L = 6.5 in.

$\dot{P}$ = 20.1 lbs./min.

$\dot{\delta}_n = 5.64 \times 10^{-4}$ in./min.

t (min.)	P (lbs.)	δ ($\times 10^{-3}$ in.)
31	624	0.4
31	16	13.6
34	72	14.0
40	56	17.6
74	50	36.8

Sample I-24:

$T = -20.0^{\circ}C$
H = 6.375 in.
D = 6.00 in.
L = 6.375 in.

$\dot{P}$ = 17.2 lbs./min.

$\dot{\delta}_n = 5.1 \times 10^{-4}$ in./min.

t (min.)	P (lbs.)	δ ($\times 10^{-3}$ in.)
32.5	560	0.4
32.5	16	12.4
35.0	50	13.0
44.0	32	18.4
76.0	32	34.6

Sample I-25:

$T = -15.0^{\circ}C$
H = 6.125 in.
D = 6.00 in.
L = 6.125 in.

$\dot{P}$ = 20 lbs./min.

$\dot{\delta}_n = 5.4 \times 10^{-4}$ in./min.

t (min.)	P (lbs.)	δ ($\times 10^{-3}$ in.)
33.5	670	0.1
33.5	64	14.0
50.0	48	23.0
70.0	40	34.0
104.0	40	52.0

Sample I-26:

$T = -6.0^{\circ}C$
H = 6.0 in.
D = 6.0 in.
L = 6.0 in.

$\dot{P}$ = 16.1 lbs./min.

$\dot{\delta}_n = 3.65 \times 10^{-4}$ in./min.

t (min.)	P (lbs.)	δ ($\times 10^{-3}$ in.)
13	210	0.1
13	48	3.5
14	32	5.5
16	16	8.0
37	16	18.5

Sample I-27:

$T = -2.0^{\circ}C$
H = 6.0 in.
D = 6.0 in.
L = 6.0 in.

$\dot{P}$ = 19.1 lbs./min.

$\dot{\delta}_n = 5.8 \times 10^{-4}$ in./min.

t (min.)	P (lbs.)	δ ($\times 10^{-3}$ in.)
5.5	105	0.1
5.5	20	4.0
7.0	10	6.0
30.0	10	19.3

Note: At t=0, P=0 and δ=0, unless noted.

Table A-3: Ice Samples I-28 to I-32 (Ice 3)

Ice (3) samples were formed from snow-ice saturated with distilled water. Average density equals 56.1 lb./cu.ft. A 5/8 in. diameter steel rod was used with samples I-28 to I-32.

Sample I-28:

$T = -10.0^{\circ}C$
H = 6.197 in.
D = 6.00 in.
L = 6.197 in.

$\dot{P}$ = 183.5 lbs./min.

$\dot{\delta}n = 4.5 \times 10^{-3}$ in./min.

t (min.)	P (lbs.)	δ ($\times 10^{-3}$ in.)
1.0	150	0.01
2.0	300	0.02
3.0	460	0.03
4.0	640	0.04
5.0	840	0.05
6.0	1060	0.06
7.0	1300	0.25
8.0	1500	0.40
8.5	1560	0.75
8.5	100	15.00
10.0	70	15.00
10.2	70	18.00
11.0	70	21.00
13.0	70	28.75
15.0	70	36.25
17.0	70	45.60

Sample I-29:

$T = -14.6^{\circ}C$
H = 6.0 in.
D = 6.0 in.
L = 6.0 in.

$\dot{P}$ = 233.3 lbs./min.

$\dot{\delta}n = 1.92 \times 10^{-3}$ in./min.

t (min.)	P (lbs.)	δ ($\times 10^{-3}$ in.)
6.15	1435	0.5
6.15	0	20.0
7.25	140	20.5
7.50	105	24.0
8.25	100	27.0
9.00	100	31.0
12.00	70	37.0
15.00	40	43.0
18.00	30	48.8

Note: At t=0, P=0 and δ=0, unless noted.

Sample I-30:

$T = -16.0^{\circ}C$
H = 6.375 in.
D = 6.00 in.
L = 6.375 in.

$\dot{P}$ = 280 lbs./min.

$\dot{\delta}n = 4.58 \times 10^{-3}$ in./min.

t (min.)	P (lbs.)	δ ($\times 10^{-3}$ in.)
2.75	880	0.25
2.75	70	13.00
3.00	70	13.20
4.00	70	18.50
5.00	60	24.75
8.00	60	41.60
11.00	50	56.60
14.00	50	70.35

Sample I-31:

$T = -6.0^{\circ}C$
H = 6.375 in.
D = 6.00 in.
L = 6.375 in.

$\dot{P}$ = 1290 lbs./min.

$\dot{\delta}n$ = **

t (sec.)	P (lbs.)	δ ($\times 10^{-3}$ in.)
20	430	** Rupture at fast rate

Sample I-32:

$T = -10.0^{\circ}C$
H = 6.5 in.
D = 6.0 in.
L = 6.5 in.

$\dot{P}$ = 258 lbs./min.

$\dot{\delta}n = 4.615 \times 10^{-3}$ in./min.

t (min.)	P (lbs.)	δ ($\times 10^{-3}$ in.)
4.00	1030	1.0
4.00	0	24.0
4.75	105	25.0
5.50	70	29.0
7.00	70	37.2
11.00	70	60.0
24.00	70	120.0

Table A-4: Frozen sand samples.

Sample S-1:

$T = -10.0^{o}C$
D = 6.0 in.*
H = 6.0 in.*
L = 6.0 in.*
v_s= 64.0 % *

d = 5/8 in.**
h = 0 (plain rod)

$\dot{P}$ = 195.5 lbs./min.

$\dot{\delta}n = 2.0 \times 10^{-3}$ in./min.

t (min.)	P (lbs.)	δ ($\times 10^{-3}$in.)
3.34***	640	0.16
4.58	890	0.22
5.50	1075	0.27
5.50	236	8.27
5.67	190	9.10
5.84	175	9.50
6.34	160	10.70
7.34	145	13.10
8.34	135	15.50

* Average values, unless noted.
** Cold-rolled steel, unless noted.
*** at t=0, P=0 and δ=0, unless noted.

Sample S-2:

$T = -10.2^{o}C$
D = 6.0 in.
H = 6.0 in.
L = 6.0 in.
v_s= 64.0 %

d = 5/8 in.
h = 0

$\dot{P}$ = 32.5 lbs./min.

$\dot{\delta}n = 5.0 \times 10^{-4}$ in./min.

t (min.)	P (lbs.)	δ ($\times 10^{-3}$in.)
21	700	0.8
29	980	1.0
38	1240	1.4
40	1300	2.2
41	1280	3.0
41	240	18.2
46	280	19.6
56	280	24.6

Sample S-3:

$T = -6.3^{o}C$
D = 6.0 in.
H = 6.0 in.
L = 6.0 in.
v_s= 64.0 %

d = 5/8 in.
h = 0

$\dot{P}$ = 29.7 lbs./min.

$\dot{\delta}n = 6.967 \times 10^{-4}$ in./min.

t (min.)	P (lbs.)	δ ($\times 10^{-3}$in.)
20.5	640	0.8
29.0	860	1.6
31.0	830	3.0
34.0	700	6.2
39.0	570	10.6
39.0	500	14.8
65.0	400	26.0

Sample S-4:

$T = -14.6^{o}C$
D = 6.0 in.
H = 6.0 in.
L = 6.0 in.
v_s= 64.0 %

d = 5/8 in.
h = 0

$\dot{P}$ = 30.7 lbs./min.

$\dot{\delta}n = 3.67 \times 10^{-4}$ in./min.

t (min.)	P (lbs.)	δ ($\times 10^{-3}$in.)
57	1790	0.8
65	2060	1.5
68	2090	2.5
69	200	50.6
78	560	51.0
80	590	51.6
84	550	54.4
87	530	56.0
99	520	60.0

Table A-4: (Cont'd)

Sample S-5:

$T = -20.1^{o}C$
$H = 5.871$ in.
$D = 6.00$ in.
$L = 5.781$ in.
$v_s = 66.3$ %

$d = 5/8$ in.
$h = 0$

$\dot{P} = 32.7$ lbs./min.
$\dot{\delta}n = 5.0 \times 10^{-4}$ in./min.

t (min.)	P (lbs.)	δ ($\times 10^{-3}$ in.)
28.0	680	0.20
47.0	1360	0.30
65.0	2080	0.35
82.0	2730	0.55
85.0	2810	1.00
85.6	2810	1.80
85.6	0	42.90
114.0	860	43.50
115.0	860	44.00
115.5	340	49.20
124.0	560	50.00
127.0	470	52.40
132.0	500	53.40
135.0	575	54.20
140.0	575	56.60

Sample S-6:

$T = -26.7^{o}C$
$H = 6.0$ in.
$D = 6.0$ in.
$L = 6.0$ in.
$v_s = 64.0$ %

$d = 5/8$ in.
$h = 0$

$\dot{P} = 37.5$ lbs./min.
$\dot{\delta}n = 6.38 \times 10^{-4}$ in./min.

t (min.)	P (lbs.)	δ ($\times 10^{-3}$ in.)
20.0	680	0.6
37.5	1360	0.8
55.0	2040	0.9
73.0	2740	1.9
73.0	110	33.7

(Continued)

Sample S-6: (COnt'd)

t (min.)	P (lbs.)	δ ($\times 10^{-3}$ in.)
91.0	800	34.5
91.3	500	38.5
97.0	680	39.3
99.5	570	41.7
104.0	610	43.3
107.0	600	44.7

Sample S-7:

$T = -26.8^{o}C$
$H = 6.0$ in.
$D = 6.0$ in.
$L = 6.0$ in.
$v_s = 64.0$ %

$d = 5/8$ in.
$h = 0$

$\dot{P} = 39.7$ lbs./min.
$\dot{\delta}n = 6.154 \times 10^{-4}$ in./min.

t (min.)	P (lbs.)	δ ($\times 10^{-3}$ in.)
20.50	720	0.40
36.75	1400	0.70
53.00	2080	0.76
70.50	2800	0.80
70.5	90	31.50
90.50	810	31.70
91.00	440	36.00
95.50	560	37.20
96.50	430	39.20
100.50	510	40.40
102.50	440	42.00
106.00	480	43.20
109.00	450	44.80
112.50	470	46.20
116.00	450	47.60

Sample S-8:

$T = -27.1^{o}C$
$H = 6.0$ in.
$D = 6.0$ in.
$L = 6.0$ in.
$v_s = 64.0$ %

$d = 5/8$ in.
$h = 0$

$\dot{P} = 20.8.2$ lbs./min.

(Continued)

Table A-4: (Cont'd)

Sample S-8: (Cont'd)

$\dot{\delta}n = 1.32 \times 10^{-3}$ in./min.

t (min.)	P (lbs.)	δ ($\times 10^{-3}$ in.)
7.00	960	0.01
15.50	3150	0.40
18.25	3800	1.00
18.50	10	50.00
25.00	1240	50.00
25.50	1320	50.40
25.75	920	54.00
26.50	950	55.40
31.00	920	60.00

Sample S-9:

T = -20.0°C
H = 5.938 in.
D = 6.00 in.
L = 6.00 in.
v_s = 64.6 %

d = 5/8 in.
h = 0

$\dot{P}$ = 210.3 lbs./min.

$\dot{\delta}n = 2.53 \times 10^{-3}$ in./min.

t (min.)	P (lbs.)	δ ($\times 10^{-3}$ in.)
11.00	2160	0.8
15.50	3260	1.2
15.50	240	35.6
18.50	960	36.4
18.75	680	40.4
28.00	580	67.2

Sample S-10:

T = -6.3°C
H = 6.0 in.
D = 6.0 in.
L = 6.0 in.
v_s = 64.0 %

d = 5/8 in.
h = 0

$\dot{P}$ = 186.7 lbs./min.

$\dot{\delta}n = 1.12 \times 10^{-3}$ in./min.

(Continued)

Sample S-10: (COnt'd)

t (min.)	P (lbs.)	δ ($\times 10^{-3}$ in.)
6.0	1180	0.2
7.5	1400	1.8
8.0	220	11.4
10.5	200	14.1
13.0	200	17.0

Sample S-11:

T = -15.1°C
H = 6.0 in.
D = 6.0 in.
L = 6.0 in.
v_s = 64.0 %

d = 5/8 in., h = 0

$\dot{P}$ = 204.6 lbs./min.

$\dot{\delta}n = 3.86 \times 10^{-3}$ in./min.

t (min.)	P (lbs.)	δ ($\times 10^{-3}$ in.)
7.50	1440	0.8
13.00	2660	1.2
13.00	220	29.0
14.75	610	29.8
15.25	450	33.6
19.00	430	46.2

Sample S-12:

T = -10.0°C
H = 6.0 in.
D = 6.0 in.
L = 6.0 in.
v_s = 64.0 %

d = 5/8 in.
h = 0

$\dot{P}$ = 222.7 lbs./min.

$\dot{\delta}n = 3.73 \times 10^{-3}$ in./min.

t (min.)	P (lbs.)	δ ($\times 10^{-3}$ in.)
6.5	1490	0.4
11.0	2450	2.6
11.0	590	20.0
11.5	480	21.6
14.5	470	32.8

Table A-4: (Cont'd)

Sample S-13:

$T = -6.0^{o}C$
$H = 6.0$ in.
$D = 6.0$ in.
$L = 6.0$ in.
$v_s = 64.0$ %

$d = 5/8$ in.
$h = 0$
$\dot{P} = 2133.3$ lbs./min.
$\dot{\delta}_n = 1.964 \times 10^{-2}$ in./min.

t (min.)	P (lbs.)	δ ($\times 10^{-3}$ in.)
0.90	1920	1.4
0.90	490	23.5
1.00	440	24.5
1.05	360	30.0
2.40	330	52.0

Sample S-14:

$T = -15.2^{o}C$
$H = 5.969$ in.
$D = 6.00$ in.
$L = 6.00$ in.
$v_s = 64.2$ %

$d = 5/8$ in.
$h = 0$
$\dot{P} = 2033.3$ lbs./min.
$\dot{\delta}_n = 3.0 \times 10^{-2}$ in./min.

t (min.)	P (lbs.)	($\times 10^{-3}$ in.)
1.6	3280	0.1
1.8	3660	0.6
1.8	480	40.0
2.0	850	40.8
2.0	600	45.0
3.0	530	75.0

Sample S-15:

$T = -10.0^{o}C$
$H = 6.0$ in.
$D = 6.0$ in.
$L = 6.0$ in.
$v_s = 64.0$ %

$d = 5/8$ in.
$h = 0$
(Continued)

Sample S-15: (Cont'd)

$\dot{P} = 1978.6$ lbs./min.
$\dot{\delta}_n = 2.13 \times 10^{-2}$ in./min.

t (min.)	P (lbs.)	δ ($\times 10^{-3}$ in.)
1.4	2770	0.4
1.4	430	30.7
1.5	780	31.6
1.6	550	33.6
2.6	440	55.0
3.0	440	62.5

Sample S-16:

$T = -25.6^{o}C$
$H = 6.0$ in.
$D = 6.0$ in.
$L = 6.0$ in.
$v_s = 64.0$ %

$d = 5/8$ in.
$h = 0$
$\dot{P} = 2210$ lbs./min.
$\dot{\delta}_n = 4.0 \times 10^{-2}$ in./min.

t (min.)	P (lbs.)	δ ($\times 10^{-3}$ in.)
1.60	3680	0.4
2.00	4420	0.7
2.00	800	16.4
2.40	1390	16.4
2.55	1630	17.8
2.60	1280	23.8
3.80	900	72.0

Sample S-17:

$T = -20.0^{o}C$
$H = 6.0$ in.
$D = 6.0$ in.
$L = 6.0$ in.
$v_s = 64.0$ %

$d = 5/8$ in.
$h = 0$
$\dot{P} = 2240$ lbs./min.
$\dot{\delta}_n = 1.32 \times 10^{-2}$ in./min.

(Continued)

Table A-4: (Cont'd)

Sample S-17: (Cont'd)

t (min.)	P (lbs.)	($x10^{-3}$in.)
1.50	3360	0.2
1.50	160	14.0
1.85	1020	14.8
1.90	860	17.5
3.00	750	30.0

Sample S-18:

T = -25.0°C
H = 6.0 in.
D = 6.0 in.
L = 6.0 in.
v_s= 64.0 %

d = 5/8 in.
h = 0
$\dot{P}$ = 5.06 lbs./min.
$\dot{\delta}_n$= $1.1x10^{-4}$ in./min.

t (min.)	P (lbs.)	δ ($x10^{-3}$in.)
340	1600	0.3
495	2400	0.9
600	2980	0.9
680	3440	2.9
680	1080	43.0
838	2460	43.0
860	2520	45.0
865	1100	48.6
995	1080	60.0

Sample S-19:

T = -10.0°C
H = 6.0 in.
D = 6.0 in.
L = 6.0 in.
v_s= 64.0 %

d = 5/8 in.
h = 0
$\dot{P}$ = 4.53 lbs./min.
$\dot{\delta}_n$= $1.66x10^{-4}$ in./min.

t (min.)	P (lbs.)	δ ($x10^{-3}$in.)
172	830	0.20
285	1350	0.45
355	1630	1.30

(Continued)

Sample S-19: (Cont'd)

t (min.)	P (lbs.)	δ ($x10^{-3}$in.)
360	1630	1.80
375	1580	3.60
440	1200	14.40

Sample S-20:

T = -6.0°C
H = 6.0 in.
D = 6.0 in.
L = 6.0 in.
v_s= 64.0 %

d = 5/8 in.
h = 0
$\dot{P}$ = 4.4 lbs./min.
$\dot{\delta}_n$= $1.0x10^{-4}$ in./min.

t (min.)	P (lbs.)	δ ($x10^{-3}$in.)
145	640	0.1
165	720	0.5
210	640	4.8
280	500	13.6
375	380	23.2

Sample S-21:

T = -15.0°C
H = 6.0 in.
D = 6.0 in.
L = 6.0 in.
v_s= 64.0 %

d = 5/8 in.
h = 0
$\dot{P}$ = 6.5 lbs./min.
$\dot{\delta}_n$= $1.86x10^{-4}$

t (min.)	P (lbs.)	δ ($x10^{-3}$in.)
165	1020	0.25
260	1860	0.50
320	2080	1.50
330	2000	5.50
332	720	15.50
335	540	21.80
370	620	23.80
470	580	31.50

Table A-4: (Cont'd)

Sample S-22:

T = -20.0°C
H = 6.0 in.
D = 6.0 in.
L = 6.0 in.
v_s= 64.0 %

d = 5/8 in.
h = 0
$\dot{P}$ = 4.4 lbs./min.
$\dot{\delta}_n$= 1.34×10^{-4} in./min.

t (min.)	P (lbs.)	δ ($\times 10^{-3}$ in.)
410.0	2550	0.4
630.0	2770	1.4
647.0	2650	4.2
647.1	1200	21.0
650.0	1000	24.6
710.0	1000	29.4

Sample S-23:

T = -10.0°C
H = 6.0 in.
D = 6.0 in.
L = 6.0 in.
v_s= 64.0 %

d = 5/8 in.
h = 0
$\dot{P}$ = 268.1 lbs./min.
$\dot{\delta}_n$= 3.83×10^{-3} in./min.

t (min.)	P (lbs.)	δ ($\times 10^{-3}$ in.)
8.80	2400	0.1
9.25	2480	1.5
9,25	240	30.0
11.00	660	31.0
11.30	660	33.0
11.75	560	35.0
16.00	540	51.0

Sample S-24:

T = -2.0°C
H = 6.0 in.
D = 6.0 in.
L = 6.0 in.
v_s= 64.0 %

d = 5/8 in.
(Continued)

Sample S-24: (Cont'd)

h = 0
$\dot{P}$ = 100 lbs./min.
$\dot{\delta}_n$= 4.0×10^{-3} in./min.

t (min.)	P (lbs.)	δ ($\times 10^{-3}$ in.)
2.50	300	0.1
3.25	390	0.8
4.00	450	2.4
4.50	450	4.1
5.25	410	7.5
6.25	330	12.3
7.25	280	16.7
8.75	240	22.7

Sample S-25:

T = -2.0°C
H = 6.0 in.
D = 6.0 in.
L = 6.0 in.
v_s= 64.0 %

d = 5/8 in.
h = 0
$\dot{P}$ = 1714.3 lbs./min.
$\dot{\delta}_n$= 3.71×10^{-2} in./min.

t (min.)	P (lbs.)	δ ($\times 10^{-3}$ in.)
0.25	520	0.5
0.35	640	2.9
0.42	720	6.1
0.45	640	10.3
0.55	370	15.0
0.90	320	28.0

Sample S-26:

T = -2.0°C
H = 6.0 in.
D = 6.0 in.
L = 6.0 in.
v_s= 64.0 %

d = 5/8 in.
h = 0
$\dot{P}$ = 2.1 lbs./min.
$\dot{\delta}_n$= 8.6×10^{-5} in./min.

(Continued)

Table A-4: (Cont'd)

Sample S-26: (Cont'd)

t (min.)	P (lbs.)	δ ($\times 10^{-3}$ in.)
35	150	0.2
65	190	1.4
100	210	3.6
150	190	8.4
250	190	16.6

Sample S-27:

T = -2.0°C
H = 6.0 in.
D = 6.0 in.
L = 6.0 in.
v_s= 64.0 %

d = 5/8 in.
h = 0
$\dot{P}$ = 26.3 lbs./min.
$\dot{\delta}_n = 6.0 \times 10^{-4}$ in./min.

t (min.)	P (lbs.)	δ ($\times 10^{-3}$ in.)
13.5	420	0.5
17.5	460	2.4
21.0	448	4.8
32.0	380	11.4
50.0	350	22.2

Sample S-28:

T = -20.0°C
H = 6.0 in.
D = 6.0 in.
L = 6.0 in.
v_s= 64.0 %

d = 5/8 in.
h = 0
$\dot{P}$ = 2478.3 lbs./min.
$\dot{\delta}_n = 3.9 \times 10^{-2}$ in./min.

t (min.)	P (lbs.)	δ ($\times 10^{-3}$ in.)
1.38	3420	0.01
1.38	320	39.00
1.69	1060	41.00
1.80	840	46.00
2.55	770	74.50

Sample S-29:

T = -15.0°C
H =6.0 in.
D = 6.0 in.
L = 6.0 in.
v_s= 64.0 %

d = 5/8 in.
h = 0
$\dot{P}$ = 220.9 lbs./min.
$\dot{\delta}_n$= **

t (min.)	P (lbs.)	δ ($\times 10^{-3}$ in.)
11.5	2540	**
11.5	400	
13.0	760	
15.0	660	
20.0	660	

** Not recorded, channel was OFF.

Sample S-30:

T = -10.0°C
H = 6.0 in.
D = 6.0 in.
L = 6.0 in.
v_s= 64.0 %

d = 3/8 in.
h = 0
$\dot{P}$ = 29.3 lbs./min.
$\dot{\delta}_n = 8.0 \times 10^{-4}$ in./min.

t (min.)	P (lbs.)	δ ($\times 10^{-3}$ in.)
30.0	880	0.8
30.5	240	7.4
31.0	200	8.8
33.0	160	11.2
39.0	140	16.0
94.0	140	60.0

Sample S-31:

T = -10.0°C
H = 6.0 in.
D = 6.0 in.
L = 6.0 in.
v_s= 64.0 %

(Continued)

Table A-4: (Cont'd)

Sample S-31: (Cont'd)

d = 3/8 in.
h = 1/16 in.*

$\dot{P}$ = 29.7 lbs./min.

$\dot{\delta}n = 5.2 \times 10^{-4}$ in./min.

t (min.)	P (lbs.)	δ ($\times 10^{-3}$ in.)
52.5	1560	1.2
53.0	1320	5.2
54.0	1040	10.4
66.0	1040	16.6

* A 90°-lug, unless noted.

Sample S-32:

T = -10.0°C
H = 6.0 in.
D = 6.0 in.
L = 6.0 in.
v_s = 64.0 %

d = 3/8 in.
h = 1/8 in.

$\dot{P}$ = 33.4 lbs./min.

$\dot{\delta}n = 5.34 \times 10^{-4}$ in./min.

t (min.)	P (lbs.)	δ ($\times 10^{-3}$ in.)
61	2040	2.0
62	1800	5.6
64	1580	9.2
72	1490	14.8
78	1520	18.0

Sample S-33:

T = -10.0°C
H = 6.0 in.
D = 6.0 in.
L = 6.0 in.
v_s = 64.0 %

d = 3/8 in.
h = 3/16 in.

$\dot{P}$ = 32 lbs./min.

$\dot{\delta}n = 5.82 \times 10^{-4}$ in./min.

(Continued)

Sample S-33: (Cont'd)

t (min.)	P (lbs.)	δ ($\times 10^{-3}$ in.)
68.5	2190	2.0
72.0	1870	6.0
76.0	1840	9.2
87.0	1830	15.6

Sample S-34:

T = -10.0°C
H = 6.0 in.
D = 6.0 in.
L = 6.0 in.
v_s = 64.0 %

d = 3/8 in.
h = 3/16 in.

$\dot{P}$ = 31.3 lbs./min.

$\dot{\delta}n = 4.212 \times 10^{-4}$ in./min.

t (min.)	P (lbs.)	δ ($\times 10^{-3}$ in.)
74	2320	2.8
85	2330	8.6
127	2800	26.0
177	3480	45.0
357	4800	132.0
360	4440	136.0
450	4800	160.0
640	4800	240.0

Sample S-35:

T = -20.0°C
H = 6.0 in.
D = 6.0 in.
L = 6.0 in.
v_s = 64.0 %

d = 3/8 in.
h = 0

$\dot{P}$ = 138.7 lbs./min.

$\dot{\delta}n = 6.944 \times 10^{-4}$ in./min.

t (min.)	P (lbs.)	δ ($\times 10^{-3}$ in.)
7.5	1040	1.0
8.0	420	9.0
26.0	300	21.5

Table A-4: (Cont'd)

Sample S-36:

$T = -20.0^{o}C$
H = 6.0 in.
D = 6.0 in.
L = 6.0 in.
$v_s = 64.0$ %

d = 3/8 in.
h = 1/16 in.

$\dot{P} = 32.8$ lbs./min.

$\dot{\delta}_n = 5.1 \times 10^{-4}$ in./min.

t (min.)	P (lbs.)	δ ($\times 10^{-3}$ in.)
55.5	1820	0.01
59.0	1650	4.60
65.0	1610	8.70
105.0	2000	26.00
145.0	3380	45.00
185.0	2440	65.00
205.0	2500	76.00
240.0	2600	94.40
275.0	2680	113.40
310.0	2660	130.40

Sample S-36:

$T = -20.0^{o}C$
H = 6.0 in.
D = 6.0 in.
L = 6.0 in.
$v_s = 64.0$ %

d = 3/8 in.
h = 1/8 in.

$\dot{P} = 37.5$ lbs./min.

$\dot{\delta}_n = 3.9 \times 10^{-4}$ in./min.

t (min.)	P (lbs.)	δ ($\times 10^{-3}$ in.)
63	2360	1.6
69	2330	5.7
110	2840	22.4
150	3340	37.4
170	3580	45.0

Sample S-38:

$T = -20.0^{o}C$
H = 6.0 in.
D = 6.0 in.
L = 6.0 in.
$v_s = 64.0$ %

d = 3/8 in.
h = 3.16 in.

$\dot{P} = 35.8$ lbs./min.

$\dot{\delta}_n = 4.1 \times 10^{-4}$ in./min.

t (min.)	P (lbs.)	δ ($\times 10^{-3}$ in.)
95	3400	0.6
103	3360	6.4
145	3900	18.4
185	4441	36.1
225	4921	46.2
265	5382	70.5
305	5722	87.5
345	6000	104.0
385	6280	118.8
425	6480	135.4
465	6620	152.6
505	6740	167.0
590	7020*	200.0

* This load caused rod yielding

Sample S-39:

$T = -10.0^{o}C$
H = 6.0 in.
D = 6.0 in.
L = 6.0 in.
$v_s = 64.0$ %

d = 3/8 in.
h = 0

$\dot{P} = 27.1$ lbs./min.

$\dot{\delta}_n = 5.0 \times 10^{-4}$ in./min.

t (min.)	P (lbs.)	δ ($\times 10^{-3}$ in.)
4.5	130	0.8
6.0	64	1.6
9.0	45	3.2
17.0	40	7.2

Table A-4: (Cont'd)

Sample S-40:

$T = -10.0^{o}C$
H = 6.0 in.
D = 6.0 in.
L = 6.0 in.
v_s= 64.0 %

d = 3/32 in.
h = 0

$\dot{P}$ = 5.3 lbs./min.

$\dot{\delta}_n = 4.32 \times 10^{-4}$ in./min.

t (min.)	P (lbs.)	δ ($\times 10^{-3}$ in.)
8	56	0.4
15	80	1.2
17	45	1.6
42	20	12.0

Sample S-41:

$T = -20.0^{o}C$
H = 6.0 in.
D = 6.0 in.
L = 6.0 in.
v_s= 64.0 %

d = 3/16 in.
h = 0

$\dot{P}$ = 15.8 lbs./min.

$\dot{\delta}_n = 5.43 \times 10^{-4}$ in./min.

t (min.)	P (lbs.)	δ ($\times 10^{-3}$ in.)
33.5	530	0.4
33.5	90	2.8
34.0	70	4.0
37.0	65	5.2
45.0	50	8.8
48.0	50	11.6

Sample S-42:

$T = -20.0^{o}C$
H = 6.0 in.
D = 6.0 in.
L = 6.0 in.
v_s= 64.0 %

d = 3/32 in.
h = 0
(Continued)

Sample S-42: (Cont'd)

$\dot{P}$ = 7.4 lbs./min.

$\dot{\delta}_n = 4.5 \times 10^{-4}$ in./min.

t (min.)	P (lbs.)	δ ($\times 10^{-3}$ in.)
20.5	152	0.2
22.0	100	2.6
29.0	80	6.0
33.0	80	7.8

Sample S-43:

$T = -10.0^{o}C$
H = 6.0 in.
D = 6.0 in.
L = 6.0 in.
v_s= 64.0 %

d = 3/8 in.
h = 1/8 in.

$\dot{P}$ = 2220 lbs./min.

$\dot{\delta}_n = 2.1 \times 10^{-2}$ in./min.

t (min.)	P (lbs.)	δ ($\times 10^{-3}$ in.)
1.0	2220	3.0
1.5	2760	13.0
2.0	3140	24.0
2.5	3540	34.0
4.0	4040	74.0
5.5	4320	97.0

Sample S-44:

$T = -10.0^{o}C$
H = 6.0 in.
D = 6.0 in.
L = 6.0 in.
v_s= 64.0 %

d = 3/8 in.
h = 1/8 in.

$\dot{P}$ = 198.1 lbs./min.

$\dot{\delta}_n = 3.36 \times 10^{-3}$ in./min.

(Continued)

Table A-4: (Cont'd)

Sample S-44: (Cont'd)

t (min.)	P (lbs.)	δ ($x10^{-3}$in.)
10.50	2080	1.6
11.75	2080	5.8
25.25	3220	37.0
36.50	3900	65.0
46.00	4220	94.4
62.00	4540	150.0
67.00	4540	167.5
94.50	4540	260.0

Sample S-45:

$T = -10.0^{o}C$
H = 6.0 in.
D = 6.0 in.
L = 6.0 in.
v_s= 64.0 %

d = 3/8 in.
h = 1/8 in.

$\dot{P}$ = 4.8 lbs./min.

$\dot{\delta}n = 7.0x10^{-5}$ in./min.

t (min.)	P (lbs.)	δ ($x10^{-3}$in.)
235	1120	2.0
280	940	9.0
300	880	11.0
340	880	14.6
390	940	18.0
470	940	24.0
520	1000	27.0
550	1000	28.4

Sample S-46:

$T = -15.0^{o}C$
H = 6.0 in.
D = 6.0 in.
L = 6.0 in.
v_s= 64.0 %

d = 3/8 in.
h = 1/8 in.

$\dot{P}$ = 30.6 lbs./min.

$\dot{\delta}n = 2.8x10^{-4}$ in./min.

(Continued)

Sample S-46: (Cont'd)

t (min.)	P (lbs.)	δ ($x10^{-3}$in.)
68	2080	1.8
72	2000	5.0
83	2000	11.0
123	2470	28.0
163	2880	44.0
203	3200	62.0
225	3360	73.0
330	3720	82.0
380	3800	94.0
760	3800	200.0

Sample S-47:

$T = -26.0^{o}C$
H = 6.0 in.
D = 6.0 in.
L = 6.0 in.
v_s= 64.0 %

d = 3/8 in.
h = 1/8 in.

$\dot{P}$ = 33 lbs./min.

$\dot{\delta}n = 5.02x10^{-4}$ in./min.

t (min.)	P (lbs.)	δ ($x10^{-3}$in.)
77	2540	2.0
100	2880	10.0
120	3200	16.0
140	3520	24.0
160	3760	32.0
180	4000	38,4
282	4980	82.0
382	5440	129.0
480	5600	185.0
630	5760	257.0
820	6080	352.0

Sample S-48:

$T = -6.0^{o}C$
H = 6.0 in.
D = 6.0 in.
L = 6.0 in.
v_s= 64.0 %

d = 3/8 in.
h = 1/8 in.

$\dot{P}$ = 32.4 lbs./min.

(Continued)

Table A-4: (Cont'd)

Sample S-48: (Cont'd)

$\dot{\delta}n = 5.7 \times 10^{-4}$ in./min.

t (min.)	P (lbs.)	δ ($\times 10^{-3}$ in.)
37	1200	2.6
65	1120	18.0
165	1680	68.0
270	1920	119.0
370	2080	176.0
382	2080	240.0

Sample S-49:

$T = -2.0^{\circ}C$
H = 6.0 in.
D = 6.0 in.
L = 6.0 in.
$v_s = 64.0$ %

d = 3/8 in.
h = 1/8 in.
$\dot{P} = 17$ lbs./min.
$\dot{\delta}n = 3.283 \times 10^{-4}$ in./min.

t (min.)	P (lbs.)	δ ($\times 10^{-3}$ in.)
26	440	1.5
36	540	5.0
46	600	10.0
56	660	15.0
66	700	20.0
76	760	24.0
126	1020	47.0
240	1390	87.0
330	1390	114.0
592	1390	200.0

Sample S-50:

$T = -10.0^{\circ}C$
H = 5.0 in.
D = 6.0 in.
L = 5.0 in.
$v_s = 64.0$ %

d = 3/8 in.
h = 0
$\dot{P} = 28.4$ lbs./min.
$\dot{\delta}n = 5.63 \times 10^{-4}$ in./min.
(Continued)

Sample S-50: (Cont'd)

t (min.)	P (lbs.)	δ ($\times 10^{-3}$ in.)
21.5	610	0.4
21.5	280	6.0
22.0	180	7.0
34.0	120	16.0
50.0	120	25.0

Sample S-51:

$T = -10.0^{\circ}C$
H = 5.312 in.
D = 6.00 in.
L = 5.312 in.
$v_s = 64.0$ %

d = 3/8 in.
h = 0
$\dot{P} = 5.2$ lbs./min.
$\dot{\delta}n = 1.14 \times 10^{-4}$ in./min.

t (min.)	P (lbs.)	δ ($\times 10^{-3}$ in.)
140	730	0.01
140	220	7.00
145	160	10.00
280	120	26.0
420	120	42.0

Sample S-52:

$T = -10.0^{\circ}C$
H = 6.0 in.
D = 6.0 in.
L = 6.0 in.
$v_s = 64.0$ %

d = 3/8 in.
h = 0
$\dot{P} = 6.3$ lbs./min.
$\dot{\delta}n = 1.4 \times 10^{-4}$ in./min.

t (min.)	P (lbs.)	δ ($\times 10^{-3}$ in.)
148	940	0.01
148	220	12.00
205	140	20.00

Table A-4: (Cont'd)

Sample S-53:

$T = -10.0^{o}C$
$H = 3.0$ in.
$D = 6.0$ in.
$L = 3.0$ in.
$v_s = 64.0$ %

$d = 3/8$ in.
$h = 0$
$\dot{P} = 24.5$ lbs./min.
$\dot{\delta}n = 5.63 \times 10^{-4}$ in./min.

t (min.)	P (lbs.)	δ ($\times 10^{-3}$ in.)
22.0	540	1.0
22.5	510	2.0
22.5	170	6.0
23.0	140	8.0
39.0	130	17.0

Sample S-54:

$T = -10.0^{o}C$
$H = 2.0$ in.
$D = 6.0$ in.
$L = 2.0$ in.
$v_s = 64.0$ %

$d = 3/8$ in.
$h = 0$
$\dot{P} = 20.4$ lbs./min.
$\dot{\delta}n = 6.5 \times 10^{-4}$ in./min.

t (min.)	P (lbs.)	δ ($\times 10^{-3}$ in.)
11.0	224	0.1
11.5	144	1.8
14.0	96	4.5
30.0	64	14.5
40.0	64	21.0

Sample S-55:

$T = -10.0^{o}C$
$H = 1.0$ in.
$D = 6.0$ in.
$L = 1.0$ in.
$v_s = 64.0$ %

$d = 3/8$ in.
$h = 0$
$\dot{P} = 9.6$ lbs./min.
(Continued)

Sample S-55: (Cont'd)

$\dot{\delta}n = 1.43 \times 10^{-4}$ in./min.

t (min.)	P (lbs.)	δ ($\times 10^{-3}$ in.)
5	48	2.0
9	48	7.0
25	28	30.0

Sample S-56:

$T = -10.0^{o}C$
$H = 1.0$ in.
$D = 6.0$ in.
$L = 1.0$ in.
$v_s = 64.0$ %

$d = 3/8$ in.
$h = 0$
$\dot{P} = 14.4$ lbs./min.
$\dot{\delta}n = 3.0 \times 10^{-4}$ in./min.

t (min.)	P (lbs.)	δ ($\times 10^{-3}$ in.)
10	144	0.16
12	96	0.80
18	94	2.60
20	64	3.2

Sample S-57:

$T = -10.0^{o}C$
$H = 6.0$ in.
$D = 6.0$ in.
$L = 6.0$ in.
$v_s = 64.0$ %

$d = 3/8$ in.
$h = 1/8$ in.
$\dot{P} = 34.7$ lbs./min.
$\dot{\delta}n = 5.433 \times 10^{-4}$ in./min.

t (min.)	P (lbs.)	δ ($\times 10^{-3}$ in.)
45	1560	0.2
48	1240	4.2
53	1060	10.0
58	1040	14.0
63	1040	16.5
105	1281	49.2
220	1640	89.6
300	2062	118.2

(Continued)

Table A-4: (Cont'd)

Sample S-57: (Cont'd)

t (min.)	P (lbs.)	δ ($\times 10^{-3}$ in.)
350	2522	152.7
420	2800	191.6
565	2920	270.0
660	2920	322.0

Sample S-58:

T = -10.0°C
H = 1.0 in.
D = 6.0 in.
L = 1.0 in.
v_s= 64.0 %

d = 3/8 in.
h = 0

$\dot{P}$ = 10.2 lbs./min.

$\dot{\delta}n = 6.0 \times 10^{-4}$ in./min.

t (min.)	P (lbs.)	δ ($\times 10^{-3}$ in.)
18.5	188	0.4
22.0	160	1.2
30.5	128	6.0
32.0	80	10.0
34.0	64	13.0
38.0	48	15.2
42.0	40	17.6

Sample S-59:

T = -10.0°C
H = 1.0 in.
D = 6.0 in.
L = 1.0 in.
v_s= 64.0 %

d = 3/8 in.
h = 0

$\dot{P}$ = 13.7 lbs./min.

$\dot{\delta}n = 6.8 \times 10^{-3}$ in./min.

t (min.)	P (lbs.)	δ ($\times 10^{-3}$ in.)
7	96	0.16
9	64	1.80
25	40	10.00
30	40	14.00

Sample S-60:

T = -15.0°C
H = 6.0 in.
D = 6.0 in.
L = 6.0 in.
v_s= 64.0 %

d = 3/8 in.
h = 0

$\dot{P}$ = 33.8 lbs./min.

$\dot{\delta}n = 1.25 \times 10^{-4}$ in./min.

t (min.)	P (lbs.)	δ ($\times 10^{-3}$ in.)
22.5	760	0.1
23.0	280	6.0
37.0	200	16.0
82.0	200	22.0

Sample S-61:

T = -26.0°C
H =6.0 in.
D = 6.0 in.
L = 6.0 in.
v_s= 64.0 %

d = 3/8 in.
h = 0

$\dot{P}$ = 24.1 lbs./min.

$\dot{\delta}n = 6.316 \times 10^{-4}$ in./min.

t (min.)	P (lbs.)	δ ($\times 10^{-3}$ in.)
36.5	880	1.0
37.0	560	5.0
50.0	400	15.0
57.0	400	19.0

Sample S-62:

T = -20.0°C
H = 6.0 in.
D = 6.0 in.
L = 6.0 in.
v_s= 64.0 %

d = 3/8 in.
h = 1/8 in.

$\dot{P}$ = 29.0 lbs./min.

$\dot{\delta}n = 4.65 \times 10^{-4}$ in./min.

(Continued)

Table A-4: (Cont'd)

Sample S-62: (Cont'd)

t (min.)	P (lbs.)	δ ($\times 10^{-3}$ in.)
56	1700	0.1
60	1740	2.0
65	1760	4.5
240	3840	73.0
290	4170	95.0
340	4300	118.8
410	4460	152.2
470	4580	178.0
603	4580	240.0

Sample S-63:

T = -2.0°C
H = 6.0 in.
D = 6.0 in.
L = 6.0 in.
v_s= 64.0 %

d = 3/8 in.
h = 0

$\dot{P}$ = 17.3 lbs./min.

$\dot{\delta}n$= 2.25×10^{-4} in./min.

t (min.)	P (lbs.)	δ ($\times 10^{-3}$ in.)
15	260	0.6
16	260	1.0
17	160	1.8
18	100	2.8
20	80	3.6
34	50	7.2

Sample S-64:

T = -6.0°C
H = 6.0 in.
D = 6.0 in.
L = 6.0 in.
v_s= 64.0 %

d = 3/8 in.
h = 0

$\dot{P}$ = 18.2 lbs./min.

$\dot{\delta}n$= 9.5×10^{-5} in./min.

t (min.)	P (lbs.)	δ ($\times 10^{-3}$ in.)
28.5	520	0.3
29.0	140	1.0
40.0	100	2.0
48.0	100	2.8

Sample S-65:

T = -15.0°C
H = 6.0 in.
D = 6.0 in.
L = 6.0 in.
v_s= 64.0 %

d = 3/8 in.
h = 0

$\dot{P}$ = 22.6 lbs./min.

$\dot{\delta}n$= 6.316×10^{-4} in./min.

t (min.)	P (lbs.)	δ ($\times 10^{-3}$ in.)
39.0	880	0.1
39.0	460	6.6
39.5	300	10.6
41.0	240	12.2
47.0	220	15.8
60.0	220	24.0

Sample S-66:

T =-20.0°C
H = 6.0 in.
D = 6.0 in.
L = 6.0 in.
v_s= 64.0 %

d = 3/8 in.
h = 0

$\dot{P}$ = 23.9 lbs./min.

$\dot{\delta}n$= 6.47×10^{-4} in./min.

t (min.)	P (lbs.)	δ ($\times 10^{-3}$ in.)
33.5	800	0.4
34.0	480	6.0
35.0	400	8.0
45.0	320	14.5
52.0	320	19.0

Sample S-67:

T = -20.0°C
H = 6.0 in.
D = 6.0 in.
L = 6.0 in.
v_s= 64.0 %

d = 3/16 in.
h = 0

(Continued)

Table A-4: (Cont'd)

Sample S-67: (Cont'd)

$\dot{P}$ = 16.3 lbs./min.

$\dot{\delta}_n$= **

t (min.)	P (lbs.)	δ ($x10^{-3}$in.)
29.5	480	**
30.0	270	
46.0	210	

** Not recorded

Sample S-68:

T = -20.0^{o}C
H = 6.0 in.
D = 6.0 in.
L = 6.0 in.
v_s= 64.0 %

d = 3/8 in.
h = 1/8 in.

$\dot{P}$ = 17.7 lbs./min.

$\dot{\delta}_n$= $2.3x10^{-4}$ in./min.

t (min.)	P (lbs.)	δ ($x10^{-3}$in.)
50	1220	0.1
150	2660	18.0
250	3140	34.0
400	3840	60.0
600	4580	112.0
620	4580	120.0

Sample S-69:

T = -25.4^{o}C
H = 6.0 in.
D = 6.0 in.
L = 6.0 in.
v_s= 64.0 %

d = 3/8 in.
h = 0

$\dot{P}$ = 21.86 lbs./min.

$\dot{\delta}_n$= $6.5x10^{-4}$ in./min.

t (min.)	P (lbs.)	($x10^{-3}$in.)
48.5	1060	0.05
49.0	640	6.60

(Continued)

Sample S-69: (Cont'd)

t (min.)	P (lbs.)	δ ($x10^{-3}$in.)
50.0	510	9.2
52.0	480	11.2
55.0	450	13.2
64.0	420	19.0

Sample S-70:

T = -10.0^{o}C

H = 6.0 in.
D = 6.0 in.
L = 6.0 in.
v_s= 64.0 %

d = 3/8 in.
h = 0

$\dot{P}$ = 12.3 lbs./min.

$\dot{\delta}_n$= $5.867x10^{-4}$ in./min.

t (min.)	P (lbs.)	δ ($x10^{-3}$in.)
28	344	0.4
29	120	6.4
30	120	7.2
45	120	16.0

Sample S-71:

T = -10.0^{o}C
H = 4.0 in.
D = 6.0 in.
L = 4.0 in.
v_s= 64.0 %

d = 3/8 in.
h = 0

$\dot{P}$ = 19.5 lbs./min.

$\dot{\delta}_n$= $6.1x10^{-4}$ in./min.

t (min.)	P (lbs.)	δ ($x10^{-3}$in.)
25.5	495	6.0
26.0	145	7.6
28.0	130	10.0
41.0	95	18.0
47.0	95	21.6

Table A-4: (Cont'd)

Sample S-72:

$T = -10.0^{o}C$
H = 6.o in.
D = 6.0 in.
L = 6.0 in.
v_s= 64.0 %

d = 3/8 in.
h = 0

$\dot{P}$ = 12 lbs./min.

$\dot{\delta}_n = 5.5 \times 10^{-4}$ in./min.

t (min.)	P (lbs.)	δ ($\times 10^{-3}$ in.)
35.5	520	0.8
35.5	120	17.6
40.0	160	19.6
60.0	160	30.6

Sample S-73:**

$T = -15.0^{o}C$
H = 6.0 in.
D = 6.0 in.
L = 6.0 in.
v_s= 64.0 %

d = 3/8 in.
h = 0

$\dot{P}$ = 25.5 lbs./min.

$\dot{\delta}_n = 4.67 \times 10^{-4}$ in./min.

t (min.)	P (lbs.)	δ ($\times 10^{-3}$ in.)
46	1170	0.4
52	1000	0.4
54	1000	0.6
70	1540	1.6
70	280	21.6
79	500	23.6
81	470	25.2
93	470	30.8

** Sample loaded, unloaded, and reloaded before rupture.

Sample S-74:

$T = -20.0^{o}C$
H = 6.0 in.
D = 6.0 in.
L = 6.0 in.
(Continued)

Sample S-74: (Cont')

v_s= 64.0 %

d = 5/8 in.
h = 0

$\dot{P}$ = 25.8 lbs./min.

$\dot{\delta}_n$= **

t (min.)	P (lbs.)	δ ($\times 10^{-3}$ in.)
118	3040	**
133	3180	
143	3240	
153	3240	
193	2880	
230	2200	
280	1640	
370	1240	

** Not recorded, equipment failure

Sample S-75:

$T = -6.0^{o}C$
H = 6.0 in.
D = 6.0 in.
L = 6.0 in.
v_s= 64.0 %

d = 3/8 in.
h = 0

$\dot{P}$ = 11.64 lbs./min.

$\dot{\delta}_n = 4.5 \times 10^{-4}$ in./min.

t (min.)	P (lbs.)	δ ($\times 10^{-4}$ in.)
44	510	0.1
55	625	3.2
55	160	14.4
60	175	17.2
69	175	21.2

Sample S-76:

$T = -10.0^{o}C$
H = 2.0 in.
D = 6.0 in.
L = 2.0 in.
v_s= 64.0 %

d = 5/8 in.
h = 0
(Continued)

Table A-4: (cont'd)

Sample S-76: (Cont'd)

$\dot{P}$ = 14.7 lbs./min.

$\dot{\delta}_n$= **

t (min.)	P (lbs.)	δ ($x10^{-3}$in.)
50	1736	**
76	1090	
84	1090	
124	900	

** not recorded, equipment failure

Sample S-77:

T = -10.0°C
H = 5.0 in.
D = 6.0 in.
L = 5.0 in.
v_s= 64.0 %

d = 3/8 in.
h = 0

$\dot{P}$ = 11.7 lbs./min.

$\dot{\delta}_n$= $4.1x10^{-4}$ in./min.

t (min.)	P (lbs.)	δ ($x10^{-3}$in.)
67	780	2.0
67	220	17.2
68	190	19.0
90	190	28.0

Sample S-78:

Leakage, Data void

Sample S-79:

T = -10.0°C
H = 3.0 in.
D = 6.0 in.
L = 3.0 in.
v_s= 64.0 %

d = 3/8 in.
h = 0

$\dot{P}$ = 13.7 lbs./min.

$\dot{\delta}_n$= $4.75x10^{-4}$ in./min.
(Continued)

Sample S-79: (Cont'd)

t (min.)	P (lbs.)	δ ($x10^{-3}$in.)
39.5	540	1.4
40.0	130	14.4
41.0	140	15.4
57.0	140	23.0

Sample S-80:

Leakage, data void.

Sample S-81:

T = -10.0°C
H = 2.0 in.
D = 6.0 in.
L = 2.0 in.
v_s= 64.0 %

d = 3/8 in.
h = 0

$\dot{P}$ = 9.0 lbs./min.

$\dot{\delta}_n$= $4.5x10^{-4}$ in./min.

t (min.)	P (lbs.)	δ ($x10^{-3}$in.)
30	270	0.8
30	90	8.8
32	60	11.4
44	60	16.8

Sample S-82:

T = -10.0°C
H = 3.0 in.
D = 6.0 in.
L = 3.0 in.
v_s= 64.0 %

d = 5/8 in.
h = 0

$\dot{P}$ = 8.2 lbs./min.

$\dot{\delta}_n$= **

t (min.)	P (lbs.)	δ ($x10^{-3}$in.)
53	430	**
80	430	

** Not recorded, equipment failure.

Table A-4: (Cont'd)

Sample S-83:

$T = -10.0^{\circ}C$
H = 2.0 in.
D = 6.0 in.
L = 2.0 in.
$v_s = 64.0\ \%$

d = 5/8 in.
h = 0

$\dot{P} = 6.8$ lbs./min.

$\dot{\delta}_n = 3.1 \times 10^{-4}$ in./min.

t (min.)	P (lbs.)	δ ($\times 10^{-3}$ in.)
42.5	290	0.6
43.0	80	9.6
80.0	80	21.0

Sample S-84:

$T = -10.0^{\circ}C$
H = 2.0 in.
D = 6.0 in.
L = 2.0 in.
$v_s = 64.0\ \%$

d = 5/8 in.
h = 0

$\dot{P} = 4.45$ lbs./min.

$\dot{\delta}_n$ = **

t (min.)	P (lbs.)	δ ($\times 10^{-3}$ in.)
55	240	**

** Not recorded, equipment failure

Sample S-85:

$T = -10.0^{\circ}C$
H = 6.0 in.
D = 6.0 in.
L = 6.0 in.
$v_s = 64.0\ \%$

d = 3/8 in.
h = 0 (Ground-Finish)

$\dot{P} = 20$ lbs./min.

$\dot{\delta}_n = 3.24 \times 10^{-4}$ in./min.
(Continued)

Sample S-85: (Cont'd)

t (min.)	P (lbs.)	δ ($\times 10^{-3}$ in.)
26.5	530	0.1
26.5	220	4.8
30.0	180	7.6
51.0	180	14.4

Sample S-86:

$T = -10.0^{\circ}C$
H = 6.0 in.
D = 6.0 in.
L = 6.0 in.
$v_s = 64.0\ \%$

d = 3/8 in.
h = 0 (Ground-Finish)

$\dot{P} = 23.3$ lbs./min.

$\dot{\delta}_n = 4.0 \times 10^{-4}$ in./min.

t (min.)	P (lbs.)	δ ($\times 10^{-3}$ in.)
0.0	100	0.01
24.5	670	0.1
24.5	170	6.8
30.0	140	12.0
35.0	140	14.0
43.0	140	17.0
113.0	140	45.0

Sample S-87:

$T = -10.0^{\circ}C$
H = 6.0 in.
D = 6.0 in.
L = 6.0 in.
$v_s = 64.0\ \%$

d = 3/8 in.
h = 1/8 in.
(45°-lug, Ground-Finish)

$\dot{P} = 23.1$ lbs./min.

$\dot{\delta}_n = 5.93 \times 10^{-4}$ in./min.

t (min.)	P (lbs.)	δ ($\times 10^{-3}$ in.)
35	810	0.4
160	2090	30.2
260	2530	78.6
360	2730	129.6
405	2730	154.6

Table A-4: (Cont'd)

Sample S-88:

$T = -10.0^{o}C$
H = 6.0 in.
D = 6.0 in.
L = 6.0 in.
v_s= 64.0 %

d = 3/8 in.
h = 0 (Shot-Blasted)

$\dot{P}$ = 18.5 lbs./min.

$\dot{\delta}n = 7.5 \times 10^{-4}$ in./min.

t (min.)	P (lbs.)	δ ($\times 10^{-3}$ in.)
94	1740	3.2
94	1600	9.6
95	1140	19.2
97	1070	24.2
100	990	28.3
160	730	69.3
175	730	80.8

Sample S-89:

$T = -10.0^{o}C$
H = 6.0 in.
D = 6.0 in.
L = 6.0 in.
v_s= 64.0 %

d = 3/8 in.
h = 1/8 in. (45^{o}-lug)

$\dot{P}$ = 25 lbs./min.

$\dot{\delta}n = 5.5 \times 10^{-4}$ in./min.

t (min.)	P (lbs.)	δ ($\times 10^{-3}$ in.)
15.6	1440	0.1
16.0	1560	9.0
66.0	2300	26.5
166.0	3160	70.0
271.0	3380	121.0
350.0	3380	165.0
523.0	3380	260.0

Sample S-90:

$T = -10.0^{o}C$
H = 6.0 in.
D = 6.0 in.
L = 6.0 in.
(Continued)

Sample S-90: (Cont'd)

v_s= 64.0 %

d = 3/8 in.
h = 1/8 in.
(45^{o}-lug, Shot-Blasted)

$\dot{P}$ = 30 lbs./min.

$\dot{\delta}n = 5.39 \times 10^{-4}$ in./min.

t (min.)	P (lbs.)	δ ($\times 10^{-3}$ in.)
72	2160	1.0
75	1960	6.0
85	1960	11.2
185	2920	52.8
370	3400	146.0
520	3400	225.0

Sample S-91:

$T = -15.0^{o}C$
H = 6.0 in.
D = 6.0 in.
L = 6.0 in.
v_s= 64.0 %

d = 3/8 in.
h = 1/8 in. (45^{o}-lug)

$\dot{P}$ = 23 lbs./min.

$\dot{\delta}n = 5.0 \times 10^{-4}$ in./min.

t (min.)	P (lbs.)	δ ($\times 10^{-3}$ in.)
85	2160	1.5
95	2160	8.0
195	2920	36.0
350	3840	84.0
560	4360	182.0
680	4360	242.0

Sample S-92:

$T = -15.0^{o}C$
H = 6.0 in.
D = 6.0 in.
L = 6.0 in.
v_s= 64.0 %

d = 3/8 in.
h = 0

$\dot{P}$ = 20.5 lbs./min.
(Continued)

Table A-4: (Cont'd)

Sample S-92: (Cont'd)

$\dot{\delta}n = 6.25 \times 10^{-4}$ in./min.

t (min.)	P (lbs.)	δ ($\times 10^{-3}$ in.)
61	1250	0.8
61	95	20.0
70	320	20.4
71	320	21.6
73	300	23.2
85	280	31.2
100	280	39.7
120	280	52.2

Sample S-93:

T = -20.0°C
H = 6.0 in.
D = 6.0 in.
L = 6.0 in.
v_s = 64.0 %

d = 3/8 in.
h = 1/8 in. (45°-lug)

$\dot{P}$ = 34.9 lbs./min.

$\dot{\delta}n = 5.2 \times 10^{-4}$ in./min.

t (min.)	P (lbs.)	δ ($\times 10^{-3}$ in.)
75	2720	0.1
80	2600	5.0
90	2600	9.6
190	3800	42.0
340	4480	116.0
420	4600	160.0
450	4640	175.0

Sample S-94:

T = -20.0°C
H = 6.0 in.
D = 6.0 in.
L = 6.0 in.
v_s = 64.0 %

d = 3/8 in.
h = 0

$\dot{P}$ = 18 lbs./min.

$\dot{\delta}n = 5.85 \times 10^{-4}$ in./min.

(Continued)

Sample S-94: (Cont'd)

t (min.)	P (lbs.)	δ ($\times 10^{-3}$ in.)
80	1440	0.2
95	1700	0.4
95	300	25.6
103	480	25.8
104.5	520	26.0
108.0	520	29.6
110.0	460	32.8
126.0	440	41.9
136.0	440	48.0

Sample S-95:

T = -26.0°C
H = 6.0 in.
D = 6.0 in.
L = 6.0 in.
v_s = 64.0 %

d = 3/8 in.
h = 0

$\dot{P}$ = 22.2 lbs./min.

$\dot{\delta}n = 6.67 \times 10^{-4}$ in./min.

t (min.)	P (lbs.)	δ ($\times 10^{-3}$ in.)
83	1840	0.1
83	240	28.0
103	800	29.0
103	680	32.0
105	600	34.0
115	640	39.0
145	640	59.0

Sample S-96:

T = -6.0°C
H = 6.0 in.
D = 6.0 in.
L = 6.0 in.
v_s = 64.0 %

d = 3/8 in.
h = 1/8 in. (45°-lug)

$\dot{P}$ = 27.6 lbs./min.

$\dot{\delta}n = 5.6 \times 10^{-4}$ in./min.

(Continued)

Table A-4: (Cont'd)

Sample S-96: (Cont'd)

t (min.)	P (lbs.)	δ ($\times 10^{-3}$ in.)
50	1380	3.0
65	1280	12.0
75	1280	17.0
175	1760	64.4
275	1960	117.0
375	2040	173.0

Sample S-97:

T = -2.0°C
H = 6.0 in.
D = 6.0 in.
L = 6.0 in.
v_s = 64.0%

d = 3/8 in.
h = 1/8 in. (45°-lug)
$\dot{P}$ = 19.34 lbs./min.
$\dot{\delta}_n = 5.67 \times 10^{-4}$ in./min.

t (min.)	P (lbs.)	δ ($\times 10^{-3}$ in.)
30	580	4.5
80	1040	23.0
160	1440	61.5
200	1520	81.5
320	1520	149.5

Sample S-98:

T = -10.0°C
H = 2.0 in.
D = 6.0 in.
L = 2.0 in.
v_s = 64.0 %

d = 5/8 in.
h = 0
$\dot{P}$ = 25 lbs./min.
$\dot{\delta}_n = 5.73 \times 10^{-4}$ in./min.

t (min.)	P (lbs.)	δ ($\times 10^{-3}$ in.)
23.5	576	0.4
23.5	170	7.2
25.0	145	8.2
40.0	145	16.8

Sample S-99:

T = 10.0°C
H = 4.0 in.
D = 6.0 in.
L = 4.0 in.
v_s = 64.0 %

d = 5/8 in.
h = 0
$\dot{P}$ = 36.9 lbs./min.
$\dot{\delta}_n = 6.67 \times 10^{-4}$ in./min.

t (min.)	P (lbs.)	δ ($\times 10^{-3}$ in.)
52	1920	1.8
52	320	21.4
58	500	23.0
62	480	24.0
80	480	36.0

Sample S-100:

T = -10.0°C
H = 3.0 in.
D = 6.0 in.
L = 3.0 in.
v_s = 64.0 %

d = 5/8 in.
h = 0
$\dot{P}$ = 31.22 lbs./min.
$\dot{\delta}_n = 5.6 \times 10^{-4}$ in./min.

t (min.)	P (lbs.)	δ ($\times 10^{-3}$ in.)
41	1280	0.8
41	460	10.4
42	300	13.6
54	290	20.4
62	290	24.8

Sample S-101:

T = -10.0°C
H = 5.0 in.
D = 6.0 in.
L = 5.0 in.
v_s = 64.0 %

d = 5/8 in.
h = 0
(Continued)

Table A-4: (Cont'd)

Sample S-101: (Cont'd)

$\dot{P}$ = 41 lbs./min.

$\dot{\delta}_n$= 6.03×10^{-4} in./min.

t (min.)	P (lbs.)	δ ($\times 10^{-3}$ in.)
76.0	3120	2.0
77.0	2920	4.0
77.5	1980	15.0
78.0	1620	20.5
79.0	1340	24.0
82.0	1250	27.5
116.0	1220	48.0

Sample S-102:

T = -10.0^{o}C
H = 6.0 in.
D = 6.0 in.
L = 6.0 in.
v_s= 64.0 %

d = 5/8 in.
h = 0

$\dot{P}$ = 41.73 lbs./min.

$\dot{\delta}_n$= 7.17×10^{-4} in./min.

t (min.)	P (lbs.)	δ ($\times 10^{-3}$ in.)
81.0	3380	1.5
83.0	2980	5.0
83.5	1700	23.5
85.0	1300	29.5
88.0	1180	32.5
130.0	1180	56.5

Sample S-103:

T = -10.0^{o}C
H = 2.0 in.
D = 6.0 in.
L = 2.0 in.
v_s= 64.0 %

d = 5/8 in.
h = 0

$\dot{P}$ = 28.1 lbs./min.

(Continued)

Sample S-103: (Cont'd)

$\dot{\delta}_n$= 5.7×10^{-4} in./min.

t (min.)	P (lbs.)	δ ($\times 10^{-3}$ in.)
35.5	980	2.4
35.5	440	8.8
36.0	290	10.8
40.0	260	13.4
60.0	260	24.8

Sample S-104:

Leakage, data void

Sample S-105:

T = -10.0^{o}C
H = 5.0 in.
D = 6.0 in.
L = 5.0 in.
v_s= 64.0 %

d = 5/8 in.
h = 0

$\dot{P}$ = 35.6 lbs./min.

$\dot{\delta}_n$= 6.25×10^{-4} in./min.

t (min.)	P (lbs.)	δ ($\times 10^{-3}$ in.)
81	2880	2
82	2520	6
83	1320	21
88	1080	27
96	1080	32

Sample S-106:

T = -10.0^{o}C
H = 2.0 in.
D = 6.0 in.
L = 2.0 in.
v_s= 64.0 %

d = 5/8 in.
h = 0

$\dot{P}$ = 25 lbs./min.

$\dot{\delta}_n$= 5.86×10^{-4} in./min.

(Contiued)

Table A-4: (Cont'd)

Sample S-106: (Cont'd)

t (min.)	P (lbs.)	δ ($\times 10^{-3}$ in.)
23	576	1.6
23	210	7.2
24	120	8.0
39	120	16.8

Sample S-107:

$T = -10.0^{\circ}C$
$h = 5.0$ in.
$D = 6.0$ in.
$L = 5.0$ in.
$v_s = 64.0$ %
$d = 5/8$ in.
$h = 0$
$\dot{P} = 38.9$ lbs./min.
$\dot{\delta}_n = 6.2 \times 10^{-4}$ in./min.

t (min.)	P (lbs.)	δ ($\times 10^{-3}$ in.)
52.5	2040	3.0
52.5	460	20.0
57.0	500	23.0
74.0	500	33.5

Sample S-108:

$T = -10.0^{\circ}C$
$H = 3.0$ in.
$D = 6.0$ in.
$L = 3.0$ in.
$v_s = 64.0$ %
$d = 5/8$ in.
$h = 0$
$\dot{P} = 26.5$ lbs./min.
$\dot{\delta}_n = 5.8 \times 10^{-4}$ in./min.

t (min.)	P (lbs.)	δ ($\times 10^{-3}$ in.)
20	530	0.01
20	160	5.60
21	130	6.40
41	130	18.00

Sample S-109:

$T = -10.0^{\circ}C$
$H = 6.0$ in.
$D = 6.0$ in.
(Continued)

Sample S-109: (Cont'd)

$L = 6.0$ in.
$v_s = 64.0$ %
$d = 5/8$ in.
$h = 0$
$\dot{P} = 35$ lbs./min.
$\dot{\delta}_n = 5.0 \times 10^{-4}$ in./min.

t (min.)	P (lbs.)	δ ($\times 10^{-3}$ in.)
56	1960	2.0
56	320	19.0
65	640	23.0
67	480	26.0
73	480	29.0
115	480	50.0

Sample S-110:

$T = -10.0^{\circ}C$
$H = 4.0$ in.
$D = 6.0$ in.
$L = 4.0$ in.
$v_s = 64.0$ %
$d = 5/8$ in.
$h = 0$
$\dot{P} = 28.2$ lbs./min.
$\dot{\delta}_n = 5.56 \times 10^{-4}$ in./min.

t (min.)	P (lbs.)	δ ($\times 10^{-3}$ in.)
17	500	0.8
17	170	4.0
20	140	8.0
30	130	14.0
60	120	31.0
66	120	34.0

Sample S-111:

$T = -10.0^{\circ}C$
$H = 5.5$ in.
$D = 6.0$ in.
$L = 5.5$ in.
$v_s = 64.0$ %
$d = 3/8$ in.
$h = 0$
(Continued)

Table A-4: (Cont'd)

Sample S-111: (Vont'd)

$\dot{P}$ = 20 lbs./min.

$\dot{\delta}_n = 6.67 \times 10^{-4}$ in./min.

t (min.)	P (lbs.)	δ ($\times 10^{-3}$ in.)
28	560	0.5
28	320	8.5
40	40	16.5
52	40	24.5

Sample S-112:

T = -10.0°C
H = 5.625 in.
D = 6.000 in.
L = 5.626 in.
v_s = 64.0 %

d = 3/8 in.
h = 0

$\dot{P}$ = 21.2 lbs./min.

$\dot{\delta}_n = 6.25 \times 10^{-4}$ in./min.

t (min.)	P (lbs.)	δ ($\times 10^{-3}$ in.)
30	640	0.1
30	240	9.5
31	100	12.0
42	80	19.0
47	80	22.0

Sample S-113:

T = -15.0°C
H = 6.0 in.
D = 6.0 in.
L = 6.0 in.
v_s = 64.0 %

d = 3/8 in.
h = 0

$\dot{P}$ = 25.2 lbs./min.

$\dot{\delta}_n = 4.75 \times 10^{-4}$ in./min.

t (min.)	P (lbs.)	δ ($\times 10^{-3}$ in.)
42	1060	0.7
42	280	14.0
58	280	21.6

Sample S-114:

T = -15.0°C
H = 6.0 in.
D = 6.0 in.
L = 6.0 in.
v_s = 64.0 %

d = 3/8 in.
h = 0

$\dot{P}$ = 25.8 lbs./min.

$\dot{\delta}_n = 4.0 \times 10^{-4}$ in./min.

t (min.)	P (lbs.)	δ ($\times 10^{-3}$ in.)
27	690	0.40
35	430*	0.16
38	430	0.18
63	1250**	0.24
63	280	14.20
64	220	14.40
68	250	15.80
78	240	19.80

* Decreased due to unloading
** Reloading

Sample S-115:

T = -10.0°C
H = 6.0 in.
D = 6.0 in.
L = 6.0 in.
v_s = 64.0 %

d = 3/8 in.
h = 0

$\dot{P}$ = 17.3 lbs./min.

$\dot{\delta}_n = 4.2 \times 10^{-4}$ in./min.

t (min.)	P (lbs.)	δ ($\times 10^{-3}$ in.)
33.5	580	1.0
33.5	160	7.4
34.0	80	9.8
74.0	30	26.6
108.0	30	33.8

Table A-4: (Cont'd)

Sample S-116:

T = -10.0°C
H = 6.0 in.
D = 6.0 in.
L = 6.0 in.
v_s= 64.0 %

d = 3/8 in.
h = 0
$\dot{P}$ = 20.3 lbs./min.
$\dot{\delta}n$= 4.84×10^{-4} in./min.

t (min.)	P (lbs.)	δ ($\times 10^{-3}$ in.)
22.5	460	0.4
22.5	170	4.4
23.0	100	7.0
33.0	40	16.6
61.0	40	25.4

Sample S-117:

T = -20.0°C
H = 6.0 in.
D = 6.o in.
L = 6.0 in.

v_s= 64.0 %

d = 3/8 in.
h = 0
$\dot{P}$ = 24.6 lbs./min.
$\dot{\delta}n$= 2.1×10^{-4} in./min.

t (min.)	P (lbs.)	δ ($\times 10^{-3}$ in.)
54	1330	0.6
54	280	12.8
59	250	16.0
87	210	23.0
113	180	27.2
160	180	36.9

Sample S-118:

T = -20.0°C
H = 6.0 in.
D = 6.0 in.
L = 6.0 in.

v_s= 64.0 %

d = 3/8 in.
(Continued)

Sample S-118: (cont'd)

h = 0
$\dot{P}$ = 22 lbs./min.
$\dot{\delta}n$= 2.8×10^{-4} in./min.

t (min.)	P (lbs.)	δ ($\times 10^{-3}$ in.)
37	810	0.1
37	330	4.4
40	200	8.8
52	170	14.0
75	170	20.4

Sample S-119:

T = -10.0°C
H = 6.0 in.
D = 6.0 in.
L = 6.0 in.
v_s= 64.0 %

d = 5/8 in.
h = 0
$\dot{P}$ = 33.4 lbs./min.
$\dot{\delta}n$= 1.17×10^{-4} in./min.

t (min.)	P (lbs.)	δ ($\times 10^{-3}$ in.)
41	1370	0.9
41	50	7.2
50	280	7.5
56	240	8.2
68	240	9.6

Samlpe S-120:

T = -10.0°C
H = 2.0 in.
D = 6.0 in.
L = 2.0 in.
v_s= 64.0 %

d = 3/8 in.**
h = 0.015 in.**
$\dot{P}$ = 170 lbs./min.
$\dot{\delta}n$= 4.6×10^{-3} in./min.

** Standard deformed bar

(Continued)

Table A-4: (Cont'd)

Sample S-120: (Cont'd)

t (min.)	P (lbs.)	δ ($x10^{-3}$in.)
2	560	0.9
4	1060	2.5
5	1260	4.0
6	1420	7.5
8	1630	13.0
10	1870	19.0
12	2030	25.0
14	2190	32.5
16	2270	40.0
17	2300	43.8
20	2300	56.5
24	2200	75.0
29	2080	100.0
53	1800	130.0
40	1610	155.6
45	1540	180.0
60	1310	250.0
81	1050	325.0

Sample S-121:

T = -10.0^{o}C
H = 3.0 in.
D = 6.0 in.
L = 3.0 in.
v_s= 64.0 %

d = 3/8 in.**
h = 0.015 in.**
$\dot{P}$ = 235 lbs./min.
$\dot{\delta}_n$= $4.5x10^{-3}$ in./min.

t (min.)	P (lbs.)	δ ($x10^{-3}$in.)
4	1102	0.5
8	2100	4.4
10	2678	8.8
12	3220	13.5
14	3378	18.5
16	3762	25.0
18	3890	31.0
21	4025	46.3
24	3940	60.5
28	3590	89.4
32	3100	117.0
36	2720	143.5
40	2470	174.0

(Continued)

Sample S-121: (Cont'd)

t (min.)	P (lbs.)	δ ($x10^{-3}$in.)
46	2300	207.0
52	2120	242.0
60	1980	282.0
68	1840	327.0

** Standard deformed bar

Sample S-122:

T = -10.0^{o}C
H = 6.0 in.
D = 6.0 in.
L = 6.0 in.
v_s= 64.0 %

d = 3/8 in.
h = 1/8 in.
$\dot{P}$ = 40 lbs./min.
$\dot{\delta}_n$= $6.7x10^{-4}$ in./min.

t (min.)	P (lbs.)	δ ($x10^{-3}$in.)
20.0	770	0.3
40.0	1600	1.8
41.0	1570	2.5
43.0	1300	7.5
46.0	1080	15.0
50.0	1120	17.5
55.0	1150	20.0
60.0	1208	23.0
70.0	1310	29.5
90.0	1450	41.2
120.0	1560	61.2
160.0	1698	88.0
170.0	1750	116.5
190.0	1750	166.5
285.0	1750	230.0

Sample S-123:

T = -10.0^{o}C
H = D = L = 6.0 in.
d = 3/8 in.
h = 0 (plain)
v_s= 42.0 %
$\dot{P}$ = 22 lbs./min.
$\dot{\delta}_n$= $8.2x10^{-4}$ in./min.

(Continued)

Table A-4: (Cont'd)

Sample S-123: (Cont'd)

t (min.)	P (lbs.)	δ ($x10^{-3}$in.)
15.0	330	0.5
15.0	113	4.5
17.5	105	6.2
21.0	96	10.0
29.5	82	17.0
32.5	82	21.0

Sample S-124:

$T = -10.0^{o}C$
H = D = L = 6.0 in.
d = 3/8 in.
h = 0
v_s= 29.6 %
$\dot{P}$ = 31.8 lbs./min.
$\dot{\delta}_n = 6.8x10^{-4}$ in./min.

t (min.)	P (lbs.)	δ ($x10^{-3}$in.)
16.5	525	0.20
16.5	60	8.25
20.0	60	10.75
30.0	60	19.62
46.0	60	30.63

Sample S-125:

$T = -10.0^{o}C$
H = L = 6.125 in.
D = 6.0 in.
d = 3/8 in.
h = 0
v_s= 53.8 %
$\dot{P}$ = 20.8 lbs./min.
$\dot{\delta}_n = 7.0x10^{-4}$ in./min.

t (min.)	P (lbs.)	δ ($x10^{-3}$in.)
10.5	225	0.1
11.0	100	2.5
21.0	85	10.5
28.0	75	15.1
34.0	75	19.6

Sample S-126:

$T = -10.0^{o}C$
H = D = L = 6.0 in.
d = 3/8 in.
h = 0
v_s= 52.7 %
$\dot{P}$ = 44 lbs./min.
$\dot{\delta}_n = 8.4x10^{-4}$ in./min.

t (min.)	P (lbs.)	δ ($x10^{-3}$in.)
16.2	710	0.4
16.2	112	9.2
18.0	145	10.0
24.0	145	15.5
29.0	245	19.2

Sample S-127:

$T = -10.0^{o}C$
H = D = L = 6.0 in.
d = 3/8 in.
h = 0
v_s= 30.3 %
$\dot{P}$ = 31.6 lbs./min.
$\dot{\delta}_n = 1.1x10^{-3}$ in./min.

t (min.)	P (lbs.)	δ ($x10^{-3}$in.)
16.6	525	0.8
17.0	135	7.5
18.0	60	8.6
21.0	60	11.9

Sample S-128:

$T = -10.0^{o}C$
H = L = 5.875 in.
D = 6.0 in.
d = 3/8 in., h = 0
v_s= 44.2 %
$\dot{P}$ = 30 lbs./min.
$\dot{\delta}_n = 8.1x10^{-4}$ in./min.

t (min.)	P (lbs.)	δ ($x10^{-3}$in.)
10.6	320	0.5
11.0	120	5.5
13.0	75	8.0
16.0	40	10.8
19.0	40	13.2

Table B-1: Ice samples CI-1 and CI-2 (Ice 3)

Sample CI-1:

T = -10.0°C
H = 5.87 in.
D = 6.00 in.
L = 5.87 in.
d = 3/8 in.(Cold-rolled)
h = 1/8 in.(90°-lug)

P (lbs.)	t (min.)	δ^c (x10^{-3}in.)
520	20	0.20
	40	0.75
	60	1.75
	80	3.00
	100	5.00
	120	18.50
	140	83.50
	160	141.00
	180	213.50
	200	286.00
	220	361.00
	240	443.50

Sample CI-2:

T = -10.0°C
H = 6.0 in.
D = 6.0 in.
L = 6.0 in.
d = 3/8 in.
h = 1/8 in.

P (lbs.)	t (min.)	δ^c (x10^{-3}in.)
200	80	0.20
	100	0.01
	200	0.10
	300	0.50
	400	0.50
	500	0.10
	600	0.10
	700	0.25
	1000	0.25
	1100	0.50
	1255	0.40
280**	0	0.40
	100	0.75
	200	1.00
	400	1.12

(Continued)

** Step loading procedure

Sample CI-2: (Cont'd)

P (lbs.)	t (min.)	δ^c (x10^{-3}in.)
280	550	1.25
	600	1.00
	690	1.00
360	0	1.00
	100	0.75
	200	0.75
	300	1.00
	500	1.00
	710	1.00
440	0	1.00
	300	1.00
	400	1.12
	500	1.50
	600	1.88
	750	2.00
	1000	2.50
	1100	3.00
	1200	3.00
	1300	3.00
	1380	3.50
520	0	3.50
	100	4.00
	200	4.50
	300	5.00
	400	6.00
	500	7.25
	600	10.00
	650	11.80
	700	15.80
	720	24.00

Table B-2: Frozen sand samples

Sample CS-1:**

T = -10.0°C
H = 6.0 in.
D = 6.0 in.
L = 6.0 in.
d = 5/8 in.
h = 0, v_s= 64.0 %

** Instant rupture at t=0.75 min., P=1420 lbs., and δc=0.0002 in.

Sample CS-2:

T = -10.0°C
H = 6.0 in.
D = 6.0 in.
L = 6.0 in.
d = 5/8 in.
h = 0 , v_s= 64.0 %

P (lbs.)	t (min.)	δc ($\times 10^{-3}$ in.)
1040	1	0.1
	2	0.7 rupture

Sample CS-3:

T = -10.0°C
H = 6.0 in.
D = 6.0 in.
L = 6.0 in.
d = 5/8 in.
h = 0 , v_s= 64.0%

P (lbs.)	t (min.)	δc ($\times 10^{-3}$ in.)
750	0.75	0.10
	34.00	0.15
910	34.00	0.20
	48.00	0.21
	66.00	0.84
	70.00	1.40 (rupture)

Sample CS-4:**

T = -10.0°C
H = D = L = 6.0 in.
d = 5/8 in., h = 0 , v_s= 64.0 %

** Instant rupture at P = 800 lbs.

Sample CS-5:

T = -10.0°C
H = D = L = 6.0 in.
d = 3/8 in.
h = 1/8 in. (90°-lug)
v_s= 64.0 %

P (lbs.)	t (min.)	δc ($\times 10^{-3}$ in.)
2300	1	9
	2	13
	3	15
	4	17
	12	27
	21	33
	40	43
	60	50
	80	57
	120	67
	160	75
	200	85
	300	101
	400	117
	600	141
	800	165
	1100	191
	1420	225
2500	1425	229
	1520	245
	1640	269
	1820	299
	2030	333
2780	2030	334
	2220	398
	2420	454
	2620	504
	2820	550
	2920	570
3020	2920	572
	2960	588
	3020	614
3180	3020	620
	3120	666
	3220	706

Table B-2: (Cont'd)

Sample CS-6:

$T = -10.0^{o}C$
$H = D = L = 6.0$ in.
$d = 3/8$ in.
$h = 1/8$ in.
$v_s = 64.0$ %

P (lbs.)	t (min.)	$\delta^c (x10^{-3}$ in.)
2800	1	15
	2	20
	3	24
	4	26
	5	38
	6	30
	7	31
	10	33
	20	45
	30	53
	40	61
	60	71
	80	81
	100	89
	150	109
	200	125
	250	139
	300	153
	350	165
	400	177
	500	203
	585	225
3080	585	229
	600	234
	700	277
	800	321
	856	351
3320	865	353
	900	383
	1000	451
	1100	518
	1200	589
3560	1200	591
	1250	641
	1300	687
	1480	833

Sample CS-7:

$T = -10.0^{o}C$
$H = D = L = 6.0$ in.
$d = 3/8$ in.
$h = 1/8$ in.
$v_s = 64.0$ %

P (lbs.)	t (min.)	$\delta^c (x10^{-3}$ in.)
3560	5	61
	10	81
	25	121
	45	156
	65	185
	100	229
	150	286
	200	349
	250	411
	275	444
	300	476
	405	625
3780	405	626
	420	664
	460	751
	500	822
	545	916
4000	580	1019
	615	1106

Sample CS-8:

$T = -10.0^{o}C$
$H = D = L = 6.0$ in.
$d = 3/8$ in.
$h = 1/8$ in.
$v_s = 64.0$ %

P (lbs.)	t (min.)	$\delta^c (x10^{-3}$ in.)
4000	1.5	33
	3.0	45
	5.0	54
	8.0	64
	12.0	74
	15.0	82
	20.0	111
	30.0	154
	45.0	204
	60.0	252
	80.0	309
	100.0	369

(Continued)

Table B-2: (Cont'd)

Sample CS-8: (Cont'd)

P (lbs.)	t (min.)	δ^c ($\times 10^{-3}$ in.)
4000	150	514
	200	654
	240	771
	275	874

Sample CS-9:

T = -10.0°C
H = D = L = 6.0 in.
d = 3/8 in.
h = 1/16 in.
v_s = 64.0 %

P (lbs.)	t (min.)	δ^c ($\times 10^{-3}$ in.)
1400	1	15
	2	20
	5	32
	10	40
	20	54
	40	74
	70	95
	100	115
	120	128
	120	143
	137	161
	137	178
	170	198
	200	210
	245	228
1560	245	230
	270	252
	300	275
	342	300
1800	342	302
	345	308
	350	320
	360	338
	370	350
	400	398
	450	450
	500	500
	550	563
	600	612
	650	670

(Continued)

Sample CS-9: (Cont'd)

P (lbs.)	t (min.)	δ^c ($\times 10^{-3}$ in.)
1800	700	710
	780	788
2080	780	790
	790	815
	800	840
	810	860
	820	875

Sample CS-10:

T = -10.0°C
H = D = L = 6.0 in.
d = 3/8 in.
h = 1/8 in.
v_s = 64.0 %

P (lbs.)	t (min.)	δ^c ($\times 10^{-3}$ in.)
1580	5	9
	10	13
	20	23
	60	33
	100	36
	145	40
	195	44
1860	195	46
	230	52
	280	56
	350	63
2140	350	65
	400	72
	450	78
	505	86
2300	505	88
	550	93
	600	100
	700	113
	800	126
	950	146
	1050	153
	1280	159

Table B-2: (Cont'd)

Sample CS-11:

T = -10.0°C
H = D = L = 6.0 in.
d = 3/8 in.
h = 3/16 in.
v_s= 64.0 %

P (lbs.)	t (min.)	δ^c(x10^{-3}in.)
2000	1	2.5
	2	4.0
	5	4.5
	10	6.0
	20	7.0
	40	8.1
	70	10.1
	100	11.1
	160	12.5
	230	13.2
2480	230	13.3
	250	16.8
	290	21.7
	350	26.7
	400	30.8
	500	36.8
	600	42.0
	700	46.4
	785	49.5
3040	785	50.2
	800	53.0
	850	58.6
	900	63.3
	970	68.5
	1040	72.7
3600	1040	73.3
	1070	76.1
	1120	84.9
	1160	88.9
	1200	92.3
	1270	98.5
4160	1270	98.9
	1300	108.4
	1350	120.4
	1400	131.6
	1500	151.6
	1600	172.4

Sample CS-12:

T = -10.0°C
H = D = L = 6.0 in.
d = 3/8 in.
h = 1/8 in.
v_s= 64.0 %

P (lbs.)	t (min.)	δ^c(x10^{-3}in.)
4000	5	96
	10	107
	15	163
	20	188
	25	212

Test stopped, LVDT OFF

Sample CS-13:

T = -10.0°C
H = D = L = 6.0 in.
d = 3/8 in.
h = 1/16 in.
v_s= 64.0 %

P (lbs.)	t (min.)	δ^c(x10^{-3}in.)
850	3	2.4
	8	6.8
	18	12.5
	38	19.6
	80	28.8
	120	33.5
	170	37.7
	230	44.0
	300	49.0
	345	51.5
1200	345	52.0
	370	64.0
	400	74.0
	450	86.0
	500	97.0
	585	114.6
1560	585	117.1
	600	133.6
	618	149.6
	1220	417.1
	1300	467.3
	1455	542.1

(Continued)

Table B-2: (Cont'd)

Sample CS-13: (Cont'd)

P (lbs.)	t (min.)	δ^c ($\times 10^{-3}$ in.)
2600	1455	592.0
	1458	652.0
	1465	727.0
	1480	829.6
	1500	989.6
	1520	1117.0
	1540	1214.6

Sample CS-14:

T = -10.0°C
H = D = L = 6.0 in.
d = 3/8 in.
h = 1/8 in.
v_s = 64.0 %

P (lbs.)	t (min.)	δ^c ($\times 10^{-3}$ in.)
4500	0	31
	2	75
	5	112
	10	156
	20	231
	32	312
	47	400
	48	475
	57	578
	72	725
	89	890
	90	950
	100	1080

Sample CS-15:

T = -10.0°C
H = D = L = 6.0 in.
d = 3/8 in.
h = 1/16 in.
v_s = 64.0 %

P (lbs.)	t (min.)	δ^c ($\times 10^{-3}$ in.)
3000	0.5	140
	1.0	280
	1.5	375
	3.0	420
	4.5	470

(Continued)

Sample CS-15: (Cont'd)

P (lbs.)	t (min.)	δ^c ($\times 10^{-3}$ in.)
3000	5.2	504
	6.0	607
	7.0	645
	8.0	670
	9.0	708
	10.0	745
	10.0	rupture

Sample CS-16:

T = -15.0°C
H = D = L = 6.0 in.
d = 3/8 in.
h = 1/8 in.
v_s = 64.0 %

P (lbs.)	t (min.)	δ^c ($\times 10^{-3}$ in.)
1500	5	1.75
	10	3.12
	20	5.38
	50	10.00
	100	15.00
	150	18.75
	200	20.88
	300	25.00
	400	28.50
	500	30.25
	600	32.50
	706	34.25
2000	706	34.38
	730	38.50
	770	41.25
	800	43.12
	850	46.00
	900	48.75
	1000	53.12
	1100	56.50
	1200	60.00
	1300	62.50
	1400	65.00
	1500	67.50
	1554	68.38
2500	1554	68.60
	1600	71.40

(Continued)

Table B-2: (Cont'd)

Sample CS-16: (Cont'd)

P (lbs.)	t (min.)	δ^c ($\times 10^{-3}$ in.)
2500	1650	76.40
	1700	79.40
	1800	86.40
	1950	95.65
	2134	104.40
3000	2134	105.65
	2150	109.40
	2200	119.40
	2300	133.15
	2450	151.15
	2600	167.65
	2750	184.15
	2938	203.15
3500	2938	205.15
	3000	225.15
	3100	255.15
	3250	295.15
	3400	325.10
	3600	375.15
	3730	415.10
4000	3730	415.60
	3800	473.65
	3880	525.15
	3935	615.15

Sample CS-17:

T = -10.0°C
H = D = L = 6.0 in.
d = 3/8 in.
h = 3/16 in.
v_s = 64.0 %

P (lbs.)	t (min.)	δ^c ($\times 10^{-3}$ in.)
2500	10	17.5
	20	25.0
	40	33.8
	70	40.0
	100	47.0
	150	53.8
	200	58.8
	275	65.0
3500	275	66.0
	300	79.5

(Continued)

Sample CS-17: (Cont'd)

P (lbs.)	t (min.)	δ^c ($\times 10^{-3}$ in.)
3500	350	91.0
	400	101.0
	500	116.0
	650	136.0
	800	151.0
	950	166.0
	1100	181.0
2500	1100	181.0
Unloading	1210	182.0
	1445	186.0

Sample CS-18:

T = 10.0°C
H = D = L = 6.0 in.
d = 3/8 in.
h = 1/8 in.
v_s = 64.0 %

P (lbs.)	t (min.)	δ^c ($\times 10^{-3}$ in.)
1220	20	6.5
	60	12.5
	100	16.7
	150	20.2
	200	22.5
	300	26.5
	450	30.0
	600	32.8
	725	35.0
1540	725	36.5
	760	38.4
	800	39.9
	900	43.2
	1050	47.5
	1200	50.9
	1350	52.8
	1450	54.6
1820	1450	55.2
	1495	58.2
	1550	60.7
	1600	62.0
	1700	66.4
	1850	74.0
	2000	80.0
	2155	86.4

(Continued)

Table B-2: (Cont'd)

Sample CS-18: (Cont'd)

P (lbs.)	t (min.)	δ^c ($\times 10^{-3}$ in.)
2100	2155	88.2
	2200	91.7
	2300	98.2
	2500	108.2
	2700	117.7
	2830	125.2
2380	2830	127.7
	2900	134.2
	3000	140.2
	3150	152.7
	3300	162.7
	3560	180.0
2100	3560	180.0
Unloading	3650	184.2
	3700	186.2
	3800	190.2
	3910	191.2
1540	3910	191.2
	4100	191.2
	4355	190.0
1220	4355	190.0
	4500	190.0
	5100	190.0

Sample CS-19:

T = -10.0°C
H = L = 5.954 in.
D = 2.781 in.
d = 3/8 in.
h = 1/16 in.
v_s= 64.0 %

P (lbs.)	t (min.)	δ^c ($\times 10^{-3}$ in.)
1500	20	70.0
	60	120.0
	100	157.5
	150	207.5
	200	251.2
	300	345.0
	400	426.2
	550	563.8
	700	713.8

(Continued)

Sample CS-19: (Cont'd)

P (lbs.)	t (min.)	δ^c ($\times 10^{-3}$ in.)
1500	800	807.5
	900	1032.5
	1000	1148.8
	1140	1317.6

Sample CS-20:

T = -10.0°C
H = D = L = 6.0 in.
d = 3/8 in.
h = 1/8 in. (at z = 4.5 in.)**
v_s= 64.0 %

** For all samples z = 3.0 in., unless noted.

P (lbs.)	t (min.)	δ^c ($\times 10^{-3}$ in.)
1500	8	10.0
	18	15.0
	38	21.2
	68	27.5
	100	32.5
	150	38.1
	200	43.8
	300	51.2
	400	57.5
	500	62.5
	650	70.0
	800	76.8
	1000	85.0
	1225	93.0
2000	1225	95.0
	1260	103.0
	1300	110.0
	1400	122.5
	1500	135.0
	1650	150.5
	1800	166.8
	2015	187.5
2500	2015	190.0
	2060	215.5
	2150	252.5
	2300	307.5
	2500	382.5
	2675	452.0

(Continued)

Table B-2: (Cont'd)

Sample CS-20: (Cont'd)

P (lbs.)	t (min.)	δ^c ($\times 10^{-3}$ in.)
3000	2675	452.5
	2735	530.0
	2800	605.0
	2900	748.8
	2960	883.8
	2960	rupture

Sample CS-21:

T = -10.0°C
H = L = 6.0 in.
D = 1.938 in.
d = 3/8 in.
h = 1/8 in.
v_s = 64.0 %

P (lbs.)	t (min.)	δ^c ($\times 10^{-3}$ in.)
1000	10	12.5
	20	17.5
	40	27.0
	70	36.3
	100	42.5
	150	50.0
	200	56.8
	300	67.0
	450	77.0
	600	83.8
	800	92.5
	1000	99.2
	1190	105.0
1740	1190	106.0
	1220	125.0
	1260	141.2
	1320	161.2
	1400	183.7
	1500	213.7
	1650	263.7
	1800	313.7
	2000	406.2
	2200	543.7
	2200	rupture

Sample CS-22:

T = -10.0°C
H = L = D = 6.0 in.
(Continued)

Sample CS-22: (Cont'd)

d = 3/8 in.
h = 1/8 in. (at z = 4.5 in.)
v_s = 64.0 %

P (lbs.)	t (min.)	δ^c ($\times 10^{-3}$ in.)
1500	10	11.2
	20	15.8
	40	21.0
	70	27.0
	100	31.5
	150	37.2
	200	42.2
	300	48.4
	550	60.3
	700	66.0
	850	73.4
	1000	78.4
	1120	81.0
2000	1120	83.4
	1200	94.7
	1300	104.4
	1500	119.1
	1700	131.6
	1840	140.4
2500	1840	143.3
	2000	176.6
	2200	221.6
	2400	259.1
	2600	301.6
	2700	321.6
3000	2700	322.0
	2850	409.5
	3000	492.0
	3200	602.0
	3370	685.0
3500	3370	687.0
	3500	874.5
	3700	1137.0
	3900	1387.0
	4060	1612.0

Sample CS-23:

T = -10.0°C
H = L = 6.0 in.
D = 1.938 in.
(Continued)

Table B-2: (Cont'd)

Sample CS-23: (Cont'd)

d = 3/8 in.
h = 1/8 in.
v_s= 64.0 %

P (lbs.)	t (min.)	δ^c(x10^{-3}in.)
1500	10	26.2
	20	38.7
	40	55.0
	70	72.5
	100	85.0
	200	122.5
	300	155.0
	450	200.0
	600	242.5
	800	325.0
	1000	437.5
	1100	512.5
	1250	682.5
	1250	rupture

Sample CS-24:

T = -6.0°C
H = L = D = 6.0 in.
d = 3/8 in.
h = 1/8 in.
v_s= 64.0 %

P (lbs.)	t (min.)	δ^c(x10^{-3}in.)
1020	20	7.1
	60	14.0
	100	17.0
	150	19.8
	200	22.9
	300	30.4
	450	35.4
	600	39.8
	800	43.6
	1000	47.3
	1115	49.8
1500	11150	51.0
	1160	57.9
	1200	61.7
	1300	67.9
	1400	73.6
	1550	81.7
	1700	87.3

(Continued)

Sample CS-24: (Cont'd)

P (lbs.)	t (min.)	δ^c(x10^{-3}in.)
1500	1840	93.0
1980	1840	96.7
	1900	110.5
	2000	128.5
	2150	145.5
	2300	163.0
	2500	188.0
	2625	203.0
2500	2625	204.0
	2660	226.0
	2700	248.0
	2800	293.0
	2950	383.0
	3100	487.0
	3300	640.0
	3400	728.0
3000	3400	778.0
	3440	890.0
	3500	1102.0
	3600	1390.0

Sample CS-25:

T = -10.0°C
H = L = 6.0 in.
D = 1.938 in.
d = 3/8 in.
h = 1/8 in.
v_s= 64.0 %

P (lbs.)	t (min.)	δ^c(x10^{-3}in.)
1500	20	30.0
	60	47.5
	100	60.0
	150	73.8
	200	85.0
	300	103.8
	400	120.0
	550	145.0
	700	170.0
	900	205.0
	1100	241.0
	1200	258.6
1980	1200	259.0

(Continued)

Table B-2: (Cont'd)

Sample CS-25: (Cont'd)

P (lbs.)	t (min.)	δ^c ($\times 10^{-3}$ in.)
1980	1240	290.0
	1300	350.0
	1350	400.0
	1400	465.0
	1490	655.0
	1490	rupture

Sample CS-26:

$T = -10.0^{o}C$
$H = D = L = 6.0$ in.
$d = 3/8$ in.
$h = 1/8$ in. (at $z = 1.5$ in.)
$v_s = 64.0$ %

P (lbs.)	t (min.)	δ^c ($\times 10^{-3}$ in.)
1020	0	0.5
	20	1.8
	40	2.5
	70	4.0
	100	4.5
	150	6.0
	200	6.5
	250	7.5
	300	8.0
	400	9.0
	500	10.0
	650	11.2
	800	12.5
	1000	14.0
	1250	15.5
	1500	16.5
	1800	17.8
	2100	18.5
	2400	20.0
	2800	21.0
1500**	0	22.0
	50	24.0
	100	25.0
	200	28.0
	300	30.0

** Step loading procedure

(Continued)

Sample CS-26: (Cont'd)

P (lbs.)	t (min.)	δ^c ($\times 10^{-3}$ in.)
1500	400	31.5
	500	33.0
	600	35.5
	740	38.0
1940	0	40.0
	50	43.8
	100	47.5
	200	55.0
	400	62.5
	500	75.0
	600	80.0
	700	85.0
	800	88.8
	900	92.5
2500	0	97.5
	50	110.0
	100	120.0
	200	140.0
	300	160.0
	450	186.2
	600	215.0
	700	235.0
	820	260.0

Sample CS-27:

$T = 10.0^{o}C$
$H = 5.594$ in.
$D = 2.781$ in.
$L = 5.594$
$d = 3/8$ in.
$h = 1/8$ in.
$v_s = 64.0$ %

P (lbs.)	t (min.)	δ^c ($\times 10^{-3}$ in.)
1020	0	0.8
	20	4.5
	40	6.5
	70	8.2
	100	9.2
	150	10.0
	200	11.0
	250	11.5
	300	12.2

(Continued)

Table B-2: (Cont'd)

Sample CS-27: (Cont'd)

P (lbs.)	t (min.)	δ^c ($\times 10^{-3}$ in.)
1020	400	13.0
	500	13.8
	650	14.5
	800	15.1
	1000	15.8
	1310	16.8
1500**	0	16.9
	30	18.2
	60	18.8
	90	19.0
	140	19.8
	190	20.8
	290	21.1
	340	22.2
	520	23.7
2020	0	23.8
	20	28.8
	70	38.8
	120	47.5
	170	53.8
	270	67.6
	370	80.0
	520	98.8
	660	115.0
2500	0	115.2
	50	143.8
	110	172.5
	260	238.8
	410	308.8
	560	381.3
	775	502.5
3000	0	505.5
	15	550.0
	15	rupture

Sample CS-28:

$T = -10.0^{\circ}C$
H = L = 6.0 in.
D = 4.0 in.
d = 3/8 in.
h = 1/8 in.
v_s = 64.0 %

(Continued)

Sample CS-28: (Cont'd)

P (lbs.)	t (min.)	δ^c ($\times 10^{-3}$ in.)
1020	50	1.0
	100	1.4
	200	2.2
	300	2.8
	500	3.0
	800	4.0
	1200	4.2
	1460	4.5
1500	0	4.5
	50	5.0
	100	5.2
	200	6.0
	350	6.5
	600	7.5
	890	8.1
1980	0	8.1
	50	8.6
	100	9.5
	200	9.8
	350	11.0
	480	11.6
2500	0	11.8
	50	14.0
	100	15.4
	200	18.2
	300	21.0
	450	24.2
	600	27.7
	750	31.0
	960	36.0
3000	0	37.2
	50	47.2
	100	56.0
	200	73.4
	300	94.2
	400	118.4
	500	219.7
	600	317.2
	700	422.2
	780	557.2

Table B-2: (Cont'd)

Sample CS-29:

$T = -10.0^{o}C$
H = D = L = 6.0 in.
d = 5/8 in.
h = 0 (plain rod)
v_s= 64.0 %

P (lbs.)	t (min.)	$\delta^c (x10^{-3}$in.)
250	50	0.500
	100	0.825
	200	1.075
	300	1.275
	450	2.000
	600	2.000
	1770	2.000
520	0	2.000
	50	2.300
	100	2.500
	200	3.200
	250	3.750
	300	4.500
	350	5.680
	400	7.380
	420	8.500
	440	11.000
	440	rupture

Sample CS-30:

$T = -10.0^{o}C$
H = L = D = 6.0 in.
d = 5/8 in.
h = 0
v_s= 64.0 %

P (lbs.)	t (min.)	$\delta^c (x10^{-3}$in.)
250	50	0.25
	100	0.50
	200	0.87
	400	1.00
	600	1.12
	900	1.50
	1200	1.75
	1400	2.00
	1620	2.00
410	0	2.00
	100	2.20

(Continued)

Sample CS-30: (Cont'd)

P (lbs.)	t (min.)	$\delta^c (x10^{-3}$in.)
410	200	3.00
	500	3.50
	730	3.50
570	0	3.50
	100	3.50
	300	3.75
	500	4.50
	720	5.82
730	0	5.82
	50	6.57
	100	7.57
	140	9.07
	160	10.32
	180	13.32
	180	rupture

Sample CS-31:

$T = -10.0^{o}C$
H = D = L = 6.0 in.
d = 5/8 in.
h = 0
v_s= 64.0 %

P (lbs.)	t (min.)	$\delta^c (x10^{-3}$in.)
160	50	0.50
	100	0.68
	200	0.88
	300	1.12
	400	1.37
	1480	1.50
240	0	1.50
	100	1.50
	200	1.50
	1665	1.50
360	0	1.50
	100	1.62
	400	1.50
	820	1.50
480	0	1.50
	200	1.50
	400	1.50
	800	1.50
	1000	3.12

(Continued)

Table B-2: (Cont'd)

Sample CS-31: (Cont'd)

P (lbs.)	t (min.)	δ^c ($\times 10^{-3}$ in.)
480	1000	1.50
	1180	1.50
600	0	1.50
	60	1.88
	100	1.50
	200	1.50
	785	1.50
720	0	1.50
	400	1.50
	460	1.62
	460	2.62
	620	3.25
840	0	3.25
	100	2.62
	200	3.00
	425	3.00
	425	1.62
	700	1.62
960	0	1.62
	100	1.62
	200	1.12
	560	1.50
	560	1.62
	680	1.62
1080	0	1.62
	40	1.62
	60	3.25
	80	6.25
	80	rupture

Sample CS-32:

T = -15.0°C
H = D = L = 6.0 in.
d = 5/8 in.
h = 0
v_s = 64.0 %

P (lbs.)	t (min.)	δ^c ($\times 10^{-3}$ in.)
240	50	1.00
	100	1.50
	200	1.75

(Continued)

Sample CS-32: (Cont'd)

P (lbs.)	t (min.)	δ^c ($\times 10^{-3}$ in.)
240	400	1.75
	740	1.75
	925	4.25
	925	1.75
	1100	1.75
	1220	2.50
	1220	1.00
	1400	1.00
	1455	2.00
	2850	2.00
400	0	2.00
	100	2.00
	200	2.00
	450	2.00
600	0	2.00
	100	2.00
	200	2.12
	1040	2.12
760	0	2.25
	100	2.25
	200	2.50
	480	2.50
920	0	2.50
	50	2.88
	100	2.50
	400	2.50
	580	2.50
1080	0	2.50
	100	2.50
	200	2.75
	400	3.00
	1280	3.00
1280	0	3.00
	100	3.50
	200	3.80
	300	4.35
	400	5.00
	500	6.25
	600	7.50
	640	8.75
	665	11.50
	665	rupture

Table B-2: (cont'd)

Sample CS-33:

$T = -15.1^{o}C$
H = D = L = 6.0 in.
d = 5/8 in.
h = 0
v_s= 64.0 %

P (lbs.)	t (min.)	δ^c ($\times 10^{-3}$ in.)
240	0	0.01
	100	0.01
	200	0.01
	840	0.01
400	0	0.01
	100	0.25
	400	0.40
	1310	0.50
560	0	0.50
	100	0.65
	200	0.90
	610	1.00
720	0	1.00
	100	1.00
	200	1.25
	400	1.38
	1270	1.50
880	0	1.50
	100	1.55
	400	1.80
	760	1.81
1040	0	1.81
	100	2.30
	150	2.55
	200	4.00
	200	rupture

Sample CS-34:

$T = -6.1^{o}C$
H = D = L = 6.0 in.
d = 5/8 in.
h = 0
v_s= 64.0 %

(Continued)

Sample CS-34: (cont'd)

P (lbs.)	t (min.)	δ^c ($\times 10^{-3}$ in.)
160	50	0.38
	100	0.50
	200	0.80
	760	1.00
280	0	1.00
	100	1.00
	710	1.25
400	0	1.25
	200	1.50
	775	1.50
520	0	1.50
	200	1.55
	600	1.60
	700	1.65
640	0	1.65
	200	1.72
	300	3.50
	400	6.00
	450	7.80
	500	12.00
	510	14.00
	520	17.75
	525	22.50
	525	rupture

Sample CS-35:

$T = -6.0^{o}C$
H = D = L = 6.0 in.
d = 5/8 in.
h = 0
v_s= 64.0 %

P (lbs.)	t (min.)	δ^c ($\times 10^{-3}$ in.)
280	50	0.50
	100	0.75
	200	1.00
	400	1.20
	530	1.25
400	0	1.25
	100	1.25
	200	1.44

(Continued)

Table B-2: (Cont'd)

Sample CS-35: (Cont'd)

P (lbs.)	t (min.)	δ^c ($\times 10^{-3}$ in.)
400	400	1.50
	860	1.75
520	0	1.75
	100	2.00
	300	2.25
	500	2.35
640	0	2.35
	100	2.60
	400	2.68
	660	2.70
720	0	2.70
	100	3.00
	200	3.08
	400	3.28
	600	3.50
	820	3.60
800	0	3.60
	100	3.80
	200	4.10
	730	4.30
920	0	4.30
	100	4.50
	200	4.80
	300	5.18
	400	5.30
	500	5.20
1040	0	5.20
	40	5.70
	60	6.58
	70	10.80
	70	rupture

Sample CS-36:

$T = -10.0^{o}C$
H = D = L = 6.0 in.
d = 3/8 in.
h = 1/8 in.
v_s = 44.5 %

P (lbs.)	t (min.)	δ^c ($\times 10^{-3}$ in.)
520	50	5.0
	100	8.5

(Continued)

Sample CS-36: (Cont'd)

P (lbs.)	t (min.)	δ^c ($\times 10^{-3}$ in.)
520	200	14.0
	300	18.0
	450	22.8
	600	26.7
	800	32.0
	1000	36.2
	1250	40.1
	1500	44.5
	1750	48.0
	2010	52.0
1080	0	52.0
	50	74.5
	100	92.0
	200	123.2
	300	152.0
	400	178.3
	500	203.2
	650	239.5
	800	275.8
	1000	321.1
	1250	377.7
	1400	411.7
	1515	437.7
1560	0	437.7
	50	507.8
	100	567.7
	150	627.5
	200	690.2
	250	760.2
	280	810.3

Sample CS-37:

$T = -10.1^{o}C$
H = L = 5.625 in.
D = 6.0 in.
d = 3/8 in.
h = 0
v_s = 32.3 %

P (lbs.)	t (min.)	δ^c ($\times 10^{-3}$ in.)
520	200	0.5
	375	1.0
	415	5.0
	480	18.1

(Continued)

Table B-2: (Cont'd)

Sample CS-37: (Cont'd)

P (lbs.)	t (min.)	δ^c ($\times 10^{-3}$ in.)
520	530	26.5
	600	37.8
	650	45.5
	800	63.3
	1000	87.1
	1200	110.9
	1400	134.7
	1700	158.4
	2000	181.2
	2200	195.2
	2370	207.3
1080	0	213.2
	50	300.0
	100	383.2
	150	485.2
	200	535.7
	250	613.2
	300	703.2

Sample CS-38:

T = -10.0°C
H = L = 5.875 in.
D = 6.0 in.
d = 3/8 in.
h = 1/8 in.
v_s = 51.6 %

P (lbs.)	t (min.)	δ^c ($\times 10^{-3}$ in.)
520	100	0.01
	290	1.25
	350	3.50
	400	6.25
	500	10.00
	650	14.38
	800	17.50
	1000	21.80
	1250	28.75
	1775	31.88
1080	0	33.12
	50	47.00
	100	55.00
	200	66.88

(Continued)

Sample CS-38: (Cont'd)

P (lbs.)	t (min.)	δ^c ($\times 10^{-3}$ in.)
1080	300	76.25
	450	90.00
	600	99.25
	800	112.50
	1000	125.75
	1250	138.72
	1500	151.68
	1600	156.88
	1800	164.63
	2050	170.63
1560	0	172.13
	50	188.12
	100	201.38
	200	228.13
	300	251.40
	450	290.60
	600	330.60
	800	385.62
	1000	443.13
	1200	509.10
	1400	584.60
	1590	668.10
1980	0	668.15
	50	730.62
	100	793.12
	150	868.12

Sample CS-39:

T = -10.0°C
H = L 5.875 in.
D = 6.0 in.
d = 3/8 in.
h = 1/8 in.
v_s = 48.6 %

P (lbs.)	t (min.)	δ^c ($\times 10^{-3}$ in.)
520	100	1.25
	200	2.60
	300	5.00
	400	7.60
	600	10.80
	800	15.1

(Continued)

Table B-2: (Cont'd)

Sample CS-39: (Cont'd)

P (lbs.)	t (min.)	δ^c ($\times 10^{-3}$ in.)
520	1000	18.9
	1250	23.2
	1500	27.6
	1800	31.8
	2100	37.0
	2400	40.8
	2700	44.5
	3015	47.5
1080	0	51.0
	50	67.0
	100	81.2
	200	106.0
	300	129.1
	450	151.0
	600	192.2
	800	234.8
	1000	276.0
	1200	316.0
	1400	361.0
1560	0	362.0
	50	424.5
	100	487.0
	150	537.0
	200	612.0
	280	712.0
	260	837.0

Sample CS-40:

$T = -10.0^{o}C$
$H = L = 6.125$ in.
$D = 6.0$ in.
$d = 3/8$ in.
$h = 1/8$ in.
$v_s = 52.8$ %

P (lbs.)	t (min.)	δ^c ($\times 10^{-3}$ in.)
520	50	6.0
	100	9.0
	200	12.8
	300	15.2
	450	17.8

(Continued)

Sample CS-40: (Cont'd)

P (lbs.)	t (min.)	δ^c ($\times 10^{-3}$ in.)
520	600	21.5
	800	24.0
	1000	27.1
	1250	29.0
	1500	31.5
	1800	32.8
	1965	34.0
720	0	35.2
	50	36.5
	100	37.8
	200	40.2
	300	41.5
	450	44.0
	600	46.5
	800	49.0
	1000	51.5
	1200	54.0
	1425	57.7
1080	0	57.8
	50	62.8
	100	65.3
	200	71.5
	300	76.6
	450	82.8
	600	89.1
	800	96.5
	1000	104.0
	1200	111.5
	1410	119.0
1240	0	120.3
	50	124.0
	100	127.8
	200	134.8
	300	142.8
	450	152.8
	600	164.0
	745	175.3
1560	0	175.5
	50	190.5
	100	205.5
	200	234.5
	300	263.0
	450	318.0
	600	393.0
	700	454.2
	820	585.5

Table B-2: (Continued)

Sample CS-41:

T = -10.0°C
H = D = L = 6.0 in.
d = 3/8 in.
h = 1/8 in.
v_s= 17.5 %

P (lbs.)	t (min.)	δ^c(x10^{-3}in.)
280	100	0.12
	200	0.25
	300	0.50
	600	0.50
	935	0.20
360	0	0.20
	100	0.25
	200	0.50
	400	0.50
	500	0.75
	740	1.00
	1300	1.00
	1445	0.75
520	0	0.50
	100	1.50
	200	2.62
	300	4.50
	400	7.75
	500	11.00
	600	18.50
	700	32.25
	840	61.00
600	0	61.00
	100	111.00
	200	161.00
	300	211.00
	400	261.00
	500	311.00
	600	367.00
	750	448.00
680	0	448.00
	100	555.00
	200	655.00
	300	780.00
	400	918.00
	500	1038.00

Sample CS-42:

T = -10.0°C
H = L = 6.0 in.
D = 1.938 in.
d = 3/8 in.
h = 1/8 in.
v_s= 64.0 %

P (lbs.)	t (min.)	δ^c(x10^{-3}in.)
520	100	1.0
	200	1.0
	300	1.0
	500	1.5
	615	3.0
720	0	3.0
	200	3.3
	500	3.5
	800	4.0
	920	5.0
1080	0	5.0
	50	8.2
	100	12.0
	200	18.0
	300	21.5
	400	25.5
	500	28.5
	615	31.5
1240	0	31.7
	100	37.0
	200	40.9
	300	44.0
	400	47.7
	550	53.4
	700	58.4
	850	59.6
	1035	65.9
1560	0	65.9
	100	75.9
	200	83.4
	300	91.5
	450	104.0
	600	117.1
	750	128.4
	940	144.6
1840	0	144.6
	50	158.4

(Continued)

Table B-2: (Cont'd)

Sample CS-42: (Cont'd)

P (lbs.)	t (min.)	δ^c ($\times 10^{-3}$ in.)
1840	100	170.9
	200	192.1
	300	217.0
	400	233.4
	500	267.0
	665	317.0
2120	0	317.0
	50	364.5
	100	426.4
	150	492.0
	210	604.5
	210	rupture

Sample CS-43:

T = -10.0°C
H = L = 6.0 in.
D = 4.0 in.
d = 3/8 in.
h = 1/8 in.
v_s = 64.0 %

P (lbs.)	t (min.)	δ^c ($\times 10^{-3}$ in.)
1080	50	6.8
	100	13.0
	200	21.0
	300	27.0
	450	31.8
	600	35.8
	800	40.8
	1000	44.5
	1150	46.4
1440	0	47.0
	50	52.0
	100	54.5
	200	59.5
	300	63.2
	450	68.5
	600	72.0
	680	75.0
1840	0	76.0
	50	83.2

(Continued)

Sample CS-43: (Cont'd)

P (lbs.)	t (min.)	δ^c ($\times 10^{-3}$ in.)
1840	100	87.0
	200	95.8
	300	103.2
	450	112.0
	600	122.0
	800	133.0
	1000	144.5
	1180	152.0
2200	0	155.0
	50	160.0
	100	168.8
	200	175.0
	300	187.5
	450	202.5
	600	218.5
	780	237.5
2560	0	237.8
	50	253.0
	100	271.0
	200	293.0
	300	317.0
	400	340.0
	500	363.0
	600	385.0
	670	403.0
2840	0	405.0
	50	433.0
	100	485.0
	200	509.0
	300	563.0
	400	613.0
	500	663.0
	600	725.5

Sample CS-44:

T = 10.0°C
H = L = 3.0 in.
D = 6.0 in.
d = 3/8 in.**
h = 0.015 in.**
v_s = 64.0 %

(Continued)

** Standard deformed bar

Table B-2: (Cont'd)

Sample CS-44: (Cont'd)

P (lbs.)	t (min.)	δ^c ($\times 10^{-3}$ in.)
1080	20	2.5
	40	5.0
	80	7.8
	130	9.8
	200	10.8
	260	13.0
	350	14.9
	450	16.8
	600	18.0
	750	19.2
	900	20.5
	1130	21.8
1560	0	21.8
	40	24.2
	100	26.1
	150	28.0
	250	30.0
	400	34.8
	600	35.5
	800	38.0
	1000	40.2
	1200	42.0
	1365	43.5
1980	0	43.5
	100	48.7
	200	53.0
	350	58.8
	500	64.2
	700	74.2
	950	88.0
	1160	104.2
	1270	124.2
2560	0	124.2
	5	144.0
	5	rupture

Sample CS-45: (Cont'd)

P (lbs.)	t (min.)	δ^c ($\times 10^{-3}$ in.)
520	40	9.3
	100	16.0
	200	21.9
	300	26.5
	450	31.5
	600	35.0
	800	40.0
	1000	43.5
	1205	45.8
800	0	46.5
	50	52.5
	100	55.8
	200	61.2
	300	66.2
	450	72.7
	800	88.3
	1000	95.8
	1130	99.3
1160	0	100.0
	50	115.3
	100	123.8
	200	141.0
	300	156.0
	450	174.3
	600	192.0
	800	216.0
	1000	241.0
	1200	266.0
	1400	292.3
	1535	313.0
1560	0	313.0
	50	403.0
	100	465.0
	200	572.0
	300	671.0
	360	743.0
	400	778.0
	455	896.0

Sample CS-45:

$T = -2.0^{\circ}C$
$H = D = L = 6.0$ in.
$d = 3/8$ in.
$h = 1/8$ in.
$v_s = 64.0$ %

(Continued)